ARSENIC AND FLUORIDE REMOVAL FROM WATER USING BONE CHAR

A Thesis submitted by

Susan Shahab Ahmed Alkurdi, MEng

For the award of

Doctor of Philosophy

2020

Dedication

To

God who gave me the power

My beloved parents who prayed for me day and night

My husband, Dr Salahddin and my children Muhammed, Sara and Ava who consistently supported me

My sisters (Media, Peyman, Havan and Sharmeen) who have always encouraged me

This thesis is dedicated to you

Abstract

Dissolved arsenic and fluorine species co-occurrence in groundwater is of great global concern due to the consequences arising from daily exposure. Millions of people around the world are experiencing health issues as a result of water contamination, especially in developing countries. Therefore, exploring a cost-effective and environmentally friendly adsorbent using waste material has gained great interest in recent years. The use of animal waste from a growing meat industry, provides a sustainable energy source and environmental benefits by reducing the amount of waste material to be disposed.

This study developed bone char and its composites using bone waste as the precursor. The initial objective was to study the effect of pyrolysis temperature (500, 650, 800 and 900 °C), variant residence time and purging gas on the characteristics of the bone char samples. The characteristics of these samples were compared using a range of analytical methods, which were used to interpret the mechanism of removal of fluoride (F^-), arsenite [As(III)] and arsenate [As(V)] from water. The samples prepared at 900 °C had the highest removal capacity for As(III) and As(V) at 4.21 and 56.79 µg/g, respectively. On the other hand, a pyrolysis temperature of 650 °C was reported as the optimum temperature for the removal of F^- from water.

Using four different isotherm models (Langmuir, Freundlich, Redlich-Peterson and Sips), the experimental data relating to As(III) and As(V) removal from water under optimal conditions was found to follow the Sips and Langmuir model, respectively. The kinetic models were examined at 0.5, 2.5, 5 and 10 mg/L of initial concentration for both As(III) and As(V) using kinetic and diffusion models. It was found that the main controlling rate of the adsorption process was intraparticle diffusion, while pore diffusion's contribution in the adsorption process was limited to the lower concentrations of 0.5 and 2.5 mg/L. The outcome of the study showed that the removal of As(III) and As(V) from water was complex. Bone char was found to have a higher removal capacity of As(III) at higher concentrations (>20 mg/L). Thus, modifications are required to either increase the As(III) uptake by the bone char samples or oxidize them to As(V) to provide higher removal capacities.

The oxidation of As(III) to As(V) was examined by producing a composite through the coating of bone char (BC) with nanoscale titanium dioxide ($nTiO_2$) as a photocatalyst. Two preparation methods were adopted for the coating process: after the pyrolysis process at 300 °C and during the pyrolysis process at 900 °C. The latter resulted in a phase change of the $nTiO_2$ from anatase to rutile and showed higher As removal (57.3 % vs 24.8%) and oxidation efficiency (3.5 times more arsenate was produced) for both species compared to the composite prepared after the pyrolysis process. It was also found to have a higher removal capacity for both As species compared to unmodified bone char. The oxidation process was examined through the examination of three different levels of UV light (4, 8, and 12 W) during the experiment. By applying 12 W of UV, a removal capacity of 281.36 µg/g was achieved for the composite, compared to the removal capacity of 195.76 µg/g using the uncoated BC900.

For the individual and simultaneous removals of As(III), As(V) and F^-, fixed bed columns packed with bone char were used to quantify influent flow rate and concentration on breakthrough time during the removal of these contaminants. Breakthrough time was found to decrease with the increase in flow rate and influent concentrations. Four models were used to fit the experimental data relating to the characteristic parameters of the columns: the Yoon-Nelson, Thomas, and Bohart and Adams models. The best fit was provided by the Yoon-Nelson and Thomas models. The presence of coexisting anions was examined and it was found that they resulted in a decreased As removal from water, with F^- posing the most significant effect. The improvement in As removal from water was examined by applying capitative deionization (CDI) technology to the columns. Promising results were achieved as there was a significant increase in breakthrough time using this combination.

This study confirms that valuable bone char and composites can be prepared from animal bio-waste to be utilized as adsorbents for various environmental applications. The structural and surface properties of bone char can be optimized by changing pyrolysis conditions to maximize the sorption capacity of the targeted contaminants.

Certification of Thesis

This Thesis is the work of Mrs Susan Alkurdi except where otherwise acknowledged, with the majority of the authorship of the papers presented as a Thesis by Publication undertaken by the Student. The work is original and has not previously been submitted for any other award, except where acknowledged.

Principal Supervisor: *Professor Jochen Bundschuh*

Associate Supervisor: *Dr Les Bowtell*

Associate Supervisor: *Dr Alla Marchuk*

Associate Supervisor: *Dr Ihsan Hamawand*

Student's and Supervisors' signatures of endorsement are held at the University of Southern Queensland.

Statement of Contribution

The following detail is the agreed share of contribution for candidate and co-authors in the presented publications in this thesis:

Paper I: Alkurdi, S.S., Herath, I., Bundschuh, J., Al-Juboori, R.A., Vithanage, M., and Mohan, D., 2019. Biochar versus bone char for a sustainable inorganic arsenic mitigation in water: What needs to be done in future research? Environment International, 127, 52-69. (**Published; Q1 journal**; Impact Factor: 7.943 and SNIP: 2.505).

Contributions:

- Susan Alkurdi formulated the existing research gaps, prepared the abstract, and outlined and composed the manuscript. The contribution made by the candidate is 70%
- Prof Jochen Bundschuh, Dr Indika Herath, Dr Read Al-Juboori, Dr Meththika Vithanage and Prof Danish Mohan assisted with the manuscript compilation, editing, and critical revision. Overall, their contribution to this manuscript is 30%.

Paper II: Alkurdi, S.S., Al-Juboori, R.A., Bundschuh, J. and Hamawand, I. (2019). Bone char as a green sorbent for removing health threatening fluoride from drinking water. Environment International, 127, 704-719. (**Published; Q1 journal**; Impact Factor: 7.943 and SNIP: 2.505).

Contributions:

- Susan Alkurdi prepared the abstract, reviewed the literature and composed the content of the manuscript. The contribution made by the candidate is 70%
- Prof Jochen Bundschuh, Dr Read Al-Juboori and Dr Ihsan Hamawand assisted with the manuscript's compilation, editing, and critical revision. Overall, their contribution to this manuscript is 30%.

Paper III: Alkurdi, S.S., Al-Juboori, R.A., Bundschuh, J., Bowtell, L. and McKnight, S., 2020. Effect of pyrolysis conditions on bone char characterization and its ability for arsenic and fluoride removal. Environmental Pollution, 262: 114221. (**Published; Q1 journal**; Impact Factor: 5.714 and SNIP: 1.578).

Contributions:

- Susan Alkurdi formulated the research questions and hypothesis, established the research objectives and methodologies, planned and conducted all experiments, collected, analyzed and interpreted all the data, and composed the content of the manuscript. The contribution made by the candidate is 80%
- Prof Jochen Bundschuh, Dr Raed Al-Juboori, Dr Les Bowtell and Mr Stafford McKnight assisted with instrumentation, XRD measurements, critical revision and final revision. Overall, their contribution to this manuscript is 20%.

Paper IV: Alkurdi, S.S., Al-Juboori, R.A., Bundschuh, J., Bowtell, L. and Marchuk, A. (2020). Arsenic removal from water using bon char: A detailed study on adsorption kinetic and isotherm models **(Submitted to the Journal of Hazardous Materials; Q1)**.

Contributions:

- Susan Alkurdi designed the experiments, collected and analyzed all the data, interpreted the results and composed the manuscript. The contribution made by the candidate is 80%
- Prof Jochen Bundschuh, Dr Raed Al-Juboori, Dr Les Bowtell and Dr Alla Marchuk assisted with the manuscript compilation, editing, and critical revision. Overall, their contribution to this manuscript is 20%.

Paper V: Alkurdi, S. S., Al-Juboori, R. A., Bundschuh, J. and Marchuk, A. (2020). Evaluating the ability of nTiO_2/bone char composite and UV radiation for simultaneous oxidation and removal of arsenite **(Prepared for submission to Environmental Pollution; Q1)**.

Contributions:

- Susan Alkurdi prepared the abstract, designed the experiments, collected and analyzed all the data, and composed the content of the manuscript. The contribution made by the candidate is 70%.
- Prof Jochen Bundschuh, Dr Raed Al-Juboori and Dr Alla Marchuk assisted with the manuscript's compilation, editing, and critical revision. Overall, their contribution to this manuscript is 30%.

Paper VI: Alkurdi, S.S., Al-Juboori, R.A., Bundschuh, J., Bowtell, L. Hamawand, I. and Kumarathilaka, P. (2020). Simultaneous immobilization of co-occurring fluoride and arsenic from water using bone char packed columns and the application of CDI for enhancing As removal. **(Prepared for submission to the Journal of Hazardous Materials; Q1)**.

Contributions:

- Susan Alkurdi formulated the research questions, established the research objectives and methodologies, planned and conducted all experiments, data collection, analysis and interpretation, and composed the content of the manuscript. The contribution made by the candidate is 80%.
- Prof Jochen Bundschuh, Dr Raed Al-Juboori, Dr Ihsan Hamawand and Mr Prasanna Kumarathilaka assisted with the manuscript's compilation, editing, and critical revision. Overall, their contribution to this manuscript is 20%.

Acknowledgement

I gratefully acknowledge the financial support of the Iraqi Government and the Australian Research Training Program provided to pursue this doctoral study. I would like to express my deepest gratitude to my principal supervisor, Prof Jochen Bundschuh for giving me this invaluable opportunity, as well as his excellent guidance and encouragement throughout my PhD study. Without his valuable support, it would not have been possible to conduct this research study successfully.

My sincere thanks and appreciation are extended to my associate supervisors, Dr Les Bowtell, Dr Alla Marchuk and Dr Ihsan Hamawand for their encouragement and guidance in the completion of this study. I greatly appreciate the collaboration of Dr Raed Al-Juboori for providing me with analytical and scientific assistance throughout my research project.

I also owe special thanks to the technical staff, particularly Dr Susette Eberhard, Mr Mohan Trada, Mr Adrian Blokland and Mr Brian Lenske for their technical support throughout my study. I would also like to sincerely thank Mrs Sandra Cochrane and Dr Barbara Harmes for their excellent English language support for my manuscripts and the thesis.

My special thanks to my friend Mrs Sara Al-Shaikhli for her friendship and support. Moreover, I wish to thank all my other fellow research colleagues, Dr Javier Rumayor, Dr Indika Herath and Mr Prasanna Kumarathilaka for their extensive support. Finally, my sincere appreciation goes to my parents, husband, children and sisters for supporting me spiritually during the entire doctoral study.

Table of Contents

Dedication i
Abstract ii
Certification of Thesis iv
Statement of Contribution v
Acknowledgement viii
Table of content ix
List of Figures xi
List of Tables xv

Chapter 1: Introduction 1
1.1 Rationale of the study 1
1.2 Research gaps 8
1.3 Research questions 8
1.4 Research aim and objectives 9
1.5 Organization of the thesis 10

Chapter 2: Literature review 13
2.1 Arsenic remediation using bone char and biochar 13
2.1.1 Introduction 13
2.1.2 Manuscript 15
2.1.3 Concluding remarks 33
2.2 Bone char as a green sorbent for Fluoride removal from water 34
2.2.1 Introduction 34
2.2.2 Manuscript 35
2.2.3 Concluding remarks 51

Chapter 3: Effect of pyrolysis conditions on bone char characterization and its ability for arsenic and fluoride removal 52
3.1 Introduction 52
3.2 Manuscript 53
3.3 Concluding remarks 67

Chapter 4: Arsenic removal from water using bon char: A detailed study on adsorption kinetic and isotherm models 68
4.1 Introduction 68
4.2 Manuscript 79
4.3 Concluding remarks 104

Chapter 5: Evaluating the ability of nTiO2/bone char composite and UV radiation for simultaneous oxidation and removal of arsenite 105
5.1 Introduction 105
5.2 Manuscript 106
5.3 Concluding remarks 125

Chapter 6: Simultaneous immobilization of co-occurring arsenic and fluoride from water used bone char packed columns and the application of CDI for enhancing As removal 126
6.1 Introduction 126
6.2 Manuscript 127
6.3 Concluding remarks 150

Chapter 7: Conclusions and Recommendations 151
7.1 Conclusions 151
7.2 Recommendations 155

References 158

Appendix A: Supplemantry materials 173

Appendix B: Graphical abstract of published papers 190

List of Figures

Chapter 1: Introduction 1

Fig. 1.1 pH-Eh diagram for aqueous As species in the system As-O_2-H_2O at 25°C and 1 bar total pressure (Akter et al. 2005) 3

Fig. 1.2 Organization of the thesis 12

Chapter 2: Literature review 13

Fig. 2.1.1 Schematic diagram of the methodology of the review 18

Fig. 2.1.2 Schematic diagram of biochar and bone char production methods from different feedstock types [adapted from (Vithanage, et al. 2017)] 19

Fig. 2.1.3 As adsorption through co-precipitation and ligand exchange mechanisms on the unmodified bone char surface 20

Fig. 2.1.4 The proposed mechanism for the surface complexation of As(V) on iron oxide coated bone char surface (Yoon et al. 2016) 21

Fig. 2.1.5 The effect of biochar modification on its specific surface area and As(V) sorption capacity 22

Fig. 2.1.6 The Mechanism of As removal in the presence of Fe and Mn oxides. 24

Fig. 2.1.7 Graphical representation of potential mechanisms for the immobilization of As on modified biochar surface 25

Fig. 2.1.8 The potential As adsorption mechanism by –NH_2 modified biochar composites 27

Fig. 2.2.1 Countries with high level of fluoride in drinking water (British Geological Survey 2018) 36

Fig. 2.2.2 Meat production by type and country (OECD et al. 2018) 37

Fig. 2.2.3 FTIR spectrum for raw bone and bone char samples pyrolyzed at different temperatures: (a) raw bone, (b) 650 °C, (c) 700 °C, (d) 800 °C, (e) 900 °C and (f) 1000 °C (Rojas-Mayorga et al. 2013) 39

Fig. 2.2.4 Mechanisms of fluoride removal on bone char. 40

Fig. 2.2.5 Most common domestic units designs for defluoridation in developing countries (Fawell et al. 2006) 46

Fig. 2.2.6 Conceptual designs for bone char columns: a) ultrasonically enhanced adsorption and b) electrically enhanced adsorption 47

Chapter 3: Effect of pyrolysis conditions on bone char characterization and its ability for arsenic and fluoride removal..... 52

Fig. 1. SEM images of bone char samples prepared at 500-900 °C, residence time 1-2 h time with or without purging N_2 gas*. (a) BC-500-1, (b) BC-500-2, (c) BC-500-N_2, (d) BC-650-1, (e) BC-650-2, (f) BC-650-N_2, (g) BC-800-1, (h) BC-800-2, (i) BC-800-N_2, (j) BC-900-1, (k) BC-900-2, (l) BC-900-N_2..... 57

Fig. 2. FTIR analysis for the samples produced at 2 different residence time. .. 58

Fig. 3. The concentration of the exchangeable cations in bone char samples made at 1 h, 2h and under N_2 stream. (a) Na, (b) Ca, (c) Mg and (d) K ion concentrations. 60

Fig. 4. Effect of pyrolysis conditions on bone char crystallinity: (a) temperature for residence time of 2 h without N_2, (b) residence time at 650 °C without N_2 and (c) with or without N_2 at 650 ℃ for 2 h. 61

Fig. 5. Removal of As(III) and As(V) on bone char samples. 62

Fig. 6. FTIR analysis for bone char samples before and after loading with (a) As(III) and As(V) and (b) F^-. 63

Fig. 7. Removal of F^- on bone char samples..... 64

Chapter 4: Arsenic removal from water using bon char: A detailed study on adsorption kinetic and isotherm models 68

Fig. 1. The effect of solution pH on the removal capacity of 1 mg/L (a) As(V) and (b) As(III) using 5 g/L BC900. 77

Fig. 2. Effect of initial concentration of As(III) and As(V) on removal capacity using 5 g/L BC900 at pH 8.6 and 7.5, respectively. 79

Fig. 3. Isotherm models fit for the experimental data of (a) As(III) and (b) As(V) using 5 g/L BC900 at pH 8.3 and 7.5, respectively. 82

Fig. 4. Fitting of the kinetic models and the experimental data for As(III) at an initial concentration of (a) 0.5 mg/L, (b) 2.5 mg/L, (c) 5 mg/L and (d) 10 mg/L using 5 g/L BC900 at pH 8.3. 91

Fig. 5. Fitting of the kinetic models of As(V) removal on bone char to the experimental data at (a) 0.5 mg/L, (b) 2.5 mg/L, (c) 5 mg/L and (d)10 mg/L using 5 g/L BC900 at pH 7.5. 94

Fig. 6. Plot of intra particle diffusion model for (a) As(III) and (b) As(V) experimental data using 5 g/L BC900 at pH 8.6 and 7.5, respectively.....99
Fig. 7. Plot of the Boyd model for different concentrations of (a) As(III) and (b) As(V) experimental data using 5 g/L bone char at pH 8.6 and 7.5, respectively. 100
Fig. 8. EDS analyses for (a) BC900, (b) As(III) and (c) As(V).....101
Fig. 9. FTIR analysis for As-loaded and unloaded BC900 (Alkurdi et al. 2020) 102

Chapter 5: Evaluating the ability of $nTiO_2$/bone char composite and UV radiation for simultaneous oxidation and removal of arsenite..... 105
Fig. 1. Experimental setup. 112
Fig. 2. EDS analyses for (a) BC900 and (b) $(BC/nTiO2)_P$ 114
Fig. 3. SEM images for (a) BC900 and (b) $(BC/nTiO_2)_P$. 116
Fig. 4. $(BC/nTiO_2)_P$ surface charge at various pH levels. 116
Fig. 5. FTIR spectra of BC900 and the composites prepared following two different procedures. 117
Fig. 6. FTIR spectra for (a) $nTiO_2$ (anatase) and after exposure to 300°C and 900°C in this study and (b) anatase and rutile (El-Sherbiny et al. 2014).....118
Fig. 7. Arsenic speciation for (a) untreated sample, (b) treated sample with UV and $(BC/nTiO_2)_{US}$ (c) treated sample with UV and $(BC/nTiO_2)_P$. 120
Fig. 8. As removal capacity with different treatment scenarios. Experimental conditions: pH = 8, As (III) initial concentration = 2.5 mg/L, adsorbent dose = 5 g/L. 121
Fig. 9. FTIR analysis for (a) As loading effect on $(BC/TiO_2)_P$ structure and (b) UV and $nTiO_2$ effect on BC900 structure. 123

Chapter 6: Simultaneous immobilization of co-occurring arsenic and fluoride from water used bone char packed columns and the application of CDI for enhancing As removal..... 125
Fig. 1. Schematic representation of the experimental setup. 132
Fig. 2. As(III) experiments and models plot at (a) 1 mg/L and (b) 1.5 mg/L at three different flow rates. 136

Fig. 3. As(V) experimental and models plot at (a) 1 mg/L and (b) 1.5 mg/L at three different flow rates.....137
Fig. 4. The removal 1 mg/L total As at 90 mL/min. 141
Fig. 5. Total As removal at 1 mg/L and 10 mL/min using (a) natural well water and (b) applying CDI using distilled water.....142
Fig. 6. Principle of CDI application (Li and Zou 2011) 143
Fig. 7. Breakthrough curve and model plot for F^- at (a) 10 mg/L and (b) 20 mg/L. 145
Fig. 8. The simultaneous removal of (a) 1 mg/L total As and (b) 10 mg/L F^- from natural well water. 147

List of Tables

Chapter 2: Literature review 13

Table 2.1.1 Advantages and disadvantages of different technologies used for arsenic removal in water. 16

Table 2.1.2 The effect of surface modification of biochar to remove arsenic from water. 23

Table 2.1.3 Desorption capability of regenerated biochar and bone char in aqueous media. 28

Table 2.1.4 The effect of co-existing anions on the removal of As by biochar and bone char. 28

Table 2.2.1 The effect of charring temperature and heating rate on the bone char surface properties and fluoride uptake (residence time =2h). 38

Table 2.2.2 The effect of charring temperature and residence time on the bone char surface properties and fluoride uptake (heating rate =10 °C/h). 39

Table 2.2.3 Removal capacity and experimental conditions for fluoride removal on bone char. 41

Table 2.2.4 List of some isotherm models (Foo and Hameed 2010). 45

Chapter 3: Effect of pyrolysis conditions on bone char characterization and its ability for arsenic and fluoride removal…… 52

Table 1. Amount of the DOC released from each bone char sample in mg/L.. . 59

Table 2. The results of the Boehm titration for bone char samples prepared at different temperatures. 60

Chapter 4: Arsenic removal from water using bon char: A detailed study on adsorption kinetic and isotherm models 68

Table 1. Characteristics of bone char. 75

Table 2. Parameters of isotherm models for As(III) and As(V) adsorption onto bone char based on nonlinear regression fitting. 84

Table 3. Error analysis comparison for As(III) isotherm parameters..... 84

Table 4. Error analysis comparison for As(V) isotherm parameters..... 86

Table 5. Kinetic models' parameters for As(III) adsorption onto bone char from nonlinear regression. 91
Table 6. Error analysis for kinetic models of As(III) adsorption onto bone char. 92
Table 7. Kinetic models' parameters for As(V) adsorption onto bone char based on the nonlinear form of the model. 95
Table 8. Error analysis for kinetic models of As(III) adsorption onto bone char at an initial concentration of 0.5 mg/L. 95

Chapter 5: Evaluating the ability of $nTiO_2$/bone char composite and UV radiation for simultaneous oxidation and removal of arsenite 105
Table 1. Optimum operating conditions for As species removal with BC900. 113
Table 2. $(BC/nTiO_2)_P$ characteristics. 115

Chapter 6: Simultaneous immobilization of co-occuring arsenic and fluoride from water used bone char packed columns and the application of CDI for enhancing As removal 125
Table 1. Parameters of column models for As(III) experimental data fittings. 139
Table 2. Parameters of column models for As(V) experimental data fittings.. 140
Table 3. The parameters calculated for the breakthrough curve at saturation. 141
Table 4. The characteristic of well water supplied by Western Downs Regional Council. 143
Table 5. Parameters of adsorption models applied for F^- removal from water. 146

CHAPTER 1

INTRODUCTION

1.1 Rationale of Study

The existence of mankind is dependent on water as it is an essential factor in the integrity of the Earth's ecosystem. However, water scarcity is a serious issue and a full-scale emergency has been declared regarding a global water shortage in coming decades. Based on the United Nations' annual environmental report, changes in consumption patterns, population and economic growth have increased the demand for water by 1% per year since the 1980s' (UN, 2019). On the other hand, while water resources are sufficient in several places around the world, deteriorating water quality may reduce access to safe drinking and irrigation water.

Groundwater is the largest fresh water source, but the most slowly renewed (Dalin et al., 2019). About 97% of fresh water available for human use is stored in aquifers (excluding glaciers/icecaps) (Figoli et al., 2016). The increased rate of groundwater usage globally (750-800 Km^3/year) has decreased the yield of wells, increased pumping costs, damaged the ecosystem and reduced land usability (Konikow and Kendy, 2005). For instance, in the last 60 years, the use of groundwater for irrigation has tripled to 20% of the total amount of water used for irrigation globally (Dalin et al., 2019). Groundwater sources are known to require minimal treatment for domestic use due to their microbiological and chemical qualities. However, changes in rainfall patterns and the unsustainable use of groundwater for irrigation and domestic uses have rendered it unsafe due to the vertical migration of contaminates through soil layers during the aquifer recharge process (Lapworth et al., 2017). Groundwater contamination is related to the natural weathering of bedrock, i.e. mobilization of geogenic contaminants into groundwater. This process can be accelerated by several orders of magnitude through anthropogenic activities such as groundwater exploitation, mining activities (Bundschuh et al. 2017) and purely anthropogenic contaminant sources (e.g. coal based thermal power plants) (Dubey et al. 2012). While in areas where groundwater resources are less exposed to geogenic and anthropogenic

water pollutants, the presence of trace elements (arsenic, fluorine, uranium, manganese, etc.) can render the quality of aquifers and pose a health hazard when used domestically.

Arsenic (As) is an abundant element in the earth crust with an average availability of 5 mg/kg (Garelick et al., 2009). The main source of As in groundwater is geogenic. Inorganic As is found in groundwater in two oxidation states: arsenite [As(III)] and arsenate [As(V)]. Arsenic is mobilized to groundwater through a series of complex chemical and biochemical interactions between aquifer sediments and water (Herath et al., 2016). The mobility of these two redox species is mainly controlled by the redox number and pH, as presented in Fig. 1.1 (Appelo and Heederik, 2008). Furthermore, the presence of organic dissolved solids and the availability of adsorptive materials such as clay minerals, oxides or hydroxide of aluminium, iron or manganese may affect their mobility. Moreover, anthropogenic sources, represented by As discharged due to agricultural and industrial activities, contribute significantly to concentrations in excess of limits specified by World Health Organization (WHO) guidelines (10 µg/L). For instance, the main source of As in Australia is geogenic and it has been accelerated by several orders of magnitude through anthropogenic activities such as mining and related activities and agricultural activities (Smith et al., 2003). Some of the As agricultural residuals also contain organochlorine pesticides (OCPs), concentrated arsenicals, concentrated arsenical mixtures, other arsenicals which have been contaminated with pesticides, cattle dip sites, and As waste from mining and mineral processing (Bordajandi et al., 2003; Edvantoro et al., 2004; Juhasz et al., 2002). Some of the issues relating to the disposal of As contaminants after treatment and without recovery are the high associated costs and that As waste is not treatable when combined with OCP (Environment Australia, 1998).

Arsenic has been reported to be a Grade I carcinogenic metalloid based on evidence that it causes several cancers (e.g. lung, skin, bladder and breast cancer) when consumed through drinking water (Khan et al., 2020). There is also limited evidence that it may affect the human liver and kidney (Rousseau et al., 2005). The main chronic health effects related to exposure to As in drinking water are Type 2 Diabetes and respiratory, renal and cardiovascular complications in adults (Khan et al., 2020). Inorganic As(III) is more mobile and toxic than As(V) (Qi et al., 2019) due to its higher cellular toxicity through replacement and binding with proteins. The higher mobility

of As(III) and its uncharged state at natural groundwater pH levels reduces its removability via electrostatic attraction and ion exchange (Clifford and Ghurye, 2001; Zeltner, 2002). Thus, developing cost effective methods for As mitigation from drinking water is a necessity.

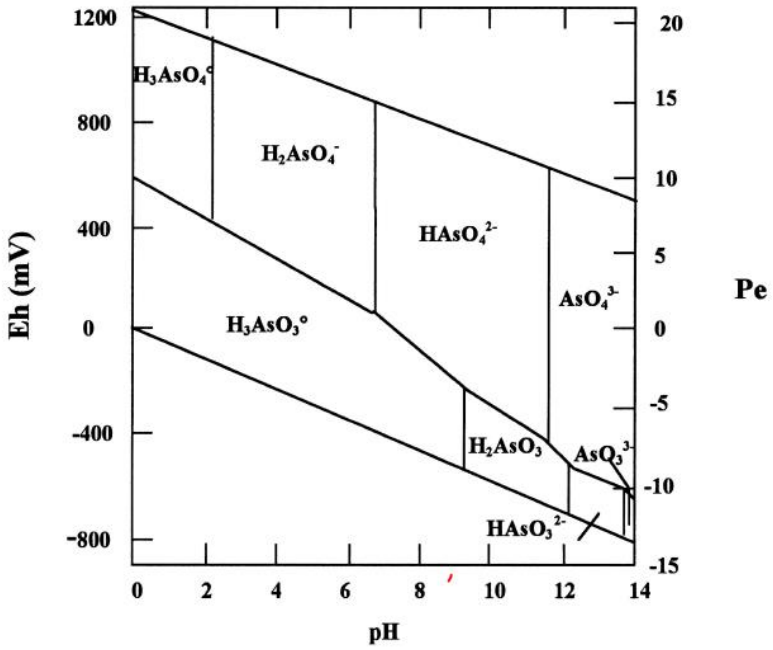

Fig. 1.1 pH-Eh diagram for aqueous As species in the system As-O_2-H_2O at 25°C and 1 bar total pressure (Akter et al., 2005)

Fluorine (F) is the lightest halogen and the most electronegative chemical element. It occurs naturally in the Earth's crust as fluoride (F^-) ions and its respective dissolved complexes in aqueous solutions. Its presence in groundwater is due to geological conditions as it exists naturally in mafic minerals, alkali rocks, and hydrothermal solutions (Hussain et al., 2003). The concentration of F^- in groundwater ranges from 0 to more than 50 mg/L (Figoli et al., 2016), with more than 200 million people in >25 countries exposed to F^- in drinking water with concentrations higher than the permissible limits of 1.5 mg/L specified by the WHO (Alarcón-Herrera et al., 2020). The release of F^- into ground water could be accelerated due to some factors, such as soil alkalinity and the levels of aluminium, calcium and magnesium oxides in the surrounding environment (Padhi and Muralidharan, 2012). The concentration of F^- in groundwater is significantly higher in arid and semi-arid areas due to the drawing of water from deeper aquifers where the occurrence of mineral dissociation is higher due

to longer rock-water interaction time (Alarcón-Herrera et al., 2013; Alarcón-Herrera et al., 2020). Fluoride ions are also discharged into aquatic environments via industrial wastewater such as those associated with semiconductor, pesticide and fertilizer, electronics, glass and aluminium manufacture (Cai et al., 2017; Rasool et al., 2017). This contamination can severely affect bone structure and result in teeth caries if concentrations in drinking water exceed the indicative limits specified by the WHO (Bundschuh et al., 2017). Its harmful effect is related to its uptake by hydroxyapatite (HAP), which is the main component in the bone structure (Bertoni et al., 1998). Fluoride ions have similar radii and charges to hydroxide ions (Gunneriusson et al., 2009) which ease the process of substituting each other in the HAP. The uptake and release of F^- by the HAP is a function of pH. According to Ramsey et al. (1973), HAP dissolution at pH 4 leads to the formation of calcium fluoride at the same pH. This increase in pH leads to the formation of fluorapatite, which is more stable and less soluble than the HAP (Bullough, 2010). Dental and skeletal issues relate to the consumption of F^- in drinking water with concentrations higher than 1.5 mg/L (Bundschuh et al., 2017), and providing safe drinking water is a critical requirement for the areas exposed to high F^- concentrations.

The co-occurrence of dissolved As and F species in groundwater is related to volcanic eruptions, mining activities and geothermal currents (Jadhav et al., 2015). The availability of these two contaminants has been reported around the world including the Americas, Europe and Asia (Alarcón-Herrera et al., 2020; Kumar et al., 2016; Rasool et al., 2015) in shallow aquifers and semi-arid regions. The immobilization of aqueous As and F to groundwater through three main processes: redox potential, microbial related reduction and desorption (Guo et al., 2014). In addition, soil composition and texture, hydraulic gradient and water circulation velocity are the main factors that control the release of As(III), As(V) and F^- into groundwater. The occurrence of these two elements is of great concern to human health and the ecosystem. Several million people are exposed to high concentrations of dissolved As and F species in drinking water, with a higher attention paid to As contaminated water due to its high toxicity. Arsenicosis and fluorosis are the main health concern related to the long exposure to As and F species in drinking water. Thus, the provision safe drinking water from groundwater sources requires some level of treatment.

Arsenic removal from water/wastewater relies on the use of various technologies such as oxidation (Zhang et al., 2019b), biological remediation (Alam and McPhedran, 2019), membrane filtration (Hubadillah et al., 2019) and flocculation and coagulation (Inam et al., 2019). Some of the methods used for F^- removal from water/wastewater are reverse osmosis (Shen et al., 2016), membrane filtration (Zhang et al., 2019a), coagulation-filtration (Long and Xu, 2017) and chemical precipitation (Huang et al., 2017). Some of these methods are also applicable for the simultaneous removal of aqueous As and F, such as chemical precipitation (Ingallinella et al., 2011), electrocoagulation (Nevárez et al., 2011) and membrane filtration. However, high expense, sensitivity to pH levels and pre- and post-treatment issues are the main limitations of these treatment processes (Asadullah et al., 2014), and more effort is required to explore green sorbents for the concurrent mitigation of these two contaminants. On the other hand, adsorption is reported to be the most widely used and efficient removal process of contaminants from water, including As and F species (Dotto et al., 2017).

Adsorption is the process of transferring substances from liquid to solid media. The adsorption process follows three stages: the transport of contaminants from the liquid to the solid surface, adsorption on the sorbent media particles, and substance transport within the sorbent particles (Patel, 2019). The main advantage of water treatment through the adsorption process is related to the possibility of regenerating the sorbent and recycling the contaminants. Different types of adsorbents have been used for the removal of dissolved As and F from water including natural materials such as zeolites (Soni and Shukla, 2019) and red mud (Rubinos and Spagnoli, 2019), industrial by-products (Nasir et al., 2019), biological and agricultural wastes including rice husk (Pillai et al., 2020; Wang et al., 2019). Furthermore, recent studies adopted thermal, chemical and physical modifications to produce composite materials (especially activated carbon composites) that are efficient for water/wastewater remediation (Jia et al., 2007). The use of activated carbon is prominent in the water treatment process, and the high cost of production and subsequent regeneration of spent carbon are the main reasons behind exploring the production of low-cost material from waste (Mohan et al., 2014).

Recently, and particularly in developing countries, the use of cost-effective and environmentally friendly materials has emerged as a promising approach due to their

efficiencies in removing contaminates from soil, water and air, and agents for soil amendment and seed germination. Environmental protection efforts are directed toward minimizing the mass of polluting chemicals added to water bodies. Land filling of organic waste and anaerobic digestion of animal waste results in the release of significant quantities of CH_4 and N_2O gases into the atmosphere. Therefore, using waste residues as a precursor for environmental remediation is an effective waste management strategy to reduce the emission of greenhouse gases and waste disposal costs. For instance, the meat industry produces millions of tonnes of animal waste including animal bone (Co-operation and Development, 2018). Recently, concerns have been raised in relation to the increased amount of animal waste due to the increase in the population. The utilization of these waste materials for environmentally sound and economically beneficial applications will contribute to significant economic and sustainability benefits. While heat treatment of the bone precursor can be utilized for energy production, the by-product of the process, i.e. bone char, has benefits for environmental applications.

Bone char (BC) is a promising alternative remediation method for many toxic and expensive treatment methods. Bone char is mainly composed of HAP [$Ca_{10}(PO_4)_6(OH)_2$] and carbon (Sternitzke et al., 2012). It is used for discoloration in the sugar industry (Choy and McKay, 2005) and it was introduced as a superior adsorbent for the removal of F^- (Abe et al., 2004; Kawasaki et al., 2009). Bone char adsorption capacity depends on its physical and chemical properties which can be controlled through the pyrolysis temperature and the purging gas during the preparation process. Furthermore, adsorbate chemical properties, pyrolysis temperature, solution pH, oxidation/reduction potential (E_h), ionic strength, etc. are all factors that need to be optimized to raise the efficiency of the removal to its maximum values. Bone chars are available commercially, but they are rarely useful for the selective removal of heavy metals/metalloids. Generally, they are used for agricultural soil amendments rather than for water treatment. Thus, bone char modification, which is referred to as engineered biochar, is applied to produce a selective sorption media by controlling its anionic and cationic exchange capacity, surface area and pore volume or the amount of functional groups on the surfaces. Furthermore, limited modification methods were developed to enhance bone char sorption capacity for the removal of As and F species from water (Liu et al., 2016; Zhu et al., 2011).

To improve the removal of aqueous As and F species, several studies have investigated the modification of adsorbents to enhance removal capacity. Bone char removes F^- from water by the ion exchange process between OH ions and F^- in the solution to form fluorapatite. Chemical modification of bone char with multivalent metal ions was found to enhance removal capacity due to their high attraction to F^- (Chatterjee et al., 2018; Delgadillo-Velasco et al., 2017; Rojas-Mayorga et al., 2013). Examination of the kinetics and the isotherm of As(V) removal from water on bone char showed that the mechanism of removal was complex (Chen et al., 2008; Czerniczyniec et al., 2007). However, the only modification of bone char for As removal using chitosan and Fe_3O_4 showed an increase in the immobilization of As(V) from water. On the other hand, As(III) removal by adsorption is typically ineffective as it is uncharged in the natural pH of groundwater. Therefore, As(III) remediation may be enhanced by oxidation of As(III) to As(V) or modifying bone char chemically or physically to increase its uptake.

Titanium dioxide (TiO_2) is reported to be one of the most effective photocatalysts due to its low toxicity, cost effectiveness, high catalytic activity, stability, high oxidation ability, etc. (Singh et al., 2013). Titanium dioxide is a semiconductor that can be used for hydrogen production from water to be used as fuel, transporting electrons in solar cells or for environmental remediations (Lazar et al., 2012). Moreover, nanoparticles of titanium dioxide ($nTiO_2$) were reported for their ability to interact with As(V) due to electrostatic force and chemical bonding (Guan et al., 2012; Li et al., 2016). In this study, $nTiO_2$ was attached to bone char samples to examine its ability to enhance the oxidation of As(III) from solution without the need for pre-treatment units and adsorbing the oxidized As(III) to As(V), while increasing the uptake of As(V) on bone char was adopted using electrochemical method. Capitative deionization (CDI) has emerged as a cost effective and energy efficient technology in water desalination (Porada et al., 2013). It is based on attracting charged ions in solutions to the oppositely charged porous carbon electrode. CDI technology has been used to efficiently remove a low concentration of As(V) (up to 0.13 mg/L) from ground water (Fan et al., 2017; Fan et al., 2016) as it is predominantly available in groundwater as negatively charged $H_2AsO_4^-$ and $HAsO_4^{2-}$. However, for the efficient removal of total As (As(III) and As(V)), peroxidation of As(III) species is required to attract it to the positively charge

electrodes. Then, combining CDI to a fixed bed adsorption column could effectively lower the concentration of As(V) below the standard limits of 1.5 µg/L.

In this research, sheep bones (*Ovis aries)* will be used as a precursor for the production of bone char and its composite to: (i) examine the effect of temperature, residence time and purging gas on bone char characteristics and their ability to remove As(III), As(V) and F^-, (ii) explore the mechanism of As(III) and As(V) removal from water, (iii) study the effectiveness of BC/nTiO_2 composite in oxidizing and adsorbing As(III) and (iv) study the simultaneous removal of dissolved As and F species in column experiments and the effect of CDI on As removal. To date, only limited research has been performed in this area. Bone char will be prepared at different temperatures.

1.2 Research gaps

1. So far, no research has been conducted on producing bone char at different temperature ranges to study its effect on As removal from water, specifically, As(III)
2. No studies have elaborated the isotherm and kinetics of As(III) removal from water using bone char to understand the mechanism of the removal
3. No studies have been conducted on the performance of coating titanium dioxide on bone char in oxidizing As(III) to As(V) under UV light
4. Bone char has not been explored for the simultaneous removal of aqueous As and F species in fixed bed adsorption
5. The effect of CDI application on As removal using fixed bed columns have not been studied before.

1.3 Research questions

1. What is the potential for animal waste to be converted it into an economically valuable resource, such as bone char and its composite, for water treatment using titanium dioxide?
2. What are the effects of temperature, purging gas and residence time on physical characteristics such as surface area, pore structure, and pore volume, and the surface chemistry of the produced bone char?

3. How does the adsorption capacity of the produced bone char vary when used to remove As and F from water?
4. Can the modification of bone char surface with TiO_2 significantly enhance the removal of As from water?
5. What mechanisms are involved in As(III) and As(V) removal onto bone char?
6. What is the impact of applying DC voltage as a driving force to increase As removal in column experiments?
7. How do As and F affect each other when they are removed simultaneously in column experiments?

1.4 Research aims and objectives

The overall aim of the project is to investigate the efficiency of modified bone char for removing As(III), As(V) and F^- contaminants from groundwater. The main objectives are as follows:

1. Studying the effect of charring temperature on the sorbent properties and adsorption performance of the bone char
2. Establishing the adsorption isotherms, process kinetics, and thermodynamics using As(III) and As(V) to elaborate the removal mechanism
3. Producing bone char by pyrolysis and coating and/or impregnating with titanium dioxide (TiO_2) to produce BC/nTiO_2 composites
4. Characterizing the newly developed bone char and BC/nTiO_2 composites in terms of properties and surface chemistry
5. Investigating the performances of BC and BC/nTiO_2 composites in oxidizing and adsorbing As water
6. Investigating the simultaneous removal of As(III), As(V) and F^- in column experiments
7. Applying CDI technology to examine the differences in bone char ability to mitigate As from water.

1.5 Organization of the thesis

This thesis has been structured in six chapters, and the organization of the thesis is represented schematically in Fig. 1.2.

Chapter 1 identifies the rationale of the study, research gaps, research questions, research aims and objectives.

Chapter 2 presents a comprehensive review of the literature associated with the major aspects of the current study. This chapter is associated with two publications: Paper I (Biochar versus bone char for a sustainable inorganic As mitigation in water: What needs to be done in future research?) which presents an overview of the production, characteristics, modification and mechanism for As removal using bone char or biochar and Paper II (Bone char as a green sorbent for removing health-threatening fluoride from drinking water) which provides a critical discussion of the application of bone char to remove F^- from water on lab and large scale. Gaps in research, identified from Paper I and II, are linked with the organization of the research study in the next chapters.

Chapter 3 presents Paper III (Effect of pyrolysis conditions on bone char characterization and its ability for arsenic and fluoride removal) which optimizes and compares the effect of charring temperature on the physical and chemical characteristics of bone char to remediate water from As and F^-.

Chapter 4 presents Paper IV (Arsenic removal from water using bon char: A detailed study on adsorption kinetics and isotherm models) which examines (for the first time) the isotherm, kinetics and the mechanism of As(III) and As(V) removal from water using bone char.

Chapter 5 presents Paper V (Evaluating the ability of $nTiO_2$/bone char composite and UV radiation for simultaneous oxidation and removal of arsenite) which investigates the effect of chemical modification using titanium dioxide nanoparticles on the oxidative state of As species and its removal capacity in the presence of UV light.

Chapter 6 presents Paper VI (Simultaneous immobilization of co-occurring fluoride and arsenic from water using bone char packed columns and the application of CDI for enhancing As removal) which discusses the removal of the two targeted

contaminants on bone char samples via column filtration. Furthermore, the study explores the application of CDI to increase the removal of As.

Chapter 7 summarizes the key outcomes of the research project and provides recommendations for practice and future research.

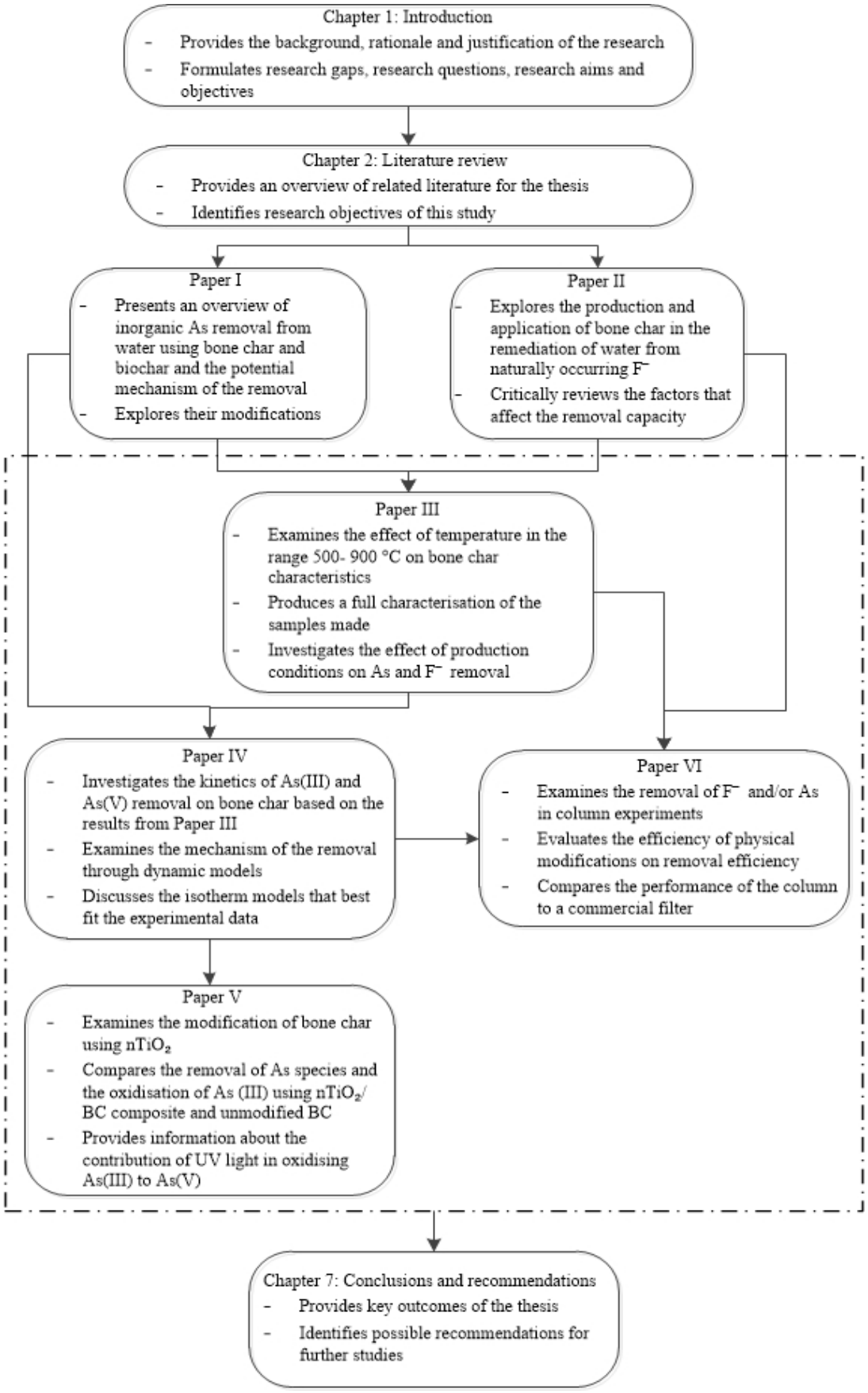

Fig. 1.2 Organization of the thesis

CHAPTER 2

Literature Review

This chapter is organized into two sections including two review articles that were published during the PhD work. The first section critically discusses the use of bone char and biochar and their modifications for inorganic As removal from water. It also provides the potential mechanisms that As species follow during the adsorption process. The second section explores the application of bone char for F^- removal from water and discusses the potential of improving the removal capacity via the proposed designs.

2.1 Arsenic removal on bone char and biochar

PAPER I

Alkurdi, S.S., Herath, I., Bundschuh, J., Al-Juboori, R.A., Vithanage, M. and Mohan, D., 2019. Biochar versus bone char for a sustainable inorganic arsenic mitigation in water: What needs to be done in future research? Environment International, 127, 52- 69. (Published).

2.1.1 Introduction

This review manuscript explores the use of low-cost adsorbent from agricultural and animal waste for the mitigation of inorganic As from water. Unlike previous review studies in the literature, this study brings together different As removal aspects on bone char and biochar, including the effectiveness of bone char and biochar as an adsorbent, the effectiveness of chemical modification methods, the research gaps in the explanation of the mechanism of As removal, the effect of the coexisting anions and

the generation methods for examining the economical validity of the adsorbents. Furthermore, it shows the lack of research into the investigation and application of bone char use for As(III) removal specifically. Finally, it explores the limitations of the applicability of using these adsorbents on a large scale for wastewater and industrial waste treatment. The overall aim of this review is to identify the existing gaps in research on the mechanism of As removal to achieve the goal of the study: providing safe potable drinking water using waste materials.

Environment International 127 (2019) 52–69

Contents lists available at ScienceDirect

Environment International

journal homepage: www.elsevier.com/locate/envint

Review article

Biochar versus bone char for a sustainable inorganic arsenic mitigation in water: What needs to be done in future research?

Susan S.A. Alkurdi[a,b], Indika Herath[a], Jochen Bundschuh[a,c,*], Raed A. Al-Juboori[a,d], Meththika Vithanage[e,f], Dinesh Mohan[g]

[a] School of Civil Engineering and Surveying, Faculty of Health, Engineering and Sciences, University of Southern Queensland, West Street, Toowoomba, 4350, Queensland, Australia
[b] Northern Technical University, Engineering Technical College, Kirkuk, Iraq
[c] UNESCO Chair on Groundwater Arsenic within the 2030 Agenda for Sustainable Development, University of Southern Queensland, West Street, Toowoomba, 4350, Queensland, Australia
[d] School of Science, Engineering and Information Technology, Federation University Australia, University Drive, Mt Helen, VIC 3350, Australia
[e] Office of the Dean, Faculty of Applied Sciences, Jayewardenepura, Nugegoda, Sri Lanka
[f] International Centre for Applied Climate Science, University of Southern Queensland, West Street, Toowoomba, 4350, Queensland, Australia
[g] School of Environmental Sciences, Jawaharlal Nehru University, New Delhi, India

ARTICLE INFO

Keywords:
Inorganic arsenic
Engineered biochar
Bone char
Surface modification
Sorption capacity
Immobilization

ABSTRACT

Arsenic (As) is an emerging contaminant on a global scale posing threat to environmental and human health. The relatively brief history of the applications of biochar and bone char has mapped the endeavors to remove As from water to a considerable extent. This critical review attempts to provide a comprehensive overview for the first time on the potential of bio- and bone-char in the immobilization of inorganic As in water. It seeks to offer a rational assessment of what is existing and what needs to be done in future research as an implication for As toxicity of human health risks through acute and chronic exposure to As contaminated water. Bio- and bone-char are recognized as promising alternatives to activated carbon due to their lower production and activation cost. The surface modification via chemical methods has been adopted to improve the adsorption capacity for anionic As species. Surface complexation, ion exchange, precipitation and electrostatic interactions are the main mechanisms involved in the adsorption of As onto the char surface. However, arsenic-bio-bone char interactions along with their chemical bonding for the removal of As in aqueous solution is still a subject of debate. Hence, the proposed mechanisms need to be scrutinized further using advanced analytical techniques such as synchrotron-based X-ray. Moving this technology from laboratory phase to field scale applications is an urgent necessity in order to establish a sustainable As mitigation in drinking water on a global scale.

1. Introduction

Arsenic (As) is a carcinogenic metalloid that exists in the environment due to geogenic sources as well as anthropogenic activities. It has been found that there are > 250 types of As bearing minerals in the environment (Rahaman et al., 2008). Arsenopyrite (FeAsS) is the most abundant As bearing mineral and other As bearing minerals such as niccolite (NiAs), enargite (Cu_3AsS_4), sperrylite ($PtAs_2$), cobaltite (CoAsS), loellingite ($FeAs_2$), realgar (AsS) and orpiment (As_2S_3) can be widely found in the natural environment (Herath et al., 2016b). Naturally occurring geochemical and biological processes tend to enhance the release of more mobile species of As from the aforementioned mineral phases into the environment. Moreover, anthropogenic activities including mining of As bearing mineral ores, coal and oil exploitation, use of As containing pesticides, herbicides and pharmaceuticals may directly contributed to the release of a variety of As species into the environment. Because of both naturally occurring sources and man-made activities, As is accumulated in environmental, geological, and biological systems at elevated concentrations.

The mobility of As and its immobilization properties in water are highly sensitive to changes in redox potential and pH (Darling, 2016). Generally, As exists in the forms of organic (methylated arsenic compounds, arsenocholine, arsenobetaine, etc.) and inorganic (mono-di-tri-tetra-arsenites and -arsenates) in the environment. However, inorganic

* Corresponding author at: Faculty of Health, Engineering and Sciences & UNESCO Chair on Groundwater Arsenic within the 2030 Agenda for Sustainable Development, University of Southern Queensland, West Street, Toowoomba, Queensland, Australia.
E-mail address: Jochen.Bundschuh@usq.edu.au (J. Bundschuh).

https://doi.org/10.1016/j.envint.2019.03.012
Received 13 December 2018; Received in revised form 15 February 2019; Accepted 4 March 2019
Available online 22 March 2019

forms of As in water is of particular concern in terms of its mobility, transformation and toxicity. In aqueous phase, As occurs in two principal inorganic forms, including arsenate [As(V)] and arsenite [(As(III)] depending on solution pH (Duker et al., 2005; Sorg et al., 2014). Under oxidizing conditions (250–750 mV), As(V) exits in four different species, including H_3AsO_4, $H_2AsO_4^-$, $HAsO_4^{2-}$ and AsO_4^{3-} (Bissen and Frimmel, 2003). In aerobic water (500–750 mV), arsenic acid (H_3AsO_4) becomes the prevalent form of As(V) at extremely acidic pHs (pH < 2), whereas As(V) occurs in the form of $H_2AsO_4^-$ and $HAsO_4^{2-}$ in a wide range of pH (pH 2–11). In mildly reducing environments (−250–+250 mV), arsenious acid (H_3AsO_3) appears at a wide range of pHs (1–9), but it tends to convert to $H_2AsO_3^-$ with the increase of solution pH up to 12 at redox potential ranging from −250 to −500 mV (Panagiotaras and Nikolopoulos, 2015). When the pH value exceeds 12, it occurs in the form of $HAsO_3^{2-}$ in extremely high reducing environments (Bissen and Frimmel, 2003). In natural systems, inorganic As(III) species are of particular interest in terms of their high toxicity, mobility and redox transformation (Mandal and Suzuki, 2002). The concentrations of As in groundwater typically are in the range of 1–2000 μg/L (Figoli et al., 2016). The World Health Organization (WHO) has revised the recommended permissible limit (guideline value) of As in drinking water from 50 μg/L, which was set by the EPA in 1975 (Yamamura et al., 2003), to 10 μg/L (WHO, 2011). However, As contaminated groundwater has been used for drinking and irrigation in many parts of the world, particularly in developing countries where treatment/mitigation options are limited due to political/regulatory lack of awareness as well as poor economic situations (Herath et al., 2016b).

Different technologies have been used for the removal of As from water. Table 1 summarizes the technologies which have been used to remove As from water including some of the advantages and disadvantages of each process. Adsorption has been extensively used for the removal of contaminants from water at different scales, ranging from single household to industrial scale. However, the suitability (including economic and environmental sustainability) depends on removal effectiveness and the possibility of regenerating the sorbent and recycling the contaminants. Different types of feedstock have been used as sorption media, including natural materials, such as zeolites (Xu et al., 2000) and red mud (Genç-Fuhrman et al., 2005; Zhang et al., 2008); industrial by-products such as hydrous titanium (Pirilä et al., 2011); biological and agricultural wastes including rice husk (Pehlivan et al., 2013), laboratory woodchip bioreactors (Hua et al., 2016), sludge waste (Tavares et al., 2012), hydrogels (Sanyang et al., 2014) and biopolymers represented by chitosan (Boddu et al., 2008; Yamani et al., 2016). In order to increase the selectivity of the removal process, recent studies have adopted thermal, chemical and physical modifications to produce composite materials that are efficient for the removal of As in water (Trakal et al., 2018; Wang et al., 2017; Zhang et al., 2016).

Biochar is a heterogeneous carbon material comprising a variety of surface functional groups produced by the thermal alteration of a variety of waste materials. A typical biochar is a carbon-rich product obtained when biomasses, such as wood, leaves, manure, municipal waste sludge, etc. is heated in a closed system with little or absence of air (Lehmann and Joseph, 2015). Biochar derived from different waste feedstocks is widely applied for the removal of organic and inorganic pollutants such as heavy metals (Xu et al., 2019), metalloids (Trakal et al., 2018), pesticides (Herath et al., 2016a) and pharmaceuticals (Zeng et al., 2019) that are present in contaminated-water. On the other hand, animal bone char is another form of biochar that can be produced under similar controlled thermal conditions to produce a phosphorus (P) rich product (Zwetsloot et al., 2016). Bone char produced from animal bones which is the result of partial calcination or the pyrolysis of meat industry waste, is mainly composed of hydroxyapatite (HAP) [$Ca_{10}(PO_4)_6(OH)_2$] and carbon (Sternitzke et al., 2012). It has been reported as a promising adsorbent for fluoride ions in water (Kaseva, 2006; Leyva-Ramos et al., 2010; Medellin-Castillo et al., 2007). However, there is a limited number of studies on the effectiveness of bone char applied in water treatment processes for the removal of metal(loid) (Chen et al., 2008), organic pollutants (Egbuchunam et al., 2016) and dyes (Sun and Yang, 2003). More than 60% of heavy metal(loid)s removal process is attributed to the interaction with the inorganic part (calcium carbonate) of the bone char (Mendoza-Castillo et al., 2015) due to three immobilization mechanisms: ion exchange, dissolution-precipitation reactions, and complexation (Sternitzke et al., 2012). In recent years, there has been increased attention on the modification of the biochar surface as an effective approach to alter the surface properties, pore volume, pore size and surface charge for the selective removal of targeted contaminants from water systems. However, there are limited studies adopting the modification of bone char for water treatment purpose, especially for As removal from water. Thus, engineered biochar and bone char, are a result of either physical or chemical modification using potential natural or synthetic materials (alkaline or acid solutions, zeolite, chitosan, polymers, etc.).

Table 1
Some advantages and disadvantages of different technologies used for arsenic removal in water.

Removal technology	Advantages	Disadvantages	Reference
Coagulation	• Applicable over a neutral pH levels • Chemicals are available commercially	• The need for post-treatment units (sedimentation and filtration) • Highly contaminated solid waste disposal/ management issues	Franco and Carro (2014) Mohan and Pittman (2007) Nicomel et al. (2016)
Adsorption and ion exchange	• Commercially available chemicals (such as activated alumina and resins) • Suitable for removing both As(V) and As(III) • Easy operation • No sludge produced • Cost-effective	• The need for further remediation (disposal/ management issues) • Regeneration issues represented by concentrated liquid waste	Chiavola et al. (2015) Mohan and Pittman (2007) Singh et al. (2015)
Chemical oxidation precipitation	• Break through monitoring is not required • Cost effective method	• Concentrated sludge disposal issues • Not suitable for large scale water treatment • Efficient pH control is required	Anjum et al. (2009) Arar et al. (2014) Bora et al. (2016)
Membrane process	• Efficiently remove both inorganic arsenic forms from water	• High energy demand and cost of reverse osmosis • Liquid waste management in membrane technologies • Fouling issues • Sensitive to pH levels • Time consuming process • Using reagents	Greenlee et al. (2009) Nicomel et al. (2016) Perez-Gonzalez et al. (2012) Shokri et al. (2016)
(Micro)biological remediation	• Economic and promising technology	• Needs more in-depth studies and skilled operators • Have some limitation related to the climate conditions	Hayat et al. (2017) Li et al. (2016)

This review provides a critical overview of the production, characterization and modification of different types of biochar and bone char along with a comprehensive evaluation of their application in the immobilization of various As species in water. Overall, the present review critically analyses and discusses the current knowledge on the As sorption capacity of different types of unmodified and engineered biochar as well as the sorption mechanisms which trigger the immobilization of As species on the biochar surface. The understanding of existing research gaps on arsenic-biochar and arsenic-bone char interactions in different water systems is of utmost importance in order to develop more innovative remediation strategies in future research which would pave the way to establish sustainable As mitigation on a global scale.

2. Methodology

The present review provides a critical assessment of existing research on the application of biochar and bone char for the removal of soluble inorganic As on laboratory and small scale experiments. The review is a collection of appropriate resources extracted from credible sources such as reputable international journals, google scholar books, governmental reports, standards and library catalogue. Fig. 1 depicts the outline of process that was followed for constructing the review. The key words “bone char”, “biochar”, “arsenic removal”, “arsenic immobilization” and “water treatment” were used to collect the relevant literature (regardless to the publication date). Firstly, the documents were collected and organized based on the source of the adsorbent (i.e. bone char or biochar). Secondly, careful screening was followed based on the modification method and the removal of As from water. In some cases, electronic mails were sent to the corresponding authors to clarify some controversial points in their research work. Google scholar alerts were also used for an update to the latest publications related to the topic of the manuscript. For the sake of effective presentation of literature results, quantitative data were compiled and summarized in tables. In some occasions, calculations were made to unify the units or to compare the percentages of As removal on bone char/biochar. Graphical representations of adsorption mechanisms were constructed based on the reported reactions in the literature. As per the knowledge of the authors, reports with controversial results and/or those that lack scientific justifications were avoided. The authors attempted to critically analyze and provide justifications for the results reported in previous studies based on their own knowledge and available information in this field.

3. Arsenic from health perspective

The toxicity of As usually depends on its change in oxidation state (Jain and Ali, 2000). The As(III) is highly cellular toxic due to its ability to hinder the metabolism of glucose, thereby interrupting the energy production through replacing phosphate (PO_4^{3-}) group in adenosine triphosphate ($C_{10}H_{16}N_5O_{13}P_3$) (Singh et al., 2011). As(III) is more toxic than As(V) as it deteriorates the function of many proteins due to binding to sulfhydryl groups (Oremland and Stolz, 2003), and has high affinity to interact with the vicinal thiols in pyruvate dehydogenase and 2-oxoglutarate dehydrogenase (National Research Council, 1999) and with the glucocorticoid receptor (Singh et al., 2011). However, As(V) can effect on metabolism in human body is due to the interaction with PO_4^{3-} receptors and it is less toxic as it needs to be reduced to As(III) to be more reactive with the cells (Molin et al., 2015). Toxicological effects of As exposure are highly associated with aberrations of skin, kidney and liver cells of numerous animal species and humans. The consumption of As contaminated water for a long time may result in various chronical health effects including cardiovascular diseases, neurological disorders, gastrointestinal disturbances, liver disease and renal disease, reproductive health effects, dermal disease and cancers (Bundschuh et al., 2017; Jomova et al., 2011). It has been reported that long-term ingestion of As at 500 μg As/L via drinking groundwater can cause one death per 10 people due to lung, bladder, and skin cancers (Smith et al., 2000). Inorganic As is extremely toxic to living organisms due to high binding ability with protein-sulphydryl (SH) groups and the overproduction of cellular reactive oxygen species (ROS) (Elia et al., 2018). Subacute concentrations of As(III) and dimethylarsinic acid (DMA(V)) are highly sensitive to the cell lines such as human hepatocellular carcinoma and epithelioma papulosum cyprinid generating excessive levels of ROS which may damage of the antioxidant defense system. In addition, the As(III) is in-vitro cytotoxic and genotoxic on human keratinocytes and in-vivo DNA damage in leukocytes and lymphocytes (Sadaf et al., 2018). Because of such critical health consequences of chronic and acute exposure to As, the remediation of As contaminated ground-surface-, drinking- and irrigated- water as well as As contaminated-wastewater through environmental friendly and cost effective strategies is an urgent necessity.

4. Biochar and bone char production and characterization

The pyrolysis temperature and type of feedstock are considered to be key factors in controlling the physio-chemical characteristics of biochar such as surface area, pore size/pore distribution, pH and surface functional groups (Vithanage et al., 2017). Many studies have been well established on the production of various types of biochar, factors affecting their properties, and their application in the remediation of contaminated soil and water systems (Cao and Harris, 2010; Meng et al., 2013; Sun et al., 2014; Vithanage et al., 2017). Biochar and bone char can be produced by using different processes, including low temperature processes, pyrolysis and gasification (Fig. 2) (Mohan et al., 2014; Novotny et al., 2015). At low temperatures (50–300 °C), hydrothermal carbonization, torrefaction and ratification processes take place. These processes produce about 80% of solids with high O/C ratio (Novotny et al., 2015). At higher temperatures (300–700 °C), pyrolysis processes take place. Fast pyrolysis involves a rapid heating of the feedstock in the absence of oxygen followed by a rapid cooling and quenching (Brewer et al., 2009). Fast pyrolysis with short residence time (< 2 s) (Mohan et al., 2006) results in about 40% bio-oil and only 12% solid fraction. The char produced from this process possesses high surface area and porosity and low O/C and H/C ratio compared to those produced via slow pyrolysis. Slow pyrolysis (conventional pyrolysis) is performed in the absence of oxygen using slow heating methods and long residence time, which ranges from hours to days (Dutta et al., 2012). The amount of char produced from this process is about 35% of the final product (Mohan et al., 2014), however the surface characteristic depends particularly on the type of feedstock and pyrolysis temperature (Ahmad et al., 2014). In gasification methods, the biomass is partially combusted in an oxidizing atmosphere producing a relatively small amount of char (about 10%) (Libra et al., 2011). The solid fraction produced via gasification is a porous media with high surface area and low O/C and H/C ratio (Novotny et al., 2015).

In general, increasing the pyrolysis temperature will result in decreasing biochar yield, while increasing ash content, cation exchange capacity (CEC) and surface area (Brewer et al., 2009; Cao and Harris, 2010; Meng et al., 2013; Sun et al., 2014). The existence of different types of functional groups on the biochar surface is related to the pyrolysis temperature and the pH of the solution. Moreover, the CEC of a biochar depends on the charring temperature. Tan et al. (2015) reported that up to a certain temperature (based on the source of the feedstock), the CEC of biochar will increase due to the change in the levels of free OH groups available on the char surface. Then the CEC tends to be decreased as the aromatic crystallites get evolved at higher charring temperature (Harvey et al., 2011). It is prudent to remark that applying pressure during the pyrolysis process may also alter the quality of the char. Cetin et al. (2004) reported that increasing pyrolysis pressure can result in decreasing the surface area of the biochar from 296 m^2/g at 0.1 MPa (1 bar) to 236 m^2/g at 2.0 MPa (20 bar) (using N_2

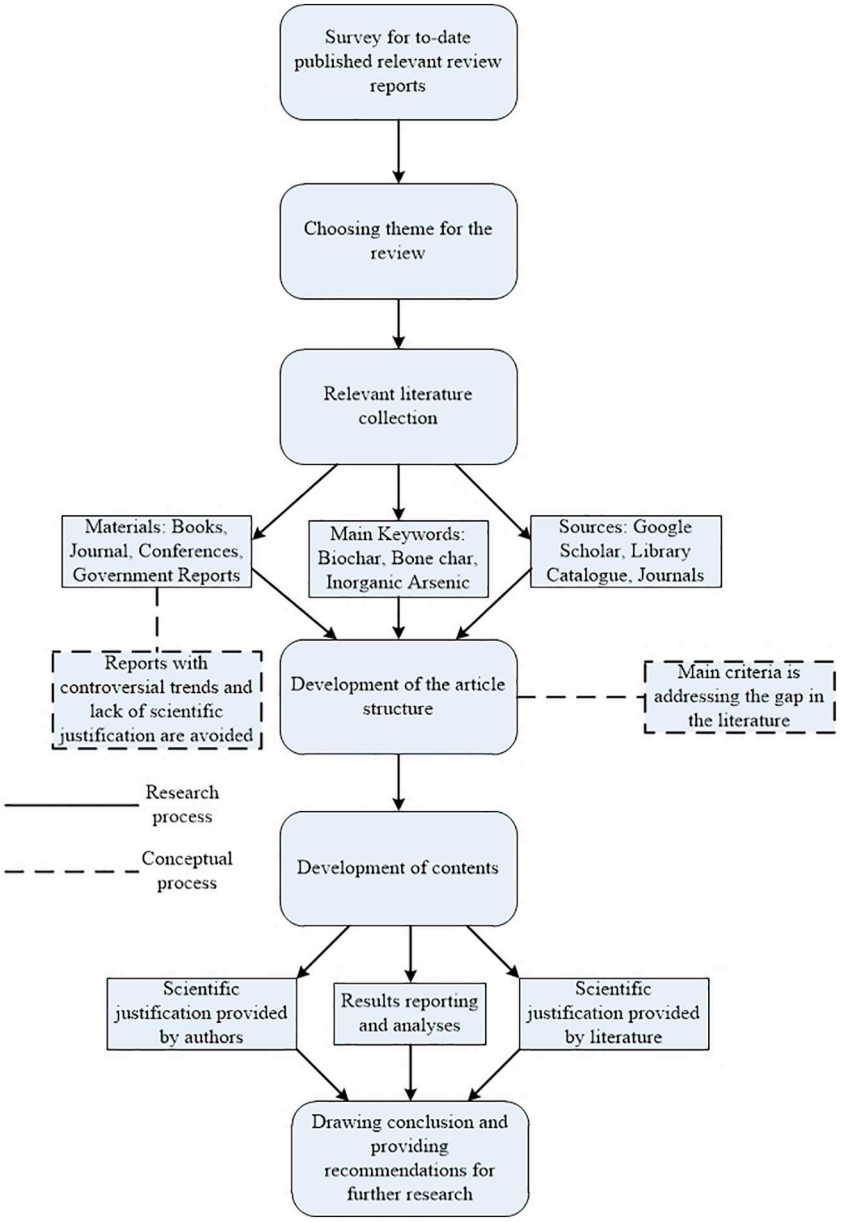

Fig. 1. Schematic diagram of the methodology of the review.

surface area measurements).

The particle size of the feedstock used for char production is also of a particular concern in order to improve the reactivity of biochar through its effect on the intraparticle heat transfer (Lei et al., 2009). It is a fact that the higher intraparticle contact area achieved with smaller particle size can enhance heat transfer inside the grain particles. However, the effect of particle size of the biochar depends on pyrolysis process and feedstock type. Up to now, there is no satisfactory data regarding the relationship between grain size and the adsorption capacity for biochar produced by slow pyrolysis. Nevertheless, it is evident that increasing residence time (Downie et al., 2009) is capable of providing sufficient heat to overcome heat transfer resistance for large particles of feedstock (Demirbas, 2004; Rapagna and Latif, 1997).

Several studies have been published with the primary goal of investigating the effect of particle size during fast pyrolysis and gasification on gas, bio-oil quality and char reactivity (Beaumont and Schwob, 1984; Huang et al., 2008; Lin et al., 2017; Septien et al., 2012). Biochar produced via fast pyrolysis is found to be more reactive and porous than those from slow pyrolysis (Zanzi et al., 1996). Generally, the particle size of biochar from organic sources is significantly lower than those of the feedstock due to the shrinkage and attrition during the pyrolysis. Nevertheless, in some other cases, there will be an increase in the particle size of the biochar due to the particles' agglomeration (Cetin et al., 2004).

The adsorption capacity of biochar for the removal of contaminants is attributed to the existence of functional groups on the biochar surface. The surface charge of the particles can be controlled through the protonation and deprotonation of the existing functional groups (Yuan et al., 2011). At pH levels less than the point of zero charge (pH_{PZC}) of the biochar surface, protonation of some surface functional groups such as carboxyl, ammine, hydroxyl etc. will take place, resulting in an overall positive surface charge on the biochar surface (Waghmare et al., 2015). Thus, the biochar having acidic pHs would favor the adsorption of negatively charged pollutants such as arsenates/arsenites, antimonates/antimonites, etc. Biochar produced at low temperatures (200–400 °C) is preferred for the removal of inorganic and polar organic contaminants due to their binding with O– containing functional groups of the biochar (Ahmad et al., 2014) and the higher O/C molar ratio for

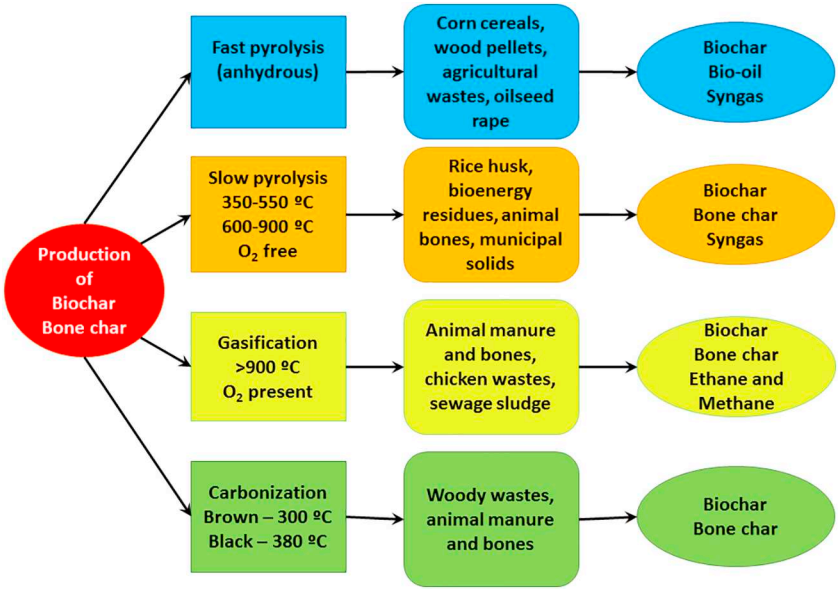

Fig. 2. Schematic diagram of biochar and bone char production methods from different feedstock types. [Adapted from (Vithanage et al., 2017)].

the biochar produced at low temperature (Uchimiya et al., 2011). Therefore it is clear that the availability of functional groups, O/C ratio, polarity indices (O + N)/C and zeta potential are crucial factors in determining the potential of biochar to remove contaminants from aqueous solutions (Samsuri et al., 2013).

5. Biochar and bone char for arsenic removal from water

Biochar produced from different types of feedstock such as pine wood and bark, oak wood and bark, solid waste, rice husks, biosolids, and animal products, has been used to test their effectiveness for As removal from water. However, unmodified biochar has been found to be possessing limited sorption ability of As in aqueous media. This is because the potential of biochar for As removal is predominantly dependent on the surface charge (Hu et al., 2015). The surface of biochar can itself carry both positive and negative charges at a range of pHs, however, the surface becomes net negative above its pH_{PZC}, while it is net positive below the pH_{PZC} (Vithanage et al., 2016). Hence, the pH_{PZC} is an influential parameter to determine the net charge of the char surface for the adsorption of As in aqueous media. The sorption capacity of both biochar and bone char can be improved by changing the surface charge through physical and/or chemical modification methods (Liu et al., 2014). Interestingly, bone char derived from cattle bones can be applied for the removal of As from water to a significant extent without any surface modification. Therefore, this review comparatively discusses the effects of modified and unmodified biochar and bone char for the removal of As from water in order to understand the gaps in existing research which need to be addressed by future research.

5.1. Bone char for arsenic removal from water

Several studies investigated the sorption mechanisms and factors affecting sorption efficiency for enhancing the removal of As(V) using bone char produced from waste animal bones such as cattle and fish bone. Czerniczyniec et al. (2007) reported that the high salinity (0.05–0.5 mol/L) and hardness levels of water can enhance the adsorption of As(V) on cow bone char in drinking water. The increment in salinity levels may result in increasing Ca^{2+} concentration in the solution due to the increase in the solubility of biogenic hydroxyapatite (HAP). High hardness levels were capable of increasing the positive surface charge on bone char, thereby increasing the interaction between negatively charged As(V) and char surface. The maximum removal (75%) was achieved onto the bone char produced at 900 °C at an initial As(V) concentration of 1 mg/L (up to 0.142 mg As/g sorbent). On the other hand, decreasing the charring temperature to 500 °C resulted in an increase of the sorption capacity by more than two-fold due to the increase in surface area (from 2.6 to 376.4 m^2/g). Bone char effectively removed As(V) from drinking water (up to 95.2%) at pH 10 and an initial As(V) concentration of 0.5 mg/L (Chen and Chai, 2008).

The effect of pH, contact time, adsorbent dosage and initial As concentration on As(V) sorption onto commercial bone char (supplied by Biochemistry Ltd., Sichuang, China) were investigated by Chen et al. (2008). This study demonstrated that As(V) sorption is rapid in the first 30 min and that the initial concentrations (0.5, 1.0 and 1.5 mg/L) did not affect the equilibrium time. The pH range of 2 to 13 and the adsorbent dose of 0.1 to 0.8 g/L significantly influenced the removal efficiency. The maximum As(V) removal was 99.18% (0.827 mg/g) at pH 10 and an initial As(V) concentration of 0.5 mg/L. This study further suggested that the maximum removal achieved at high pH levels may be attributed to co-precipitation between $HAsO_4^{2-}$ and HAP in the presence of Ca^{2+} and ion exchange between hydroxyl and As(V) ions (Fig. 3). Similarly, Begum et al. (2016) investigated As(V) removal using commercial bone char (produced at 450 °C and purchased from Anthracite Filter Media Company) in the pH range of 1–11, initial As(V) concentrations of 0.1–1 mg/L and adsorbate dose of 1–5 g/L. A maximum adsorption capacity of bone char of 0.134 mg/g was achieved at pH 4, As(V) concentration of 1 mg/L and adsorbate dose of 3 g/L which agreed with the predicted value by Langmuir isotherm model. This indicates that As(V)adsorption was a monolayer one with the homogenous bone char surface. Liu et al. (2014) studied the adsorption of As (V) from wastewater onto a commercially produced cow bone char at 500 °C having a surface area of 1.51 m^2/g, via batch and column experiments. Using the Langmuir isotherm model to fit the experimental results, the maximum sorption capacity for As(V) was 0.335 mg/g at pH 4 and an initial As(V) concentration of 10 mg/L. The mechanisms that trigger the removal of As(V) were found to be dissolution, ligand exchange and electrostatic attraction as expressed by Eqs. (1)–(3) (Liu et al., 2014).

$$Ca_5(PO_4)_3{\cdot}OH \rightarrow 5\,Ca^{2+} + 3PO_4^{3-} + OH^- \quad (1)$$

$$Ca_5(PO_4)_3{\cdot}OH + H_2AsO_4^- \rightarrow Ca_5(PO_4)_3{\cdot}H_2AsO_4 + OH^- \quad (2)$$

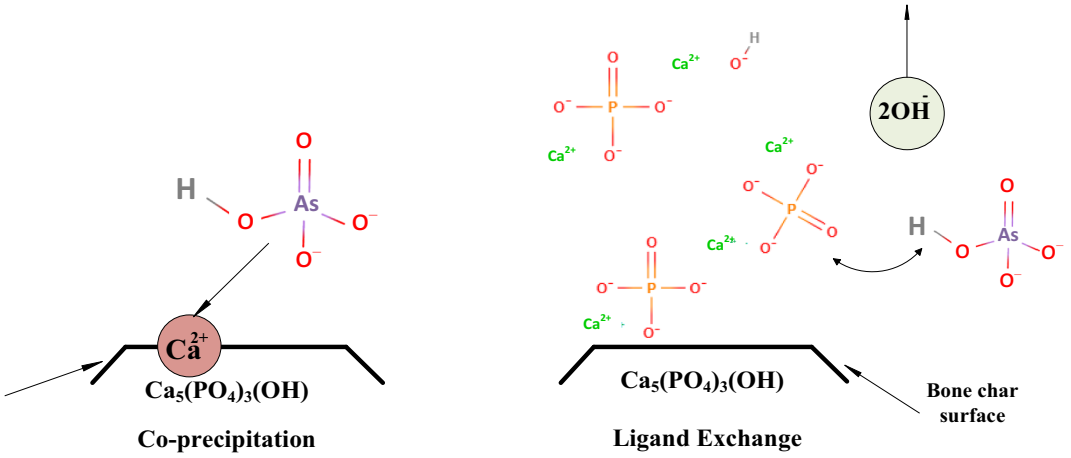

Fig. 3. As adsorption through co-precipitation and ligand exchange mechanisms on the unmodified bone char surface.

$$Ca_5(PO_4)_3{\cdot}OH_2^+ + H_2AsO_4^- \rightarrow Ca_5(PO_4)_3{\cdot}OH_2^+ \cdots\cdots H_2AsO_4^- \quad (3)$$

Synthetic HAP, which is an emerging bioceramic used in biomedical applications possesses many similarities to the naturally occurring HAP in animal bone and teeth (Nayak, 2010). Hence, it is acceptable to utilize this structural similarity to predict the efficiency and gain understanding of As removal mechanisms with bone char (Fig. 3). Sneddon et al. (2005) compared the performance of synthesized HAP with barite (HAP + B) (produced from commercially available bonemeal, from Vitax Ltd) and granular activated carbon (GAC) for the removal As(V) from aqueous solution. A maximum removal of As(V) by HAP + B was observed to be 0.32 mg/g at 4 mg/L initial As concentration, 10 g/L bone char dose and initial pH of 5.0. Because unmodified bone chars are less effective for the removal of As from water, some recent studies have used modified bone char to increase the removal efficiency of As from aqueous solutions. It is noteworthy to remark that up to date, only single study is available on the investigation of As(III) removal by bone char possessing a maximum removal capacity of 0.22 mg/g (Mlilo et al., 2009). Thus, further study is recommended to investigate this aspect, as it would be more cost-effective to eliminate the pre-oxidation of As(III) to As(V).

5.2. Modified bone char for arsenic removal

To our knowledge, the effect of coating bone char with Fe oxide nanoparticles on the removal of As(V) has been studied for the first time by Soltani et al. (2017). In this study, composites of cattle bone char, Fe_3O_4 nanoparticles (with diameter < 50 nm) and chitosan biopolymer were applied for the immobilization of As(V) in an aqueous solution at a range of pH 2-11. The removal capacity of As(V) decreased under both extreme acidic and basic conditions due to the formation of H_3AsO_4 at pH < 2.0, and the increase in OH^- competing ions at high pH levels, respectively. The maximum As(V) removal capacity estimated by the Langmuir isotherm model was found to be 112 μg/L. This composite has been recognized as a spontaneous adsorbent for As(V) removal from aqueous solution. The removal mechanism proposed by this study is electrostatic interaction force between negatively charged As(V) species and the positively charged $Fe_3O_4^-$ nanocomposite surface at neutral pH range. However, it is noteworthy to mention that the adsorption mechanism of As(III) on such iron oxide coated char surfaces is strongly affected by a surface complexation mechanism. Fig. 4 depicts the proposed mechanisms for the adsorption of As(V) and As(III) in iron oxide modified bone char surface. As(III) and As(V) are capable of adsorbing onto the iron oxide coated bone char surface by an inner-sphere ligand-exchange mechanism. In this ligand exchange, As oxyanion gets exchanged with surface −OH or $-OH_2$ groups which are directly coordinated on Fe^{3+} at the iron oxide surface. For the adsorption of As (V), the absorbed As(V) is usually coordinated to two adjacent structural Fe^{3+} cations by iron oxide (Fig. 4(a)) which is a bidentate binuclear-bridging complex. In contrast, in the adsorption of As(III), both bidentate binuclear-bridging complexes and monodentate complexes can exist (Fig. 4(b)). A monodentate complex is formed when a single oxygen atom of the As(III) oxyanion coordinates with a single structural Fe^{3+} at the iron oxide surface. It has been confirmed that the bonding of As(III) on iron oxide surface predominantly takes place through either a monodentate bond or the formation of an outer-sphere complex (Yoon et al., 2016). In an outer sphere complex, the ligand is not coordinated directly to the structural Fe^{3+}, instead it is bound to the surface −OH or $-OH_2$ groups through hydrogen bonds (Fig. 4(c)). Therefore, it is predicted to be a strong and easy adsorption of As(III) onto adsorbents modified with Fe_3O_4 than As(V) in the adsorption process.

A commercial bone char (from Sichuan Biochemistry Co. Ltd. in China) was effectively modified by using nano-sized manganese (using $MnSO_4$ solution) for As removal in water (Liu et al., 2016). The modification of bone char surface with manganese resulted in increasing the specific surface area of uncoated bone char from 1.51 m^2/g to a maximum of 4.6 m^2/g for the modified bone char at 15 g/L initial Mn^{2+} concentration. The results of this study revealed that the adsorption capacity of modified bone char for As(V) is 78 times higher than the uncoated bone char, and the removal efficiency linearly increases with increasing the manganese concentration (0.025–14.5 mg/g). The maximum As(V) removal was 9.46 mg/g at 30 g/L of manganese coated bone char, which was much higher than that of the uncoated bone char (0.12 mg/g). Such a modification of char surface for As(V) removal was presumably attributed to the enhancement of electrostatic interactions between As(V) and the bone char surface.

Liu et al. (2010) proposed a chemical modification method to remove As(V) from simulated groundwater (with initial concentration of 0.195–0.959 mg/L) by doping Cu onto synthesized HAP. Copper doping onto the HAP (CuHAP) significantly increased the surface area from 6.63 m^2/g of unmodified bone char to 77.5 m^2/g of modified bone char. As a result, the maximum As(V) uptake by CuHAP was 0.048–1.091 mg/g at pH 7.7–8.0 which was 1.6–9.1 times higher than that of untreated HAP (0.03–0.1199 mg/g). The adsorption mechanism of As(V) by CuHAP may be a complex process due to the formation of different Ca-HAP complexes with other metal impurities in bone char such a $Ca_{(10-3\times/2)}$ $Al_x(PO_4)_6(OH)_2$, $Ca_{(10-x)}$ $Mg_x(PO_4)_6(OH)_2$, and $Ca_{(10-3\times/2)}$ $La_x(PO_4)_6(OH)_2$ (Chen et al., 2018). Therefore, chemical characterization of bone char would be a critical step before the surface modification via metal doping.

Moreover, Passman et al. (2014) added a layer of commercial bone char to a clay filter in a prototype model to investigate the removal of

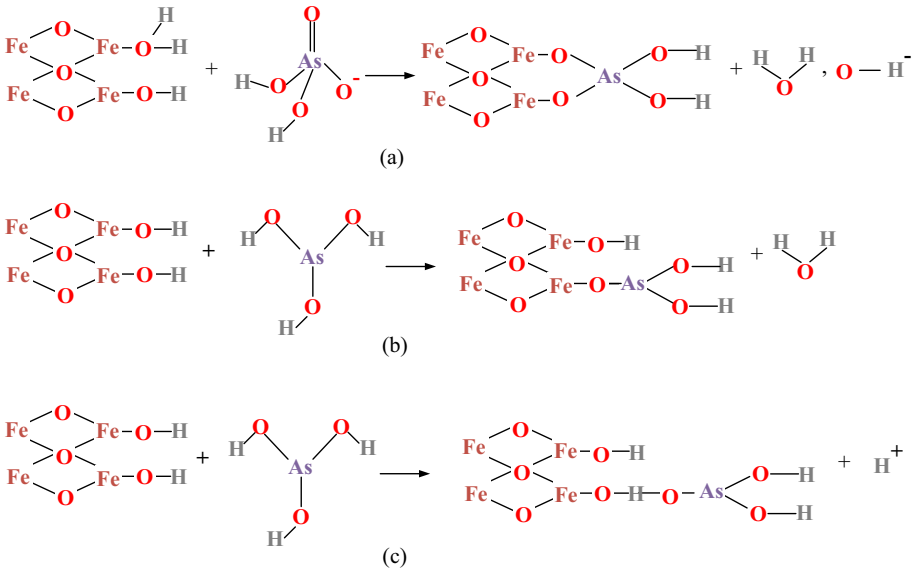

Fig. 4. The proposed mechanism for the surface complexation of As(V) on iron oxide coated bone char surface (Yoon et al., 2016).

As as well as the removal of microorganisms in drinking water. In this method, two types of filters including clay and bone char were attached to each other and the water was passed through the filters to remove coliform bacteria on the clay filter and subsequently As species on the bone char layer. This modified system interestingly decreased the As concentration from 0.5 mg/L to < 0.01 mg/L in the effluent (below WHO and United States Environmental Protection Agency (US EPA) standard limits). Hence, the application of this type of materials in large scale would be a promising strategy for lowering the concentration of As below 10 μg/L in drinking water.

5.3. Biochar for arsenic removal

Recent studies have recognized different types of feedstock including agricultural, solid and sludge wastes and industrial by-products as promising sources for the production of biochar which will also be an alternative waste management option in the environment. Biochar derived from waste materials and agricultural residues has been widely investigated for the immobilization of As species in water (Vithanage et al., 2017). For instance, Agrafioti et al. (2014a) studied the adsorption and desorption at different initial As(V) concentrations (90–850 μg/L) in aqueous solutions using three types of biochar produced from rice husk (BC–RH), solid wastes (BC–SW), and sewage sludge (BC–SS). For an initial As(V) concentration of 90 μg/L, the maximum As(V) removal by BC–RH (8 g/L adsorbent dose and surface area of 155 m^2/g) was only 2.813 μg/g. On the other hand, the maximum As(V) removal was 2.98 and 3.094 μg/g on the BC–SS and BC–SW, respectively. The BC–SW biochar, having a high ash content of 32% w/w with 49.38% of CaO, is likely to be efficient in As(V) removal at pH 9.5 due to its strong interactions with the biochar surface. On the other hand, in an alkaline solution with high Ca content, As(V) removal takes place through the precipitation. The removal of As(V) by BC–SS was increased at low pH due to the presence of the ferrous oxide on the biochar surface in which the sorption mechanism is governed by a redox reaction between As(V) and Fe(II).

Mohan et al. (2007) investigated the adsorption of As(III) onto biochar produced by fast pyrolysis from barks and woods of oak and pine at 450 °C. At pH levels < 2, oak-bark biochar removed a maximum of 70% of As(III) from the solution. The removal of As(III) by oak and pine wood biochar increased from 0 to 20% at pH 2–4. The optimal As (III) removal was 12.15 mg/g at pH 3.5 on pine bark char as predicted by the Langmuir isotherm model. The higher removal capacity of pine bark biochar was due to its higher surface area and pore volume compared to the other biochar samples.

Industrial activities distributed throughout the world tend to generate solid wastes at excessive quantities. The use of industrial by-products as a low-cost sorbent will contribute to improve waste disposal management in developed as well as developing countries due to improper waste handling and disposal practices. Examining the possibility of reusing the by-product of these processes for environmental remediation may justify their validity as an alternative for fossil fuels. For instance, Yadav et al. (2014) used sponge iron char (SIC) having a surface area of 78.63 m^2/g for As(III) and As(V) removal from wastewater. The maximum As removal was found to be at pH 12, adsorbent dosage of 6 g/L, initial As concentration of 150 μg/L and equilibrium contact time of 3 h. The maximum adsorption capacity predicted by the Langmuir isotherm model was 28.58 and 27.85 μg/g for As(V) and As (III), respectively.

Up to date, limited studies exist on biochar produced from the by-products of biological processes for As removal from water. For instance, the high surface area and positively charged surface functional groups have been observed in anaerobically digested sugar beet tailing based biochar. Such biochar types are supposed to be more suitable for anionic contaminant reclamation (Yao et al., 2011). Moreover, the existence of large amount of nano-sized MgO on the biochar surface provides a strong binding ability to remove negatively charged contaminants in an aqueous solution (Yao et al., 2011). The mechanism of As(V) and As(III) immobilization on biochar are not fully understood due to heterogeneous nature of biochar surface with various types of functional groups; however, a small number of studies have proposed some mechanisms including ion exchange (Begum et al., 2016) and co-precipitation (Liu et al., 2014). Therefore, the immobilization mechanisms of different As species on the biochar surface need to be addressed by future research.

5.4. Enhancing arsenic removal by engineered biochar

Engineered biochar has been recognized as a viable option to enhance the effectiveness of As removal from water and soil systems (Rajapaksha et al., 2016). Modification of biochar via chemical and physical methods has endeavored to improve the surface area and surface functional groups of biochar, thereby enhancing its sorption capacity (Zhou et al., 2013). Physical modification of biochar, conducted through purging steam, N_2, CO_2, or Ar, provides a smooth

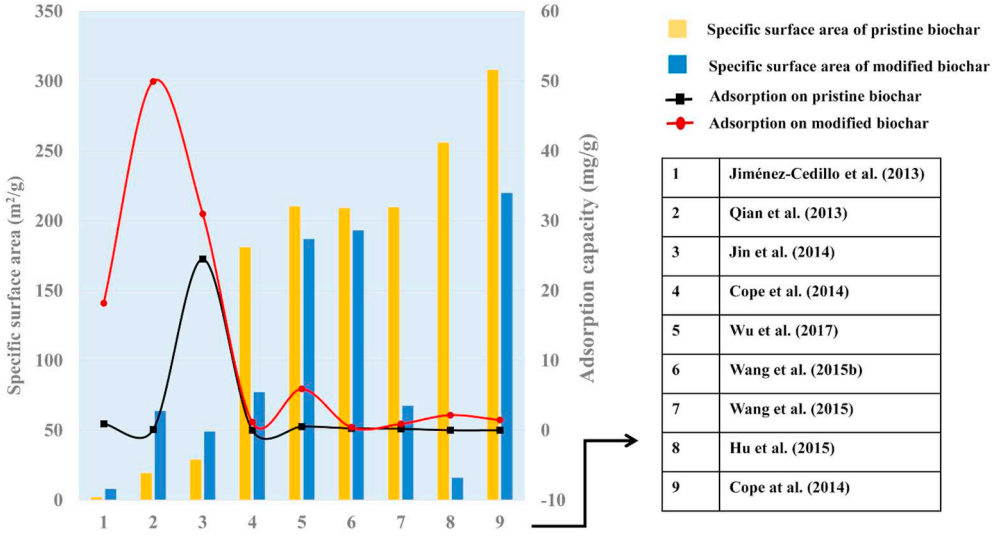

Fig. 5. The effect of biochar modification on its specific surface area and As(V) sorption capacity.

biochar surface along with high surface area and uniform pore distribution (Mohan et al., 2014). Chemical activation is performed either prior to or during combustion through the addition of some chemicals such as mild acids, alkaline solutions, organic solvents, and other chemicals such as NaOH, $Ca(OH)_2$, Fe salts, or Fe oxide minerals depending on the type of contaminant and its application (Niazi et al., 2016). Activation of the biochar surface by acidic solutions plays an important role in removing metallic residues and impurities from the biochar surface, while alkaline solutions remove ashes from the surface leading to higher surface area and pore volume (Liou and Wu, 2009; Rajapaksha et al., 2016). Chemical and physical methods can be used either separately or combined together to improve the capability of biochar to remove contaminants from water. Fig. 5 shows the effect of biochar modification on the specific surface area and the sorption capacity of the biochar before and after modification. Cho et al. (2013) reported that the surface area of marine macro-algae-derived biochar can be increased up to 57.9 and 1287 m^2/g after physical (steam activation) and chemical activation (with KOH solution), respectively. Several studies reported that chemical modification of biochar, specifically impregnation with chemical elements results in a decrease in the surface area due to clogging the pores of the biochar surface. However, such alteration can increase the adsorption capacity due to surface chemistry alteration (Cope et al., 2014; Hu et al., 2015; Wang et al., 2015a).

For As removal from water, the activation of municipal waste sludge biochar using 2 M of KOH solution increased the adsorption capacity for As(V) nearly 1.3-fold higher than that of unmodified biochar (Jin et al., 2014). Such an efficient removal of As(V) is attributed to the enhancement of surface area and porous texture of the biochar after the modification with KOH. The modification resulted in a replacement in the functional groups and an increase in the positive surface charge of the biochar, which resulted in a higher affinity of As(V) species to the biochar surface (Jin et al., 2014). Compared to acid-wash, alkali-modification increases surface aromaticity increasing C/H ratio while decreasing O/C ratio (Ahmed et al., 2016b). Thus, the higher aromaticity of the base-leaching derived biochar and its high carbon content prompt the alkaline agent crosslinking to the biochar surface (Ma et al., 2014).

Chemical modification of biochar surface is an effective strategy for enhancing the sorption capacity. Chemical substances that are newly introduced to the biochar surface provide a great affinity for contaminants to form surface complexes through strong inter-molecular interactions (Rajapaksha et al., 2016). However, the disadvantages of some chemical activation methods include the use of corrosive activating agents, such as strong acids and bases, and the need for washing after the chemical treatment (Rashidi and Yusup, 2016). In order to treat As contaminated water, chemically engineered biochar can effectively be used for such purposes. However, compared to the chemical modification methods adopted for the removal of inorganic contaminants in recent studies, application of biochar for the removal of As(III) (Jiménez-Cedillo et al., 2013; Lin et al., 2017; Van Vinh et al., 2015) and As(V) (Cho et al., 2017; Hu et al., 2015; Qian et al., 2013; Wang et al., 2015a; Zhang and Gao, 2013) species is very limited and mostly focuses on the removal of As(V) rather than As(III).

5.4.1. *Biochar coating with metals and/nano-sized metals*

Biochar coating with metal oxides, carbon nanotubes or graphene was recently adopted to improve biochar properties for selective removal of contaminants such as pharmaceuticals and heavy metals (Rajapaksha et al., 2016). However, the only coating method found in the literature for improving As removal is the coating of metal oxides with different particle sizes (ranging from micro to nano scale). Modification of biochar using nanoparticles has been reported as a promising method for improving sorption capacity of biochar for water and soil remediation due to the special physical and chemical properties of added nanomaterials including their particle size, surface area, chemical properties, photo-electronic and photocatalytic properties (Liu et al., 2011). Metal-containing nanoparticles, carbonaceous nanomaterials, zeolites and dendrimers are able to enhance sorption capacities for water treatment purposes (Savage and Diallo, 2005). Zhang and Gao (2013) stated that modification of biochar with nanoparticles increases the sorption capacity for different contaminants such as heavy metals, metalloids, PO_4^{3-}, NO_3^- and organic compounds.

Impregnation of $Zn(NO_3)_2$ on pine cone biochar increased the surface charge thereby improving As(III) removal through electrostatic interactions (Van Vinh et al., 2015). This Zn-loaded biochar showed a higher removal capacity for As(III) at pH 2–4, at which As(III) is dominant as neutral H_3AsO_3 and $H_2AsO_3^-$. Similarly, rice, soybean, and peanut straw biochar coated with Al(III) showed an increased sorption capacity for the removal of As(V) due to shifting zeta potential-pH curves to a positive direction under acidic conditions (Qian et al., 2013). The Al(III) modification on aforementioned biochar significantly increased the sorption of As(V) compared to the unmodified biochar (Table 2). Zhang and Gao (2013) developed a composite material from biochar and AlOOH nanoparticles to improve the As(V) sorption capacity in aqueous media. This study reported that the biochar-AlOOH composite can be used as an effective material for As(V) removal from polluted water although it takes quite a long time (12h) to reach the

Table 2
The effect of surface modification of biochar to remove arsenic from water.

Biochar	As(III) removal mg/g	As(V) removal mg/g	pH	Initial concentration mg/L	Charring temperature °C	Surface area m^2/g	Pore volume cm^3/g	Author
Soybean straw (SSB)	_	Negligible	5	22.5–89.9	350	1 ± 0.2	_	Qian et al. (2013)
Peanut straw (PSB)						2.1 ± 0.5		
Rice straw (RSB)						19.3 ± 1.1		
0.3M-Al/SSB		33.32				72.7 ± 2.7		
0.6M-Al/SSB		48.37				89 ± 3.5		
0.6M-Al/PSB		48.37				39.9 ± 1.5		
0.6M-Al/RSB		49.95				63.9 ± 2.7		
Biochar/AlOOH nanocomposite	_	17.41	_	50	600	_	_	Zhang and Gao (2013)
Pine cone biochar (PC)	0.0057	_	4	_	500	6.598	0.016	Van Vinh et al. (2015)
Zn-loaded PC	0.007		4			11.543	0.028	
Mn oxide/Pine biochar	_	0.59	7	1.0–20	600	463.1	0.022	Wang et al. (2015a)
Birnessite/Pine biochar		0.91				67.7	0.066	
Unmodified pine biochar		0.2				209.6	0.003	
Amorphous Mn/Grape stalk biochar	_	34.1[a]	7.0	74.922	600	44	_	Trakal et al. (2018)
Corn stem biochar	2.89		3	0.2–50	620	60.9		Lin et al. (2017)
Fe-Mn/Corn biochar	8.25					208.8		
Pinewood biochar with Ni/Mn oxides	_	0.549	_	0–20	600	125		Wang et al. (2016)
Ni/Mn-layered double Hydroxides/Pinewood biochar	_	6.25	_	0–40		282.8		
Wheat straw biochar	Negligible	_	9.3	5–200	500	124.44		Zhu et al. (2016)
Bismuth/wheat straw	16.2					190.4		
Empty fruit bunch biochar (EFBB)	18.9	5.5	For As(III) at pH 8–9, For As(V) at pH 6	3–300	_	1.89	_	Samsuri et al. (2013)
Rice husk biochar (RH)	19.3	7.1				25.161		
Fe/EFBB	31.4	15.2						
Fe/RH	30.7	16.9						
Oedogonium/Fe biochar	_	80.7	_	0.0075–749.22	300	_	_	Johansson et al. (2016)
Gracilaria/Fe biochar	_	62.5						
Petroselinum crispum/Fe^{3+}	0.06	0.19	6.5	0.05–2	500	1.13	0.006	Jiménez-Cedillo et al. (2013)
Petroselinum crispum biochar/Fe^{3+}	0.31	18.17				8.05	0.008	
Rise husk (RHC)	_	Negligible	4	0–2.5	550	181	_	Cope et al. (2014)
Fe/RHC		1.15 ± 0.1				77.3		
RHC		Negligible			950	308		
Fe/RHC		1.46 ± 0.11				220		
11.4% Rice husk-Ca^{2+}	_	> 0.095	10.8	8	300	_	_	Agrafioti et al. (2014b)
11.41% Rice husk-Fe^0		0.029	7.4					
11.4% Rice husk-Fe^{3+}		> 0.76	2.4					
11.4% Solid waste-Fe^0		> 0.063	10.9					
11.4% Solid waste-Fe^{3+}		> 0.38	2.8					
2.3% Rice husk-Fe^0		0.025	7					
2.3% Rice husk-Fe^{3+}		0.036	6.8					
2.3% Solid waste-Fe^0		> 0.063	10.4					
2.3% Solid waste-Fe^{3+}		> 0.063	9					
Hickory chips biochar	_	Negligible			600	256	_	Hu et al. (2015)
Fe-impregnated biochar		2.16	5.8	0–55		16		
Pinewood biochar	_	0.265	7	1–50	600	209.6	_	Wang et al. (2015b)
Hematite biochar (HPB)		0.429				193.1		
Rice straw biochar	0.448	0.522	As(V) at pH 6 As(III) at pH 10	1–50	600	210.29	_	Wu et al. (2017)
Rice straw/Red mud	0.52	5.923				186.95		
Water hyacinth biochar-Fe^{2+}/Fe^{3+}		7.41	5.3	2–105	250	69		Zhang et al. (2016)
Magnetic biochar with colloidal ϒ-Fe_2O_3	_	3.147	_	0–200	700	_	_	Zhang et al. (2013)
Kans grass straw biochar-Fe^{3+}/Fe^{2+}	2	3.1	13.5	0.4–0.8	500	31.45	0.177	Baig et al. (2014)
Rice straw biochar	_	3.681	4	0.2–50	450	_	_	Liu et al. (2017)
Magnetic biochar		10.6	3			_	_	
Chitosan magnetic biochar		17.88	5			_	_	
Chestnut shell biochar	_	17.5	4	0.2–50	500	_	_	Zhou et al. (2017)
Magnetic gelatin/Chestnut shell biochar	_	45.5				_	_	
Municipal waste sludge biochar	_	24.49		5–400	500	29.1	0.039	Jin et al. (2014)
KOH/Municipal waste sludge	_	30.98				49.1	0.357	
Hydrogel/Rice husk biochar	_	28.32	6	1–150	_	_	_	Sanyang et al. (2016)
Rice husk biochar		_						
$FeCl_3$/Coffee ground under CO_2	_	8.9	4.5	12.4–95	700	512	0.249	Cho et al. (2017)
$FeCl_3$/Coffee ground under N_2		13.1				8.3	0.018	

(*continued on next page*)

Table 2 (*continued*)

Biochar	As(III) removal mg/g	As(V) removal mg/g	pH	Initial concentration mg/L	Charring temperature °C	Surface area m^2/g	Pore volume cm^3/g	Author
Granular and activated sludge biochar	Negligible	Negligible	_	50	300	_	_	Zwetsloot et al. (2016)
$FeCl_3$/Granular sludge biochar	6.1	11.5			500			
ZVI/Red oak biochar	15.58 (Total As)		7–7.5	0–25	900	_	_	Bakshi et al. (2018)
ZVI/Switchgrass biochar	7.92 (Total As)							

[a] Data calculated from the information reported in the article.

equilibrium adsorption.

Table 2 summarizes the efficiency of engineered biochar over unmodified biochar for the removal of As from aqueous solutions. Hydrous manganese oxides and birnessite have the ability to immobilize soluble As(V) due to different mechanisms including adsorption, surface complexion or precipitation (Trakal et al., 2018). Wang et al. (2015a) studied the kinetics and sorption capacity of As(V) sorption onto unmodified pine wood biochar (PB) and modified PB with $MnCl_2.4H_2O$ (MPB) and birnessite (BPB). The sorption capacity of BPB for As(V) was 0.59 mg/g, which is significantly higher than that of PB (0.20 mg/g), and the highest sorption capacity of BPB is due to strong redox interaction with birnessite particles. The surface structure of the biochar used for As removal is of a great deal in the effectiveness of the composite in removing the targeted contaminants. Following the same procedure to produce a biochar birnessite composite, Trakal et al. (2018) reported a higher removal capacity (3.42 mg/g) for As(V) using grape stalks as a feedstock. Modifying the same biochar using amorphous manganese (AMO) had resulted in a greater removal of As(V) from solution. Compared to the limited ability of the unmodified biochar, the removal capacity was increased from 64 to 91% (about 34.1 mg/g) after increasing the AMO ratio coated on the char. This was explained by the higher CEC of the composite compared to the unmodified biochar (Trakal et al., 2018). A higher adsorption capacity (8.25 mg/g) for As(III) resulted from the impregnation of Mn and Fe oxides onto corn stem biochar (Lin et al., 2017). Higher removal capacity of the ferromanganese oxide is due to enhanced specific surface area (208 m^2/g) compared to that of unmodified biochar (61 m^2/g), thereby providing a large surface area to promote the oxidation of As (III) to As(V). In the removal mechanism, Mn(III) oxides promote mainly the oxidation of As(III) to As(V), while Fe oxides act as sorption sites for As(V) to be adsorbed onto the biochar surface (Fig. 6). Therefore, it is clear that the Fe-Mn oxides incorporated with biochar play an important role in strengthening the adsorption capacity of corn steam biochar.

Moreover, Wang et al. (2016) synthesized two biochar composites through pyrolysis of pinewood biochar with Ni/Mn oxides (NMMF) as well as precipitation of Ni/Mn-layered double hydroxides (LDHs) onto the pinewood biochar (NMMB) using $MnCl_2.4H_2O$ and $Ni(NO_3)_2.6H_2O$. The removal efficiency of NMMB and NMMF at 12 mg/L of As(V) solution was 98 and 10.6%, respectively and hence, the maximum As(V) sorption capacity of NMMF and NMMB (0.549 g/kg and 6.520 g/kg, respectively) was improved compared to the unmodified biochar. The most significant mechanisms which govern the removal of As(V) by both modified adsorbents were found to be electrostatic interactions and surface complexation with hydroxyl (-OH) at pH 8 (Wang et al., 2016). Fig. 7 illustrates the potential mechanisms which trigger the immobilization of As on a modified biochar surface. Since the pH_{PZC} for both NMMB and NMMF was higher than solution pH 8, the surface of biochar becomes positively charged which facilitates strong electrostatic forces between As(V) and the surface (Fig. 7). On the other hand, $HAsO_4^{2-}$ is capable of complexing with −OH groups that are present on the LDHs and thereby exchanging other negatively charged ions such as Cl^- and NO_3^-, which provides a greater stability for As(V) removal from water.

The As(III) was effectively removed from water using wheat straw biochar impregnated with bismuth (by sonication) at pyrolytic temperatures of 400, 500 and 600 °C (Zhu et al., 2016). The highest As(III) removal capacity of bismuth activated biochar produced at 500 °C was achieved at pH 9.3. At this level, the surface of modified biochar gets protonated while promoting a Lewis acid-base reaction between the active adsorption site and the neutral H_3AsO_3. Similarly, a column packed with a composite of wheat straw biochar and periphyton was able to remove a maximum of 95.4% of As(III) at initial concentration

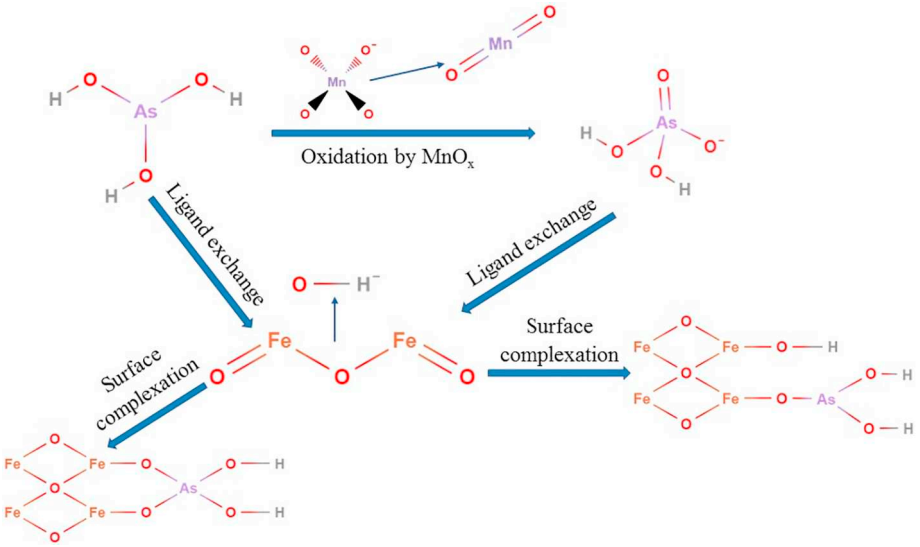

Fig. 6. The Mechanism of As removal in the presence of Fe and Mn oxides.

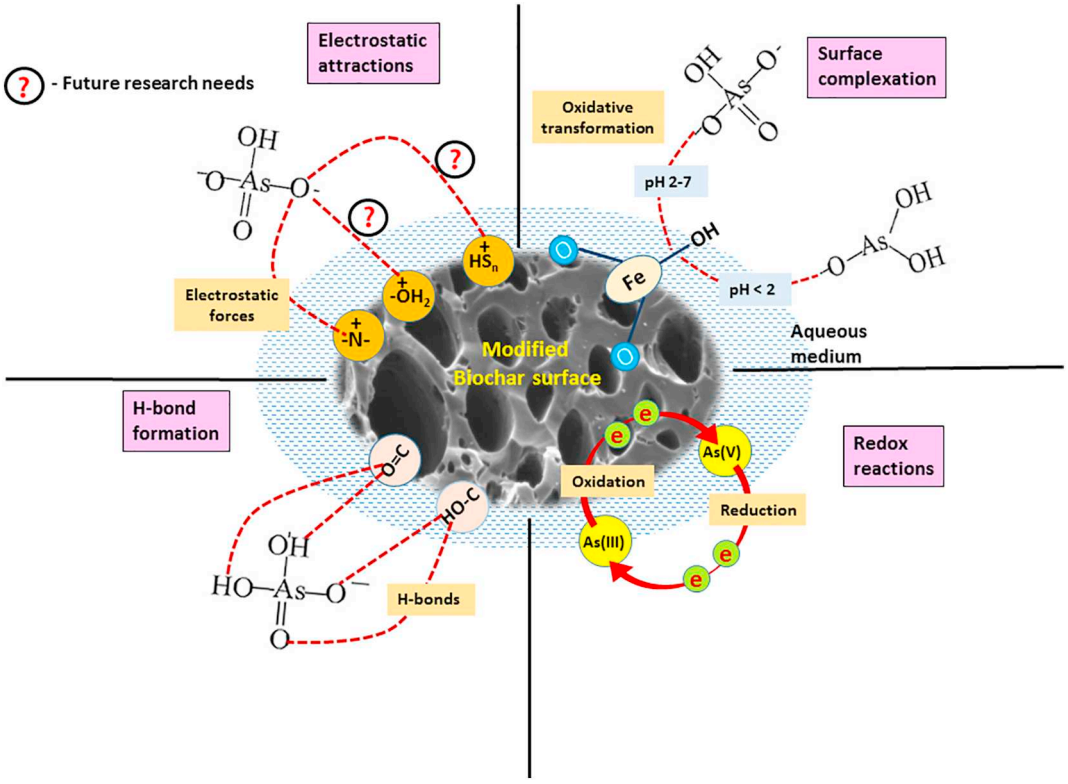

Fig. 7. Graphical representation of potential mechanisms for the immobilization of As on modified biochar surface.

of 2 mg/L and flow rate of 1 mL/min (Zhu et al., 2017). The mechanisms which trigger the immobilization of geogenic As species in the presence of Fe oxides under natural conditions have also been recently discussed (Herath et al., 2016b). Naturally occurring Fe oxides, particularly ferrihydrite ($Fe_2O_3{\cdot}2H_2O$) tend to immobilize the mobile species of As through a ligand exchange mechanism with HO_2^- and OH^- in the coordination spheres of the surface structural Fe atoms (Fig. 4). The existing knowledge regarding these mechanisms has been recently applied in producing modified biochar materials for the remediation of water. For example, nano-zero valent iron [(Fe(0)] incorporated into biochar can enhance the immobilization of As(V) species in water through strong chemisorption interactions produced from an oxidation and reduction reaction on the biochar surface (Fig. 7). During the oxidation of Fe(0), As(V) gets partially reduced to As(III) which possesses a high affinity to be adsorbed on the hydrous ferric oxides (HFO) formed on the biochar surface during the oxidation of Fe(0). Moreover, magnetic biochar has been investigated as a promising adsorbent for As removal, since the presence of Fe oxides as magnetite on the biochar surface provides more favorable adsorptive sites increasing the removal efficiency (Rajapaksha et al., 2016; Zhang et al., 2013; Zhu et al., 2016). Similarly, Samsuri et al. (2013) investigated the effect of Fe coating on the removal of As(III) and As(V) using empty fruit bunch biochar (EFBB) and a rice husk biochar (RHB). Regardless of the higher surface area of the RHB, both EFBB and RHB showed almost similar adsorption efficiencies for As(III) from water. Thus, the total amount of oxygen-containing functional groups, the lower zeta potentials (−24 mV for EFBB at pH 4; and −14.3 mV for RHB at pH 6), O/C ratio (0.61 and 0.37 for EFBB and RHB, respectively), and polarity indices (O + N)/C (0.64 and 0.38 for EFBB and RHB, respectively) were considered as important factors in determining the removal efficiency of As (III) on biochar.

Studies have been carried out on the effects of biochar produced from macroalgae wastes such as *Gracilaria* and *Oedogonium* that were treated with Fe as a mean of removing As from mining effluents (Johansson et al., 2016). A higher removal capacity was observed after pre-treating the *Gracilaria* waste and *Oedogonium* algae with Fe^{3+} during fast pyrolysis. The Fe-biochar derived from *Oedogonium* had a higher adsorption capacity (80.7 mg/g) than that of biochar produced from *Gracilaria* waste (62.5 mg/g) for As removal from mining effluents. Jiménez-Cedillo et al. (2013) applied biochar produced from *Petroselinum crispum* which was modified with iron particles in removing As(III) and As(V) from an aqueous solution. The biomass (non-pyrolyzed) modified with Fe^{3+} was ineffective (0.007%) in removing both As species in the solution, whereas the maximum adsorption capacity of modified biochar for As(III) and As(V) was a 5- and 95-fold increase, respectively compared to that of Fe^{3+} modified non-pyrolyzed biomass at pH 6.5. With regard to the immobilization of As(III), at pH 6.5, As(III) is dominantly present in the form of H_3AsO_3, which is more reactive with the $FeOH_2^+$ on the Fe^{3+} modified biochar than the FeO- group available on the surface of Fe^{3+} modified non-pyrolyzed biomass due to their respective pH_{PZC} values of 9.73 and 4.43. Similarly, high removal efficiency of As(V) by Fe^{3+} modified biochar at pH 6.5 is attributed to strong electrostatic forces between positively charged $FeOH_2^+$ present on the modified biochar surface (pH_{PZC} = 9.73) and anionic As species including $H_2AsO_4^-$ and $HAsO_4^{2-}$ (Jiménez-Cedillo et al., 2013). In addition, the surface area of Fe^{3+} modified biochar was nearly 4-fold higher than that of unmodified biochar (2.02 m^2/g) which further facilitated the removal of As species from the aqueous solution. Investigations have shown that a combined modification of rice husk and municipal solid wastes biochar impregnated with CaO, Fe^0 and Fe^{3+} can improve the removal of As(V) from water (Agrafioti et al., 2014b). Modification of biochar with Ca^{2+} and Fe^{3+} removed 95% of As(V), whereas the rice husk biochar impregnated with zero valent iron (ZVI) was able to remove only 58% of As(V) from aqueous solutions. Precipitation and electrostatic interactions are likely to be the mechanisms which trigger the removal of As(V) from aqueous solutions. However, the modification of biochar can cause a reduction of the surface area, while increasing the sorption capacity of As because of an increased O/C ratio after the modification (Hu et al., 2015). The pyrolysis of pine wood biochar in the presence of natural hematite mineral

and the formation of magnetic hematite-biochar have a great effect on the biochar ability to remove As(V) from an aqueous solution due to the presence of γ-Fe_2O_3 particles on the biochar surface, which provides sorption sites for As to be adsorbed on the surface (Wang et al., 2015b). The mechanisms of As adsorption by this type of modified biochar can be explained by the same reaction pathway shown in Fig. 4. Magnetic biochar derived from invasive water hyacinth biomass chemically modified through co-precipitation of Fe^{2+}/Fe^{3+} followed by pyrolysis at 250 °C demonstrated high potential to remove aqueous As(V) (Zhang et al., 2016). This modified biochar resulted in a 90% removal of As(V) at a wide range of pH (3 − 10) along with a sorption capacity of 7.41 mg/g which is higher than the results previously reported by Zhang et al. (2013). Ligand exchange and hydrogen bond formation were recognized as the mechanisms which are responsible for the adsorption of As(V) on magnetic biochar (Fig. 7).

5.4.2. Biochar modification using polymers/biopolymers

Crosslinked polymeric and biopolymeric materials including, poly (acrylamide) and *N*,*N*′-methylenebisacrylamide have been successfully used to boost the As sorption ability of biochar (Barakat and Sahiner, 2008; Sanyang et al., 2016). Hydrogels possess a high affinity to interact with negatively charged As species due to the protonation ability of hydrophilic surface functional groups such as −OH, −COOH, $-NH_2$, $-CONH_2$, and $-SO_3H$ that are present in the hydrogel molecules (Ozay et al., 2009; Sanyang et al., 2014). Hydrogel prepared from poly(3-acrylamidopropyl) trimethylammonium chloride was capable of removing 99.7% of As(V) at 1.5 g/L of hydrogel and pH 9 for 50 mg/L of As(V) aqueous solution (Barakat and Sahiner, 2008). In a similar study, a hydrogel-biochar composite prepared by embedding rice husk biochar into poly(acrylamide) hydrogel with *N*,*N*′-methylenebisacrylamide was able to remove a maximum of 94.85% of As(V) with a sorption capacity of 28.32 mg/g (Sanyang et al., 2016).

Biochar-chitosan composites are also utilized as a natural, low-cost, abundantly-available, non-toxic pre-cursor material (chitin) for the removal of heavy metals and metalloids from aqueous solutions (Gerente et al., 2007; Zhou et al., 2013). Such modified biochar composites take advantage of its surface modification via amine (-NH_2) functional groups and well-developed porous structure. In a recent study, a magnetic chitosan-biochar composite (Fe^{2+}/Fe^{3+} molar ratio of 2:3) was able to remove 90% of As(V) from aqueous solution at pH 5 resulting in a sorption capacity of 11.96 mg/g which was nearly 4-fold higher than that of its unmodified biochar (3.68 mg/g) (Liu et al., 2017). At pH 5, the $-NH_2$ group present on chitosan tends to be protonated into H_2N^+ as the solution pH is lower than the pH_{PZC} (5.25) and hence the positively charged biochar surface gets strongly attracted by negatively charged $H_2AsO_4^-$ or $HAsO_4^{2-}$ through electrostatic forces. This composite has been recognized as a superior adsorbent for As(V) removal from water due to its higher removal capacity compared to all other magnetic biochar types tested in previous studies (Baig et al., 2014; Zhang et al., 2016; Zhang et al., 2013). Furthermore, the As(III) adsorption mechanism on biochar modified with $-NH_2$ groups can be explained by a type of Bechamp reaction due to the presence of aromatic $-NH_2$ (similar to aniline) in the biochar composite structure (Fig. 8). In this reaction pathway, aromatic rings bearing with -NH_2 groups can react with arsenic acids (As(III)) followed by an electrophilic aromatic substitution to produce arsanilic acid which is a strong chemisorption interaction.

5.5. Summary of arsenic removal mechanisms on modified biochar

It is obvious that the capacity of unmodified biochar to remove oxyanion pollutants including As is relatively low due to their negative surface charge and poor anion exchange capacity. Therefore, the surface of biochar needs to be transformed to gain a high adsorption capacity for the removal of negatively charged As species. In order to achieve this, the reactivity of As with ions or oxides of metals such as Al, Mn, Ca, Fe, Mg, etc. are widely used to increase the positive charge and ligand-binding density of biochar, thereby enhancing its removal capacity. Surface modification by hydrous iron oxide (Fe−O) and manganese oxide (Mn−O), Mg−Al and Fe−Al type layered double hydroxides and activated magnesium oxide (Mg−O) attributed to increase the adsorption capacity for the removal of As from water as discussed in the previous section. Surface complexation, electrostatic interactions, ion exchange, chemical reduction and oxidation (redox reactions), and precipitation are the principal mechanisms which trigger the removal of As by modified biochar from aqueous solutions (Fig. 7) (Tan et al., 2016).

Carbothermal alteration of biomass into metal-biochar composites results in a change in surface zeta potential as well as promotes a porous carbon structure, thereby improving the chemical composition for more active sorption sites of biochar surface (Li et al., 2018). Inorganic As species, including AsO_3^{3-} and AsO_4^{3-} can undergo redox reactions in the presence of strong oxidizing (O_2, H_2O_2, MnO_4^-, CrO_3, etc.) and reducing agents (Fe, Al, Zn, Mn, Mg, etc.) on the biochar surface resulting in strong chemisorption interactions between As and biochar surface. For example, the removal of As(V) species is predominantly governed by chemical reduction on the biochar surface modified with zero valent iron (Fe^0) (Wang et al., 2017) and FeOOH (Hu et al., 2015). In the natural environment, microbes play a vital role in the control of oxidation and reduction reactions of As and hence, the inoculation of bacteria into such modified biochar would be highly efficient in the remediation of As contaminated water. Apart from redox reactions, the adsorption of As(III) by a ZnO loaded biochar is likely to be due to ligand exchange at Zn-OH producing a new As-O-Zn complex on the biochar surface (Van Vinh et al., 2015). Furthermore, in MnO_x-biochar composites, the adsorption of As(V) is mainly through surface complexation and ligand exchange with Mn−O and Mn−OH (Liu et al., 2016). Depending on the pH of the medium, some functional groups present on biochar surface, particularly ammine (−NH), alcoholic (−OH) and carboxyl (−COOH) groups, become protonated making the biochar surface more positively charged which promotes strong electrostatic interactions with negatively charged As species (Fig. 7). On the other hand, sulfur is a strong electrophile and thus the modification of biochar surface via thiol groups to produce sulfur-biochar composites will be of particular interest in future research for the removal of As from contaminated water. However, molecular level studies based on X-ray absorption synchrotron techniques such as extended X-ray absorption fine structure (EXAFS) and X-ray absorption near edge structure (XANES) are an urgent necessity to confirm the formation, and stability such chemical bonds between the As and biochar surface.

6. Influence of co-existing solutes on arsenic removal by biochar and bone char

Natural water resources contain various inorganic and mineral ions such as F^-, Cl^-, PO_4^{3-}, NO_3, HCO_3^- and SbO_4^{3-} due to naturally occurring geochemical processes as well as anthropogenic sources (Guo et al., 2018; Herath et al., 2017). Therefore, the knowledge on the existing competing anions present in natural water systems such as mining water, geothermal fluids and surface/groundwater is very important in order to design water treatment schemes for the removal of As species from such water bodies. Table 4 summarizes the effect of the existence of some oxyanions on bone char and biochar efficiency to remove As species. The complication in water treatment methods is mainly associated with the existence of other competing metal/metalloid species and inorganic ions, since such competing ions tend to impede the removal efficiency of As species on the adsorbent surface by competitively binding on the active sites (Mack et al., 2007). The effect of F^- on simultaneous removal of As(III) and As(V) by cattle bone char (with specific surface area of 99.2 m^2/g) was investigated (Mlilo et al., 2009). This study showed that the maximum sorption capacity of As(III) and As(V) was 0.022 and 0.065 mg/g, respectively in the absence of F^-,

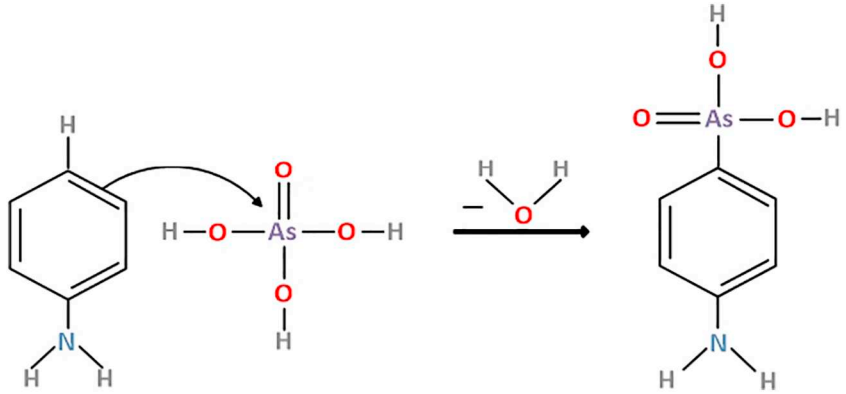

Fig. 8. The potential As adsorption mechanism by $-NH_2$ modified biochar composites (adapted from Gibaud and Jaouen, 2010).

whereas in the presence of F^-, the sorption capacity decreased up to 0.015 and 0.024 mg/g, respectively. In a similar study, the presence of 10 mg/L of F^- affected the removal of As(V) on fish bone char which was about 0.06 mg/g, as predicted by the Langmuir isotherm. In contrast to these findings, a previous study reported that fish bone char is capable of removing F^- and As(V) simultaneously with minimal competition in the water sample (Brunson and Sabatini, 2009).

Coexisting ions, including Al^{3+} and Mn^{2+} were found to enhance the sorption capacity of bone char surface due to the formation of amorphous Al and Mn coating on the bone char surface, while the presence of SO_4^{2-}, PO_4^{3-}, and SiO_3^{2-} oxyanions showed negative impacts on the immobilization of As(V) sorption on bone char because of strong competition with AsO_4^{3-} for the available sorption sites on bone char surface (Liu et al., 2014). These findings are corroborated by a previous study which showed that the negative effect of coexisting oxyanions (concentration range of 0.5–20 mg/L) in the removal of As(V) by cellulose-carbonated HAP nanocomposites decreases in the order of $SiO_3^{2-} > PO_4^{3-} > NO_3^- > SO_4^{2-}$ (Islam et al., 2011). The presence of 1 mg/L of PO_4^{3-} has a similar competition effect as 10 mg/L of $SSiO_3^{2-}$ in reducing the adsorption of As(V) onto rice husk biochar (Cope et al., 2014). It has been reported that the PO_4^{3-} has a great effect on the reduction of As adsorption on magnetic Kans grass biochar where the removal efficiency of this biochar for As(III) and As(V) was decreased by 20 and 80%, respectively at 1.0 mmol/L of PO_4^{3-} concentration (Baig et al., 2014). Similarly, the increase in the ionic strength of PO_4^{3-} from 1 mmol/L to 100 mmol/L resulted in decreasing the removal efficiency of As(III) onto Fe—Mn oxide impregnated with corn stem biochar by 22% (Lin et al., 2017). Therefore, it is clear that the PO_4^{3-} is the most competitive oxyanion to As(V) ions followed by SiO_3^{2-} and SO_4^{2-}, since the HPO_4^{2-} species can form almost similar surface complexes to the $HAsO_4^{2-}$ ion (Hu et al., 2015). The higher reduction capacity for the As (V) removal in the presence of SiO_3^{2-} and PO_4^{3-} may be attributed to their relatively large ionic radii as well as the degree of the anionic charge which are considered to be main factors for determining the effect of coexisting anions in adsorption processes. Moreover, the pH of solution plays a vital role and the immobilization of As species on bone char would be preferable at neutral or alkaline pH levels since there will be a higher release of PO_4^{3-} anions in acidic conditions.

Furthermore, Soltani et al. (2017) examined the effect of some inorganic and organic compounds present in aqueous solutions on the removal As(V) by Fe_3O_4-bone char nanocomposite. This nanocomposite removed 96% of As(V) from the solution compared to the control, whereas the removal efficiency of As(V) decreased up to 25, 34, 38 and 23% in the presence of PO_4^{3-}, SO_4^{2-}, NO_3^- and humic acid, respectively. Natural water systems such as ground-surface-water, geothermal water, and mining water may be contaminated with oxyanions of antimony (Sb) particularly antimonates [$Sb(OH)_5$, SbO_3^-] which are likely to coexist with As in the natural environment (Herath et al., 2017). On the other hand, these species possess similar toxicological effects as As in environmental and biological compartments. To our knowledge, there is no information available on the application of biochar and bone char in simultaneous removal of As in the presence of such chemically and structurally equivalent oxyanions. Therefore, future research should be more inclined towards expanding the use of adsorption technology using biochar and bone char in order to develop water treatment facilities to remediate such multi-metal contaminated water systems which would pave the way for a sustainable As mitigation on a global scale.

7. Regeneration of biochar and bone char

Biochar regeneration is an important aspect that determines the economic benefits and environmental sustainability of biochar as a sorbent for the removal of As from water (Inyang and Dickenson, 2015). Several techniques such as the use of chemicals at different concentrations to displace adsorbed metals, controlling the pH of the solution, purging gas or fluid and changing the partial pressure are used for releasing the adsorbed contaminants from modified biochar (Ahmed et al., 2016b). Zhang et al. (2016) examined the reusability of a magnetic biochar for As(V) removal from water by using a 0.1 M HCl solution in which the removal capacity decreased from 100% to 80, 65.5 and 50.8% after four regeneration cycles, respectively. Similarly, a regeneration study of bone char-Fe_3O_4 nanocomposite using 0.1 M HCl solution revealed a reduction of < 20% within three repeated runs over 60 min at 1 g/L of adsorbent dosage, 100 μg/L of initial As(V) concentration (Soltani et al., 2017). Table 3 summarizes the results obtained from previous As desorption experiments for a better understanding of the extent of regeneration capability of biochar and bone char. It is convenient to remark that among all the solutions used for As (V) desorption experiments, regeneration of biochar samples is not applicable with acidic solutions or water. The higher desorption rate (up to 98%) was through using NaOH solution with different concentration. Using 0 .5M NaOH solution resulted in flushing out 68% of As(III) from magnetic Kans grass biochar but at very high pH level (13.5) (Baig et al., 2014). The high pH levels where the maximum desorption was achieved are not applicable for water treatment facilities. In addition, using 0.05 mol/L $NaHCO_3$ resulted in 85% As(V) removal from water at pH 8.5. With regards to As(III) desorption, further investigations need to be conducted as the only examination for As(III) desorption was reached at a very high pH value (Baig et al., 2014). The application of regenerated char as a sustainable waste management strategy in the remediation of water is an urgent necessity. The potential options for disposing the As loaded adsorbents are dumping in landfills, mixing with livestock waste and mixing with building construction materials (Sullivan et al., 2010). On the other hand, the disposal of the concentrated As solution after regeneration of the adsorbent can be overcome by reusing the solution in green industry. For instance, (Riveros et al., 2001) reported the suitability of using As waste after precipitating them with Fe(III) (to form insoluble ferric arsenate

Table 3
Desorption capability of regenerated biochar and bone char in aqueous media.

Biochar	Targeted As species	Used agent	pH	Desorption rate of adsorbed As (%)	Reference
Fe impregnated hickory biochar	As(V)	0.05 mol/L $NaHCO_3$	5.8	85	Hu et al. (2015)
Solid waste biochar	As(V)	Deionized water	–	4	Agrafioti et al. (2014a)
Sewage sludge biochar				10	
Rice husk biochar				0	
Magnetic chitosan/Biochar (after 5 cycles)	As(V)	1.0 mol/L NaOH	–	68	Liu et al. (2017)
NMMB	As(V)	0.1 M NaOH	–	81.7	Wang et al. (2016)
NMMF				75.0	
Fe coated rice husk biochar	As(V)	30% HCl	1.5	12.3	Pehlivan et al. (2013)
		1 M NaOH	14	90.6	
Bone char	As	Ultra-pure water	4	30	Liu et al. (2016)
Mn coated bone char				0.2–0.6	
ZVI/Pine biochar composite	As(V)	0.1 M NaOH	–	98.2	Wang et al. (2017)
Bone char	As(V)	Distilled water and 0.1 M NaOH	–	50–70	Liu et al. (2014)
Magnetic kans grass biochar	As(III)	0.5 M NaOH	13.5	68	Baig et al. (2014)
	As(V)			89	

Table 4
The effect of co-existing anions on the removal of As by biochar and bone char.

Anions	Concentration	Reduction in As(V) removal (%)	Reduction in As(III) removal (%)	Adsorbent	Reference
NO_3^-	0.5 mg/L	9	–	HAP (synthesized)	Islam et al. (2011)
	> 2 mg/L	The effect levelled off			
SiO_3^{2-}	0.5–10 mg/L	30	–		
	> 10 mg/L	40			
PO_3^{4-}	< 2 mg/L	12	–		
	0.5–20 mg/L	32			
SO_4^{2-}	At any concentration	No significant effect	–		
PO_4^{3-}	1.0 mM	20	70	Kans grass straw biochar-Fe^{3+}/Fe^{2+}	Baig et al. (2014)
Cl^-	1.0 mM	5	12		
HCO_3^-	1.0 mM	5	10		
PO_4^{3-}	1.0 mM	44	–	Fe_3O_4/Bone char in chitosan biopolymer	Soltani et al. (2017)
SO_4^{2-}	1.0 mM	35	–		
NO_3^-	1.0 mM	31	–		
Humic acid	1.0 mM	46			
PO_4^{3-}	1.0 M	23[a]	–	Chitosan magnetic biochar	Liu et al. (2017)
SO_4^{2-}	1.0 M	10[a]	–		
CO_3^{2-}	1.0 M	10[a]	–		
NO_3^-	1.0 M	8.2[a]	–		
Cl^-	1.0 M	8.2[a]	–		
PO_4^{2-}	5 mg/L	24		hickory chips biochar	Hu et al. (2015)
	50 mg/L	58			
SO_4^{2-}	5 mg/L	4			
PO_4^{3-}	1 mg/L	17.18[a]	–	Fe/RHC	Cope et al. (2014)
	10 mg/L	34.93[a]	–		
SiO_3^{2-}	10 mg/L	15.76[a]	–		
SO_4^{2-}	10 mg/L	4.79[a]	–		
F-	10 mg/L	63.1[a]	31.8	Bone char	Mlilo et al. (2009)

[a] Reduction in As removal due to competition of co-existing ions was calculated based on the following formula: $Reduction\ (\%) = \frac{Removal\ without\ competing\ ions - Reduction\ with\ competing\ ions}{Removal\ without\ competing\ ions}$.

compounds) which can be used in metallurgical industry.

8. Cost effectiveness

The amount of the timber and agricultural organic wastes produced in Australia in the financial year 2016–2017 was about 2.1 Mt and 16.1 Mt, respectively (Bagasse, cotton gin trash and manures) (Pickin et al., 2018). In 2018 (until September 2018), the red meat production in Australia was 2,608,866 metric tons (Australian Bureau of Statistics, 2018), generating over 313,064 t of bones as a waste by-products to be disposed in the landfills. Only 1.97 Mt (million tons) out of 67 Mt total waste produced has been used as an energy source (90% were by capturing methane from landfills). The high cost spent for the treatment of waste can be avoided by developing suitable thermal treatment plants for biofuel production and char produced as a waste product can be used for environmental remediation processes. For instance, the Australian government invests about US$ 60.000 per year on handling cotton industry residues which can be used as a source of energy and biochar for environmental remediation via thermal treatment (Hamawand et al., 2016). Extensive studies inspected the energy balance and the annual revenue of biochar production confirming a positive energy balance for the biochar production using cotton gin trash (Coates, 2000), oil palm empty fruit bunches (Harsono et al., 2013), late stover, early stover, switch grass and yard waste (Zhang et al., 2019).

The cost of biochar/bone char production may vary depending on the production conditions such as energy consumption during the charring process, the cost of transportation, feedstock treatment and drying the precursor, equipment, maintenance and labor cost (Ahmed et al., 2016a). For instance, the net energy consumed in the production

of biochar using electricity is higher than those produced using diesel fuel (Harsono et al., 2013). Moreover the cost of biochar production through slow pyrolysis is lower than those produced via fast pyrolysis (Kung et al., 2014). Generally, in the case of feedstock from forests residues and food industry (such as nut shells, grains and fruits bunches), biochar has been reported as a source of positive energy (Zhang et al., 2019). In addition, the amount of the net energy production and GHG emission is related to the production process and the type of equipment used.

The literature available for the cost benefits and revenue from biochar market is mainly concentrated on the application of biochar as a soil amendment, whereas there is a lack of relevant information available for bone char market and production cost. In water treatment applications, biochar takes much attention as an alternative to activated carbon (AC) due to its environmental benefits in terms of waste management, mitigation of climate change, soil improvement, and energy co-generation (Lehmann and Joseph, 2015). The cost of biochar production was estimated to be US$ 246/ton versus US$ 1500/ton for AC (Inyang and Dickenson, 2015), while the cost of biochar production can vary from US$ 0.09/kg in Philippines to US$ 8.85/kg in United Kingdom (Tan et al., 2017). The cost of bone char production for As removal needs to be investigated as it is only reported for water defluoridation. The economic benefits represented by the use of low cost waste materials as a precursor, bioenergy production, and non-activation requirements during the production process (Ahmad et al., 2013; Zhang et al., 2015) justify the use of biochar as a promising alternative for AC. With regards to the economical validity of biochar, it has been reported that the estimated break-even price of biochar is 1/6 of commercially available AC (Zhang et al., 2015). Moreover, the regeneration of AC may be costly compared to that of biochar when it is used as a sorbent in wastewater treatment processes at a commercial scale (Ahmad et al., 2014; Gupta and Ali, 2012; Mohan et al., 2014).

9. Limitations of current research and what needs to be done in future

Environmental consequences of toxic As species present in water have been significant over the past decades. The relatively brief history of the application of adsorption technology using biochar and bone char has endeavored to implement the removal or immobilization of As from aqueous solutions to a considerable extent.

The high pH_{PZC} values of most of biochar types makes their surface more negatively charged, which promotes repulsive forces between the biochar surface and negatively charged As species. Because of that, selecting a suitable type of unmodified biochar for the removal of As from aqueous solutions is indeed a challenging task; this is the major problem to be overcome by future research for the remediation of As contaminated water. Although the engineered char performs well over unmodified char in the removal of As from water, drawbacks associated with the modification methods such as high cost, less regeneration capacity, and use of toxic chemicals are of particular concern. Furthermore, the stability of the modified char is of great concern to maintain the reagents used in the modification method and thereby minimizing environmental contamination (Trakal et al., 2018).

The utilization of different types of organic and biological waste materials which are available at large quantities in the environment for the production of biochar and bone char, will be a promising waste management strategy in the environment. Additionally, using these materials will facilitate the reduction of global warming and greenhouse gas emission from landfills. As the present review demonstrated, the existing research related to regeneration of used bone char and biochar are insufficient and therefore, the disposal of the As adsorbed chars is essentially taken into consideration in future research. Mechanistic understanding of biochar-As and bone char-As interactions has so far attached little research concern and hence there is a significant research gap in the interpretation and confirmation of potential mechanisms and types of chemical bonds which trigger the adsorption of As species onto the adsorbent surface. Synchrotron-based X-ray techniques, particularly EXAFS and XANES are essential in future research to understand the change in oxidation state of As species and certain types of chemical bonding between As and bio-bone-char surface. The removal efficiency of As by particular types of biochar or bone char is greatly decreased in the presence of chemically or structurally equivalent oxyanions, so that the application of this technology for the remediation of wastewater is still subject to debate. Moreover, research of the use of biochar and bone char is limited to laboratory scale experiments and hence, moving this technology from laboratory phase to field scale applications, needs to be undertaken by future research in order to establish a sustainable mitigation of toxic As species in drinking-surface-ground-and irrigated water systems. However, the application of these adsorbents on a commercial or industrial scale is limited due to several restriction issues raised in some countries. The main limitation for the use of bone char as an adsorbent for water treatment purpose is related to some cultural and religious beliefs. For instance, the use of bone char for fluoride removal from water were rejected in Ethiopia based on cultural and religious reasons (Osterwalder et al., 2014; Saxena and Patel, 2018). The effect of the charring temperature on the biochar production is a crucial factor in terms of environmental pollution due to the emission of other toxic particulate matter. Hamawand et al. (2016) reported that biochar produced at temperatures below 600 °C has the potential of releasing toxic elements and heavy metals to the environment (formaldehyde, arsenic and cadmium), and raising charring temperature to > 800 °C may lead to releasing more N_2 gas and providing more GHG to the environment (Hamawand et al., 2016).

10. Conclusions

Inorganic As is extremely toxic to living organisms due to high binding ability with protein-sulfydryl (SH) groups and the overproduction of cellular reactive oxygen species. Hence, the application of bio- and bone-char for As removal from water has been thoroughly scrutinized in this review with the aim of shedding light on recent achievements and pinpointing the gaps in this research area. The higher point of zero charge of most of the char types makes its surface more negatively charged, promoting repulsive forces between the surface and negatively charged As species. Hence, selecting a suitable char type for the removal of As has become a challenging task. The surface modification via chemical methods has been adopted to alter the surface charge and surface area to improve the adsorption capacity for anionic As species. Nano-sized manganese coated bone char increases the removal of As(V) by 78-fold compared to the non-modified bone char. The removal of As(V) by bone char produced at 500 °C was 2-fold higher than that which is produced at 900 °C. A magnetic chitosan-biochar composite removes 90% of As(V) from aqueous solution at pH 5 resulting in a sorption capacity of 11.96 mg/g which was 4-fold higher than that of its unmodified biochar. The main proposed mechanisms of As removal using bio- or bone- char are surface complexation, ion exchange, electrostatic interaction and co-precipitation. These mechanisms are governed by surface area, ion exchange capacity, surface functional groups and pH_{PZC}. In addition to the advantage of the char being a product of recycled waste, it has another attractive trait of being regenerative using acidic or alkaline wash. Overall the present review concludes that the engineered biochar can effectively remove As while unmodified bone derived char itself possessing a great adsorption capacity for As removal from aqueous solution. However, more research is essential in the future to fully understand the As-char interactions along with their bonding nature under various environmental conditions to develop more reliable and sustainable char types for water treatment applications on an industrial scale.

Acknowledgements

This research was supported in part by the Iraqi Government/ Ministry of Higher Education, Scientific Research and Australian Research Training Program and the fund of Postgraduate Research Scholarship of University of Southern Queensland, Australia.

References

Agrafioti, E., Kalderis, D., Diamadopoulos, E., 2014a. Arsenic and chromium removal from waterusing biochars derived from rice husk, organic solid wastes and sewage sludge. J. Environ. Manag. 133, 309–314.
Agrafioti, E., Kalderis, D., Diamadopoulos, E., 2014b. Ca and Fe modified biochars as adsorbents of arsenic and chromium in aqueous solutions. J. Environ. Manag. 146, 444–450.
Ahmad, M., Lee, S.S., Rajapaksha, A.U., Vithanage, M., Zhang, M., Cho, J.S., Lee, S.-E., Ok, Y.S., 2013. Trichloroethylene adsorption by pine needle biochars produced at various pyrolysis temperatures. Bioresour. Technol. 143, 615–622.
Ahmad, M., Rajapaksha, A.U., Lim, J.E., Zhang, M., Bolan, N., Mohan, D., Vithanage, M., Lee, S.S., Ok, Y.S., 2014. Biochar as a sorbent for contaminant management in soil and water: a review. Chemosphere 99, 19–33.
Ahmed, M.B., Zhou, J.L., Ngo, H.H., Guo, W., 2016a. Insight into biochar properties and its cost analysis. Biomass Bioenergy 84, 76–86.
Ahmed, M.B., Zhou, J.L., Ngo, H.H., Guo, W., Chen, M., 2016b. Progress in the preparation and application of modified biochar for improved contaminant removal from water and wastewater. Bioresour. Technol. 214, 836–851.
Anjum, S., Gautam, D., Gupta, B., Ikram, S., 2009. Arsenic removal from water: an overview of recent technologies. J. Chem. 2, 7–52.
Arar, O., Kabay, N., Sánchez, J., Rivas, B.L., Bryjak, M., Peña, C., 2014. Removal of arsenic from water by combination of electro-oxidation and polymer enhanced ultrafiltration. Environ. Prog. Sustain. Energy 33, 918–924.
Australian Bureau of Statistics, 2018. Livestock Products, Australia, Sep 2018. Australian Government.
Baig, S.A., Zhu, J., Muhammad, N., Sheng, T., Xu, X., 2014. Effect of synthesis methods on magnetic Kans grass biochar for enhanced As (III, V) adsorption from aqueous solutions. Biomass Bioenergy 71, 299–310.
Bakshi, S., Banik, C., Rathke, S.J., Laird, D.A., 2018. Arsenic sorption on zero-valent iron-biochar complexes. Water Res. 137, 153–163.
Barakat, M., Sahiner, N., 2008. Cationic hydrogels for toxic arsenate removal from aqueous environment. J. Environ. Manag. 88, 955–961.
Beaumont, O., Schwob, Y., 1984. Influence of physical and chemical parameters on wood pyrolysis. Ind. Eng. Chem. Process. Des. Dev. 23, 637–641.
Begum, S.A., Hyder, A.G., Vahdat, N., 2016. Adsorption isotherm and kinetic studies of As (V) removal from aqueous solution using cattle bone char. J. Water Supply Res. T. 65, 244–252.
Bissen, M., Frimmel, F.H., 2003. Arsenic—a review. Part I: occurrence, toxicity, speciation, mobility. Acta Hydrochim. Hydrobiol. 31, 9–18.
Boddu, V.M., Abburi, K., Talbott, J.L., Smith, E.D., Haasch, R., 2008. Removal of arsenic (III) and arsenic (V) from aqueous medium using chitosan-coated biosorbent. Water Res. 42, 633–642.
Bora, A.J., Gogoi, S., Baruah, G., Dutta, R.K., 2016. Utilization of co-existing iron in arsenic removal from groundwater by oxidation-coagulation at optimized pH. J. Environ. Chem. Eng. 4, 2683–2691.
Brewer, C.E., Schmidt-Rohr, K., Satrio, J.A., Brown, R.C., 2009. Characterization of biochar from fast pyrolysis and gasification systems. Environ. Prog. Sustain. Energy 28, 386–396.
Brunson, L.R., Sabatini, D.A., 2009. An evaluation of fish bone char as an appropriate arsenic and fluoride removal technology for emerging regions. Environ. Eng. Sci. 26, 1777–1784.
Bundschuh, J., Maity, J.P., Mushtaq, S., Vithanage, M., Seneweera, S., Schneider, J., Bhattacharya, P., Khan, N.I., Hamawand, I., Guilherme, L.R., 2017. Medical geology in the framework of the sustainable development goals. Sci. Total Environ. 581, 87–104.
Cao, X., Harris, W., 2010. Properties of dairy-manure-derived biochar pertinent to its potential use in remediation. Bioresour. Technol. 101, 5222–5228.
Cetin, E., Moghtaderi, B., Gupta, R., Wall, T., 2004. Influence of pyrolysis conditions on the structure and gasification reactivity of biomass chars. Fuel 83, 2139–2150.
Chen, Y.-N.; Chai, L.-Y. Equilibrium and Kinetics of Arsenic (V) Sorption by Bone Char. Bioinformatics and biomedical engineering, 2008 ICBBE 2008 the 2nd International Conference on: IEEE; 2008.
Chen, Y.-N., Chai, L.-Y., Shu, Y.-D., 2008. Study of arsenic (V) adsorption on bone char from aqueous solution. J. Hazard. Mater. 160, 168–172.
Chen, Z., Liu, Y., Mao, L., Gong, L., Sun, W., Feng, L., 2018. Effect of cation doping on the structure of hydroxyapatite and the mechanism of defluoridation. Ceram. Int. 44, 6002–6009.
Chiavola, A., D'Amato, E., Gavasci, R., Sirini, P., 2015. Arsenic removal from groundwater by ion exchange and adsorption processes: comparison of two different materials. Water Sci. Technol. Water Supply 15, 981–989.
Cho, H.J., Baek, K., Jeon, J.-K., Park, S.H., Suh, D.J., Park, Y.-K., 2013. Removal characteristics of copper by marine macro-algae-derived chars. Chem. Eng. J. 217, 205–211.
Cho, D.-W., Yoon, K., Kwon, E.E., Biswas, J.K., Song, H., 2017. Fabrication of magnetic biochar as a treatment medium for As (V) via pyrolysis of FeCl3-pretreated spent coffee ground. Environ. Pollut. 229, 942–949.
Coates, W., 2000. Using cotton plant residue to produce briquettes. Biomass Bioenergy 18, 201–208.
Cope, C.O., Webster, D.S., Sabatini, D.A., 2014. Arsenate adsorption onto iron oxide amended rice husk char. Sci. Total Environ. 488, 554–561.
Czerniczyniec, M., Farías, S., Magallanes, J., Cicerone, D., 2007. Arsenic (V) adsorption onto biogenic hydroxyapatite: solution composition effects. Water Air Soil Pollut. 180, 75–82.
Darling, B.K., 2016. Geochemical factors controlling the mobilization of arsenic at an artificial recharge site, Clearwater. Florida. J. Contemp. Water Res. Educ. 105–116.
Demirbas, A., 2004. Effects of temperature and particle size on bio-char yield from pyrolysis of agricultural residues. J. Anal. Appl. Pyrolysis 72, 243–248.
Downie, A., Crosky, A., Munroe, P., 2009. Physical properties of biochar. Biochar for environmental management: Science Technol. 13–32.
Duker, A.A., Carranza, E., Hale, M., 2005. Arsenic geochemistry and health. Environ. Int. 31, 631–641.
Dutta, B., Raghavan, G., Ngadi, M., 2012. Surface characterization and classification of slow and fast pyrolyzed biochar using novel methods of pycnometry and hyperspectral imaging. J. Wood Chem. Technol. 32, 105–120.
Egbuchunam, T.O., Obi, G., Okieimen, F.E., Yetgin, S., 2016. Adsorptive removal of p-nitrophenol from aqueous solution by bone char: equilibrium and kinetic studies. J. Chem. 10, 325–335.
Elia, A.C., Magara, G., Caruso, C., Masoero, L., Prearo, M., Arsieni, P., Caldaroni, B., Dörr, A.J.M., Scoparo, M., Salvati, S., 2018. A comparative study on subacute toxicity of arsenic trioxide and dimethylarsinic acid on antioxidant status in Crandell Rees feline kidney (CRFK), human hepatocellular carcinoma (PLC/PRF/5), and epithelioma papulosum cyprini (EPC) cell lines. J. Toxic. Environ. Health A 81, 333–348.
Figoli, A., Hoinkis, J., Bundschuh, J., 2016. Membrane Technologies for Water Treatment: Removal of Toxic Trace Elements with Emphasis on Arsenic, Fluoride and Uranium Ed. CRC Press.
Franco, M., Carro, P., 2014. Arsenic removal in water by means of coagulation-flocculation processes. Rev. Int. Contam. Ambie. 30, 177–190.
Genç-Fuhrman, H., Bregnhøj, H., McConchie, D., 2005. Arsenate removal from water using sand–red mud columns. Water Res. 39, 2944–2954.
Gerente, C., Lee, V., Cloirec, P.L., McKay, G., 2007. Application of chitosan for the removal of metals from wastewaters by adsorption—mechanisms and models review. Crit. Rev. Environ. Sci. Technol. 37, 41–127.
Gibaud, S., Jaouen, G., 2010. Arsenic-Based Drugs: From Fowler's Solution to Modern Anticancer Chemotherapy. In: Jaouen, G., Metzler-Nolte, N. (Eds.), Medicinal Organometallic Chemistry. Top. Organomet. Chem. 32. Springer Berlin Heidelberg, Berlin, Heidelberg, pp. 1–20. https://doi.org/10.1007/978-3-642-13185-1_1.
Greenlee, L.F., Lawler, D.F., Freeman, B.D., Marrot, B., Moulin, P., 2009. Reverse osmosis desalination: water sources, technology, and today's challenges. Water Res. 43, 2317–2348.
Guo, X., Zuo, R., Meng, L., Wang, J., Teng, Y., Liu, X., Chen, M., 2018. Seasonal and spatial variability of anthropogenic and natural factors influencing groundwater quality based on source apportionment. Int. J. Environ. Res. Public Health 15, 279.
Gupta, V.K., Ali, I., 2012. Environmental Water: Advances in Treatment, Remediation and Recycling Ed. Newnes.
Hamawand, I., Sandell, G., Pittaway, P., Chakrabarty, S., Yusaf, T., Chen, G., Seneweera, S., Al-Lwayzy, S., Bennett, J., Hopf, J., 2016. Bioenergy from cotton industry wastes: a review and potential. Renew. Sust. Energ. Rev. 66, 435–448.
Harsono, S.S., Grundman, P., Lau, L.H., Hansen, A., Salleh, M.A.M., Meyer-Aurich, A., Idris, A., Ghazi, T.I.M., 2013. Energy balances, greenhouse gas emissions and economics of biochar production from palm oil empty fruit bunches. Resour. Conserv. Recycl. 77, 108–115.
Harvey, O.R., Herbert, B.E., Rhue, R.D., Kuo, L.-J., 2011. Metal interactions at the biochar-water interface: energetics and structure-sorption relationships elucidated by flow adsorption microcalorimetry. Environ. Sci. Technol. 45, 5550–5556.
Hayat, K., Menhas, S., Bundschuh, J., Chaudhary, H.J., 2017. Microbial biotechnology as an emerging industrial wastewater treatment process for arsenic mitigation: a critical review. J. Clean. Prod. 151, 427–438.
Herath, I., Kumarathilaka, P., Al-Wabel, M.I., Abduljabbar, A., Ahmad, M., Usman, A.R., Vithanage, M., 2016a. Mechanistic modeling of glyphosate interaction with rice husk derived engineered biochar. Microporous Mesoporous Mater. 225, 280–288.
Herath, I., Vithanage, M., Bundschuh, J., Maity, J.P., Bhattacharya, P., 2016b. Natural arsenic in global groundwaters: distribution and geochemical triggers for mobilization. Current Pollution Reports 2, 68–89.
Herath, I., Vithanage, M., Bundschuh, J., 2017. Antimony as a global dilemma: geochemistry, mobility, fate and transport. Environ. Pollut. 223, 545–559.
Hu, X., Ding, Z., Zimmerman, A.R., Wang, S., Gao, B., 2015. Batch and column sorption of arsenic onto iron-impregnated biochar synthesized through hydrolysis. Water Res. 68, 206–216.
Hua, G., Salo, M.W., Schmit, C.G., Hay, C.H., 2016. Nitrate and phosphate removal from agricultural subsurface drainage using laboratory woodchip bioreactors and recycled steel byproduct filters. Water Res. 102, 180–189.
Huang, Y.F., Kuan, W., Lo, S., Lin, C., 2008. Total recovery of resources and energy from rice straw using microwave-induced pyrolysis. Bioresour. Technol. 99, 8252–8258.
Inyang, M., Dickenson, E., 2015. The potential role of biochar in the removal of organic and microbial contaminants from potable and reuse water: a review. Chemosphere 134, 232–240.
Islam, M., Mishra, P.C., Patel, R., 2011. Arsenate removal from aqueous solution by cellulose-carbonated hydroxyapatite nanocomposites. J. Hazard. Mater. 189, 755–763.
Jain, C., Ali, I., 2000. Arsenic: occurrence, toxicity and speciation techniques. Water Res. 34, 4304–4312.

Jiménez-Cedillo, M., Olguín, M., Fall, C., Colin-Cruz, A., 2013. As (III) and As (V) sorption on iron-modified non-pyrolyzed and pyrolyzed biomass from Petroselinum crispum (parsley). J. Environ. Manag. 117, 242–252.
Jin, H., Capareda, S., Chang, Z., Gao, J., Xu, Y., Zhang, J., 2014. Biochar pyrolytically produced from municipal solid wastes for aqueous As (V) removal: adsorption property and its improvement with KOH activation. Bioresour. Technol. 169, 622–629.
Johansson, C.L., Paul, N.A., de Nys, R., Roberts, D.A., 2016. Simultaneous biosorption of selenium, arsenic and molybdenum with modified algal-based biochars. J. Environ. Manag. 165, 117–123.
Jomova, K., Jenisova, Z., Feszterova, M., Baros, S., Liska, J., Hudecova, D., Rhodes, C., Valko, M., 2011. Arsenic: toxicity, oxidative stress and human disease. J. Appl. Toxicol. 31, 95–107.
Kaseva, M., 2006. Optimization of regenerated bone char for fluoride removal in drinking water: a case study in Tanzania. J. Water Health 4, 139–147.
Kung, C.-C., McCarl, B.A., Chen, C.-C., 2014. An environmental and economic evaluation of pyrolysis for energy generation in Taiwan with endogenous land greenhouse gases emissions. Int. J. Environ. Res. Public Health 11, 2973–2991.
Lehmann, J., Joseph, S., 2015. Biochar for Environmental Management: Science, Technology and Implementation Ed. Routledge.
Lei, H., Ren, S., Julson, J., 2009. The effects of reaction temperature and time and particle size of corn stover on microwave pyrolysis. Energy Fuel 23, 3254–3261.
Leyva-Ramos, R., Rivera-Utrilla, J., Medellin-Castillo, N., Sanchez-Polo, M., 2010. Kinetic modeling of fluoride adsorption from aqueous solution onto bone char. Chem. Eng. J. 158, 458–467.
Li, B., Deng, C., Zhang, D., Pan, X., Al-misned, F.A., Mortuza, M.G., 2016. Bioremediation of nitrate-and arsenic-contaminated groundwater using nitrate-dependent Fe (II) oxidizing clostridium sp, *Strain pxl2*. Geomicrobiol. J. 33, 185–193.
Li, R., Wang, J.J., Gaston, L.A., Zhou, B., Li, M., Xiao, R., Wang, Q., Zhang, Z., Huang, H., Liang, W., 2018. An overview of carbothermal synthesis of metal–biochar composites for the removal of oxyanion contaminants from aqueous solution. Carbon 129, 674–687.
Libra, J.A., Ro, K.S., Kammann, C., Funke, A., Berge, N.D., Neubauer, Y., Titirici, M.-M., Fühner, C., Bens, O., Kern, J., 2011. Hydrothermal carbonization of biomass residuals: a comparative review of the chemistry, processes and applications of wet and dry pyrolysis. Biofuels 2, 71–106.
Lin, L., Qiu, W., Wang, D., Huang, Q., Song, Z., Chau, H.W., 2017. Arsenic removal in aqueous solution by a novel Fe-Mn modified biochar composite: characterization and mechanism. Ecotoxicol. Environ. Saf. 144, 514–521.
Liou, T.-H., Wu, S.-J., 2009. Characteristics of microporous/mesoporous carbons prepared from rice husk under base- and acid-treated conditions. J. Hazard. Mater. 171, 693–703.
Liu, G., Talley, J.W., Na, C., Larson, S.L., Wolfe, L.G., 2010. Copper doping improves hydroxyapatite sorption for arsenate in simulated groundwaters. Environ. Sci. Technol. 44, 1366–1372.
Liu, Y., Su, G., Zhang, B., Jiang, G., Yan, B., 2011. Nanoparticle-based strategies for detection and remediation of environmental pollutants. Analyst 136, 872–877.
Liu, J., Huang, X., Liu, J., Wang, W., Zhang, W., Dong, F., 2014. Adsorption of arsenic (V) on bone char: batch. column and modeling studies. Environ. Earth Sci. 72, 2081–2090.
Liu, J., He, L., Dong, F., Hudson-Edwards, K.A., 2016. The role of nano-sized manganese coatings on bone char in removing arsenic (V) from solution: implications for permeable reactive barrier technologies. Chemosphere 153, 146–154.
Liu, S., Huang, B., Chai, L., Liu, Y., Zeng, G., Wang, X., Zeng, W., Shang, M., Deng, J., Zhou, Z., 2017. Enhancement of As (v) adsorption from aqueous solution by a magnetic chitosan/biochar composite. RSC Adv. 7, 10891–10900.
Ma, Y., Liu, W.-J., Zhang, N., Li, Y.-S., Jiang, H., Sheng, G.-P., 2014. Polyethylenimine modified biochar adsorbent for hexavalent chromium removal from the aqueous solution. Bioresour. Technol. 169, 403–408.
Mack, C., Wilhelmi, B., Duncan, J., Burgess, J., 2007. Biosorption of precious metals. Biotechnol. Adv. 25, 264–271.
Mandal, B.K., Suzuki, K.T., 2002. Arsenic round the world: a review. Talanta 58, 201–235.
Medellin-Castillo, N.A., Leyva-Ramos, R., Ocampo-Perez, R., Garcia de la Cruz, R.F., Aragon-Pina, A., Martinez-Rosales, J.M., Guerrero-Coronado, R.M., Fuentes-Rubio, L., 2007. Adsorption of fluoride from water solution on bone char. Ind. Eng. Chem. Res. 46, 9205–9212.
Mendoza-Castillo, D.I., Bonilla-Petriciolet, A., Jáuregui-Rincón, J., 2015. On the importance of surface chemistry and composition of Bone char for the sorption of heavy metals from aqueous solution. Desalination Water Treat. 54, 1651–1662.
Meng, J., Wang, L., Liu, X., Wu, J., Brookes, P.C., Xu, J., 2013. Physicochemical properties of biochar produced from aerobically composted swine manure and its potential use as an environmental amendment. Bioresour. Technol. 142, 641–646.
Mlilo, T., Brunson, L., Sabatini, D., 2009. Arsenic and fluoride removal using simple materials. J. Environ. Eng. 136, 391–398.
Mohan, D., Pittman, C.U., 2007. Arsenic removal from water/wastewater using adsorbents—a critical review. J. Hazard. Mater. 142, 1–53.
Mohan, D., Pittman, C.U., Steele, P.H., 2006. Pyrolysis of wood/biomass for bio-oil: a critical review. Energy Fuel 20, 848–889.
Mohan, D., Pittman, C.U., Bricka, M., Smith, F., Yancey, B., Mohammad, J., Steele, P.H., Alexandre-Franco, M.F., Gómez-Serrano, V., Gong, H., 2007. Sorption of arsenic, cadmium, and lead by chars produced from fast pyrolysis of wood and bark during bio-oil production. J. Colloid Interface Sci. 310, 57–73.
Mohan, D., Sarswat, A., Ok, Y.S., Pittman, C.U., 2014. Organic and inorganic contaminants removal from water with biochar, a renewable, low cost and sustainable adsorbent–a critical review. Bioresour. Technol. 160, 191–202.
Molin, M., Ulven, S.M., Meltzer, H.M., Alexander, J., 2015. Arsenic in the human food chain, biotransformation and toxicology–review focusing on seafood arsenic. J. Trace Elem. Med. Biol. 31, 249–259.
National Research Council, 1999. Arsenic in Drinking Water edˆ. National Academies Press.
Nayak, A.K., 2010. Hydroxyapatite synthesis methodologies: an overview. Int. J. ChemTech Res. 2, 903–907.
Niazi, N.K., Murtaza, B., Shahid, M., White, J., Nawaz, M., Bashir, S., Shakoor, M., Choppala, G., Murtaza, G., Wang, H., 2016. Removal and recovery of metals by biosorbents and biochars derived from biowastes. Environmental materials and waste: resource recovery and pollution. Prevention 149–177.
Nicomel, N., Leus, K., Folens, K., Van Der Voort, P., Du Laing, G., 2016. Technologies for arsenic removal from water: current status and future perspectives. Int. J. Environ. Res. Public Health 13 (62).
Novotny, E.H., Maia, C.M.B.d.F., Carvalho, M.T.d.M., Madari, B.E., 2015. Biochar: pyrogenic carbon for agricultural use-a critical review. Rev. Bras. Cienc. Solo 39, 321–344.
Oremland, R.S., Stolz, J.F., 2003. The ecology of arsenic. Science 300, 939–944.
Osterwalder, L., Johnson, C.A., Yang, H., Johnston, R.B., 2014. Multi-criteria assessment of community-based fluoride-removal technologies for rural Ethiopia. Sci. Total Environ. 488, 532–538.
Ozay, O., Ekici, S., Baran, Y., Aktas, N., Sahiner, N., 2009. Removal of toxic metal ions with magnetic hydrogels. Water Res. 43, 4403–4411.
Panagiotaras, D., Nikolopoulos, D., 2015. Arsenic occurrence and fate in the environment; a geochemical perspective. J. Earth Sci. Clim. Change 6 (1).
Passman, S.D., White, T.J., Lewis, R.D., 2014. Point-of-use water filtration for arsenic: a sustainable and simple solution in resource-poor settings. IJSLE 9, 79–91.
Pehlivan, E., Tran, T., Ouédraogo, W., Schmidt, C., Zachmann, D., Bahadir, M., 2013. Removal of As (V) from aqueous solutions by iron coated rice husk. Fuel Process. Technol. 106, 511–517.
Perez-Gonzalez, A., Urtiaga, A.M., Ibanez, R., Ortiz, I., 2012. State of the art and review on the treatment technologies of water reverse osmosis concentrates. Water Res. 46, 267–283.
Pickin, J., Randell, P., Trinh, J., Grant, B., 2018. National Waste Report 2018. In: Department of the Environment and Energy Blue Environment Pty Ltd.
Pirilä, M., Martikainen, M., Ainassaari, K., Kuokkanen, T., Keiski, R.L., 2011. Removal of aqueous As (III) and As (V) by hydrous titanium dioxide. J. Colloid Interface Sci. 353, 257–262.
Qian, W., Zhao, A.-z., Xu, R.-k., 2013. Sorption of As (V) by aluminum-modified crop straw-derived biochars. Water Air Soil Pollut. 224, 1610.
Rahaman, M., Basu, A., Islam, M., 2008. The removal of As (III) and As (V) from aqueous solutions by waste materials. Bioresour. Technol. 99, 2815–2823.
Rajapaksha, A.U., Chen, S.S., Tsang, D.C., Zhang, M., Vithanage, M., Mandal, S., Gao, B., Bolan, N.S., Ok, Y.S., 2016. Engineered/designer biochar for contaminant removal/immobilization from soil and water: potential and implication of biochar modification. Chemosphere 148, 6e291.
Rapagna, S., Latif, A., 1997. Steam gasification of almond shells in a fluidised bed reactor: the influence of temperature and particle size on product yield and distribution. Biomass Bioenergy 12, 281–288.
Rashidi, N.A., Yusup, S., 2016. An overview of activated carbons utilization for the post-combustion carbon dioxide capture. J CO2 Utilization 13, 1–16.
Riveros, P., Dutrizac, J., Spencer, P., 2001. Arsenic disposal practices in the metallurgical industry. Can. Metall. Q. 40, 395–420.
Sadaf, N., Kumar, N., Ali, M., Ali, V., Bimal, S., Haque, R., 2018. Arsenic trioxide induces apoptosis and inhibits the growth of human liver cancer cells. Life Sci. 205, 9–17.
Samsuri, A.W., Sadegh-Zadeh, F., Seh-Bardan, B.J., 2013. Adsorption of As (III) and As (V) by Fe coated biochars and biochars produced from empty fruit bunch and rice husk. J. Environ. Chem. Eng. 1, 981–988.
Sanyang, L., Ghani, W.A.W.A.K., Idris, A., Mansor, A., 2014. Zinc removal from Wastewater using hydrogel modified biochar. Appl. Mech. Mater. 625, 842–846.
Sanyang, M.L., Ghani, W.A.W.A.K., Idris, A., Ahmad, M.B., 2016. Hydrogel biochar composite for arsenic removal from wastewater. Desalination Water Treat. 57, 3674–3688.
Savage, N., Diallo, M.S., 2005. Nanomaterials and water purification: opportunities and challenges. J. Nanopart. Res. 7, 331–342.
Saxena, A., Patel, A., 2018. Role of bioremediation as a low-cost adsorbent for excessive fluoride removal in groundwater. Handbook of Environmental Materials Management 1–32.
Septien, S., Valin, S., Dupont, C., Peyrot, M., Salvador, S., 2012. Effect of particle size and temperature on woody biomass fast pyrolysis at high temperature (1000–1400 C). Fuel 97, 202–210.
Shokri, E., Yegani, R., Pourabbas, B., Kazemian, N., 2016. Preparation and characterization of polysulfone/organoclay adsorptive nanocomposite membrane for arsenic removal from contaminated water. Appl. Clay Sci. 132, 611–620.
Singh, A.P., Goel, R.K., Kaur, T., 2011. Mechanisms pertaining to arsenic toxicity. Toxicol. Int. 18, 87.
Singh, R., Singh, S., Parihar, P., Singh, V.P., Prasad, S.M., 2015. Arsenic contamination, consequences and remediation techniques: a review. Ecotoxicol. Environ. Saf. 112, 247–270.
Smith, A.H., Lingas, E.O., Rahman, M., 2000. Contamination of drinking-water by arsenic in Bangladesh: a public health emergency. Bull. World Health Organ. 78, 1093–1103.
Sneddon, I., Garelick, H., Valsami-Jones, E., 2005. An investigation into arsenic (V) removal from aqueous solutions by hydroxylapatite and bone-char. Mineral. Mag. 69, 769–780.
Soltani, R.D.C., Safari, M., Maleki, A., Rezaee, R., Shahmoradi, B., Shahmohammadi, S., Ghahramani, E., 2017. Decontamination of arsenic (V)-contained liquid phase

utilizing Fe3O4/bone char nanocomposite encapsulated in chitosan biopolymer. Environ. Sci. Pollut. R 1–10.
Sorg, T.J., Chen, A.S., Wang, L., 2014. Arsenic species in drinking water wells in the USA with high arsenic concentrations. Water Res. 48, 156–169.
Sternitzke, V., Kaegi, R., Audinot, J.-N., Lewin, E., Hering, J.G., Johnson, C.A., 2012. Uptake of fluoride from aqueous solution on nano-sized hydroxyapatite: examination of a fluoridated surface layer. Environ. Sci. Technol. 46, 802–809.
Sullivan, C., Tyrer, M., Cheeseman, C.R., Graham, N.J., 2010. Disposal of water treatment wastes containing arsenic—a review. Sci. Total Environ. 408, 1770–1778.
Sun, Q., Yang, L., 2003. The adsorption of basic dyes from aqueous solution on modified peat–resin particle. Water Res. 37, 1535–1544.
Sun, Y., Gao, B., Yao, Y., Fang, J., Zhang, M., Zhou, Y., Chen, H., Yang, L., 2014. Effects of feedstock type, production method, and pyrolysis temperature on biochar and hydrochar properties. Chem. Eng. J. 240, 574–578.
Tan, X., Liu, Y., Zeng, G., Wang, X., Hu, X., Gu, Y., Yang, Z., 2015. Application of biochar for the removal of pollutants from aqueous solutions. Chemosphere 125, 70–85.
Tan, X.-f., Liu, Y.-g., Gu, Y.-l., Xu, Y., Zeng, G.-m., Hu, X.-j., Liu, S.-b., Wang, X., Liu, S.-m., Li, J., 2016. Biochar-based nano-composites for the decontamination of wastewater: a review. Bioresour. Technol. 212, 318–333.
Tan, X.-f., Liu, S.-b., Liu, Y.-g., Gu, Y.-l., Zeng, G.-m., Hu, X.-j., Wang, X., Liu, S.-h., Jiang, L.-h., 2017. Biochar as potential sustainable precursors for activated carbon production: multiple applications in environmental protection and energy storage. Bioresour. Technol. 227, 359–372.
Tavares, D.S., Lopes, C.B., Coelho, J.P., Sánchez, M.E., Garcia, A.I., Duarte, A.C., Otero, M., Pereira, E., 2012. Removal of arsenic from aqueous solutions by sorption onto sewage sludge-based sorbent. Water Air Soil Pollut. 223, 2311–2321.
Trakal, L., Michálková, Z., Beesley, L., Vítková, M., Ouředníček, P., Barceló, A.P., Ettler, V., Číhalová, S., Komárek, M., 2018. AMOchar: Amorphous manganese oxide coating of biochar improves its efficiency at removing metal (loid) s from aqueous solutions. Sci. Total Environ. 625, 71–78.
Uchimiya, M., Chang, S., Klasson, K.T., 2011. Screening biochars for heavy metal retention in soil: role of oxygen functional groups. J. Hazard. Mater. 190, 432–441.
Van Vinh, N., Zafar, M., Behera, S., Park, H.-S., 2015. Arsenic (III) removal from aqueous solution by raw and zinc-loaded pine cone biochar: equilibrium, kinetics, and thermodynamics studies. Int. J. Environ. Sci. Technol. 12, 1283–1294.
Vithanage, M., Herath, I., Joseph, S., Bundschuh, J., Bolan, N., Ok, Y.S., Kirkham, M., Rinklebe, J., 2016. Interaction of arsenic with biochar in soil and water: a critical review. Carbon 113, 219–230.
Vithanage, M., Herath, I., Joseph, S., Bundschuh, J., Bolan, N., Ok, Y.S., Kirkham, M.B., Rinklebe, J., 2017. Interaction of arsenic with biochar in soil and water: a critical review. Carbon 113, 219–230.
Waghmare, S., Arfin, T., Rayalu, S., Lataye, D., Dubey, S., Tiwari, S., 2015. Adsorption behavior of modified zeolite as novel adsorbents for fluoride removal from drinking water: surface phenomena, kinetics and thermodynamics studies‖. IJSET 4, 4114–4124.
Wang, S., Gao, B., Li, Y., Mosa, A., Zimmerman, A.R., Ma, L.Q., Harris, W.G., Migliaccio, K.W., 2015a. Manganese oxide-modified biochars: preparation, characterization, and sorption of arsenate and lead. Bioresour. Technol. 181, 13–17.
Wang, S., Gao, B., Zimmerman, A.R., Li, Y., Ma, L., Harris, W.G., Migliaccio, K.W., 2015b. Removal of arsenic by magnetic biochar prepared from pinewood and natural hematite. Bioresour. Technol. 175, 391–395.
Wang, S., Gao, B., Li, Y., 2016. Enhanced arsenic removal by biochar modified with nickel (Ni) and manganese (Mn) oxyhydroxides. J. Ind. Eng. Chem. 37, 361–365.
Wang, S., Gao, B., Li, Y., Creamer, A.E., He, F., 2017. Adsorptive removal of arsenate from aqueous solutions by biochar supported zero-valent iron nanocomposite: batch and continuous flow tests. J. Hazard. Mater. 322, 172–181.
WHO, 2011. Guidelines for drinking-water quality. WHO Chronicle 38, 104–108.
Wu, C., Huang, L., Xue, S.-G., Huang, Y.-Y., Hartley, W., Cui, M.-q., Wong, M.-H., 2017. Arsenic sorption by red mud-modified biochar produced from rice straw. Environ. Sci. Pollut. R 24, 18168–18178.
Xu, Y.H., Ohki, A., Maeda, S., 2000. Removal of arsenate, phosphate, and fluoride ions by aluminium-loaded shirasu-zeolite. Toxicol. Environ. Chem. 76, 111–124.
Xu, Y., Luo, G., He, S., Deng, F., Pang, Q., Xu, Y., Yao, H., 2019. Efficient removal of elemental mercury by magnetic chlorinated biochars derived from co-pyrolysis of Fe (NO3) 3-laden wood and polyvinyl chloride waste. Fuel 239, 982–990.
Yadav, L.S., Mishra, B.K., Kumar, A., Paul, K.K., 2014. Arsenic removal using bagasse fly ash-iron coated and sponge iron char. J. Environ. Chem. Eng. 2, 1467–1473.
Yamamura, S., Bartram, J., Csanady, M., Gorchev, H.G., Redekopp, A., 2003. Drinking water guidelines and standards. Arsenic, Water, and Health: The State of the. Art.
Yamani, J.S., Lounsbury, A.W., Zimmerman, J.B., 2016. Towards a selective adsorbent for arsenate and selenite in the presence of phosphate: assessment of adsorption efficiency, mechanism, and binary separation factors of the chitosan-copper complex. Water Res. 88, 889–896.
Yao, Y., Gao, B., Inyang, M., Zimmerman, A.R., Cao, X., Pullammanappallil, P., Yang, L., 2011. Removal of phosphate from aqueous solution by biochar derived from anaerobically digested sugar beet tailings. J. Hazard. Mater. 190, 501–507.
Yoon, Y., Park, W.K., Hwang, T.-M., Yoon, D.H., Yang, W.S., Kang, J.-W., 2016. Comparative evaluation of magnetite–graphene oxide and magnetite-reduced graphene oxide composite for As (III) and As (V) removal. J. Hazard. Mater. 304, 196–204.
Yuan, J.-H., Xu, R.-K., Zhang, H., 2011. The forms of alkalis in the biochar produced from crop residues at different temperatures. Bioresour. Technol. 102, 3488–3497.
Zanzi, R., Sjöström, K., Björnbom, E., 1996. Rapid high-temperature pyrolysis of biomass in a free-fall reactor. Fuel 75, 545–550.
Zeng, Z., Ye, S., Wu, H., Xiao, R., Zeng, G., Liang, J., Zhang, C., Yu, J., Fang, Y., Song, B., 2019. Research on the sustainable efficacy of g-MoS2 decorated biochar nanocomposites for removing tetracycline hydrochloride from antibiotic-polluted aqueous solution. Sci. Total Environ. 648, 206–217.
Zhang, M., Gao, B., 2013. Removal of arsenic, methylene blue, and phosphate by biochar/AlOOH nanocomposite. Chem. Eng. J. 226, 286–292.
Zhang, S., Liu, C., Luan, Z., Peng, X., Ren, H., Wang, J., 2008. Arsenate removal from aqueous solutions using modified red mud. J. Hazard. Mater. 152, 486–492.
Zhang, M., Gao, B., Varnoosfaderani, S., Hebard, A., Yao, Y., Inyang, M., 2013. Preparation and characterization of a novel magnetic biochar for arsenic removal. Bioresour. Technol. 130, 457–462.
Zhang, M., Ahmad, M., Al-Wabel, M.I., Vithanage, M., Rajapaksha, A.U., Kim, H.S., Lee, S.S., Ok, Y.S., 2015. Adsorptive removal of trichloroethylene in water by crop residue biochars pyrolyzed at contrasting temperatures: continuous fixed-bed experiments. J. Chem. 2015, 1–6.
Zhang, F., Wang, X., Xionghui, J., Ma, L., 2016. Efficient arsenate removal by magnetite-modified water hyacinth biochar. Environ. Pollut. 216, 575–583.
Zhang, Z., Zhu, Z., Shen, B., Liu, L., 2019. Insights into biochar and hydrochar production and applications: a review. Energy 171, 581–589.
Zhou, Y., Gao, B., Zimmerman, A.R., Fang, J., Sun, Y., Cao, X., 2013. Sorption of heavy metals on chitosan-modified biochars and its biological effects. Chem. Eng. J. 231, 512–518.
Zhou, Z., Liu, Y.-g., Liu, S.-b., Liu, H.-y., Zeng, G.-m., Tan, X.-f., Yang, C.-p., Ding, Y., Yan, Z.-l., Cai, X.-x, 2017. Sorption performance and mechanisms of arsenic (V) removal by magnetic gelatin-modified biochar. Chem. Eng. J. 314, 223–231.
Zhu, N., Yan, T., Qiao, J., Cao, H., 2016. Adsorption of arsenic, phosphorus and chromium by bismuth impregnated biochar: adsorption mechanism and depleted adsorbent utilization. Chemosphere 164, 32–40.
Zhu, N., Zhang, J., Tang, J., Zhu, Y., Wu, Y., 2017. Arsenic removal by periphytic biofilm and its application combined with biochar. Bioresour. Technol. 248, 49–55.
Zwetsloot, M.J., Lehmann, J., Bauerle, T., Vanek, S., Hestrin, R., Nigussie, A., 2016. Phosphorus availability from bone char in a P-fixing soil influenced by root-mycorrhizae-biochar interactions. Plant Soil 408, 95–105.

2.1.3 Concluding remarks

Biochar and bone char are relatively cost-efficient waste materials that demonstrate significant contribution to the removal of As from aqueous solutions. The present review addressed the production, modification and application of biochar and bone char for environmental remediation as a replacement strategy for existing costly adsorbents. The physical properties and the surface chemistry and texture are the main factors that must be controlled to provide a selective removal of targeted contaminants. However, the negative surface charge of these adsorbents offers a limited ability to remove As from solution. The review revealed that chemical modification of biochar increased removal efficiency of As. However, little work has been carried out for the modification of bone char for the same purpose, especially for the removal of As(III). The mechanism of As removal was found to be complexation, electrostatic interaction and ligand exchange. Application of these adsorbents requires further investigation in the direction of regeneration and recovery of the spent As. Most of the reported studies were performed in the lab. This gives a platform for the examination of large-scale systems with industrial applications at the commercial level also.

2.2 Fluoride removal using bone char as a green sorbent

PAPER II

Alkurdi, S.S., Al-Juboori, R.A., Bundschuh, J. and Hamawand, I. (2019). Bone char as a green sorbent for removing health threatening fluoride from drinking water. Environment International, 127, 704-719. (Published).

2.2.1 Introduction

This review manuscript explores the pyrolysis conditions: temperature range, residence time and the purging gas effects on F^- mitigation from water using bone char. Furthermore, it critically reviews the factors that affect the efficiency of removal such as pH, equilibrium contact time, initial concentration and temperature. The mechanism of removal is elucidated, and the role of various modification methods discussed. This study also provides an overview of the effect of the presence of some other oxyanions on the ability of the bone char to adsorb fluoride. The regeneration of the adsorbents are examined, and some proposed models for the possible application of this waste-based material in industrial wastewater treatment are elaborated. Cost validity of the production is also estimated based on production costs reported in the literature and the commercially available bone char for water treatment.

Environment International 127 (2019) 704–719

Contents lists available at ScienceDirect

Environment International

journal homepage: www.elsevier.com/locate/envint

Review article

Bone char as a green sorbent for removing health threatening fluoride from drinking water

Susan S.A. Alkurdi[a,b], Raed A. Al-Juboori[a,c], Jochen Bundschuh[a,d,*], Ihsan Hamawand[e]

[a] School of Civil Engineering and Surveying, Faculty of Health, Engineering and Sciences, University of Southern Queensland, West Street, Toowoomba, 4350, Queensland, Australia
[b] Northern Technical University, Engineering Technical College, Kirkuk, Iraq
[c] School of Science, Engineering and Information Technology, Federation University Australia, University Drive, Mt Helen, VIC 3350
[d] UNESCO Chair on Groundwater Arsenic within the 2030 Agenda for Sustainable Development, University of Southern Queensland, West Street, Toowoomba, 4350, Queensland, Australia
[e] Research and Engineering Services, Toowoomba, QLD, 4350, Australia

ARTICLE INFO

Keywords:
Fluoride removal by bone char
Surface modification
Sorption capacity
Mechanism of fluoride removal
Cost
Conceptual designs

ABSTRACT

Millions of people around the world suffer from or prone to health problems caused by high concentration of fluoride in drinking water sources. One of the environmentally friendly and cost-effective ways for removing fluoride is the use of bone char. In this review, the structural properties and binding affinity of fluoride ions from different water sources was critically discussed. The effect of experimental conditions on enhancing the adsorption capacity of fluoride ions using bone char samples was addressed. It appears that surface properties, and conditions of the bone char production such as temperature and residence time play an important role in designing the optimal fluoride removal process. The optimum temperature for fluoride removal seems to be in the range of 500–700 °C and a residence time of 2 h. Applying various equilibrium adsorption isotherms for understanding fluoride adsorption mechanism was presented. The effect of bone char modification with different elements were discussed and recommendations for a further increase in the removal efficiency was proposed. Cost of bone char production and large-scale treatment systems were also discussed based on information available from scientific and commercial sources. Challenges with existing domestic defluoridation designs were highlighted and suggestions for new conceptual designs were provided.

1. Introduction

Fluorine is the most reactive electronegative element. Fluorine's leaching and dissolution into groundwater and thermal gases occurs due to the processes of weathering and water circulation within soil layers and rocks. It also has a high affinity to acquire electrons and form negative fluoride ions (F^-). Thus, fluoride forms complexes with several cations, which constitutes about (0.6–0.9%) of the Earth's crust. Its concentration is about 1 mg/L in sea water, 0.5 mg/L in lakes and rivers (Fawell et al., 2006) and (1–35 mg/L) in groundwater (Tripathy et al., 2006). The concentration of fluoride in groundwater resources depends on the geographical location and is largely associated with the presence of nearby volcanic activities and fumarolic gases. Some of the high fluoride concentrations belts extend on lands along the East African Rift, between Turkey and China, USA, South America, Japan, Australia etc. (Maheshwari, 2006). There are a wide variety of fluoride minerals present in the soil texture such as fluorspar, rock phosphate, apatite, cryolite, mica, sellaite, phlogopite, topaz, etc. (Elango and Jagadeshan, 2018). In addition, soil conditions such as alkalinity, high levels of aluminum and low concentrations of calcium and magnesium oxides are important factors that increase F^- leaching into groundwater (Padhi and Muralidharan, 2012). On the other hand, anthropogenic sources of F^- in the environment are due to two main sources. Firstly, the release and mobilization of fluoride of a geological origin into the environment from some processes such as coal combustion, and secondly from the improper discharge of waste products by various industries, including nickel, steel, copper and aluminum smelting; and the industrial manufacture of masonry, ceramics, semiconductors, phosphate fertilizers and glass (Cai et al., 2017; Rasool et al., 2017; Tovar-Gómez et al., 2013; Waghmare et al., 2015) are also responsible for fluoride availability in water resources.

Fluoride is categorized as an essential substance as it contributes in

* Corresponding author at: Faculty of Health, Engineering and Sciences, UNESCO Chair on Groundwater Arsenic within the 2030 Agenda for Sustainable Development, University of Southern Queensland, West Street, Toowoomba, Queensland, Australia.
E-mail address: Jochen.Bundschuh@usq.edu.au (J. Bundschuh).

https://doi.org/10.1016/j.envint.2019.03.065
Received 20 December 2018; Received in revised form 5 March 2019; Accepted 27 March 2019
Available online 15 April 2019

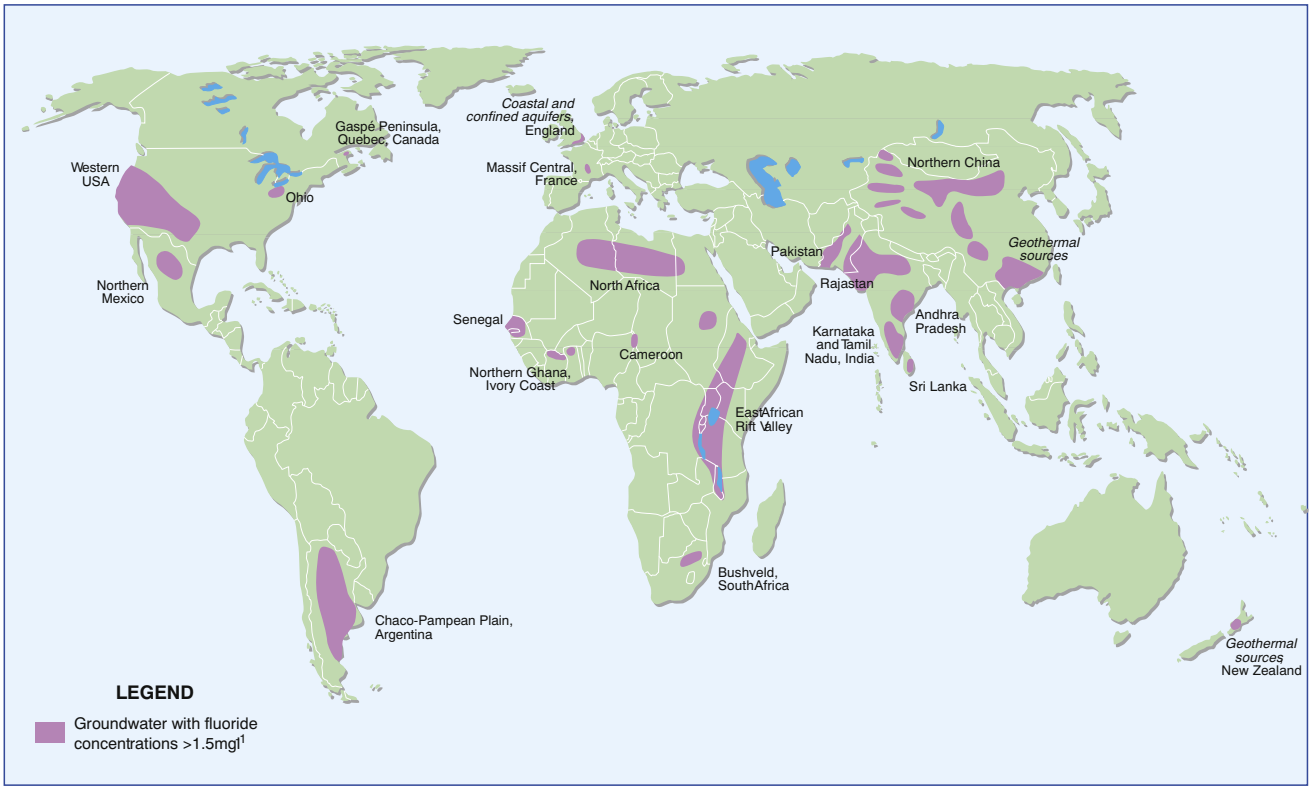

Fig. 1. Countries with high level of fluoride in groundwater. Reproduced with the permission of the British Geological Survey ©UKRI, All rights Reserved, Permit Number: CP19/030 (Edmunds and Smedley, 2013).

the development and the maintenance of dental health. However, some health hazards have been associated with the ingestion of high concentrations of fluoride via drinking water. The absorption of fluoride ions, its distribution to the tissues and bio-accumulation in bones and teeth results in many well-recognized adverse effects. According to a UNICEF report, tens of millions of people have endemic fluorosis in 25 countries globally; especially countries in volcanic areas (Petrone et al., 2013). Fluorosis emanating from excess presence of fluoride in drinking water is a serious issue worldwide as it was reported that > 35 countries worldwide have excess of fluoride in drinking water (Ayoob et al., 2008) (see Fig. 1). Most of the countries highlighted in Fig. 1 are situated in regions with from sediments of marine origin, volcanic rocks and granitic and gneissic rocks such as those in the geographical line extending from Jordan valley to Eastern Africa and central Asia trough the Mediterranean region (Fawell et al., 2006). Other health effects related to consuming high fluoride concentrations (higher than 1.0 mg/L) are effects on the immune and human reproductive systems, children's neurodevelopment, kidney and gastrointestinal tract health (Harrison, 2005). Furthermore, it was reported that fluoride can form strong bonds with other toxic metals such as aluminum and lead, altering the toxicity of the substance when digested (Jackson et al., 2002). Therefore, much research effort was focused on developing technologies for fluoride removal from aqueous media in order to reduce its concentrations to levels below 1.5 mg/L, which is the current WHO and Australian guidelines limit for F^- in drinking water (Fawell et al., 2006).

Some of the methods used to remove fluoride from water include co-precipitation (Chigondo et al., 2018), precipitation-coagulation (Ye et al., 2018), electrocoagulation (Changmai et al., 2018; Zhu et al., 2007), adsorption (Mourabet et al., 2015; Wang et al., 2013), ion exchange (Meenakshi et al., 2008) and membrane processes (Jeihanipour et al., 2018; Lhassani et al., 2001; Pan et al., 2018), or a combination of these technologies (Wei et al., 2015; Zhang and Jia, 2018). However, these methods have issues including high operating cost, waste production, strict pH and other experimental conditions and the use of toxic chemicals, all of which are limiting factors for their use in water defluoridation. Of all these methods, adsorption has been reported to be the most promising method for the removal of fluoride from water due to the high removal efficiency, superior adsorption rate, ease of operation and the availability of a wide range of adsorbents. Among many different types of adsorbent materials including activated carbon (Raychoudhury et al., 2017), cellulosic materials (Nagaraj et al., 2017), zeolites (Abaei et al., 2017; Lai et al., 2018), aluminum (Karmakar et al., 2017), nanomaterials (Maity et al., 2018; Rostamia et al., 2017), biochars (Dewage et al., 2018; Roy, 2018; Wang et al., 2018) and bone char (Delgadillo-Velasco et al., 2017; Ismail and AbdelKareem, 2015; Medellin-Castillo et al., 2007). Bone char has gained considerable attention owing to its low cost, ease of preparation and biocompatibility (Nunes-Pereira et al., 2018).

This work aims to review bone char's removal capacity of fluoride from water, with the main focus of providing a comprehensive overview of bone char preparation, modification techniques and their respective fluoride removal efficiencies. The effect of several parameters, such as pH, initial concentration, bone char dosage rate and temperature, on fluoride uptake will be discussed. These factors are of great significance, as any change in these parameters may significantly alter the fluoride removal efficiency of the adsorbent. Therefore, a general knowledge of the effect of these parameters is critical in designing the appropriate drinking water treatment facilities. Cost of bone char production, successful industrial bone char treatment attempts and design aspects were also discussed in this study.

2. Bone char production and characteristics

Globally, millions of tons of bone waste are produced annually due to the meat industry. According to the Organisation for Economic Co-operation and Development (OECD) reports (OECD, 2018), it is expected that there will be an increase of 40 million metric tons in meat

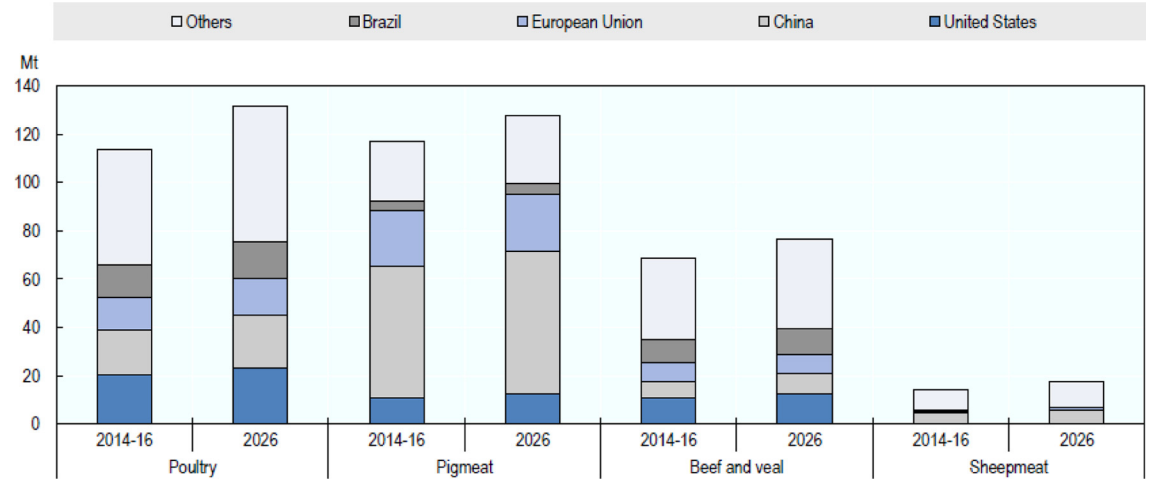

Fig. 2. Meat production by type and country (OECD, 2018).

production within the next ten years, including 13% in poultry, 10% in pig meat and > 21% in sheep meat. As a consequence, there will be a significant increase in meat and bone meal waste produced globally. Fig. 2 shows meat production statistics between 2014 and 2016, and the expected increase in meat production by 2026 in some countries. It is important to highlight here that in spite of the expected increase in waste bone, its application for defluoridation can be hampered by the customs and religious beliefs of people (e.g. char originated from cow bones is not acceptable by Hindus and similarly pigs bone char is not acceptable by Muslims). Thus, educating communities is essential for applying bone char for defluoridation.

The similarity in the bone structure of poultry and red meat species (Field et al., 1974) makes harnessing bone waste for fluoride removal a topic of interest globally as some countries may consume a certain type of meat more than others as shown in Fig. 2. However, it is important to note that the bone structure of a certain animal species may differ with age and parity (Field et al., 1974; Keene et al., 2004). The bone structure can also differ from one part to another in the animal body. Interestingly, it was found that calcium to nitrogen ratio increased in bones with age for red meat species and poultry (Field et al., 1974) and this may serve well fluoride removal given the capacity of calcium in binding with fluoride (Meenakshi et al., 2008).

Thermal treatment of animal bones is one of the methods used for safe disposal of bone waste through incineration, to ensure destruction of any pathogens. This process is mainly carried out through co-incineration in cement kilns, or by stand-alone incineration plants. However, attention to energy recovery from waste and environmental benefits of the process have attracted the attention of many researchers in order to provide a clean energy source as an alternative to fossil fuel (Usón et al., 2013). Bone char is considered as one of the adsorbents with low negative impact on the environment and human health as oppose to other waste-based adsorbents such as aluminum oxide amended wood char and activated alumina (Yami et al., 2015). The ability of regenerating bone char is an attractive trait and it makes the char a promising green sorbent for water defluoridation. However, the lifespan of bone char can only be estimated based on several factors such as F^- initial concentration, the capacity of the plant and the removal capacity of the bone char (Naliaka, 2016). The regeneration aspect of bone char will be explained in detail in Section 6.

Combustion in a limited oxygen environment through pyrolysis and gasification has been adopted in recent years for the purpose of energy generation from bone waste and use of the solid product (bone char) for environmental remediation and soil amendment applications. For maximizing the energy recovery of bone char production, gasification would be the preferred method as the produced syngas can be used as fuel to power gasification reactor. Limited number of studies have investigated this approach and were successful in producing syngas and bone char (Soni et al., 2009, 2011). However, the focus of these studies was on increasing the amount of gases produced with high heating values and bone char was only a by-product. To have a balanced approach perhaps a multi-factor optimization of gasification process taking into account energy consumed, gas produced, heating value of the gases and bone char produced should be conducted to identify the optimal operating parameters for this process.

Appetites are minerals that are widely distributed in igneous rocks. Bioapatite is the biological form of inorganic calcium phosphate salts (Liu et al., 2013) with a general formula of $Ca_5(PO_4,CO_3)_3(OH,F,Cl,CO_3)$ (Skinner and Jahren, 2004). Bone apatite is a carbonate apatite with 6–9% carbonate composition in the apatite structure (Ishikawa et al., 2018). However, bone sintering process leads to change the form of apatite minerals in bones to hydroxyapatite (HAP). Figueiredo et al. (2010) examined the effect of calcination temperature on the apatite form using bovine bones reporting that bone char samples produced up to 600 °C were made of carbonate apatite, while raising the temperature up to 900 and 1200 °C resulted in the formation of HAP. Thus, the amount and the form of apatite content of a bone char is related to the charring temperature and thermal treatment period.

Bone char has long been used as an absorbent for decolorization in the sugar industry (Kader et al., 1996). It has high pollutant removal efficiency attributed to its principal characteristics represented by the textural properties of bone char and the hydroxyapatite content. Bone char is made of 70–76% hydroxyapatite (HAP), 7–9% calcium carbonate and 9–11% amorphous carbon (Mendoza-Castillo et al., 2015; Reynel-Avila et al., 2016; Rojas-Mayorga et al., 2015a). However, in a different scenario, bone char was reported to be made of 80–90% HAP and 10% amorphous carbon (Lambert and Graham, 1989). Hydroxyapatite ($Ca_{10}(PO_4)_6(OH)_2$), which is an inorganic material, was reported as an advantageous material due to its applications in electrochemistry (Goodman et al., 2013), as a catalyst (Mohamed and Baeissa, 2013; Xie et al., 2013), and for environmental remediation (Li et al., 2018; Oladipo and Gazi, 2017; Thanh et al., 2017).

Carbonization of crushed animal bones includes heat treatment of a carbonaceous precursor at temperatures mainly higher than 500 °C and below 700 °C (Cheung et al., 2001b), in a limited oxygen environment to pyrolyze the raw material into a porous material (Cheung et al., 2001a). In such a process, partial evolution of the volatile matter from the carbonaceous precursor will take place. Further increase in pyrolyzation temperature exceeding 700 °C will alter the physical properties of the bone char. Rojas-Mayorga et al. (2015a) reported that after raising the temperature from 650 °C up to 1000 °C, a gradual color changing of the bone to white was noticed, which indicates the

Table 1
The effect of charring temperature and heating rate on the bone char surface properties and fluoride uptake (residence time = 2 h).

Factors		Effect			Purging gas	Reference
Temperature (°C)	Heating rate (°C/min)	BET surface area (m^2/g)	Total pore volume (cm^3/g)	Fluoride uptake (mg/g)		
650	5	–	–	6.7	N_2 gas	Rojas-Mayorga et al. (2013)
	10	118	0.24	6.51		
700	5	–	–	6.96		
	10	110	0.233	7.32		
800	5	–	–	6.67		
	10	–	0.224	6.71		
900	5	–	–	2.99		
	10	–	–	3.03		
1000	5	–	–	1.34		
	10	–	–	1.24		
650	5	–	–	5.52 ± 0.08	CO_2 gas	Rojas-Mayorga et al. (2015c)
	10	62	0.2	5.33 ± 0.14		
700	5	–	–	5.78 ± 0.05		
	10	69	0.3	5.92 ± 0.03		
800	5	–	–	0.74 ± 0.13		
	10	9	0.16	0.81 ± 0.02		
900	5	–	–	0		
	10	4	0.04	0		
1000	5	–	–	0		
	10	2	0.02	0		

complete elimination of the organic matter in the bone char structure. Kawasaki et al. (2009) reported that high pyrolysis temperature results in the degradation of the functional groups and lowering the efficiency of water defluoridation.

Calcination temperature has a great effect on the surface area and pore volume of bone char. For instance, raising calcination temperature from 650 °C to 700 °C under a CO_2 atmosphere resulted in an increase of the specific surface area from 62 to 69 m^2/g and the total pore volume from 0.2 to 0.23 cm^3/g of cow bone char, respectively (Rojas-Mayorga et al., 2015a). However, further increase in the temperature to 1000 °C reduced the surface area and the pore volume of the material to 2 m^2/g and 0.02 cm^3/g; and altered the color of the bone char to white. The latter was used as an indication for fluoride removal capacity of the bone char, which was reduced from 5.92 to 0 mg/g after raising pyrolysis temperature from 700 to 900 °C. Tables 1 and 2 show the effect of charring temperature at different residence times and heating rates on the BET surface area of bone char.

Pyrolyzing conditions are critical factors that affect the textural and chemical composition of bone char. Residence time and heating rate are essential factors to control the quality of the bone char produced at different temperatures. Generally, based on the bone source, pyrolysis between 500 and 700 °C seems to be a critical pyrolysis temperature for bone char used for water defluoridation (taking into account the limitations related to the residence time and the rate of temperature). Lowering the temperature below 500 °C will result in adding more organic matter to the treated water due to the incomplete removal of organic matter in the bone structure. On the other hand, raising the charring temperature will result in the dihydroxylation of the HAP. Table 1 presents a summary of the outcome of previous studies on the effect of temperature and heating rate on bone char properties.

Purging gas used during pyrolysis is an important factor in controlling bone char quality for different environmental applications. Rojas-Mayorga et al. (2015a) examined the effect of pyrolyzed cattle bone in CO_2 and N_2 atmospheres for the purpose of fluoride removal from water. While both samples were exhibiting a mesoporous structure, bone char samples pyrolyzed in an N_2 environment had higher specific surface area and total pore volume of 85 m^2/g, 0.24 cm^3/g than those pyrolyzed at the same temperature, residence time and heating rate with CO_2 as a purging gas (Tables 1 and 2). Although the removal of F^- on the bone char surface was due to their exchange with OH functional groups (i.e. chemical reaction), the increase in the surface area and the pore volume was vital in providing a higher contact possibility of F^- with the active functional groups.

Bone source and calcination temperature may have an effect on the FTIR signals received from bone chars, but the main components of bone char are well defined. The inorganic components (calcium and phosphate) of any bone char are reported to be almost the same but with different fractions (Tovar-Gómez et al., 2013). FTIR spectra of bone char pyrolyzed at different temperatures are always those of typical hydroxyapatite but with varying peaks intensity (Fig. 3). Tovar-Gómez et al. (2013) examined two commercial bone chars, namely BCM from Carbones Mexicanos (Mexico) and BCB (Brimac 216) from Brimac Carbon Services (United Kingdom), for their fluoride uptake capacity using both bone char dispersion in the medium (henceforth referred to as batch) and column experiments. The study suggested that the higher removal capacity of the BCM than BCB samples related to their chemical composition. The higher oxygen and hydrogen content (consequently, hydroxyl groups) for the BCM samples were the reason behind its higher adsorption capacity of fluoride as illustrated in Eq. (1):

$$Ca_{10}(PO_4)_6OH + 2F^- \rightarrow Ca_{10}(PO_4)_6F_2 + 2OH^- \quad (1)$$

2.1. Removal mechanism

As mentioned previously, the effectiveness of bone char for fluoride removal is due its hydroxyapatite content. The removal mechanisms of fluoride on bone char is illustrated in Fig. 4. As it can be seen from this figure that there are three removal mechanisms; ion exchange, precipitation and electrostatic interaction (Sternitzke et al., 2012) or a combination of these mechanisms.

The ion exchange is the main mechanism of F^- due to the high affinity of F^- to substitute the hydroxide group in the structure of the HAP to form the fluorapatite ($Ca_{10}(PO_4)_6F_2$). However, the electrostatic interaction between the bone char surface and the F^- plays an important role in the removal process. This mechanism is affected by the changes in the pH of the solution, in which it controls the isoelectric point of the bone char surface and hence affects its electrical attraction to entities in proximity to it. At pH levels below the point of zero charge (this will be discussed further in Section 3.3), the surface of the bone char is positively charged and this will increase the affinity of the

Table 2
The effect of charring temperature and residence time on the bone char surface properties and fluoride uptake (heating rate = 10 °C/h).

Factors		Effect			Purging gas	Reference
Temperature (°C)	Residence time (h)	BET Surface area (m^2/g)	Total pore volume (cm^3/g)	Fluoride uptake (mg/g)		
200	1	2	–	2.55[a]	Limited O_2	Terasaka et al. (2014)
400	1	114	–	2.85[a]		
600	1	73	–	1.65[a]		
650	2	118	0.24	6.51	N_2 gas	Rojas-Mayorga et al. (2013)
	4		–	6.63		
700	2	110	0.233	7.32		
	4		–	7.16		
800	2	96	0.224	6.71		
	4	–	–	6.57		
900	2	–	–	3.03		
	4	–	–	3.01		
1000	2	–	–	1.24		
	4	–	–	1.25		
650	2	62	0.2	5.33 ± 0.014	CO_2 gas	Rojas-Mayorga et al. (2015c)
	4	–	–	5.45 ± 0.06		
700	2	69	0.3	5.92 ± 0.03		
	4	–	–	5.72 ± 0.09		
800	2	9	0.16	0.81 ± 0.02		
	4	–	–	0.67 ± 0.08		
900	2	4	0.04	0		
	4	–	–	0		
1000	2	2	0.02	0		
	4	–	–	0		
400	1	98.626	0.291	–	Limited O_2	Patel et al. (2015)
	2	114.149	0.294	–		
	3	92.402	0.315	–		
450	1	98.138	0.305	–		
	2	83.948	0.302	–		
500	1	78.172	0.294	–		
	2	69.788	0.321	–		
600	1	57.939	0.293	–		
	2	50.37	0.305	–		

[a] Data were calculated from the figures and the data available in the article.

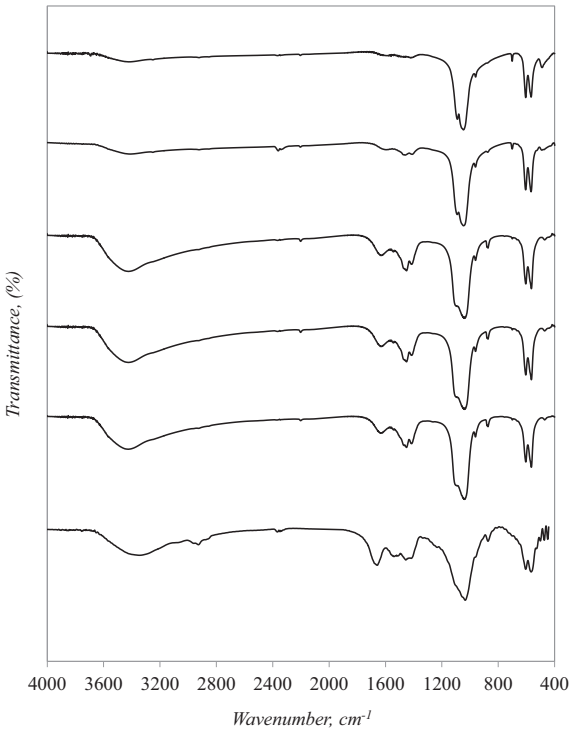

Fig. 3. FTIR spectrum for raw bone and bone char samples pyrolyzed at different temperatures: (a) raw bone, (b) 650 °C, (c) 700 °C, (d) 800 °C, (e) 900 °C and (f) 1000 °C (Rojas-Mayorga et al., 2013).

negatively charged F^- ions to adsorb onto the char. The formation of fluoride precipitants on the surface of the bone char takes part with high F^- concentrations (Herath et al., 2018) or in the case of metal coated bone char with cations such as Al^{3+}, Fe^{3+} etc. In this case, precipitants such as CaF_2, AlF_3 or FeF_3 will be formed on the char surface (Nigri et al., 2017b; Rojas-Mayorga et al., 2015b; Zhu et al., 2011). So, the prominence of the mechanisms in the removal process depends on the characteristics of the water being treated (e.g. pH and fluoride concentration).

2.2. Bone char modification

Suitable activation methods can lead to improve the adsorption capacity of carbonaceous materials via increasing the surface area, pore volume or providing a diversity of pore sizes to the adsorbent; or altering surface functional groups in a way that increases the selectivity of the adsorbent toward specific contaminants. However, bone char examinations after different modification methods indicate that there are no significant increments in the surface area (Delgadillo-Velasco et al., 2017). Thus, considerations regarding improvement in adsorption capacity of bone chars are mostly related to altering the functional groups on the surface. Table 3 summarizes the effect of different modification methods and experimental conditions on the removal capacity of F^- on bone char samples. Zúñiga-Muro et al. (2017) doped two different cerium precursors (Ce^{3+} and Ce^{4+}) onto cattle bone char for enhancing fluoride removal from water. The composite was reported to be beneficial for its stability for different pH ranges and potential antibacterial properties. The results showed a significant increase in the removal capacity of F^- on the Ce^{4+} modified bone char from 5.47 to 13.6 mg/g at pH 7. The acidic characteristic of the cerium

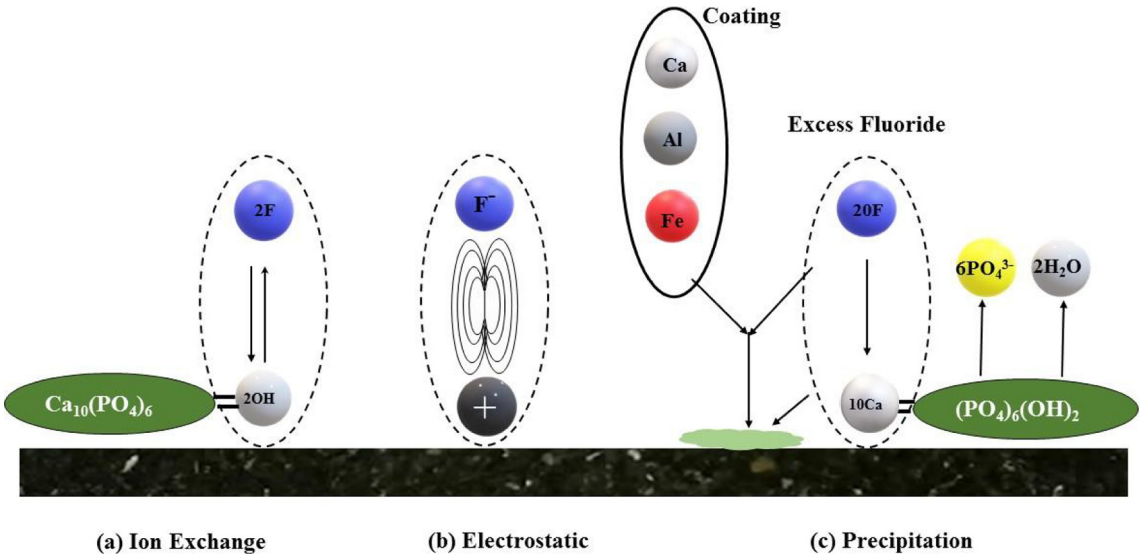

Fig. 4. Mechanisms of fluoride removal on bone char.

solution resulted in the dissolution of hydroxyapatite and release of phosphate to solution, which reacted with the cerium precursors and subsequently precipitated on the adsorbent surface. Then, an ion exchange between the calcium content of the HAP and the cerium precursor was the main mechanism behind the removal of fluoride ions on the modified bone char. On the other hand, the Ce^{3+} doped bone's ability to remove fluoride from water was lower than that of the pristine bone char in some cases due to the dissolution of Ce^{+3} in the washing stages. As a consequence, the adsorbent lost the active calcium and cerium sites after being washed out from the char surface at pH 7.

Zhu et al. (2011) used cattle bone char after modifying it with different aluminum salts ($AlCl_3$, $AlNO_3$, $NaAlO_2$, $Al_2(SO_4)_3$) to remove fluoride from water. The maximum removal onto $AlCl_3$ modified bone char was 97% at pH 7, for a 10 mg/L F^- initial concentration, 10 g/L adsorbent dosage and 72 h contact time. Similarly, bone char modification using $AlCl_3.6H_2O$ resulted in a maximum removal capacity of 6.8 mg F^-/g bone char from water (Nigri et al., 2017b), while bone char pre-treatment with $Ca(OH)_2$, $FeCl_3$, $CaCl_2$ and $MgCl_2$ were reported to be less effective for fluoride removal (4.4, 1.56, 5.1 and 4.2 mg/g, respectively). Rojas-Mayorga et al. (2015c) examined the effect of doping aluminum sulfate onto bovine bone char (pyrolyzed at 700 °C) for fluoride removal from water using packed bed micro-columns. The bed capacity to remove fluoride was 3.3–18.5 mg/g at pH 7, F^- feed concentration 10–100 mg/L and feed rate of 0.18–0.36 L/h. The Al doped bone char removed about 500% fluoride more than the commercial bone char samples used by Tovar-Gómez et al. (2013), but with different column dimensions and experimental conditions. Bone char coated with aluminum sulfate was examined for its effectiveness by comparing it to another 3 metal salts for fluoride removal from water in a batch reactor (Rojas-Mayorga et al., 2015b). Different metals ($Al(OH)_xF_y$, Fe_xF_y, and CaF_2) doped onto the bone char surface contributed significantly to the improvement of the removal efficiency. The maximum adsorption capacity achieved was 31 mg/g using aluminum sulfate doped bone char at pH 7 and 100 mg/L initial F^- concentration. In contrast, the maximum removal on the unmodified bone char was only 7.32 mg/g (Rojas-Mayorga et al., 2013), which means that there was a significant improvement in the removal capacity of fluoride ions from solution after modification. Chatterjee et al. (2018) used aluminum sulfate in combination with calcium oxide to chemically treat carbonized bone meal (a mixture of chicken and cattle bones) for fluoride removal at high initial concentrations (20–1000 mg/L). The new modified bone char resulted in enhancing the removal capacity of fluoride from 14 to 150 mg/g. Delgadillo-Velasco et al. (2017) studied the effect of doping colloidal Ag onto commercial bone char samples at different temperatures (300, 400 and 500 °C) for fluoride removal from water. The results showed that the thermal treatment at 400 °C was the most appropriate temperature for bonding Ag colloids to the bone char surface. However, thermal treatment of bone char at the same temperature showed that the increase in fluoride uptake on the bone char with and without Ag colloids are almost the same (about 20% more than the untreated bone char), but the antibacterial effect of doping Ag was a new characteristic for the composite. The thermally treated commercial bone char resulted in removal of 1.65 mg/g fluoride from solution, owing to the irreversible loss of lattice water and its effect on the lattice dimension of the hydroxyapatite in the temperature range 200–400 °C. Another explanation for this improvement in F^- removal was due to the dehydration of the hydroxyapatite after the thermal treatment of the bone char, which was considered to be equivalent to the effect of charring bone samples at 850 °C in which the dislocation of lattice will occur (Liao et al., 1999). Eq. 2 shows the OH group loss due to thermal treatment of hydroxyapatite (Rojas-Mayorga et al., 2013):

$$2Ca_5(PO_4)_3OH \rightarrow Ca_{10}(PO_4)_6(OH)_{(2-2x)}O_x\square_x + xH_2O \quad (2)$$

where □ represents a vacancy. It is clear from the observations on bone char modification that such a practice can improve the char absorptivity of F^-, however the extent of improvement varies from one element to another. Fluoride ions in solution will be highly attracted to multivalent metal ions (such as aluminum, iron, zinc etc.) owing to their small size and high electronegativity (Tchomgui-Kamga et al., 2010). Thus, the difference in the electronegativity of the used multivalent metal ions are the main reason behind their higher removal capacity of some metal ions. For instance, the higher difference in electronegativity between fluoride and Al(III) than that with Fe(III) resulted in higher removal capacity of fluoride ions from solution with Al(III) coated bone char.

2.3. Bone char treatment cost for industrial scale systems

Bone char was reported as an adsorbent for water defluoridation since 1937 (Dahi, 2016), while the first full-scale defluoridation plant using bone char was constructed in South Dakota in 1953 followed by several others distributed over different locations in California. Groundwater that was treated in these plants contained F^- concentrations of 9–12 mg/L (State of South Carolina Department of Health and Environmental Control Water Supply Division, 1980). In 1988, household scale bone char filters, with incorporation of charcoal, were

Table 3
Removal capacity and experimental conditions for fluoride removal on bone char.

Bone Char	F^- removal mg/g	pH	Initial concentration mg/L	Charring temperature °C	Surface area m^2/g	Pore volume cm^3/g	Contact time	Isotherm model	References
Cattle BC	11.9 2.71	3.0 7.0	1–20	_	104	_	2–3 d	Langmuir and Freundlich	Medellin-Castillo et al. (2007)
Commercial BC	7.74	5.0	1–20	_	104	_		Langmuir, Freundlich and Radke-Prausnitz	Medellin-Castillo et al. (2014)
HAP	11.1	7.0		_	62.9				
Fish BC	2.15 ± 0.121			300 °C	24.2 ± 2.19	_	1 h	Langmuir and Freundlich	Brunson and Sabatini (2009)
Fish BC	5.01 ± 0.015			400 °C	98.7 ± 0.3				
Fish BC	4.85 ± 0.025			500 °C	111 ± 1.63				
Fish BC	3.89 ± 0.230			600 °C	112 ± 2.29				
Cow BC	5.96 ± 0.322			400 °C	110 ± 1.35				
Commercial BC	2.72		2–200		_	_	20 h	Langmuir and Freundlich	Sani et al. (2016)
0.1 M HCL washed cow BC	6.2	7.7 ± 0.2	10	700–800	138.8	0.308	50 h	Langmuir and Freundlich	Nigri et al. (2017a)
Al-impregnated cow bone char	6.3	6.4 ± 0.3							
Ox BC	0.64	8.4–11.3	0.26–1.05 mmol/L	580	_	_	24 h	_	Larsen et al. (1993)
Commercial BC		4.9–9.2	0–20	_	_	_	3 h	Freundlich	Abe et al. (2004)
Al modified cattle BC	0.97	7	2–20				72 h	_	Zhu et al. (2007)
Commercial BC		7	1–20	_	104	0.3	2d	Langmuir, Freundlich and Prausnitz-Radke	Leyva-Ramos et al. (2010)
Cattle BC modified with Ce^{+4}	13.6	7	10–300	700 under N_2	_	_	840 min	Langmuir, Freundlich and Sips	Zúñiga-Muro et al. (2017)
BC for synthesized water	0.056	7.6	1–6	500–600	_	_	10 h	Langmuir and Freundlich	Smittakorn et al. (2010)
BC for field groundwater	0.157		3.5						
Commercial BC	0.8	_	5–50	_	65	0.098	72 h	_	Delgadillo-Velasco et al. (2017)
Ag doped thermally treated BC	1.28			400	59	0.109			
Cow BC	7.32	7	10–50	700	110	0.233	24 h	Langmuir and Freundlich	Rojas-Mayorga et al. (2013)
Cow BC under CO_2 environment	5.92 ± 0.03	7	5–80	700	69	0.23	24 h	_	Rojas-Mayorga et al. (2015c)
Cow BC under NO_2 environment	7.32				85	0.24			
Al doped cow BC	3.3–18.5	7	10–100	700	85	_	_	_	Rojas-Mayorga et al. (2015a)
Al sulfate doped BC	31	7	10–100	700	_	_	_	Langmuir	Rojas-Mayorga et al. (2015b)
Carbonized bone meal (CBM)	14	6.1	20–1000	550	58	0.01	24 h	Langmuir, Freundlich and Dubinin-Radushkevich	Chatterjee et al. (2018)
Chemically treated CBM	150				110	0.3			
Cuttlefish BC	0.283	4.5	2.5–10	_	0.07 ± 0.002	_	60 min	_	Nasr et al. (2011)
Carbones Mexicanos BC	2.26–5.0	7	9–40	_	104	_	1.5–3.0 min	Langmuir, Freundlich and Sips	Tovar-Gómez et al. (2013)
Brimac 216 BC	0.47–2.47				129				

used for water defluoridation in Thailand (Phantumvanit et al., 1988). Bone char filters were also used in many areas affected by high F^- concentrations in water sources in Tanzania and Kenya. One of the most efficient plants were constructed in Nakuru city to serve the city and the surrounding areas through the work of four different types of filters with different capacities ranging from 10 to 2,000,000 L/day (Näslund and Snell, 2005). With regards to the removal capacity of large scale bone char systems, a study conducted by Yami et al. (2015) showed that 496 kg bone char/100 m^3 water is required for reducing F^- concentration from 10 to 1.5 mg/L. Generally, the main cost elements of water treatment facilities are capital cost and operation and maintenance cost. Hansen et al. (1979) estimated the cost of constructing a water defluoridation system to range from ~$55,380 USD to ~$168,620 USD (about $192,008.41 to $584,623.66 USD in 2019 after adding the inflation, respectively) for a plant capacity of 2.57 and 126 m^3/h, respectively. Thereby the operation cost was reported to be ~$9180 USD to ~$25,010 USD (about $31,828.05 and $86,721.36 USD in 2019 after adding the inflation, respectively) for the same plants.

It seems that there is limited scientific detailed reports on the cost estimation for bone char production on a large scale, and what is available is confined to limited commercial reports. This can be attributed to the fact that the cost of the production is subjective and depends on various factors that are location specific in nature such as capital cost, availability and cost of labor, raw materials etc. Arrenberg (2010) reported that the cost of producing five tons of bone char (using mainly, goat, camel, cattle and sheep bones from different suppliers) by CDN's company was estimated to be $1609.87 USD (about $1858.35 in 2019 after adding the inflation). The cost of production included the energy consumption, cost related to materials and chemicals, and labor salaries, which represents about 20.6, 58.6 and 20.8% of the total cost, respectively. The recent cost figures for bone char production can be inferred from the available market sale prices as advertised by commercial companies. Surely the cost of production would be less than the sale prices or have been compensated by the energy gain from other product of the bone pyrolysis (i.e. useful gases produced from gasification). The recent advertised price of 25 kg of bone char produced from cow bones at 800 °C is $299 USD (~$12 USD/kg) (Bulk Bone Char® Promolife Inc), while the same amount of cattle bone char can cost about $1.2 USD based on Alibaba online company price (only big bulk orders of 20 metric tons at least) (Alibaba.com). This shows that bone char cost can be very low if it is produced on a large scale.

3. Effect of adsorption parameters

3.1. Equilibrium contact time

Adsorption equilibrium is the period of time in which adsorption and desorption processes reach equilibrium. In other words, the amount of the adsorbed material from the solution is equal to the amount of the desorbed material from the adsorbent (Çeçen and Aktas, 2011). Equilibria data is essential for assessing adsorption process, characterizing an adsorbent, examining the removal capacity of the adsorbate and the respective rate of adsorption for their application in industrial processes (Leyva-Ramos et al., 2010).

Adsorption of fluoride on bone char has been shown to follow a general trend of adsorption in which the removal capacity is fast at the beginning of the reaction owing to the availability of large numbers of active sites on the surface. Then, adsorption rate slows down gradually until the equilibrium is reached. Leyva-Ramos et al. (2010) studied the rate of fluoride adsorption on bone char in terms of diffusional and kinetic models reporting that the rate of fluoride removal is mainly controlled by the pore volume. In contrast, Abe et al. (2004) reported that the removal of fluoride ions from solution is due to the ion exchange between the phosphate dissociated from the calcium phosphate composition of bone char at low pH levels and fluoride ions in solution.

Fluoride adsorption rates for different bone chars were reported to reach equilibrium in the range of 20 h to 5 days, which is a long period when considering fluoride removal for industrial applications. Zúñiga-Muro et al. (2017) determined the removal rate of fluoride ions onto cow bone char, based on the results achieved using a pseudo second order equation, to range between 2.3×10^{-3} and 4.89×10^{-3} g/mg min. This result is comparable to the results reported by Rojas-Mayorga et al. (2013) (from 8.02×10^{-4} to 2.94×10^{-3} g/mg min) and to a lesser extent Rojas-Mayorga et al. (2015b) (from 1.71×10^{-5} to 3.11×10^{-5} g/mg min) for an equilibrium time of 24 h to remove fluoride using cow bone char and Al doped bone char, respectively, using the same kinetic model, but with different experimental conditions.

Chatterjee et al. (2018) reported a very rapid reduction in fluoride concentration in solution from 10 to 0.13 mg/L in 1 h (about 98.7%) using aluminum sulfate and calcium oxide thermally treated bone meal. Equilibrium reached after 24 h with a removal efficiency of 99.6%. The difference in the column dimensions, inter-bead voids, flow rate and hydrodynamic effects are the key factors to control the removal capacity of a contaminate. Issues related to the non-uniform void ratio through column filtration will affect the efficiency of the columns. Generally, increasing the number of beds in a column provides more active sites for contaminants to settle and a higher break through curve, which are due to the increase in the mass transfer zone. However, increasing the number of beds will also be accompanied by the use of longer columns and thus providing channeling issues and accordingly reducing the efficiency of filtration.

3.2. Effect of initial concentration and adsorbent dose

It is essential to examine the effect of changing the solute initial concentration in an adsorption process to find out the optimum conditions for substance uptake. Up to a certain limit, the removal percentage (removal efficiency) of fluoride ions on bone char increases with increasing fluoride initial concentration. Then, no more adsorption will take place owing to the limited vacant sites available for adsorbate particles. This may be explained based on the Fickian definition, which suggest that the gradient of the concentration is the driving force for molecular transport in solution (Ruthven, 2008). Smittakorn et al. (2010) examined the influence of raising fluoride initial concentration on the removal efficiency a homemade bone char using synthetic water (1–6 mg/L) and field water samples (3.5 mg/L). Their findings revealed that both samples have almost the same removal capacity (0.130 and 0.157 mg/g, respectively) at 3.5 mg/L initial F^- concentration regardless to the availability of other ions in the field ground water, whilst F^- uptake declined after increasing the initial concentration to 6 mg/L (for the synthetic samples). In contrast, (Nasr et al., 2011) reported that increasing initial concentration from 2.5 to 10 mg/L resulted in a slight decrease in the adsorption capacity of cuttlefish bone char from 80% to 78% using a 15 g/L adsorbent dose and 1 h contact time. Increasing the bone char dose from 5 to 15 g/L enhanced the char uptake from 40 to 85%, but no more significant increases were noticed above 15 mg/L. Nevertheless, determining the removal capacity of the unit weight of the bone char shows that it removed fluoride of about 0.283 mg/g, which is less than the removal capacity of a thermally regenerated bone char (Kaseva, 2006). Similarly, Zhu et al. (2007) reported a removal capacity of 97% of F^- on Al doped cattle bone char at 1 mg/L F^- initial concentration and 10 g/L adsorbent dosage. The removal efficiency in this case is not representative of the adsorbent intake as it is equivalent to 0.97 mg/g F^- uptake, which is again less than the fluoride adsorption capacity of a commercial bone char (Leyva-Ramos et al., 2010; Medellin-Castillo et al., 2014; Medellin-Castillo et al., 2007). It is convenient to remark that adsorbent ability to uptake contaminants should be explained in unit weight of the substance adsorbed per unit weight of the adsorbent. This means, that the effect of initial concentration needs to be compared based on the adsorbent dose used in the experiments.

The percentage removal shows misleading results as it does not show the amount of adsorption sites occupied by the adsorbate. Different experimental conditions represented by the initial concentrations and bone char dose can significantly alter the results of F^- removal on bone char. For instance, Nasr et al. (2011) used 15 g/L bone char for the removal of 2.5–10 mg/L fluoride, which represents a high dose compared to the literature. Thus, the availability of more active sites on the adsorbent surface in solution eliminate the effect of the driving force due to the concentration gradient.

The effect of adsorbent dose was examined by Larsen et al. (1993) to remove 9.88 mg/L F^- from water using Ox bone char pyrolyzed at 580 °C. Increasing the bone char dose from 2.5 to 7.5 g/L resulted in decreasing fluoride concentrations in solution from 8.55 to about 5.5 mg/L. Sani et al. (2016) reported that fluoride removal efficiency increased significantly from 63.2 to 86.7% after increasing bone char dose from 4 to 10 g/L in batch experiments, but a contrary result where reported after calculating the uptake of fluoride per unit weight bone char 1.58 and 0.87 mg/g. This outcome is an indication for the reduction in the active sites available for occupying more F^- at higher solution concentrations.

3.3. Effect of pH value

Although most studies have examined fluoride removal from aqueous solution on bone char in neutral pH ranges (Leyva-Ramos et al., 2010; Nigri et al., 2017b; Zhu et al., 2007), the adsorption capacity of fluoride can be greatly influenced by change of pH range in the solution. The point of zero charge (pH_{PZC}), which represent the pH value at which the surface charge is zero, for bone char samples from different origins is reported to range between 7.4 and 10 (Ip et al., 2010; Medellin-Castillo et al., 2007; Nigri et al., 2017b). Medellin-Castillo et al. (2014) examined the effect of ionic strength on pH_{PZC} of a commercial bone char using 0.01 and 0.1 M NaCl. The results showed that increasing the ionic strength resulted in the raising the surface charge of the BC, but that the isoelectric point was not affected (pH_{PZC} = 8.4). In contrast, Dimović et al. (2009) reported that raising charring temperature will result in the raising of the surface charge and thus, the pH_{PZC} value from 7.37 to 10. Fluoride removal capacity will increase due to the interaction between the positively charged bone char surface (below pH_{PZC}) and negative fluoride ions. However, at very low pH values (< 3), bone char dissolution will occur and P will be released into the solution (Larsen et al., 1993) according to eq. (3) (Warren et al., 2009):

$$Ca_5(PO_4)_3OH + 7H^+ \rightarrow 5Ca^{2+} + 3H_2PO_4^- + H_2O \quad (3)$$

Bone char surface washing with acid solutions can enhance the removal capacity due to the protonation of the functional groups of the HAP at pH values lower than pH_{PZC} (as they mainly are > 7). Accordingly, protonation reactions will provide a positive charge to the surface and increase the affinity of F^- to the surface. Nigri et al. (2017b) reported that a maximum removal of 6.2 mg/g of F^- was achieved after washing a commercial bone char with 0.1 M HCl owing to the increase in the positive surface charge. Surface protonation followed the equations below (Medellin-Castillo et al., 2014):

$$\equiv P - OH + H^+ \rightarrow \equiv POH_2^+ \quad (4)$$

$$\equiv Ca - OH + H^+ \rightarrow \equiv Ca - OH_2^+ \quad (5)$$

Medellin-Castillo et al. (2007) investigated the impact of different pH values (3, 5, 7, 10, 11 and 12) on F^- removal from water using commercially produced granular cattle bone char (Fija Fluor) with a specific surface area of 104 m^2/g. The pH_{PZC} was reported to be about 8.4. Therefore, the maximum removal capacity (2.71 mg/g) at an initial F^- concentration of 1 mg/L was achieved at a low pH value (3.0). In addition, the authors found that the bone char removal capacity is 1.3 times smaller than a polymeric resin and greater than activated aluminum and activated carbon by 2.8 and 36 times, respectively. Similarly, Abe et al. (2004) reported that there is a negative relationship between pH levels in solution and F^- removal capacity on bone char. A maximum F^- removal of 82% onto bone char surface was achieved with pH 4.6 (at 20 mg/L initial F^- concentration) when examining the effect of pH onto F^- removal capacity in the range between 4.6 and 9.2. It is noteworthy that, the surface charge of the adsorbent can significantly alter the removal capacity of fluoride on bone char. pH change affects the two adsorption mechanisms, i.e. electrostatic interaction and the chemical interaction resulting from the bone dissolution. Thus, shifting pH_{PZC} to acidic levels by altering the surface properties will provide a higher removal capacity of fluoride than at neutral pH levels.

3.4. Solution temperature

Different relationships between fluoride uptake on bone char and solution temperatures were reported in the literature. Abe et al. (2004) stated that fluoride uptake reaction on bone char is endothermic process due to the heat consumption during ion exchange process. Raising temperature from 9.85 to 39.85 °C had resulted in increasing the removal capacity of fluoride onto bone char from about 2.7 to 3.5 mg/g. Similar trend of reaction were reported by Zúñiga-Muro et al. (2017) examined the effect of temperature on fluoride uptake by Ce modified bone char. Increasing the temperature from 30 to 40 °C raised the removal capacity of the coated bone char by about 33% (13.6 mg/g), with an enthalpy change of 42 kJ/mol. The enthalpy change of fluoride adsorption reported by Rojas-Mayorga et al. (2015b) (26.67 kJ/mol) also indicated an endothermic reaction of fluoride adsorption onto Al(III) doped bone char. By contrast, a much lower enthalpy change (< 8.36 kJ/mol) was reported by Medellin-Castillo et al. (2007), which indicated that increasing temperature from 15 to 35 °C had no effect on fluoride uptake using commercial bone char. These different results are due to the difference in the ion exchange performance of fluoride with available ions on bone char or coated bone char (coating with metal). It is also noteworthy to remark that the increase in the solution temperature will increase the solubility of the metal oxides coated on bone char surface and thus, alter the removal capacity of F^- from solution. In addition, based on the ionic strength of the solution, the changes in the zeta potential of adsorbent due to changing solution temperature may affect the performance of the adsorbent to remove contaminants from solution.

On the other hand, an exothermic behavior of the fluoride adsorption on aluminum sulfate and calcium oxide treated bone char, with a negative enthalpy change of −44.8 kJ/mol, was observed by Chatterjee et al. (2018). Increasing solution temperature from 30 °C to 50 °C resulted in a decrease in fluoride uptake from 25 to 10 mg/g, which was related to the inverse relationship between mass transfer coefficient and temperature (9×10^{-4} and 8.5×10^{-4} m/s at 30 and 50 °C, respectively). The effective diffusivity of fluoride ions in solution within the pores was reported to be unaffected by the change of the solution temperature (5.8×10^{-12} and 6.2×10^{-12} m^2/s at 30 and 50 °C, respectively). The effect of solution temperature on fluoride adsorption lies in its effect on the balance of the adsorbent-adsorbate system, which in turn shifts the position of the equilibrium to counter this change.

3.5. Adsorbent particle size

Adsorbent particle size is an important factor that affects the adsorption capacity and rate of fluoride adsorption from aqueous solution. Particle size also plays an important role in altering the rate and capacity of fluoride adsorption. Chatterjee et al. (2018) demonstrated that when the size of carbonized bone meal particles decreased from 0.5 mm to 0.15 mm, the fluoride adsorption capacity showed an increase from 12 to 14 mg/g. Similarly, Kaseva (2006) also reported that a decrease of

bone char particle size produced from cattle bones resulted in an increase in fluoride adsorption from water. The examinations were made using different ranges of particle sizes. The residual fluoride decreased from 15.2 mg/L to 11.26 mg/L after a contact time of 120 min using 2.5–3 and 0.5–1.0 mm particle size, respectively. Similar results have also been reported by Zhu et al. (2011) who observed that the smaller the grain particle, the higher the removal efficiency of the bone char filter, and recorded a maximum of 70.64% F^- removal from drinking water. Thus, reducing the bone char particle size increases the effective surface area, provides more active sites for fluoride removal and eases the diffusivity of the adsorbate to penetrate the pores of the adsorbent (Gupta et al., 2011). However, for water treatment applications (filters) it is quite important to have a suitable particle size distribution in order to avoid clogging issues. On the other hand, large particles may provide a suitable environment for bacterial growth on carbon particles due to the availability of high surface area, pores and functional groups (Lin et al., 2010). The study reported an increase in the particle size in the effluent from 5 to 25 μm after filtration. The accumulation of organics and bacteria on the porous surface of activated carbon provided a good environment for microorganism growth. Consequently, biodegradation of the organics attached to the surface and of the functional groups of the carbon surface occurred and the newly attached particles to the carbon surface were separated from the carbon surface to form larger particles in the effluent. The latter desired more strength against chlorine disinfection due to the presence of extensive bacterial colonization in the large porous particles. Furthermore, there was an increase in anion concentrations (due to bacterial effect) and metallic substance in the effluent. Thus, optimizing the size range of particles is a necessity for fluoride removal via filtration, as it could act as a suitable environment for microorganism growth.

4. Adsorption isotherms

Aquatic system equilibrium is based on the law of thermodynamics, which provides an estimation of particles transport and reactivity in the system. Estimations of the final composition of a system after all reactions have occurred is based on thermodynamic approaches (Mason, 2013). Thus, the ability of different adsorbents to uptake contaminants varies based upon adsorption isotherm models (Smittakorn et al., 2010). The latter are usually determined by equilibrating the solution with varying concentrations of solid particles (contaminants). According to Barakat (2011), the sorption process follows three stages; mainly (i) the transport of contaminants from the liquid to solid surface, (ii) adsorption on the sorbent media particles, and (iii) finally the substance transport within the sorbent particles. Howe et al. (2012) described adsorption as an equilibrium reaction in which the adsorbate distributes between the adsorbent and the solution according to an adsorption isotherm. An adsorption isotherm is a curve constructed from measurements of progressive adsorption at reaction equilibrium at constant pH and temperature. As illustrated in Table 4, different isotherm models were used to predict the adsorption of contaminants from water/wastewater onto sorbents.

Langmuir and Freundlich isotherm models have commonly been applied to describe the equilibrium adsorption of fluoride by bone char. The Langmuir model assumes that all adsorption sites are identical and therefore, there is an equivalent affinity between each adsorbate and adsorbent molecules. Accordingly, the reaction enthalpy and sorption activation energy are constant. This model can be applied to monolayer adsorption with even distribution of heat and affinities when adsorption occurs over the homogeneous surface (Langmuir, 1918). On the other hand, the Freundlich isotherm model assumes a non-ideal, reversible multilayer adsorption process on a heterogeneous adsorbent surface (Foo and Hameed, 2010). Generally, the simulation of the isotherm model of fluoride on bone char in recent studies was based on Langmuir and Freundlich models. However, in rare cases, some other models were examined such as Sips, Dubinin-Radushkevich and Radke-Prausnitz isotherms. Sani et al. (2016) reported that adsorption of F^- onto bone char followed the Langmuir model, which indicated that the adsorption mechanism followed monolayer adsorption. Medellin-Castillo et al. (2007) applied the Langmuir and Freundlich isotherms to describe the adsorption equilibrium data of F^- on bone char. The results showed that the adsorption behavior of F^- removal on a commercial bone char was well presented by both models. However, the results of Freundlich model were more representative at high F^- concentrations. Similarly, Abe et al. (2004) found that the experimental data of F^- was fitted well to use of the Freundlich isotherm.

The Sips model is a combination of the Langmuir and Freundlich isotherm models and can better describe the adsorption process on heterogeneous surfaces (Günay et al., 2007). Fluoride removal on Ce^{4+} modified bone char was best fitted to the Sips model indicating the availability of more than one binding sites (Ca^{2+} and Ce^{4+}) on the surface (Zúñiga-Muro et al., 2017). For a commercial bone char, Tovar-Gómez et al. (2013) reported that both the Langmuir and Sips isotherms were best determined the isotherm of F^- removal compared to the Freundlich model.

Based on the adsorbate concentration, Radke-Prausnitz isotherm model can be reduced to linear model change to the Freundlich or Langmuir model (Ayawei et al., 2017). It best fits the data at low adsorbate concentration. With regards to F^- removal on commercial bone char, Radke-Prausnitz best fitted the data since it is a three parameters model compared to the Langmuir and Freundlich isotherm models (Leyva-Ramos et al., 2010). Medellin-Castillo et al. (2014) used Langmuir, Freundlich and Radke-Praustniz models to investigate the adsorption equilibrium of F onto commercial bone chat. The results implied that the Radke-Praustniz model well fitted the adsorption data based on the lower average absolute percentage deviation obtained values from the Radke-Praustniz compared to those obtained by the other two models.

Chatterjee et al. (2018) applied three isotherms (including Langmuir, Freundlich and Dubinin–Radoshkevitch models) to describe the adsorption equilibrium data of F^- on chemically treated carbonized bone meal followed the Langmuir model, and found that the experimental data was fitted better at different temperatures by the Langmuir model than by other models.

Nigri et al. (2017a) found that the adsorption of F^- with thermally regenerated bovine bone char followed the Freundlich and Redlich-Peterson isothermal plots well when compared to the results achieved by applying Langmuir, Temkin and Sips isotherms. The higher R^2 of 0.9964 of the Freundlich isotherm suggested that the adsorption took place on the heterogeneous surface of the adsorbent.

The mechanism for F^- ion removal onto HAP, which is the effective component of the bone char, was attributed to either surface sorption, substitution or precipitation depending on the reaction conditions (Sternitzke et al., 2012). However, the mechanism is dependent on the F^- initial concentration in solution (Sani et al., 2016). The general consensus suggests that fluoride removal on bone char mostly followed an ion exchange process between F^- and hydroxyl ions to compose fluorapatite (Abe et al., 2004; Kawasaki et al., 2009; Medellin-Castillo et al., 2014). Hence the isotherm that best correlates with these reactions would be the best fit for describing fluoride removal using bone char. The suitability of a model to represent the isotherm of F^- removal from water may also be related to the availability of the active sites on the surface of the adsorbent particles, in which the diffusion of the F^- will occur after the surface sites become less available (which is again related to the adsorbent-adsorbate ratio of the system).

5. Effect of oxyanions on fluoride removal

Medellin-Castillo et al. (2007) examined the impeding effect of chloride, nitrate, nitrite, sulfate and phosphate in natural water on fluoride removal. Examining the concentration of the anions in solution after the adsorption process showed that there was no decrease in the

Table 4
List of some isotherm models (Foo and Hameed, 2010).

Isotherm	Nonlinear form	Linear Form	Plot
Langmuir	$q_e = \frac{Q_0 b C_e}{1 + bC_e}$	$\frac{C_e}{q_e} = \frac{1}{bQ_o} + \frac{C_e}{Q_o}$	$\frac{C_e}{q_e}$ vs C_e
		$\frac{1}{q_e} = \frac{1}{Q_o} + \frac{1}{bQ_o C_e}$	$\frac{1}{q_e}$ vs $\frac{1}{C_e}$
		$q_e = Q_o - \frac{q_e}{bC_o}$	$q_e$vs $\frac{q_e}{bC_o}$
		$\frac{q_e}{C_e} = bQ_0 - bq_e$	$\frac{q_e}{C_e}$vs q_e
Freundlich	$q_e = K_F C_e^{1/n}$	$\log q_e = \log K_F + \frac{1}{n} \log C_e$	$\log q_e$vs $\log C_e$
Dubinin–Radushkevich	$q_e = (q_s) \exp(-k_{ad}\varepsilon^2)$	$ln(q_e) = ln(q_s) - k_{ad}\varepsilon^2$	$ln(q_e)$ vs ε^2
Tempkin	$q_e = \frac{RT}{b_T} \ln A_T C_e$	$q_e = \frac{RT}{b_T} ln\, A_T + \left(\frac{RT}{b_T}\right) ln\ C_e$	$q_e$vsC_e
Flory-Huggins	$\frac{\theta}{C_0} = K_{FH}(1-\theta)^{n_{FH}}$	$log\left(\frac{\theta}{C_0}\right) = log(K_{FH}) + n_{FH} log(1-\theta)$	$log\left(\frac{\theta}{C_0}\right)$ vs $log(1-\theta)$
Hill	$q_e = \frac{q_{sH} C_e^n H}{K_D + C_e^n H}$	$log\left(\frac{q_e}{q_{sH} - q_e}\right) = n_H log(C_e) - log(K_D)$	$log\left(\frac{q_e}{q_{sH} - q_e}\right)$ vs $log(C_e)$
Redlich-Peterson	$q_e = \frac{K_R C_e}{1 + a_R C_e^g}$	$ln\left(K_R \frac{C_e}{q_e} - 1\right) = g ln(C_e) + ln(a_R)$	$ln\left(K_R \frac{C_e}{q_e} - 1\right)$ vs $ln(C_e)$
Sips	$q_e = \frac{K_s C_e^{\beta} s}{1 + a_S C_e^{\beta} s}$	$\beta\ ln(C_e) = -ln\left(\frac{K_s}{q_e}\right) + ln(a_s)$	$ln\left(\frac{K_s}{q_e}\right)$vs $ln(C_e)$
Toth	$q_e = \frac{K_T C_e}{(a_T + C_e)^{1/t}}$	$ln\left(\frac{q_e}{K_T}\right) = ln(C_e) - \frac{1}{t} ln(a_T + C_e)$	$ln\left(\frac{q_e}{K_T}\right)$vs $ln(C_e)$
Koble–Corrigan	$q_e = \frac{A\, C_e^n}{1 + BC_e^n}$	$\frac{1}{q_e} = \frac{1}{AC_e^n} + \frac{B}{A}$	–
Khan	$q_e = \frac{q_s b_K C_e}{(1 + b_K C_e)^{a_K}}$	–	–
Radke–Prausnitz	$q_e = \frac{a_{RP} r_R C_e^{\beta_R}}{a_{RP} + r_R C_e^{\beta_R - 1}}$	–	–
BET	$q_e = \frac{q_s C_{BET} C_e}{(C_s - C_e)[1 + (C_{BET} - 1)(C_e / C_s)]}$	$\frac{C_e}{q_e(C_s - C_e)} = \frac{1}{q_s C_{BET}} + \frac{(C_{BET} - 1)}{q_s C_{BET}} \frac{C_e}{C_s}$	$\frac{C_e}{q_e(C_s - C_e)}$vs $\frac{C_e}{C_s}$
FHH	$ln\left(\frac{C_e}{C_s}\right) = -\frac{\alpha}{RT}\left(\frac{q_s}{q_e d}\right)^r$	–	–
MET	$q_e = q_s\left(\frac{k}{ln(C_s / C_e)}\right)^{1/3}$	–	–

concentration, indicating that the presence of these anions had no effect on F^- uptake on bone char. On the other hand, adsorption experiments showed a reduction in the carbonate concentration indicating a competition with F^- ions on the bone char surface. However, the higher amount of F^- adsorbed compared to the carbonate, confirmed that the bone char surface would selectively remove F^- rather than carbonate. The same results were confirmed by Medellin-Castillo et al. (2014) while investigating the influence of these anions. The decrease of anion affinities toward bone char (at concentration < 0.3 meq/L) was in the following order $F^- > Cl^- > CO_3^{2-} > NO_2^- \approx NO_3^- \approx HCO_3^- \approx SO_4^{2-}$. Smittakorn et al. (2010) also reported that the presence of anions had no effect on F^- removal on Thai bone char, but the presence of cations such as aluminum and magnesium will contribute by enhancing the defluoridation process from water due to the formation of complexes that easily precipitate on the char surface. Similarly, Abe et al. (2004) reported that the presence of NaCl salts in water improved the uptake of F^- from water due to the hydration of dissolute NaCl salts, providing a lower potential of F^- dissolution in water. Increasing the ionic strength from 0.01 to 1 M resulted in increasing the removal capacity of F^- on bone char from about 2.75 to 3.86 mg/g. The increase in the adsorption of F^- with increasing ionic strength could be attributed to the effect of the latter on reducing the electric double layer leading to better electrostatic interaction (Al-Juboori et al., 2016a). Larsen et al. (1993) compared the effectiveness of ox bone char to remove F^- from water with and without the presence of brushite (BSH) and calcium hydroxide, reporting that the removal capacity of the bone char increased from 0.64 to 3.88 mg/g after adding 0.05 g BSH and 0.015 g $Ca(OH)_2$ to the solution.

The simultaneous removal of As and F^- using bone char was also investigated in a recent research, reporting the suitability of fish bone charred at 500 °C for the simultaneous removal of As(V) and F^- from water. However, a higher removal capacity of fluoride was achieved due to exchanging ions between hydroxyapatite composition of the bone char and fluoride ions in solution.

6. Regeneration

Regeneration capacity is of utmost importance to evaluate the reusability of bone char efficiency in the removal of contaminants from water. Regeneration of bone char could provide recovery of pollutants, reusability of adsorbents, reducing the process cost and reducing wastes to be processed. Kaseva (2006) examined the effect of thermal regeneration in the temperature range of 100–800 °C, with regeneration time of (30–240 min) on the bone char efficiency for fluoride removal from water. Kaseva (2006) proposed the release of hydrogen fluoride (HF) gas from saturated bone char upon exposure to thermal treatment as a regeneration mechanism. Technically, this can probably happen when there is a source of hydrogen to react with fluoride.

The result showed that the F^- adsorption capacity of the regenerated bone char increased from 0.2 to 0.75 mg/g after raising the regeneration temperature from 100 to 500 °C for 120 min residence time. However, further increases in the regeneration temperature resulted in decreasing the uptake capacity of F^- on bone char. Nigri et al. (2017a) examined the effect of thermal regeneration on bovine commercial bone char at different temperatures. The results of X-ray diffraction (XRD) showed the presence of F^- ions in the structure of the bone char after regeneration, but the composition of the bone char was not altered by applying thermal treatment. This contradicts with the proposed regeneration mechanism of Kaseva (2006) where fluoride is suggested to be released in a form of HF gas. Fluoride diffusion seems to be more acceptable in explaining the thermal regeneration of bone char as opposed to HF formation especially if there is no source of hydrogen whether directly applied or released due to chemical reactions. The optimum conditions for the regeneration in the study by Nigri et al.

(2017a) were different from the results reported by Kaseva (2006) as the experimental conditions were different. The optimum temperature for the regeneration process of the bone char was 400 °C resulting in 2.25 mg/g F^- uptake capacity.

Chatterjee et al. (2018) reported that F^- uptake on chemically treated carbonized bone meal was decreased by 18% and 31% in the second and third cycle respectively, after regenerating the adsorbent with 0.1 M NaOH. Medellin-Castillo et al. (2007) examined the desorption of fluoride from commercial bone char by placing the adsorbent in water at pH values of 7 and 12. Fluoride desorption at pH 12 performed better than neutral pH due to the abundant availability of exchangeable hydroxyl groups, indicating a reversible F^- adsorption process. On a large scale, the most efficient regeneration process for bone char was reported by the use of 1–2 M NaOH solution for the regeneration of 2500 L of saturated bone char (Catholic Diocese of Nakuru, Water Quality, and Muller, 2007). The intermittent flushing of the bone char with NaOH is followed by washing with water to reduce the pH of the outflow and then suppling CO_2 enriched water to lower the pH below 8. The waste water generated from the regeneration process were precipitated with CaOH or $CaCl_2$ to form CaF_2, which have low solubility and can retain fluoride. The cost of the process was reported to be around $ 280 USD (339.27 USD in 2019 after adding the inflation rate)

The disposal of the concentrated fluoride solution resulting from the bone char regeneration can be a challenge. Such a problem can be overcome by recycling the concentrated fluoride into green industries. Zhu et al. (2013) used calcium fluoride sludge for producing strong corrosion resistant ceramic that locks fluoride well and prevents it from leaching out of the structure. In another study, fluorapatite was applied as a reusable catalyst in solvent-free epoxidation (Ichihara et al., 2003).

7. Bone char defluoridation units -existing and conceptual designs

After discussing the factors affecting bone char defluoridation efficiency, it is important to look into the designs of units used in such applications. Most of the designs available were developed to be affordable and practical for low economic and remote communities. Examples of the most common designs used for defluoridation are illustrated in Fig. 5. Fawell et al. (2006) compared the advantages and disadvantages of these designs and the column was found to be the best one. Some more sophisticated designs were also implemented in Africa and India where bone char was used in a bed configuration for the precipitation of fluoride with calcium (Nalgonda technique), this technique is termed as contact precipitation (Ayoob et al., 2008). Theses designs were commercialized and are readily available for communities at affordable prices (Kinyua, 2016). An example for the commercial supplier for these designs is the Nakuru Deflouridation Company in Kenya using bone from many different sources such as goat, camel, cattle and sheep bones (Nakuru Defluoridation Company Ltd). The challenge with these simple designs is monitoring fluoride removal levels and the adsorption capacity of the char throughout the operation period. In 2005, the Catholic Diocese of Nakuru, Water Quality (CDN WQ) (Catholic Diocese of Nakuru, Water Quality, and Muller, 2007) adopted a new design of a kiln to produce about 10 tons bone char per batch using animal bones from different sources. The best defluoridation process was reported to be with bone char produced at 400 °C for 1–5 days. To improve the quality of the produced bone char, the outlet of the air and the amount of the oxygen entering the kiln was controlled by adjusting the size of the chimney and reusing the air of the outlet by mixing it with a limited amount of oxygen. The regeneration processes of bone char used in these designs has to be done with relatively strong alkaline solution which would be problematic to handle and store especially when the setups used in village communities. This means that researching more advanced designs is inevitable.

In this study, we propose some conceptual designs that have the capacity to prolong bone char adsorption capacity and are self-cleaning as shown in Fig. 6. As it can be seen from this figure, column configuration is used in both designs. The designs apply electrical and ultrasonic enhancing adsorption mechanisms. The electric-enhancing column should be made of non-conductive material (e.g. plastic), while the ultrasonic-enhancing column should be made of magnetostrictive materials (e.g. nickel) due to its efficiency in generating ultrasonic vibration (Al-Juboori et al., 2016b). It is noteworthy that the two designs require only low level of electrical power which can be sourced from solar energy. For example, applying electrolysis should not exceed the low voltage of 1.23 V as water electrolysis occurs beyond this level (Qi,

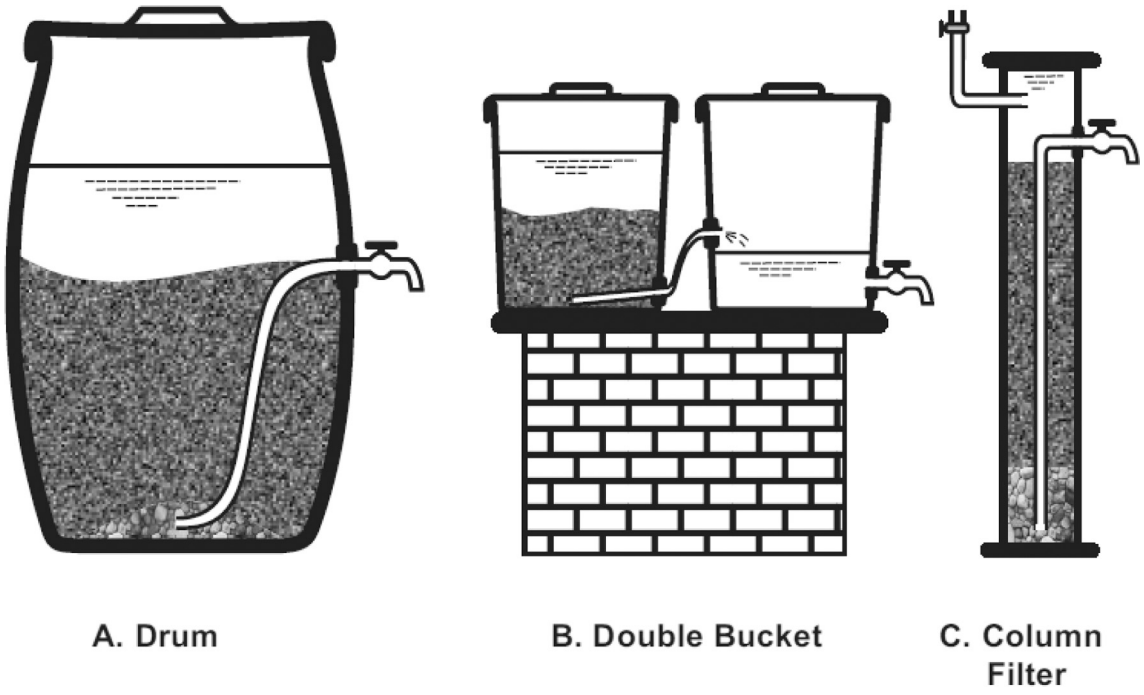

Fig. 5. Most common domestic units designs for defluoridation in developing countries (Fawell et al., 2006).

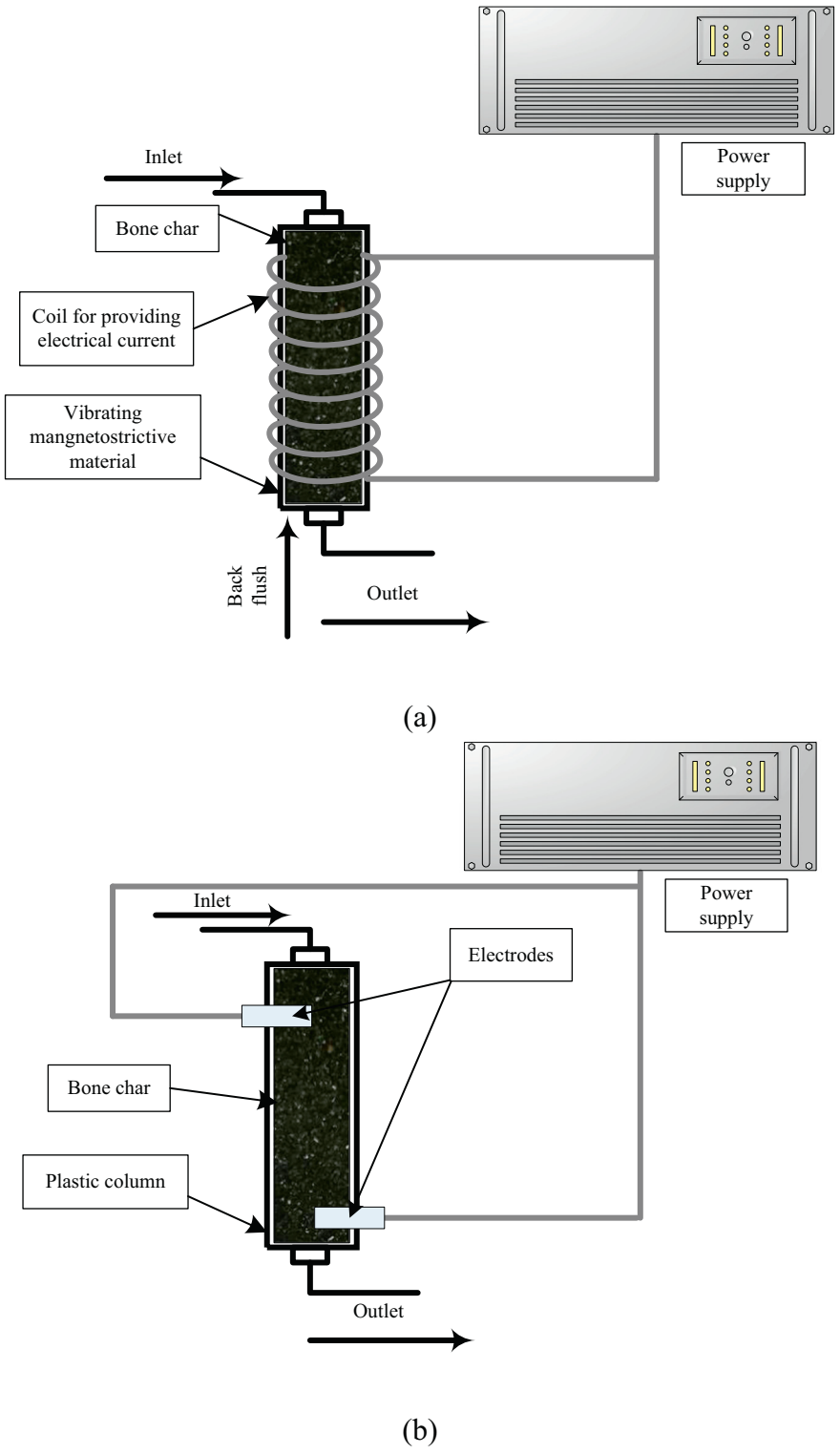

Fig. 6. Conceptual designs for bone char columns: a) ultrasonically enhanced adsorption and b) electrically enhanced adsorption.

2013). Similarly, only low level of energy is required for vibrating magnetostrictive materials with ultrasound. For instance, the domain wall energy for iron is 1.1×10^{-3} J/m^2 (Thoelke, 1993). It is hard to indicate energy demands for the proposed designs as these figures depend on several factors such as size of the column, quality of the char, flowrate, thickness of the column, number of the coil turns, etc. The electrically enhanced adsorption design promotes the electrostatic mechanisms of fluoride adsorption onto the char by the small voltage applied through the electrodes. To make the design more environmentally friendly, these electrodes can be used from recycled batteries and this in turn would reduce batteries disposal problem. The electrically enhanced adsorption design can be regenerated by charge reversal. The ultrasonically enhanced adsorption design relies on reducing the dead area of the char particles resulting from packing and prevents the formation of channels in column bed due to the continuous vibration. This design can be regenerated by back flush with treated

water applying the same or slightly higher vibration level as that used with adsorption.

8. Conclusion and future directions

The health concerns associated with the high fluoride concentration in drinking water sources were highlighted in this study. Due to the feasibility of bone char as a green adsorbent for fluoride removal, a comprehensive review addressing all the important aspects of this technology was provided. The optimum temperature range and production conditions for bone char were evaluated. Bone char samples produced at 500–700 °C seem to have the best defluoridation capacity. In addition, the effectiveness of coating with multivalent ions and the experimental conditions for batch and column filtrations were discussed. Among all coating cations, aluminum appears to be promising for increasing the removal capacity of F^- removal from water. Despite these findings, further studies are required to optimize the rate of fluoride removal on bone char as most of the studies showed that equilibrium was achieved after 24 h. The possibility of regenerating bone char and the reduction of solid waste justify the energy requirements for bone char production processes. In the case of gasification, energy for bone char production can be compensated by syngas generation. The recent low commercial price of bulk bone char indicates the drop in the cost production of the char. Possible utilization of concentrated fluoride generated from bone char regeneration for green industry application was also suggested. Challenges with existing domestic defluoridation designs were pinpointed and new conceptual designs were discussed.

More extensive works are required to examine the effective particle size for fluoride removal using column filters to avoid issues related to bacterial growth through filter layers. Further investigations are also required to examine the removal of fluoride from industrial wastewater as it can form more complex compounds due to the presence of high fluoride concentrations of various contaminants in the wastewater system. Research into the proposed defluoridation designs would be beneficial for the advancement of removal technologies.

Acknowledgements

This research was supported in part by the Iraqi Government/ Ministry of Higher Education and Scientific Research and the Australian Research Training Program.

References

Abaei, Z., Faghihian, H., Esmaeeli, N., 2017. Preparation and application of zeolitic adsorbents for removal of fuoride from aqueous solution; equilibrium, kinetic and thermodynamic studies. Der Chemica Sinica 8 (6), 524–534.
Abe, I., Iwasaki, S., Tokimoto, T., Kawasaki, N., Nakamura, T., Tanada, S., 2004. Adsorption of fluoride ions onto carbonaceous materials. J. Colloid Interface Sci. 275 (1), 35–39.
Alibaba.com Sky Bone Ash PVT from Russian Federation Inc. https://m.alibaba.com/amp/product/133373450.html.
Al-Juboori, R.A., Yusaf, T., Aravinthan, V., Pittaway, P.A., Bowtell, L., 2016a. Investigating the feasibility and the optimal location of pulsed ultrasound in surface water treatment schemes. Desalin. Water Treat. 57 (11), 4769–4787.
Al-Juboori, R.A., Bowtell, L.A., Yusaf, T., Aravinthan, V., 2016b. Insights into the scalability of magnetostrictive ultrasound technology for water treatment applications. Ultrason. Sonochem. 28, 357–366.
Arrenberg, A., 2010. Production Models for Bone Char Defluoridation. Naivsha, Kenya. MSc Thesis. Cranfield University School of Applied Sciences, Cranfield, UK.
Ayawei, N., Ebelegi, A.N. and Wankasi, D. (2017) Modelling and interpretation of adsorption isotherms. J. Chem. (Hindawi) 2017, ID 3039817.
Ayoob, S., Gupta, A., Bhat, V.T., 2008. A conceptual overview on sustainable technologies for the defluoridation of drinking water. Crit. Rev. Env. Sci. Tec. 38 (6), 401–470.
Barakat, M., 2011. New trends in removing heavy metals from industrial wastewater. Arab. J. Chem. 4 (4), 361–377.
Brunson, L.R., Sabatini, D.A., 2009. An evaluation of fish bone char as an appropriate arsenic and fluoride removal technology for emerging regions. Environ. Eng. Sci. 26 (12), 1777–1784.
Bulk Bone Char® Promolife Inc. https://www.promolife.com/bulk-bone-char-for-water-filter-systems/.
Cai, Q., Turner, B.D., Sheng, D., Sloan, S., 2017. Application of kinetic models to the design of a calcite permeable reactive barrier (PRB) for fluoride remediation. Water Res. 130, 300–311.
Catholic Diocese of Nakuru, Water Quality, Muller, K., 2007. CDN's Experiences in Producing Bone Char. Catholic Diocese of Nakuru, Nakuru, Kenya and Swiss Federal Institute of Aquatic Science and Technology (EAWAG), Dübendorf, Switzerland.
Çeçen, F., Aktas, Ö., 2011. Activated Carbon for Water and Wastewater Treatment: Integration of Adsorption and Biological Treatment. John Wiley & Sons.
Changmai, M., Pasawan, M., Purkait, M., 2018. A hybrid method for the removal of fluoride from drinking water: parametric study and cost estimation. Sep. Purif. Technol. 206, 140–148.
Chatterjee, S., Mukherjee, M., De, S., 2018. Defluoridation using novel chemically treated carbonized bone meal: batch and dynamic performance with scale-up studies. Environ. Sci. Pollut. R 25, 18161–18178.
Cheung, C., Chan, C.K., Porter, J.F., McKay, G., 2001a. Film-pore diffusion control for the batch sorption of cadmium ions from effluent onto bone char. J. Colloid Interf. Sci. 234 (2), 328–336.
Cheung, C., Porter, J., McKay, G., 2001b. Sorption kinetic analysis for the removal of cadmium ions from effluents using bone char. Water Res. 35 (3), 605–612.
Chigondo, M., Paumo, H.K., Bhaumik, M., Pillay, K., Maity, A., 2018. Rapid high adsorption performance of hydrous cerium-magnesium oxides for removal of fluoride from water. J. Mol. Liq. 265, 496–509.
Dahi, E., 2016. Africa's U-turn in defluoridation policy: from the Nalgonda technique to bone char. Fluoride 49 (4), 401–416.
Delgadillo-Velasco, L., Hernández-Montoya, V., Cervantes, F.J., Montes-Morán, M.A., Lira-Berlanga, D., 2017. Bone char with antibacterial properties for fluoride removal: preparation, characterization and water treatment. J. Environ. Manag. 201, 277–285.
Dewage, N.B., Liyanage, A.S., Pittman Jr., C.U., Mohan, D., Mlsna, T., 2018. Fast nitrate and fluoride adsorption and magnetic separation from water on α-Fe_2O_3 and Fe_3O_4 dispersed on Douglas fir biochar. Bioresour. Technol. 263, 258–265.
Dimović, S., Smičiklas, I., Plećaš, I., Antonović, D., Mitrić, M., 2009. Comparative study of differently treated animal bones for Co^{2+} removal. J. Hazard. Mater. 164 (1), 279–287.
Edmunds, W.M., Smedley, PL., 2013. Fluoride in natural waters. Ch 13. Revised edition In: Selinus, O, Alloway, B, Centeno, J A, Finkelman, RB, Fuge, R, Lindh, U, Smedley, PL. (Eds.), Essentials of Medical Geology. Springer, pp. 311–336.
Elango, L., Jagadeshan, G., 2018. Clean and Sustainable Groundwater in India. Springer, pp. 13–23.
Fawell, J.K., Bailey, K., Chilton, J., 2006. Fluoride in drinking-water. World Health Organization, Geneva, Switzerland.
Field, R.A., Riley, M., Mello, F., Corbridge, J., Kotula, A., 1974. Bone composition in cattle, pigs, sheep and poultry. J. Anim. Sci. 39 (3), 493–499.
Figueiredo, M., Fernando, A., Martins, G., Freitas, J., Judas, F., Figueiredo, H., 2010. Effect of the calcination temperature on the composition and microstructure of hydroxyapatite derived from human and animal bone. Ceram. Int. 36 (8), 2383–2393.
Foo, K.Y., Hameed, B.H., 2010. Insights into the modeling of adsorption isotherm systems. Chem. Eng. J. 156 (1), 2–10.
Goodman, P.A., Li, H., Gao, Y., Lu, Y., Stenger-Smith, J., Redepenning, J., 2013. Preparation and characterization of high surface area, high porosity carbon monoliths from pyrolyzed bovine bone and their performance as supercapacitor electrodes. Carbon 55, 291–298.
Günay, A., Arslankaya, E., Tosun, I., 2007. Lead removal from aqueous solution by natural and pretreated clinoptilolite: adsorption equilibrium and kinetics. J. Hazard. Mater. 146 (1–2), 362–371.
Gupta, V., Gupta, B., Rastogi, A., Agarwal, S., Nayak, A., 2011. A comparative investigation on adsorption performances of mesoporous activated carbon prepared from waste rubber tire and activated carbon for a hazardous azo dye—Acid Blue 113. J. Hazard. Mater. 186 (1), 891–901.
Hansen, S.P., Gumerman, R.C., Culp, R.L., 1979. Estimating Water Treatment Costs: Cost Curves Applicable to 2,500 gpd to 1 mgd Treatment Plants. US Environmental Protection Agency.
Harrison, P.T., 2005. Fluoride in water: a UK perspective. J. Fluor. Chem. 126 (11 − 12), 1448–1456.
Herath, H., Kawakami, T., Tafu, M., 2018. Repeated heat regeneration of bone char for sustainable use in fluoride removal from drinking water. Healthcare (Basel) 6 (4), 143.
Howe, K.J., Crittenden, J.C., Hand, D.W., Trussell, R.R., Tchobanoglous, G., 2012. Principles of Water Treatment, 3rd edition. John Wiley & Sons.
Ichihara, J., Kambara, A., Iteya, K., Sugimoto, E., Shinkawa, T., Takaoka, A., Yamaguchi, S., Sasaki, Y., 2003. Cetylpyridinium dodecatungstate on fluorapatite: efficient and reusable solid catalyst for solvent-free epoxidation. Green Chem. 5 (5), 491–493.
Ip, A.W., Barford, J.P., McKay, G., 2010. A comparative study on the kinetics and mechanisms of removal of Reactive Black 5 by adsorption onto activated carbons and bone char. Chem. Eng. J. 157 (2–3), 434–442.
Ishikawa, K., Miyamoto, Y., Tsuchiya, A., Hayashi, K., Tsuru, K., Ohe, G., 2018. Physical and histological comparison of hydroxyapatite, carbonate apatite, and β-tricalcium phosphate bone substitutes. Materials (Basel) 11 (10) (12 pages).
Ismail, Z.Z., AbdelKareem, H.N., 2015. Sustainable approach for recycling waste lamb and chicken bones for fluoride removal from water followed by reusing fluoride-bearing waste in concrete. Waste Manag. 45, 66–75.
Jackson, P., Harvey, P., Young, W., 2002. Chemistry and Bioavailability Aspects of Fluoride in Drinking Water. WRc-NSF, Marlow, Buckinghamshire.
Jeihanipour, A., Shen, J., Abbt-Braun, G., Huber, S.A., Mkongo, G., Schäfer, A.I., 2018. Seasonal variation of organic matter characteristics and fluoride concentration in the Maji ya Chai River (Tanzania): impact on treatability by nanofiltration/reverse osmosis. Sci. Total Environ. 637, 1209–1220.

Kader, A.A., Aly, A., Girgis, B., 1996. Bone char decolorisation efficiency. A laboratory study over four consecutive cycles. Int. Sugar J. (Worldwide Sugar Edition) 98 (1174), 542–554.
Karmakar, S., Bhattacharjee, S., De, S., 2017. Experimental and modeling of fluoride removal using aluminum fumarate (AlFu) metal organic framework incorporated cellulose acetate phthalate mixed matrix membrane. JECE 5 (6), 6087–6097.
Kaseva, M., 2006. Optimization of regenerated bone char for fluoride removal in drinking water: a case study in Tanzania. J. Water Health 4 (1), 139–147.
Kawasaki, N., Ogata, F., Tominaga, H., Yamaguchi, I., 2009. Removal of fluoride ion by bone char produced from animal biomass. J Oleo Sci 58 (10), 529–535.
Keene, B., Knowlton, K., McGilliard, M., Lawrence, L., Nickols-Richardson, S., Wilson, J., Rutledge, A., McDowell, L., Van Amburgh, M., 2004. Measures of bone mineral content in mature dairy cows. J. Dairy Sci. 87 (11), 3816–3825.
Kinyua, L., 2016. A Study of Defluoridation Techniques and the Current State of Defluoridation in Kenya. BSc Thesis. University of Nairobi, Nairobi, Kenya.
Lai, Y.-q., Kai, Y., Chao, Y., Tian, Z.-l., Guo, W.-c., Jie, L., 2018. Thermodynamics and kinetics of fluoride removal from simulated zinc sulfate solution by La (III)-modified zeolite. T. Nonferr. Metal Soc. 28 (4), 783–793.
Lambert, S., Graham, N., 1989. Adsorption methods for treating organically coloured upland waters. Environ. Technol. 10 (9), 785–798.
Langmuir, I., 1918. The adsorption of gases on plane surfaces of glass, mica and platinum. J. Am. Chem. Soc. 40 (9), 1361–1403.
Larsen, M., Pearce, E., Jensen, S., 1993. Defluoridation of water at high pH with use of brushite, calcium hydroxide, and bone char. J. Dent. Res. 72 (11), 1519–1525.
Leyva-Ramos, R., Rivera-Utrilla, J., Medellin-Castillo, N., Sanchez-Polo, M., 2010. Kinetic modeling of fluoride adsorption from aqueous solution onto bone char. Chem. Eng. J. 158 (3), 458–467.
Lhassani, A., Rumeau, M., Benjelloun, D., Pontie, M., 2001. Selective demineralization of water by nanofiltration application to the defluorination of brackish water. Water Res. 35 (13), 3260–3264.
Li, W., Liao, P., Oldham, T., Jiang, Y., Pan, C., Yuan, S., Fortner, J.D., 2018. Real-time evaluation of natural organic matter deposition processes onto model environmental surfaces. Water Res. 129, 231–239.
Liao, C.-J., Lin, F.-H., Chen, K.-S., Sun, J.-S., 1999. Thermal decomposition and reconstitution of hydroxyapatite in air atmosphere. Biomaterials 20 (19), 1807–1813.
Lin, T., Chen, W., Wang, L., 2010. Particle properties in granular activated carbon filter during drinking water treatment. J. Environ. Sci. 22 (5), 681–688.
Liu, Q., Huang, S., Matinlinna, J.P., Chen, Z., Pan, H., 2013. Insight into biological apatite: physiochemical properties and preparation approaches. Biomed. Res. Int. 2013, 1–13 929748.
Maheshwari, R., 2006. Fluoride in drinking water and its removal. J. Hazard. Mater. 137 (1), 456–463.
Maity, J.P., Hsu, C.-M., Lin, T.-J., Lee, W.-C., Bhattacharya, P., Bundschuh, J., Chen, C.-Y., 2018. Removal of fluoride from water through bacterial-surfactin mediated novel hydroxyapatite nanoparticle and its efficiency assessment: adsorption isotherm, adsorption kinetic and adsorption thermodynamics. Environ. Nanotechnol. Monit. Manage 9, 18–28.
Mason, R.P., 2013. Trace Metals in Aquatic Systems. John Wiley & Sons.
Medellin-Castillo, N.A., Leyva-Ramos, R., Ocampo-Perez, R., Garcia de la Cruz, R.F., Aragon-Pina, A., Martinez-Rosales, J.M., Guerrero-Coronado, R.M., Fuentes-Rubio, L., 2007. Adsorption of fluoride from water solution on bone char. Ind. Eng. Chem. Res. 46 (26), 9205–9212.
Medellin-Castillo, N., Leyva-Ramos, R., Padilla-Ortega, E., Perez, R.O., Flores-Cano, J., Berber-Mendoza, M., 2014. Adsorption capacity of bone char for removing fluoride from water solution. Role of hydroxyapatite content, adsorption mechanism and competing anions. J. Ind. Eng. Chem. 20 (6), 4014–4021.
Meenakshi, S., Sundaram, C.S., Sukumar, R., 2008. Enhanced fluoride sorption by mechanochemically activated kaolinites. J. Hazard. Mater. 153 (1–2), 164–172.
Mendoza-Castillo, D.I., Bonilla-Petriciolet, A., Jáuregui-Rincón, J., 2015. On the importance of surface chemistry and composition of bone char for the sorption of heavy metals from aqueous solution. Desalin. Water Treat. 54 (6), 1651–1662.
Mohamed, R., Baeissa, E., 2013. Preparation and characterisation of Pd–TiO2–hydroxyapatite nanoparticles for the photocatalytic degradation of cyanide under visible light. Appl. Catal. A Gen. 464, 218–224.
Mourabet, M., El Rhilassi, A., El Boujaady, H., Bennani-Ziatni, M., El Hamri, R., Taitai, A., 2015. Removal of fluoride from aqueous solution by adsorption on hydroxyapatite (HAp) using response surface methodology. J. Saudi Chem. Soc. 19 (6), 603–615.
Nagaraj, A., Sadasivuni, K.K., Rajan, M., 2017. Investigation of lanthanum impregnated cellulose, derived from biomass, as an adsorbent for the removal of fluoride from drinking water. Carbohydr. Polym. 176, 402–410.
Nakuru Defluoridation Company Ltd http://www.cdnwaterquality.co.ke/.
Naliaka, B., 2016. Evaluation of Bone Char Defluoridation of Water using Adsorption Isotherms and the Bed Depth Service Time (BDST) Model. MSc Thesis. University of Nairobi, Nairobi, Kenia.
Näslund, J., Snell, I., 2005. GIS-Mapping of Fluoride Contaminated Groundwater in Nakuru and Baringo District, Kenya. MSc Thesis. Luleå University of Technology, Luleå, Sweden.
Nasr, A.B., Walha, K., Charcosset, C., Amar, R.B., 2011. Removal of fluoride ions using cuttlefish bones. J. Fluor. Chem. 132 (1), 57–62.
Nigri, E.M., Bhatnagar, A., Rocha, S.D.F., 2017a. Thermal regeneration process of bone char used in the fluoride removal from aqueous solution. J. Clean. Prod. 142, 3558–3570.
Nigri, E.M., Cechinel, M.A.P., Mayer, D.A., Mazur, L.P., Loureiro, J.M., Rocha, S.D., Vilar, V.J., 2017b. Cow bones char as a green sorbent for fluorides removal from aqueous solutions: batch and fixed-bed studies. Environ. Sci. Pollut. R 24 (3), 2364–2380.
Nunes-Pereira, J., Lima, R., Choudhary, G., Sharma, P., Ferdov, S., Botelho, G., Sharma, R., Lanceros-Méndez, S., 2018. Highly efficient removal of fluoride from aqueous media through polymer composite membranes. Sep. Purif. Technol. 205, 1–10.
OECD, 2018. OECD-FAO Agricultural Outlook 2018–2027.
Oladipo, A.A., Gazi, M., 2017. Application of hydroxyapatite-based nanoceramics in wastewater treatment: Synthesis, characterization, and optimization. In: Mishra, A.K. (Ed.), Sol-Gel Based Nanoceramic Materials: Preparation, Properties and Applications. Springer, pp. 231–251.
Padhi, S., Muralidharan, D., 2012. Fluoride occurrence and mobilization in geo-environment of semi-arid granite watershed in southern peninsular India. Environ. Earth Sci. 66 (2), 471–479.
Pan, J., Zheng, Y., Ding, J., Gao, C., Van der Bruggen, B., Shen, J., 2018. Fluoride removal from water by membrane capacitive deionization with monovalent anion selective membrane. Ind. Eng. Chem. Res. 57 (20), 7048–7053.
Patel, S., Han, J., Qiu, W., Gao, W., 2015. Synthesis and characterisation of mesoporous bone char obtained by pyrolysis of animal bones, for environmental application. J. Environ. Chem. Eng 3 (4), 2368–2377.
Petrone, P., Guarino, F.M., Giustino, S., Gombos, F., 2013. Ancient and recent evidence of endemic fluorosis in the Naples area. J. Geochem. Explor. 131, 14–27.
Phantumvanit, P., Songpaisan, Y., Möller, I.J., 1988. A defluoridator for individual households. Wld. Hlth. Forum 9 (4), 555–558.
Qi, Z., 2013. Proton Exchange Membrane Fuel Cells. CRC Press.
Rasool, A., Farooqi, A., Xiao, T., Ali, W., Noor, S., Abiola, O., Ali, S., Nasim, W., 2017. A review of global outlook on fluoride contamination in groundwater with prominence on the Pakistan current situation. Environ. Geochem. Health 1–17.
Raychoudhury, T., Boindala, S.P., Kalidindi, S., 2017. Performance evaluation of metal impregnated activated carbon composite for removal of fluoride under varying solution chemistry. Water Sci. Tech-W Sup. 17 (5), 1377–1385.
Reynel-Avila, H.E., Mendoza-Castillo, D.I., Bonilla-Petriciolet, A., 2016. Relevance of anionic dye properties on water decolorization performance using bone char: adsorption kinetics, isotherms and breakthrough curves. J. Mol. Liq. 219, 425–434.
Rojas-Mayorga, C., Bonilla-Petriciolet, A., Aguayo-Villarreal, I.A., Hernandez-Montoya, V., Moreno-Virgen, M., Tovar-Gómez, R., Montes-Morán, M., 2013. Optimization of pyrolysis conditions and adsorption properties of bone char for fluoride removal from water. J. Anal. Appl. Pyrolysis 104, 10–18.
Rojas-Mayorga, C.K., Silvestre-Albero, J., Aguayo-Villarreal, I.A., Mendoza-Castillo, D.I., Bonilla-Petriciolet, A., 2015a. A new synthesis route for bone chars using CO_2 atmosphere and their application as fluoride adsorbents. Micropo. Mesopo. Mater. 209, 38–44.
Rojas-Mayorga, C.K., Bonilla-Petriciolet, A., Silvestre-Albero, J., Aguayo-Villarreal, I.A., Mendoza-Castillo, D.I., 2015b. Physico-chemical characterization of metal-doped bone chars and their adsorption behavior for water defluoridation. Appl. Surf. Sci. 355, 748–760.
Rojas-Mayorga, C.K., Bonilla-Petriciolet, A., Sánchez-Ruiz, F.J., Moreno-Pérez, J., Reynel-Ávila, H.E., Aguayo-Villarreal, I., Mendoza-Castillo, D., 2015c. Breakthrough curve modeling of liquid-phase adsorption of fluoride ions on aluminum-doped bone char using micro-columns: effectiveness of data fitting approaches. J. Mol. Liq. 208, 114–121.
Rostamia, I., Mahvib, A.H., Dehghanib, M.H., Baghania, A.N., Marandid, R., 2017. Application of nano aluminum oxide and multi-walled carbon nanotube in fluoride removal. Desalin. Water Treat. 1, 1–6.
Roy, S., 2018. Synthesis of graphene oxide using tea-waste biochar as green substitute of graphite and its application in de-fluoridation of contaminated water. Am. J. Chem. Res. 1, 1–19.
Ruthven, D.M., 2008. Fundamentals of adsorption equilibrium and kinetics in microporous solids. In: Karge, H.G., Weitkamp, J. (Eds.), Adsorption and Diffusion. Springer, Berlin, Heidelberg, pp. 1–43.
Sani, T., Gómez-Hortigüela, L., Pérez-Pariente, J., Chebude, Y., Díaz, I., 2016. Defluoridation performance of nano-hydroxyapatite/stilbite composite compared with bone char. Sep. Purif. Technol. 157, 241–248.
Skinner, H., Jahren, A., 2004. Biomineralization 8.04. In: Treatise on Geochemistry. vol. 6. pp. 182–216.
Smittakorn, S., Jirawongboonrod, N., Mongkolnchai-Arunya, S., Durnford, D., 2010. Homemade bone charcoal adsorbent for defluoridation of groundwater in Thailand. J. Water Health 8 (4), 826–836.
Soni, C., Wang, Z., Dalai, A., Pugsley, T., Fonstad, T., 2009. Hydrogen production via gasification of meat and bone meal in two-stage fixed bed reactor system. Fuel 88 (5), 920–925.
Soni, C.G., Dalai, A.K., Pugsley, T., Fonstad, T., 2011. Steam gasification of meat and bone meal in a two-stage fixed-bed reactor system. Asia Pac. J. Chem. Eng. 6 (1), 71–77.
State of South Carolina Department of Health and Environmental Control Water Supply Division, 1980. Fluoride Reduction in Community Water Supplies.
Sternitzke, V., Kaegi, R., Audinot, J.-N., Lewin, E., Hering, J.G., Johnson, C.A., 2012. Uptake of fluoride from aqueous solution on nano-sized hydroxyapatite: examination of a fluoridated surface layer. Environ. Sci. Technol. 46 (2), 802–809.
Tchomgui-Kamga, E., Alonzo, V., Nanseu-Njiki, C.P., Audebrand, N., Ngameni, E., Darchen, A., 2010. Preparation and characterization of charcoals that contain dispersed aluminum oxide as adsorbents for removal of fluoride from drinking water. Carbon 48 (2), 333–343.
Terasaka, S., Kamitakahara, M., Yokoi, T., Ioku, K., 2014. Effect of preparation temperature on the ability of bone char to remove fluoride ion and organic contaminants. J. Ceram. Soc. Japan. 122 (1432), 995–999.
Thanh, D.N., Novák, P., Vejpravova, J., Vu, H.N., Lederer, J., Munshi, T., 2017. Removal of copper and nickel from water using nanocomposite of magnetic hydroxyapatite nanorods. J. Magn. Magn. Mater. 456, 451–460.
Thoelke, J.B., 1993. Magnetization and Magnetostriction in Highly Magnetostrictive Materials. MSc Thesis. Iowa State University, Ames, Iowa.

Tovar-Gómez, R., Moreno-Virgen, M., Dena-Aguilar, J., Hernández-Montoya, V., Bonilla-Petriciolet, A., Montes-Morán, M., 2013. Modeling of fixed-bed adsorption of fluoride on bone char using a hybrid neural network approach. Chem. Eng. J. 228, 1098–1109.

Tripathy, S.S., Bersillon, J.-L., Gopal, K., 2006. Removal of fluoride from drinking water by adsorption onto alum-impregnated activated alumina. Sep. Purif. Technol. 50 (3), 310–317.

Usón, A.A., López-Sabirón, A.M., Ferreira, G., Sastresa, E.L., 2013. Uses of alternative fuels and raw materials in the cement industry as sustainable waste management options. Renew. Sust. Energ. Rev. 23, 242–260.

Waghmare, S., Arfin, T., Rayalu, S., Lataye, D., Dubey, S., Tiwari, S., 2015. Adsorption behavior of modified zeolite as novel adsorbents for fluoride removal from drinking water: surface phenomena, kinetics and thermodynamics studies‖. IJRRSET 4 (12), 4114–4124.

Wang, X.-H., Song, R.-H., Yang, H.-C., Shi, Y.-J., Dang, G.-B., Yang, S., Zhao, Y., Sun, X.-F., Wang, S.-G., 2013. Fluoride adsorption on carboxylated aerobic granules containing Ce (III). Bioresour. Technol. 127, 106–111.

Wang, J., Chen, N., Li, M., Feng, C., 2018. Efficient removal of fluoride using polypyrrole-modified biochar derived from slow pyrolysis of pomelo peel: sorption capacity and mechanism. J. Polym. Environ. 26 (4), 1559–1572.

Warren, G., Robinson, J., Someus, E., 2009. Dissolution of phosphorus from animal bone char in 12 soils. Nutr. Cycl. Agroecosys. 84 (2), 167–178.

Wei, F., Cao, C., Huang, P., Song, W., 2015. A new ion exchange adsorption mechanism between carbonate groups and fluoride ions of basic aluminum carbonate nanospheres. RSC Adv. 5 (17), 13256–13260.

Xie, J., Meng, X., Zhou, Z., Li, P., Yao, L., Bian, L., Gao, X., Wei, Y., 2013. Preparation of titania/hydroxyapatite (TiO2/HAp) composite photocatalyst with mosaic structure for degradation of pentachlorophenol. Mater. Lett. 110, 57–60.

Yami, T.L., Du, J., Brunson, L.R., Chamberlain, J.F., Sabatini, D.A., Butler, E.C., 2015. Life cycle assessment of adsorbents for fluoride removal from drinking water in East Africa. Int. J. Life Cycle Assess. 20 (9), 1277–1286.

Ye, Y., Yang, J., Jiang, W., Kang, J., Hu, Y., Ngo, H.H., Guo, W., Liu, Y., 2018. Fluoride removal from water using a magnesia-pullulan composite in a continuous fixed-bed column. J. Environ. Manag. 206, 929–937.

Zhang, Y.-X., Jia, Y., 2018. Fluoride adsorption on manganese carbonate: ion-exchange based on the surface carbonate-like groups and hydroxyl groups. J. Colloid. Interf. Sci. 510, 407–417.

Zhu, J., Zhao, H., Ni, J., 2007. Fluoride distribution in electrocoagulation defluoridation process. Sep. Purif. Technol. 56, 184–191.

Zhu, H., Wang, H., Wang, G., Zhang, K., 2011. Removal of fluorine from water by the aluminum-modified bone char. In: 2010 International Conference on Biology, Environment and Chemistry IPCBEE. vol.1. IACSIT Press, Singapore, pp. 455–457.

Zhu, P., Cao, Z., Ye, Y., Qian, G., Lu, B., Zhou, M., Zhou, J., 2013. Reuse of hazardous calcium fluoride sludge from the integrated circuit industry. Waste Manag. Res. 31 (11), 1154–1159.

Zúñiga-Muro, N., Bonilla-Petriciolet, A., Mendoza-Castillo, D., Reynel-Ávila, H., Tapia-Picazo, J., 2017. Fluoride adsorption properties of cerium-containing bone char. J. Fluor. Chem. 197, 63–73.

2.2.2 Concluding remarks

The health consequences associated with the high fluoride (F^-) concentration in water sources were investigated in this study. The application of bone char for F^- removal from water has been thoroughly scrutinized in this review with the aim of highlighting the recent achievements and addressing the gaps in this research area. The manuscript provides a comprehensive review regarding the optimum production conditions of bone char and evaluates the factors that control removal efficiency. Bone char samples pyrolysed at 500–700 °C have the highest removal capacity of F^- from water. However, further increase in the pyrolysis temperature affected the hydroxyapatite composition, and thus lowered the removal capacity significantly. Modification using multivalent ions, such as aluminum, was found to enhance the removal capacity of F^- on bone char. This is due to the high electronegativity of F^-, which provides a strong ability to form complexes with metal ions. The experimental conditions represented by the pH, contact time, temperature, particle size and initial concentrations had a significant effect on the removal capacity of bone char. The mechanism of removal was found to be ion exchange between the F^- and OH^- of the hydroxyapatite. The possibility of regenerating the F^- loaded bone char via thermal and chemical methods justifies the energy and cost of the production.

CHAPTER 3

Effect of pyrolysis conditions on bone char characterization and its ability for arsenic and fluoride removal

Paper III

Alkurdi, S.S., Al-Juboori, R.A., Bundschuh, J., Bowtell, L. and McKnight, S., 2020. Effect of pyrolysis conditions on bone char characterization and its ability for arsenic and fluoride removal. Environmental Pollution, 262: 114221. (Published).

3.1 Introduction

The manuscript presents the characteristics of bone char samples produced in a temperature range of 500-900 °C for a holding time of 1 and 2 h, with and without N_2 gas. A range of characterization methods was used to examine the effect of altering the pyrolysis temperature on the surface chemistry and the physical characteristics of the samples. Fourier-transform infrared spectroscopy (FTIR), X-ray diffraction, zeta potential and scanning electron microscopy were employed, along with quantitative analyses of Boehm titration, cation exchange capacity (CEC), proximate analysis and dissolved organic carbon (DOC) measurements for tracking the change in bone char properties. The suitability of the samples for water treatment from a health perspective were based on the results of the DOC. The samples were used to examine the effect of pyrolysis conditions on the removal of As(III), As(V) and F^- from water. The mechanism of the removal was predicted based on the results of the characterization.

Environmental Pollution 262 (2020) 114221

Contents lists available at ScienceDirect

Environmental Pollution

journal homepage: www.elsevier.com/locate/envpol

Effect of pyrolysis conditions on bone char characterization and its ability for arsenic and fluoride removal

Susan S.A. Alkurdi [a, b], Raed A. Al-Juboori [c], Jochen Bundschuh [a, d, *], Les Bowtell [e], Stafford McKnight [f]

[a] School of Civil Engineering and Surveying, Faculty of Health, Engineering and Sciences, University of Southern Queensland, West Street, Toowoomba, 4350, Queensland, Australia
[b] Northern Technical University, Engineering Technical College/Kirkuk, Iraq
[c] Water Engineering Research Group, Department of Civil and Environmental Engineering, Aalto University, P.O. Box 15200, Aalto, FI-00076, Espoo, Finland
[d] UNESCO Chair on Groundwater Arsenic Within the 2030 Agenda for Sustainable Development, University of Southern Queensland, West Street, Toowoomba, 4350, Queensland, Australia
[e] School of Mechanical and Electrical Engineering, Faculty of Health, Engineering and Sciences, University of Southern Queensland, Toowoomba, 4350, QLD, Australia
[f] School of Science, Engineering and Information Technology, Federation University Australia, University Drive, Mt Helen, 3350, Victoria, Australia

ARTICLE INFO

Article history:
Received 24 November 2019
Received in revised form
2 February 2020
Accepted 16 February 2020
Available online 19 February 2020

Keywords:
Bone char
Pyrolysis conditions
Surface chemistry
Arsenic
Fluoride

ABSTRACT

This study examined arsenite [As(III)], arsenate [As(V)] and fluoride (F^-) removal potential of bone char produced from sheep (*Ovis aries*) bone waste. Pyrolysis conditions tested were in the 500 °C–900 °C range, for a holding time of 1 or 2 h, with or without N_2 gas purging. Previous bone char studies mainly focused on either low or high temperature range with limited information provided on As(III) removal. This study aims to address these gaps and provide insights into the effect of pyrolysis conditions on bone char sorption capacity. A range of advanced chemical analyses were employed to track the change in bone char properties. As pyrolysis temperature and holding time increased, the resulting pH, surface charge, surface roughness, crystallinity, pore size and CEC all increased, accompanied by a decrease in the acidic functional groups and surface area. Pyrolysis temperature was a key parameter, showing improvement in the removal of both As(III) and As(V) as pyrolysis temperature was increased, while As(V) removal was higher than As(III) removal overall. F^- removal displayed an inverse relationship with increasing pyrolysis temperature. Bone char prepared at 500 °C released significantly more dissolved organic carbon (DOC) then those prepared at a higher temperature. The bone protein is believed to be a major factor. The predominant removal mechanisms for As were surface complexation, precipitation and interaction with nitrogenous functional groups. Whereas F^- removal was mainly influenced by interaction with oxygen functional groups and electrostatic interaction. This study recommends that the bone char pyrolysis temperature used for As and F^- removal are 900 °C and 650 °C, respectively.

1. Introduction

Concerns relating to the environmental issues represented by climate change and their foreseen negative consequences require the provision of solutions for recycling the large amounts of continuously produced waste. Solid waste represents a potential renewable energy source globally. Animal bone is one of the main biomass waste sources in meat processing industries, representing about 10–15% of the animal body (Grace, 1983). According to the Australian Bureau of Statistics (2018), the total number of livestock (excluding poultry) slaughtered in Australia for the first 8 months up until September 2018 was about 40 million animals, or a red meat production of 2.6 million tons. This production level corresponds to about 0.3 million tons of bone waste.

The thermal transformation of solid waste into char has been extensively studied as a promising waste disposal solution. The by-

* Corresponding author. Faculty of Health, Engineering and Sciences & UNESCO Chair on Groundwater Arsenic within the 2030 Agenda for Sustainable Development, University of Southern Queensland, West Street, Toowoomba, Queensland, Australia.
E-mail addresses: Susan.Alkurdi@usq.edu.au (S.S.A. Alkurdi), raed.al-juboori@aalto.fi (R.A. Al-Juboori), Jochen.Bundschuh@usq.edu.au (J. Bundschuh), Les.Bowtell@usq.edu.au (L. Bowtell), s.mcknight@federation.edu.au (S. McKnight).

https://doi.org/10.1016/j.envpol.2020.114221
0269-7491/

product of this process is a valuable material that can be used for a range of environmental remediation purposes (Cruz et al., 2019; Leinweber et al., 2019; Siebers et al., 2014). The synthesis of bone char involves the carbonization of the raw bone by pyrolysis (an oxygen lacking environment) to obtain a char with a high porous structure.

Adsorption is one of the most widely used methods in water treatment process (Dotto et al., 2017). Bone char has been traditionally used for discoloration in the sugar industry (de Melo et al., 2018). In recent years, bone char has been used as an efficient adsorbent for fluoride (F^-) removal from water, on laboratory and larger system scales (Herath et al., 2018; Shahid et al., 2019). Bone char has shown a great potential for removing heavy metals and metalloids from water such as cadmium (Cd), zinc (Zn), nickel (Ni), copper (Cu) and arsenic (As) (Alkurdi et al., 2019a; Hernández-Hernández et al., 2017; Ko et al., 2000; Liu et al., 2016; Rojas-Mayorga et al., 2016).

The properties of bone char depend on the feedstock's source and the pyrolysis conditions, such as pyrolysis temperature, residence time, heating rate and purging gas (Alkurdi et al., 2019b). Generally speaking, bone char can be produced at a temperature range of 350–900 °C, depending on the bone type and the intended application. Bone char has a lower surface area compared to plant originated biochar or activated carbon. However, the inorganic structure of phosphate and calcium make bone char an attractive adsorbent for the removal of anionic contaminants such as As (Chen et al., 2008).

Arsenic and fluoride contaminated groundwater crises are a global concern. The main source of As and F^- co-occurrence in groundwater are geological, with higher concentration in arid and semi-arid areas (Alarcón-Herrera et al., 2013). Alarcón-Herrera et al. (2020) reported that > 300 million people around the world are at risk of drinking As contaminated water, with over 30 million people exposed to a high As concentration drinking water in Bangladesh alone (Van Geen et al., 2002). Bone deformation and fragility as a consequence of high F^- concentrations in drinking water are alarming issues in more than 25 countries around the world (Alarcón-Herrera et al., 2020). While As and F^- removal from water have been extensively studied using a variety of technologies and treatment methods (Jiang, 2001; Litter et al., 2010; Mohan and Pittman Jr, 2007; Mohapatra et al., 2009), adsorption has been reported as the most cost effective and environmentally friendly method. Bone char has been reported as a superior adsorbent for F^- removal from drinking water. However, more studies are needed for testing its potential for treating highly F^- contaminated industrial wastewater or groundwater (Alkurdi et al., 2019b). Similarly, there are limited studies that investigate the effect of charring temperature on As removal from water using bone char, especially arsenite [As(III)]. Several studies have used commercial bone char samples to investigate arsenate [As(V)] removal from water (Begum et al., 2016; Chen and Chai, 2008; Chen et al., 2008; Kumar et al., 2019; Liu et al., 2014; Sneddon et al., 2005; Soltani et al., 2017). To our knowledge, there have been a limited number of investigations that examined the effect of pyrolysis temperature on As(V) uptake. For instance, a study conducted by Czerniczyniec et al. (2007) investigated only a low temperature of 500 °C and a higher temperature of 900 °C, while temperatures in between were not investigated. This study mainly investigated the effect of water salinity and hardness on the char's removal capacity, rather than focusing on the effect of other pyrolysis conditions.

The mechanisms controlling removal of contaminants with bone char is strongly influenced by its characteristics and their effect on the solution being treated. Pyrolysis conditions can affect both removal mechanisms and energy consumption of the bone char preparation process. Thus, a comprehensive investigation on the effect of pyrolysis conditions on bone char characteristics and its removal capacity of hazardous contaminants such as As and F^- is of great benefit for environmental remediation research. The goal of this study is to address the research gaps highlighted above and provide better understanding for the effect of pyrolysis conditions on bone char properties and its removal capacity for F^- and As species. As and F were selected in this study as model contaminants due to the great risk they impose to public health and the environment. A range of advanced analytical and chemical techniques were applied for detecting and evaluating the changes occur in bone char characterization with different pyrolysis conditions. Correlations between different characteristics were also tested and reported. Bone char removal of F^- and As at different pyrolysis conditions was investigated, and results were analyzed in light of the obtained information on bone char characterizations. The significance of the change observed in bone char characteristics and obtained correlations were examined for their significance using common statistical tools.

2. Materials and methods

2.1. Bone char preparation

Sheep leg bones were obtained from a local butcher shop located in Toowoomba, Queensland, Australia. The bones were cut into uniform 1.5 cm segments and thoroughly cleaned to remove any remaining meat and fat. The bones were pressure cooked in tap water for 30 min for an easier removal of tissues and bone marrow. This procedure was repeated 2–3 times until cleaning was completed. Bone samples were allowed to cool and then the trabecular bone inside was removed to obtain uniform compact bone samples. Bone samples were pyrolyzed in a limited oxygen environment using a Rio Grande brand kiln (model CS2 from USA).

The pyrolysis process used a temperature ramp-up rate of 10 °C per min to four different temperature setpoints of 500 °C, 650 °C, 800 °C and 900 °C. Two holding times were examined for each of the temperature setpoints; 1 or 2 h. These same procedures were followed to produce additional bone char samples at the same experimental conditions but with the addition of N_2 as a purging gas, at a rate of 400 mL/min. For the bone char samples produced at 500 and 650 °C, the samples were held at the targeted temperature for 2 h. This holding time was applied to reduce the concentration of total organic matter released which was found to be high for a residence time of 1 h. The 1 h residence time was used for samples produced under N_2 gas at temperatures of 800 °C and 900 °C, as it was found that a holding time of 2 h with such high temperatures could transform the color of the bone char to white, indicating diminished functional groups on the surface of the bone char (Kawasaki et al., 2009). The produced bone char sample was crushed and sieved to an average particle size of 1–2 mm, then washed with deionized water repeatedly until a stable low electrical conductivity (EC) was reached indicating all mineralized ash was removed, before being sealed and stored for later use.

2.2. Bone char characterization

Different characterization methods were used to examine the effects of altering the pyrolysis conditions on the properties of the bone char. All the measurements in this study were performed in triplicate to ensure the quality and repeatability of the work.

2.3. FTIR spectroscopy

Fourier transform infrared (FTIR) spectroscopy was used to identify functional groups on the bone char surface. To obtain

absorption spectra, bone char samples were mixed with spectroscopic grade dried KBr (BDH Chemicals Ltd, Poole, England) and then compressed into pellets. FTIR spectra were recorded between wavenumber of 4000 cm^{-1} and 400 cm^{-1} with an IRAffinity-1S FTIR spectrometer supplied by Shimadzu, at a basic resolution of 0.5 cm^{-1}. Prior to FTIR analyses, all bone char samples and KBr were oven-dried overnight at 60 °C.

2.3.1. Surface analysis

The morphology of bone char particles was tested using a scanning electron microscope (SEM) (JEOL, model JSM-6000 Plus). Elemental composition of the samples prepared at 500 °C and 900 °C were examined using Phenom Prox Desktop SEM with Energy Dispersive X-Ray analysis (EDS), Gen 5.

The textural properties of the samples were performed by Particle and Surface Sciences Pty Limited using a TriStar 3000 V6.08 A. The specific surface area (S_{BET}), was estimated using Brunauer–Emmer–Teller (BET) equation based on N_2 adsorption at 77.3 K and $P/P0$ of 0.05–0.25. The pore volume was measured at the single point of $P/P0 = 0.99$. The pore sizes of the samples were obtained from 4 V/A by BET.

2.4. Surface charge and point of zero charge

The surface charge of bone char was measured by a dynamic light scattering topology, using a Nano-S Zetasizer (Malvern Instruments Ltd., UK) at 22 °C. In brief, the ground bone char was further crushed and sieved prior to the samples' addition to deionized water to produce a suspension with a concentration of 5 g/L. The quality of the samples was examined via the count rate (kilo count per second) indicated by the instrument (Clogston and Patri, 2011). The suspension was shaken for 20 h at 25 °C.

The electrophoretic mobility of the bone char particles was studied using static methods with a Nano S Zetasizer (Malvern Instruments). The electrophoretic mobility of a spherical particle is related to the zeta potential through Henry's equation;

$$U_E = \frac{2\varepsilon\, z\, f(Ka)}{3\eta} \quad (1)$$

where z is the zeta potential (mV), U_E is the electrophoretic mobility, is the viscosity, ε is the dielectric mobility and $f(Ka)$ is Henry's function.

The suspensions were prepared by mixing 20 mg of bone char powder with 20 mL of deionized water. To determine the point of zero charge, the suspensions' pHs were then adjusted in the range from pH 2 to pH 8 by addition of 0.1 M NaOH or HCl. Aliquots of the suspensions were then passed through the measurement cell. Each mobility value presented was an average of 9 values, and two series of measurements were carried out.

2.4.1. Surface pH and EC

Surface pH and EC were measured following the procedure reported in Dang et al. (2018). Approximately 0.2 g of each bone char sample was separately added to 100 mL of deionized water (pH 7.0) and was then shaken on a Ratek rotary shaker for 30 min at 120 rpm. The pHs and ECs of the solutions were measured using Orion Star benchtop meters models A111 and A212, respectively.

2.4.2. Proximate analysis

Proximate analysis of the bone char samples, including moisture and ash content, volatile matter and fixed carbon ratio was conducted following ASTM standards (ASTM D1762-84). One gram of each sample was placed in the OHAUS MB120 Moisture Balance at 105 °C to determine the moisture content. The dried samples were utilized to determine the volatile matter by calculating weight differences before and after heating samples in covered crucibles, using a programmable muffle furnace at 950 °C for 11 min. The same procedure was applied to determine the ash content; however, the furnace temperature was set at a lower temperature of 750 °C and the sample crucibles were not covered.

2.4.3. Cation exchange capacity

Cation Exchange Capacity (CEC) was determined following the procedures reported by Dang et al. (2018). After washing the samples with deionized water repeatedly until an EC value of 50 μS/cm was reached, 2 g of the bone char sample was added to 50 mL of 0.5 M NH_4Cl solution and shaken for 1 h using a Ratek shaker at 140 rpm. Solutions were filtrated using Advantec No.1 filter paper and the exchangeable cations were determined using ICP-MS (PerkinElmer NEXION 300 ICP/MS).

2.4.4. Dissolved organic carbon (DOC)

Carbon release from bone char was detected by applying extraction with deionized water. One gram of bone char was mixed with 50 mL deionized water and shaken at 240 rpm for 24 h. Later, the mixture was filtered through Advantec Grade GB140 Glass Fibre Filters (0.45 μm) with the released dissolved carbon measured using a Shimadzu Total Organic Carbon Analyzer (TOC-VCSH) following the standard high-temperature combustion method (5310 B) (Eaton et al., 2005).

2.4.5. Bohem titration

Bohem titration was used to determine acidic and basic functional groups on the surface of the bone char, following the procedure reported by Boehm (1994). Each of the 0.5 g of bone char samples was added to 0.05 M $NaHCO_3$ (Chem-Supply, AR), Na_2CO_3 (Chem-Supply, AR) and NaOH (Labscan Asia Co. Ltd, AR) to determine the amount of the acid sites on the surface. For the determination of the basic sites, the same amount of each sample was added to 0.05 M HCl solution (32%, AR grade, RCI Labscan). The samples were sealed and shaken for 24 h at 200 rpm then filtrated to separate the bone char. N_2 gas was used to purge excess CO_2 gas from the solution and then the samples used to determine the acid sites were neutralized with excess 0.05 M HCl. The excess HCl was determined by potentiometric back-titration with 0.05 M NaOH and the concentration of different functional groups was calculated.

2.5. XRD analyses

XRD analyses were obtained on a Panalytical X'Pert Pro diffractometer at Federation University, equipped with an incident beam BBHD Co Kα monochromator and an X'Celerator linear detector, operated at 40 kV and 25 mA over 5–70° 2θ with a step size of 0.017° 2θ at a rate of 0.08° 2θ per second. Phases were identified by search-match of the 2019 ICDD minerals database. Crystallite sizes of the treated chars were determined from line broadening of the apatite (002) peak using the Scherrer calculator from Panalytical HighScore Plus and a high purity crystalline apatite as a standard.

2.6. Adsorption experiments

The impact of pyrolysis temperature in the range of 500 °C and 900 °C on the F^-, As(III) and As(V) adsorption capacity of bone char was examined using synthetic samples prepared from high purity salts and stock solutions with double distilled water as described in 2.3.1. The removal capacity was calculated using the following formula:

$$R = \frac{C_0 - C_f}{w} * v \quad (2)$$

where R is the removal in mg/g, C_0 is the initial concentration in mg/L, C_f is the final concentration in mg/L, v is the volume of the solution in L and w is the weight of the adsorbent in g.

2.7. As and F^- adsorption experiments

The batch adsorption experiments were conducted using a 500-mL Erlenmeyer flask. A stock solution of As(III) and As(V) of 1000 mg/L in 2% HNO_3 was purchased from High-Purity Standards. An initial As concentration of 1 mg/L was prepared by diluting the stock solution with double distilled water in a 500 mL volumetric flask and was used for kinetic experiments. This concentration was chosen based on average As concentrations in the groundwater in different areas around the world (Herath et al., 2016; Mukherjee et al., 2006).

A dose of 5 g/L of each bone char sample was placed in a 50 mL container. Solutions were placed in the container and shaken for 24 h using a medium orbital shaker from Ratek (model EOM5). The samples were centrifuged and filtrated using Whatman qualitative filter paper, Grade 1. Residual As levels were measured using ICP-MS.

For the F^- batch experiment, a stock solution with a concentration of 50 mg/L was prepared by dissolving NaF (AR grade, Chem-Supply) in double distilled water. Afterwards, 50 mL of 10 mg/L of F^- solution was poured into 250 mL glass-stoppered Erlenmeyer flasks along with 1 g of each bone char. Samples were sealed and agitated at 120 rpm at room temperature for 24 h using a medium orbital shaker (Ratek, EOM5). Samples were filtered after shaking using 0.45 μm cellulose membrane. F^- concentration in the solution was measured using Thermo Scientific Dionex ICS-2000 ion chromatography (accuracy ± 2%SD).

2.8. Statistical analysis

Data was analyzed using MINITAB 19 software. Analysis of variance (ANOVA), significance and fit testing were applied to study the changes in the measured characteristics and the obtained correlations. The Tukey's Honest Significant Difference test was performed when significant differences existed among the factors (as indicated by the F-ratio) in order to determine which pair-wise interactions were significantly different at $P < 0.05$. All data was reported as mean ± standard deviation ($n = 3$).

3. Results and discussion

3.1. pH, surface charge, point of zero charge and EC

Physicochemical properties such as pH, EC, point of zero charge and surface charge are useful indicators for the char quality that can easily be used on an industrial scale. Hence, they were measured for the prepared bone char samples in this study and presented in the supplementary materials (Table SM1). The pH of the bone char increased from 8.4 to 11.6 after raising the pyrolysis temperature from 500 °C to 900 °C indicating the reduction of oxygen surface functional groups on the bone char and their substitution with neutral or basic aromatic groups (Gezahegn et al., 2019; Luo et al., 2015). However, there was a slight decrease detected in pH for samples prepared under a purged N_2 environment as opposed to those prepared under a limited oxygen environment. Similarly, the EC and surface charge of bone char samples prepared at lower temperatures (500 °C) were found to be less than those prepared at higher temperatures.

The surface charge of solid particles in water is related to the ability of water to dissolve ions and develop an electrical double layer on the surface of the particles (Fairhurst, 2013). In an aqueous solution, surface charge is mainly related to the protonation/deprotonation reaction of surface functional groups in solution. The basic surface pH of the samples presented in Table SM1, indicates the presence of oxygen functional groups, which are likely to dissociate and release protons from the surface of the hydroxyl groups (Butt et al., 2003). For bone char samples, the negative surface charge can be related to the presence of calcium hydroxide and phosphate sites at pH > 5 (Rocha et al., 2012). However, this value varies based on the pyrolysis temperature and feedstock type. Increases in the surface charge with increasing pyrolysis temperature is also likely due to the thermal alteration of surface functional groups. In other words, the dissociation of acid groups will cause increased negative surface charge (Prado et al., 2011).

Fig. SM1 in supplementary materials compares the evolution of the zeta potential of bone char powder suspensions at different pH values. It was observed that the bone char surface was negatively charged in pure water at neutral pH. The sign of the zeta potential of the bone chars reversed at pH values ranging from 6 to 8.5. These points of zero charge (pH_{PZC}) values were close to those values reported in literature (7.4–10) (Alkurdi et al., 2019b), except for the samples prepared at lower temperatures (500 °C and 650 °C). The shift in pH_{PZC} is a significant indication of altered sample surface properties, due to the different experimental conditions. This could prove to be a good assessment criterion for optimizing pyrolysis conditions to meet specific requirements.

3.2. Proximate analysis

Bone char moisture content, ash content, volatile matter and the fixed carbon ratio of the prepared bone char are shown in Table SM2. The results revealed that increasing the pyrolysis temperature decreased the volatile matter and moisture content, while the reverse trend was observed for ash content and fixed carbon levels. When residence time was increased, a similar negative trend was observed for moisture content, volatile matter and fixed carbon levels. The ash content of bone char made at 800 °C was lower than that of commercial bone char made at the same temperature by about 36%, as reported by Mendoza-Castillo et al. (2015). In comparison, OA et al. (2019) reported that the moisture content, ash content, volatile matter and fixed carbon for bone char made from cow bones at 700 °C were 22.5%, 6.65%, 7.76% and 62.42%, respectively. These results showed a higher volatile matter and moisture content, but a lower ash content compared to the results achieved in this study. This may be explained by the difference in the feedstock used and the operational conditions (Luo et al., 2015).

For the samples prepared with purging N_2 gas during the carbonization process, the results showed lower volatile matter and ash levels, but higher fixed carbon content when compared to samples produced under similar conditions but without N_2 purging gas (Table SM3).

Links between changes in proximate analysis and sorption capacity of bone char have not been clearly established in literature and the studies that address this point are limited. A study conducted by (Gumus et al., 2012) investigated the change in absorption capacity of cow bone char with three pyrolysis temperature of 300 °C, 400 °C and 600 °C, reporting on the corresponding changes in proximate analyses. This study showed that as the pyrolysis temperature increased, moisture content decreased and ash content increased. This coincided with a decrease in the adsorption capacity of synthetic color prepared from dark brown sugar. In this study the investigated temperature range was higher and the

targeted contaminants were As and F^-. Addressing the removal of As and F^- in later sections could show how these changes along with the changes in other properties affect the adsorption capacity of the prepared bone char.

3.3. Surface characterization

Fig. 1 shows SEM images for bone char samples prepared at different charring temperatures and holding time with or without purging N_2 gas. In general, bone char SEM images showed rough morphology, a surface with few or no pores and undefined geometry, which was in alignment with the findings of other studies on bone char (Rojas-Mayorga et al., 2016). It was noticed that the sample's surface texture became rougher and more porous when either the charring temperature or the residence time increased. At 500 °C, the sample had a relatively flat surface without clearly visible pores. Raising the temperature to 900 °C effectively changed the surface morphology and more pores were observed. However, the use of N_2 purging gas and increasing the residence time did not significantly affect surface morphology of the chars produced under the same conditions.

Several studies reported that surface texture is a function of

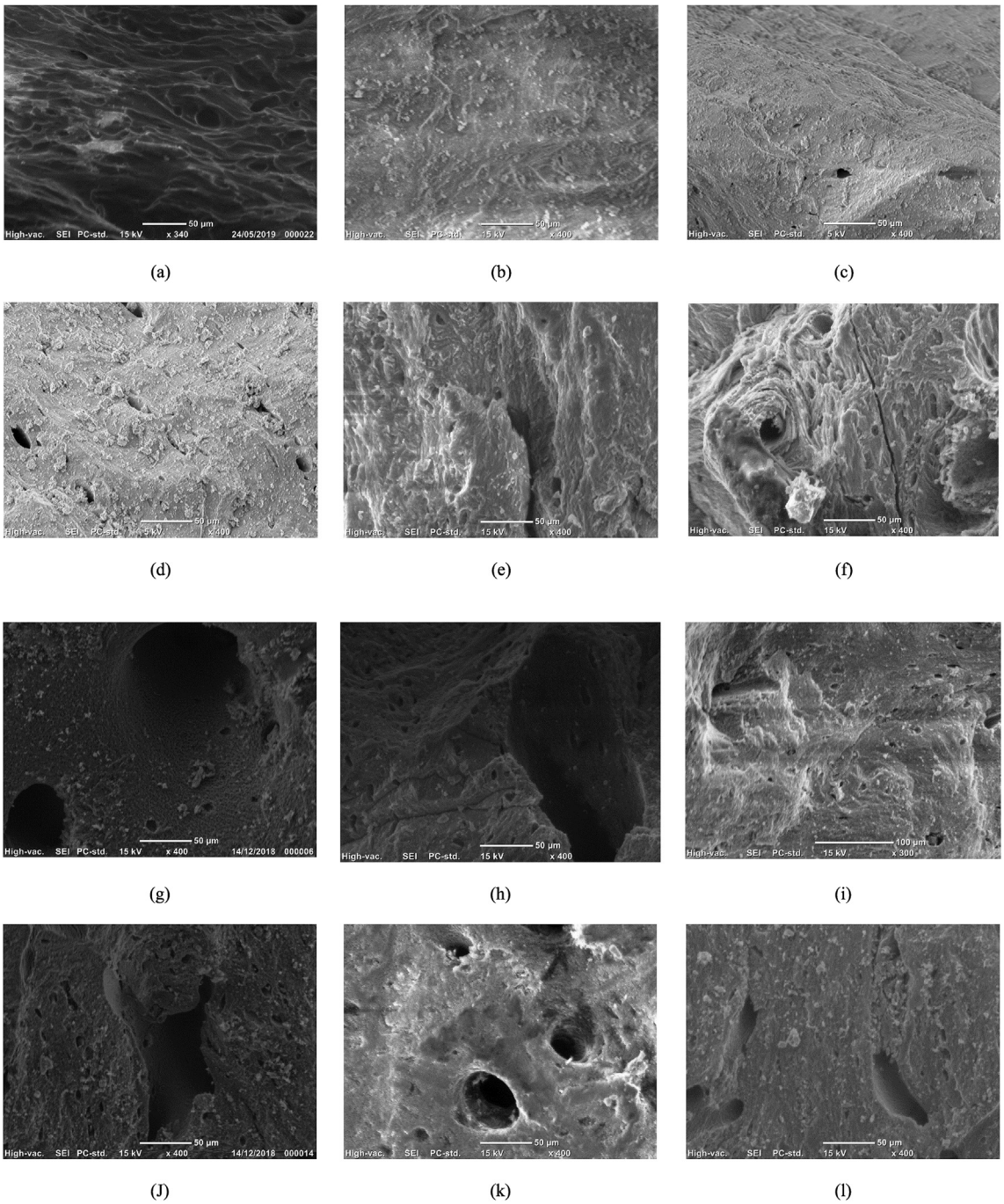

Fig. 1. SEM images of bone char samples prepared at 500–900 °C, residence time 1–2 h time with or without purging N_2 gas*. (a) BC-500-1, (b) BC-500-2, (c) BC-500-N_2, (d) BC-650-1, (e) BC-650-2, (f) BC-650-N_2, (g) BC-800-1, (h) BC-800-2, (i) BC-800-N_2, (j) BC-900-1, (k) BC-900-2, (l) BC-900-N_2.

pyrolysis temperature. Increasing pyrolysis temperature to a certain limit (about 550 °C) reportedly resulted in an increase to the surface area and pore volume of the charred material, due to devolatilization of some biomass components (Angın and Şensöz, 2014; Brunson and Sabatini, 2014). Similarly, in this study, the BET surface area of the bone char prepared at 500 °C was 120.031 m^2/g (Table SM4). However, further increases in the charring temperature resulted in decreasing the surface area (89.06 m^2/g at 900 °C) due to shrinkage and realignment in the char structure (Angın and Şensöz, 2014). Changes in surface characteristics are also related to other factors such as the feedstock source, experimental conditions and equipment used (Brunson and Sabatini, 2014). For instance, Rojas-Mayorga et al. (2013) reported that there were no significant variations in the surface morphology, surface area and porosity of cow bone char produced in the temperature range of 650 °C–800 °C. Conversely, Patel et al. (2015) found a decrease in sample porosity of the samples after raising the temperature, due to the increase in the crystal size and the grain growth, which will be addressed in XRD analysis in Section 3.7. Our study indicates a slight reduction in pore volume from 0.283 to 0.235 m^3/g, and an increase in pore size from 9.444 to 13.588 nm after raising the pyrolysis temperature from 500 °C to 900 °C (Table SM4).

Elemental analyses using SEM EDS technology provided that increasing pyrolysis temperature from 500 °C to 900 °C had resulted in decreasing the oxygen and sodium percentages in the char from 50.88 to 0.53 to 48.02 and 0.43, respectively (Fig. SM2). Contrary to this, there was an increase in the percentage amount of carbon, calcium and phosphorus from 21.69, 12.0 and 6.66 to 27.44, 15.04 and 8.47%, respectively. However, 7.84% nitrogen was detected on the bone char produced at 500 °C, but it was not detected for the 900 °C prepared bone char, while 0.51% magnesium was only detected in samples prepared at 900 °C.

3.4. FTIR analysis

FTIR spectroscopy was used to analyze the structural changes of bone char samples produced under different pyrolysis conditions. Deconvolution was used to determine the number and the position of the overlapped bands. The second spectral derivatives were used to provide a reasonable estimate of overlapped bands in a selected region (Smith, 2011). FTIR spectra of bone char with different holding time values and charring temperatures are shown in Fig. 2, while changes in the bone char characteristics due to the presence of N_2 gas during pyrolysis are provided in the supplementary document (Fig. SM3).

Results revealed an influence of pyrolysis temperature on the surface chemistry of bone char. Spectra of the all bone char samples provided evidence of hydrogen bonds, as carboxylic acid OH stretches at around 3400 cm^{-1} and OH at 960 cm^{-1}. Carboxylic groups are composed of C=O which can be detected around 1749–1728 cm^{-1}. Due to the overlap band of these peaks in the area of interest, they were detected by determining the second derivative of the peaks, as demonstrated in Fig. SM4. These peaks, along with the C–O peak at around 1320 cm^{-1} were clear evidence of the presence of carboxylic groups (Smith, 2018).

Lactones can be identified from the peaks shown around 1610 cm^{-1} (Shen et al., 2008). Both peaks' intensities decreased after increasing temperature and residence time (this will be discussed further in the following section). The shift in the peaks' positions after raising the pyrolysis temperature is an indication of thermal alteration of the bone char composition. Although a very low concentration of phenol groups was detected through neutralizing bone char samples with NaOH (data presented in the next section), peaks related to phenol groups were not detected in

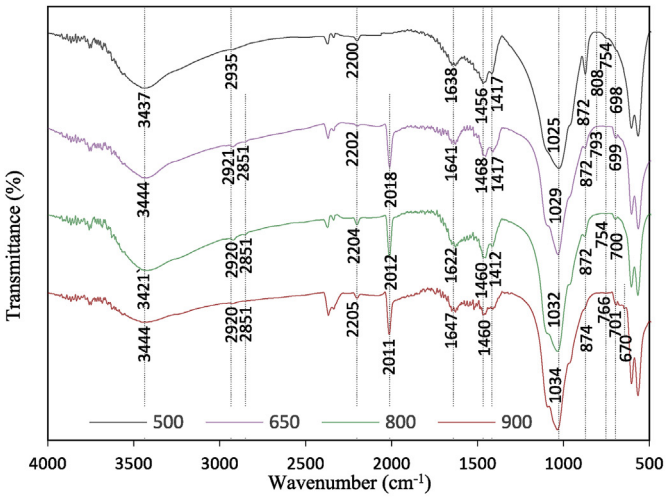

(a) Residence time of 1h

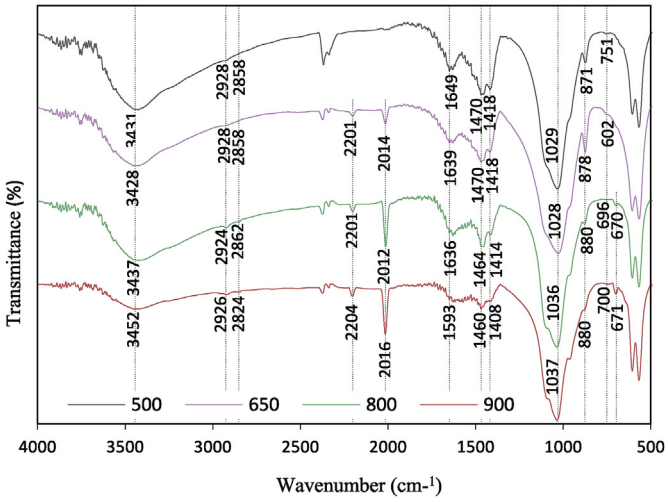

(b) Residence time of 2h

Fig. 2. FTIR analysis for the samples produced at 2 different residence time.

FTIR analysis.

The growing peak at 700-610 cm^{-1} with rising temperature suggests the presence of C≡C–H bend (broad strong absorption) (Stuart, 2000). The appearance of aliphatic symmetric and asymmetric C–H stretching bands at around 2924 and 2864 cm^{-1}, respectively, indicates the presence of saturated carbon (Stuart, 2000).

The hydroxyapatite structure was not affected by raising the pyrolysis temperature. Bands at 563 and 603 cm^{-1} indicated the presence of PO_4^{3-} v_4 antisymmetric bending (Lopes et al., 2018), while the peak at 1100 cm^{-1} was assigned to PO_4^{3-} v_3 antisymmetric stretching (Boskey and Mendelsohn, 2005). Moreover, the band at 962 cm^{-1} was due to PO_4^{3-} v_1 (Gu et al., 2013). To examine the changes in bone char structure that accompany the color changes (color alteration to grey) at 900 °C for a 2-h residence time, an FTIR scan was used to demonstrate the structural difference

between the grey and the black samples. As can be seen in Fig. SM5, surface functional groups almost completely disappeared.

The C–O stretching bond was due to the presence of PO_4^{3-} CO_3^{2-} groups. The peak at 873 cm^{-1} was assigned to $PO_4^{3-}v_2$, while the peaks in the range of 1400–1550 cm^{-1} were related to PO_4^{3-} stretching (Boskey and Mendelsohn, 2005). The bands at 1585–1720 cm^{-1} were associated with the presence of H_2O and amide I. Increasing pyrolysis temperature led to a broader peak indicating the degradation of the amide compounds when temperature increased to 900 °C. The effect of raising the pyrolysis temperature on bone char structure could also be noticed in the formation of a new sharp peak at around 2013 cm^{-1} (Fig. 2). This is likely to be due to the degradation of the protein available in the bone structure and the formation of isocyanate (–NCO), thiocyanate (SCN–) and isothiocyanate groups (–N=C=S) (Tomasini et al., 2012). The formation of the latter groups was attributed to S=O stretching, which was distinguished by the peak at 1030 cm^{-1} (Stuart, 2000). The degradation of proteins was also indicated earlier in the elemental analysis of bone char through the decreasing percentage of nitrogen.

It is believed that the protein structure contributes to the release of carbon from bone char at low temperatures and the degradation of such structures with increasing pyrolysis temperature decreases carbon release from the bone char. This conjecture was tested with correlations between the measured DOC from bone char suspension (Table 1) and the area and intensity of the peak around 2013 cm^{-1}. For the samples prepared in a limited oxygen environment, the area and intensity of the peak in FTIR analyses were negatively correlated to the concentration of the corresponding DOC. However, the correlation with peak area was much clearer than that of the intensity as the latter had some outliers. The holding time has a similar effect to that of the temperature, as doubling the holding time resulted in a drop in DOC by almost 50%, from 50.34 to 26.48 mg/L. The correlation coefficient was $R = -0.986$ (p-value < 0.005) and $R = -0.997$ (p-value < 0.005) for a residence time of 2 and 1 h, respectively. A similar relationship ($R = -0.998$, p-value < 0.01) between the amount of DOC and the peak area were examined for the samples prepared in an N_2 atmosphere. These results agree with the results reported by Patel et al. (2015) and Figueiredo et al. (2010), which confirm that the majority of organics decomposition occurs in temperature range of 500 °C–600 °C. However, the results achieved in this study show that the decomposition continued until 900 °C, but at lesser rates.

Correlating the intensity of the same peak with released DOC were in accordance with those examined using peak area, but with a lower significance value. The correlation coefficients for samples made at a residence time of 1 h, 2 h and in N_2 atmosphere were −0.83, −0.81 and −0.85, respectively. Accordingly, the significance of correlations was >0.11, >0.3 and >0.08, respectively. Thus, it can be said that the peak area at 2013 cm^{-1} is a good representation of carbon degradation in bone char and can be used to estimate the amount of carbon released from the char.

Table 1
Amount of the DOC released from each bone char sample in mg/L.

Temperature (°C)	Holding time (h)	Limited oxygen environment	N_2 gas purging
500	1	50.34 ± 0.19	–
	2	26.48 ± 0.02	41.86 ± 0.18
650	1	5.68 ± 0.02	–
	2	5.007 ± 0.14	5.668 ± 0.03
800	1	4.192 ± 0.04	2.79 ± 0.06
	2	4.11 ± 0.01	–
900	1	3.87 ± 0.03	2.75 ± 0.06
	2	3.67 ± 0.11	–

3.5. Boehm titration

Pyrolysis temperature is the most significant factor effecting the concentration and the strength of bone char surface functional groups (Li et al., 2014). Bone char samples were produced in a limited oxygen environment, and hence exhibited various concentrations of oxygen surface functional groups. These include carboxylic, lactonic, and phenolic groups. Examining the presence of these groups and their concentrations is important for understanding the adsorption mechanisms. The measured concentrations of these groups for different bone char samples are shown in Table 2 and SM5.

Generally, increasing the temperature and holding time decreased the acidic functional groups, which was in agreement with the results provide by the SEM EDS analysis. However, use of N_2 did not significantly affect carboxylic groups, but did decrease other acidic groups. Boehm titration results indicated that carboxylic and the lactonic functional groups decreased with an increase in pyrolysis temperature, which is assigned to the peaks around 1718 and 1610 cm^{-1}, as previously mentioned. Phenolic hydroxyl was detected in very small concentrations at the lower pyrolysis temperatures. Similarly, the total acidity decreased from 4.933 to 3.526 mmol/g and from 4.085 to 2.235 mmol/g for 1 h and 2 h residence time after raising the pyrolysis temperature. This correlated well with the results presented in Table SM1.

The rise in the surface pH is evidence of the presence of basic surface oxides on the surface of the bone char samples. Boehm (1994) reported that these oxides are always available on the carbon surface, due to the chemisorption process of atmospheric oxygen during cooling and later in aqueous solution. The levels of the basic functional groups were also presented in Table 1 and SM5. As can be seen from the results, there is no change in the basic groups' concentrations with changing experimental conditions. The amount of the acidic and basic functional groups on the bone char samples presented in this study are significantly higher than those reported by Ip et al. (2010) using a commercial bone char sample (0.13 and 3.07 mmol/g, respectively).

3.6. Cation exchange capacity

Cation exchange capacity is an important indication for the material's ability to adsorb cations and is a relatively simple technique for examining the adsorption capacity of bone char. In this study, the cation exchange capacity was determined based on the concentration of the exchangeable Na, K, Mg and Ca concentration released from samples. The results showed that there was a gradual increase in the CEC after raising the pyrolysis temperature from 500 to 800 °C for both sample groups (with or without N_2 purging) followed by a sharp increase after 800 °C (Fig. SM6). These results are in agreement with the findings reported by Waghmare et al. (2015). The higher CEC of the 900 °C sample, was due to the higher exchangeable Mg concentration released, while there was only a slight difference in the concentration of the rest of the cations, as shown in Fig. 3. However, the CEC for samples charred under an N_2 environment were found to be slightly lower, than those without N_2 gas purging at the same temperature. The increase in the CEC was due to the changes in the porosity and the surface chemistry of the bone char with temperature, which was well correlated with the SEM, Boehm titration and FTIR results.

3.7. XRD analyses

The effect of pyrolysis conditions on bone char crystallinity was

Table 2
The results of the Boehm titration for bone char samples prepared at different temperatures.

Charring temperature (°C)	Holding time (h)	Carboxylic groups (mmol/g)	Phenolic groups (mmol/g)	Lactonic groups (mmol/g)	Basic groups (mmol/g)
500	1	3.954 ± 0.06	0.310 ± 0.06	0.589 ± 0.08	2.309 ± 0.02
	2	3.211 ± 0.12	0.262 ± 0.09	0.487 ± 0.11	2.439 ± 0.06
650	1	3.497 ± 0.03	0.211 ± 0.10	0.481 ± 0.12	2.444 ± 0.11
	2	3.180 ± 0.06	0.162 ± 0.13	0.388 ± 0.05	2.468 ± 0.09
800	1	3.379 ± 0.11	0.158 ± 0.08	0.271 ± 0.09	2.421 ± 0.09
	2	2.277 ± 0.12	0.140 ± 0.03	0.217 ± 0.07	2.435 ± 0.07
900	1	3.295 ± 0.06	0.069 ± 0.05	0.169 ± 0.10	2.382 ± 0.12
	2	2.175 ± 0.08	0.045 ± 0.12	0.105 ± 0.06	2.580 ± 0.06

captured using XRD analysis as depicted in Fig. 4. The diffractograms shown in Fig. 4 exhibit a typical hydroxyapatite structure, indicated by the appearance of its typical indices (Fig. 4 a) (Rojas-Mayorga et al., 2016). It was noticed that the peak's width decreased, and the height increased with temperature rise. These results agree with those reported by Patel et al. (2015). This trend is believed to be associated with the increase in crystallinity, which is a measure of crystallite size (Person et al., 1995). The crystallite size for different pyrolysis conditions were measured according to the method reported by Kang et al. (2018) as presented in Fig. SM7. It is clear that raising the pyrolysis temperature or increasing the residence time increases the crystallite size. However, increasing the time from 1.5 to 2 h did not lead to a significant increase in the crystallite size. Similar results were obtained by other studies (Figueiredo et al., 2010). The increase in crystallinity of bone char corresponded with a decrease in carbon content of the char (Figueiredo et al., 2010), and this in line with the results presented in Table SM2 and surface analysis. Contrary to temperature and residence time effects, using nitrogen as a purging gas resulted in lower crystallinity.

4. Application of the bone char as an adsorbent

4.1. Kinetic experiments for As removal at various conditions

Preliminary experiments were conducted to examine the effect of charring conditions on bone char properties and their ability to adsorb As(III) and As(V). To examine the effect of pyrolysis conditions, other experimental parameters such as initial concentration, pH and the bone char dose were kept constant. Arsenic adsorption capacities of the bone char samples at different pyrolysis conditions are presented in Fig. 5. The results of the experiments indicated that the pyrolysis temperature and the residence time have a significant effect on As adsorption (p-value < 0.01). On the other hand, the purging gas has an insignificant effect on the bone char ability to remove As (p-value > 0.05).

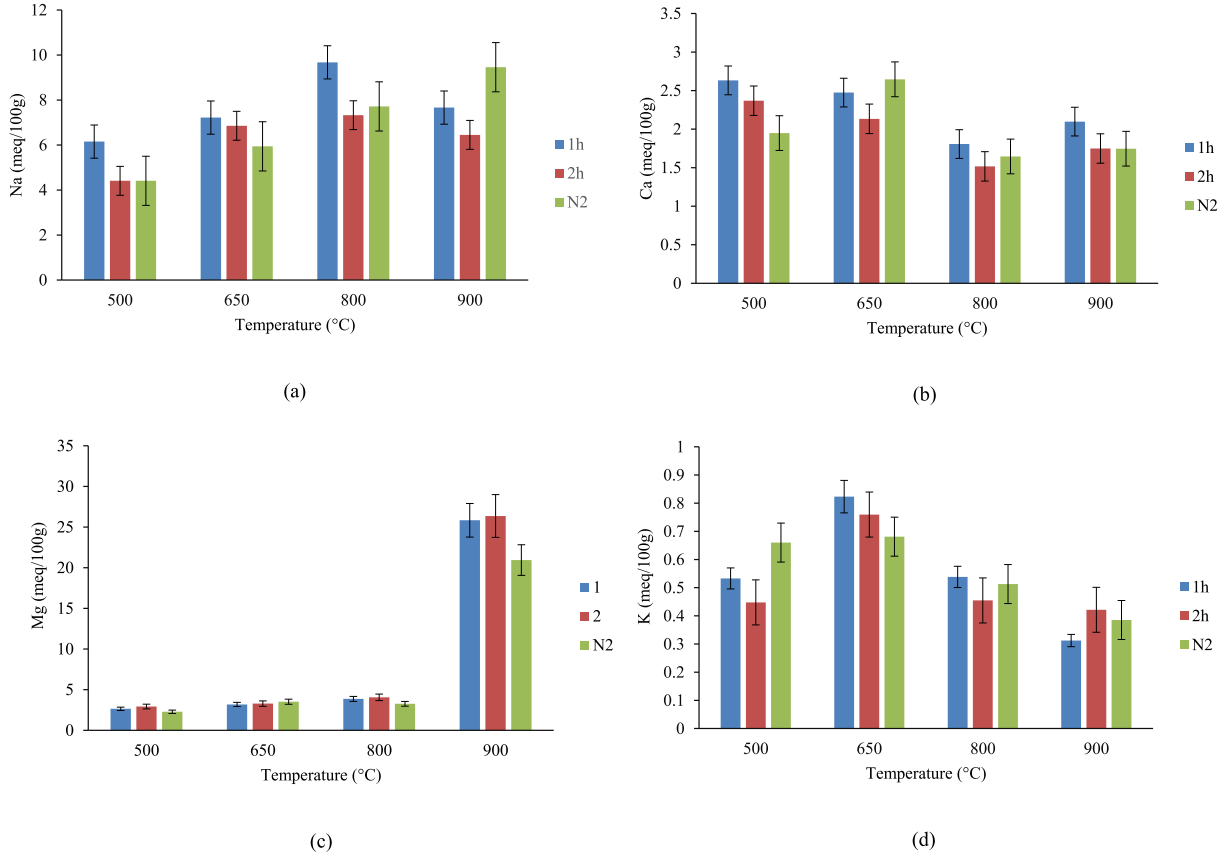

Fig. 3. The concentration of the exchangeable cations in bone char samples made at 1 h, 2 h and under N_2 stream. (a) Na, (b) Ca, (c) Mg and (d) K ion concentrations.

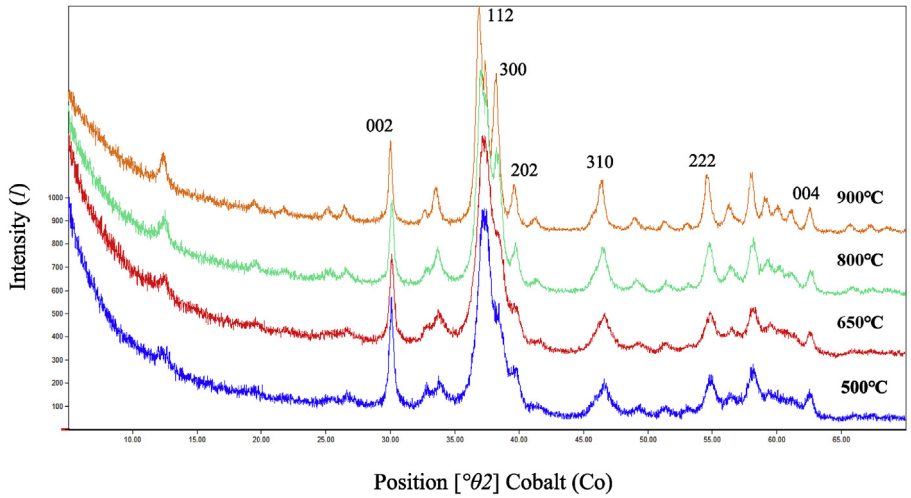

(a)

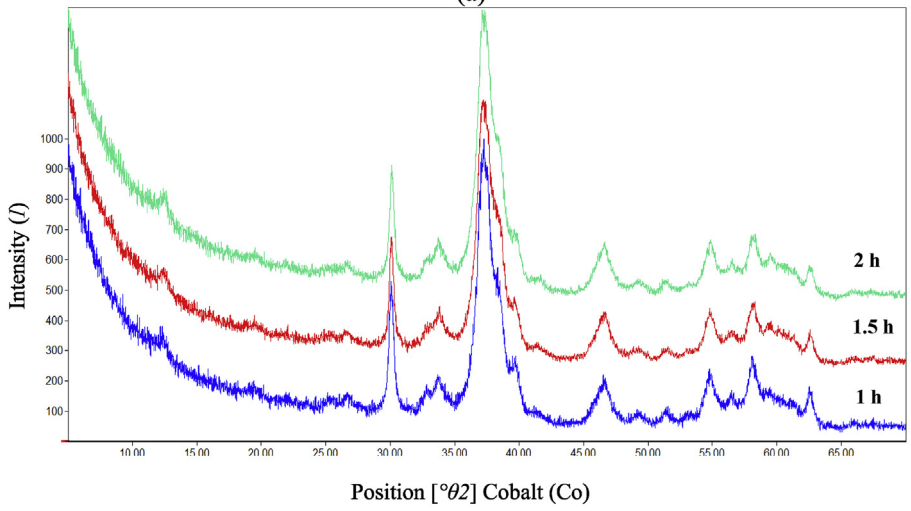

(b)

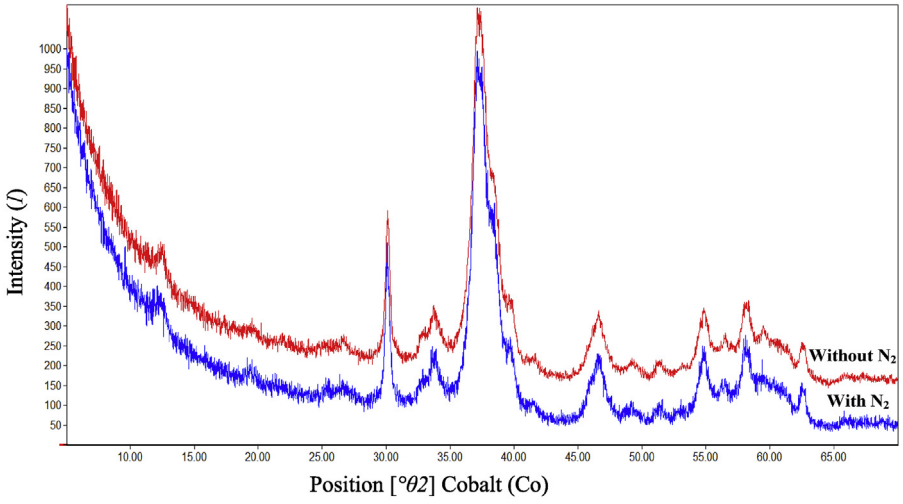

(c)

Fig. 4. Effect of pyrolysis conditions on bone char crystallinity: (a) temperature for residence time of 2 h without N_2, (b) residence time at 650 °C without N_2 and (c) with or without N_2 at 650 °C for 2 h.

Bone char samples prepared at 500 °C for a residence time of 1 h showed a very low removal capacity for both As(III) and As(V) (0.96 and 6.11 μg/g, respectively). This may be explained by the high DOC released during the agitation process (Grafe et al., 2002). However, samples prepared at the same temperature but with a 2 h residence time and in N_2 environment were more effective in removing As(V) than As(III). For both As species, a bone char sample prepared at 900 °C has the greatest removal capacity compared to other temperatures, while the residence time and purging gas had no effect on As(V) removal from water at 900 °C. On the other hand, As(III) uptake on bone char was significantly affected by pyrolysis conditions during the pyrolysis process. The difference in the bone char ability to uptake different As species is related to the difference in their oxidation state, which is the determinant factor in the immobilization of As species during adsorption/desorption process. The smaller ionic radius of As(V) as opposed to As(III) (Ali and Aboul-Enein, 2002) makes the latter more readily absorbed by the porous structure. This, along with the increase of bone char charge and pore size as temperature increases, may explain the higher absorption of As(V) compared to As(III).

For As(III), there was a slight decrease in the removal capacity of the bone char for the samples produced in the presence of N_2 gas. As it can be seen from Fig. 5, increasing the residence time from 1 to 2 h resulted in a slight increase in As(III) uptake of the bone char at 500 °C. However, the reverse effect was observed for the highest temperature of 900 °C. This is likely to be related to the effect of pyrolysis temperature on surface functional groups as discussed previously.

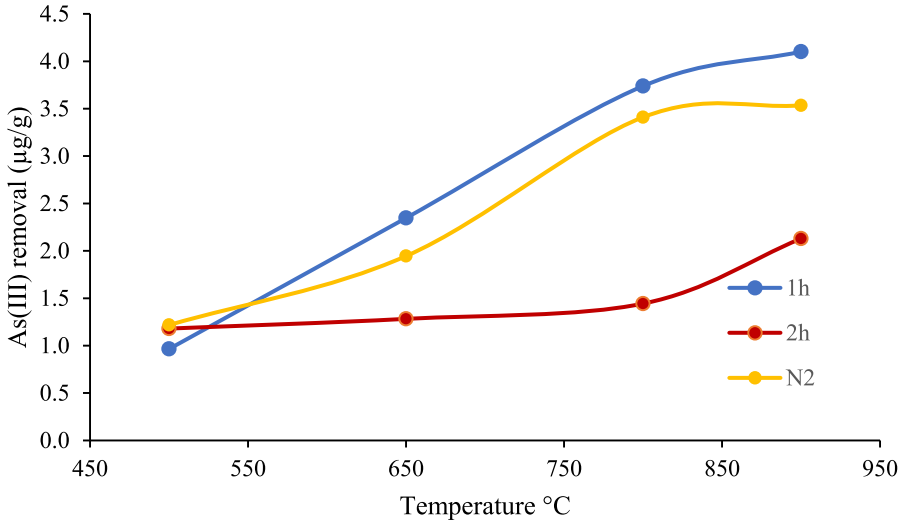

(a) As(III) removal

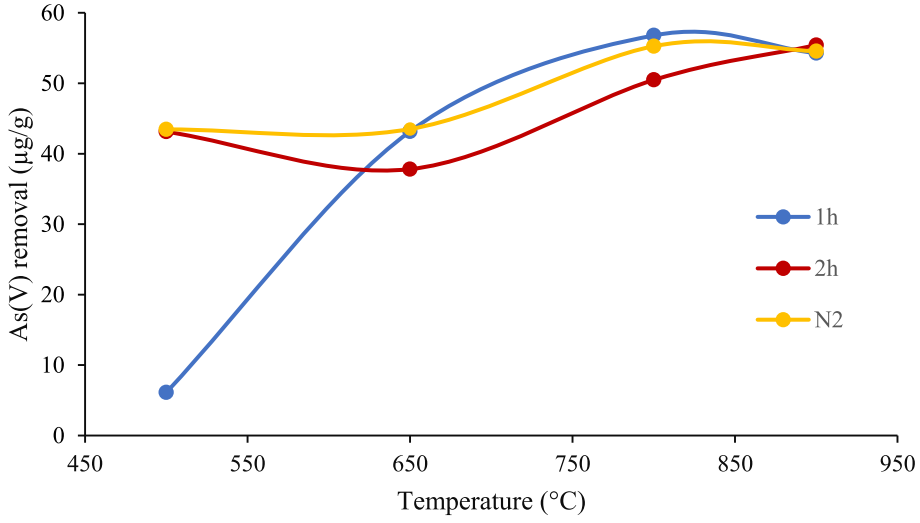

(b) As(V) removal

Fig. 5. Removal of As(III) and As(V) on bone char samples.

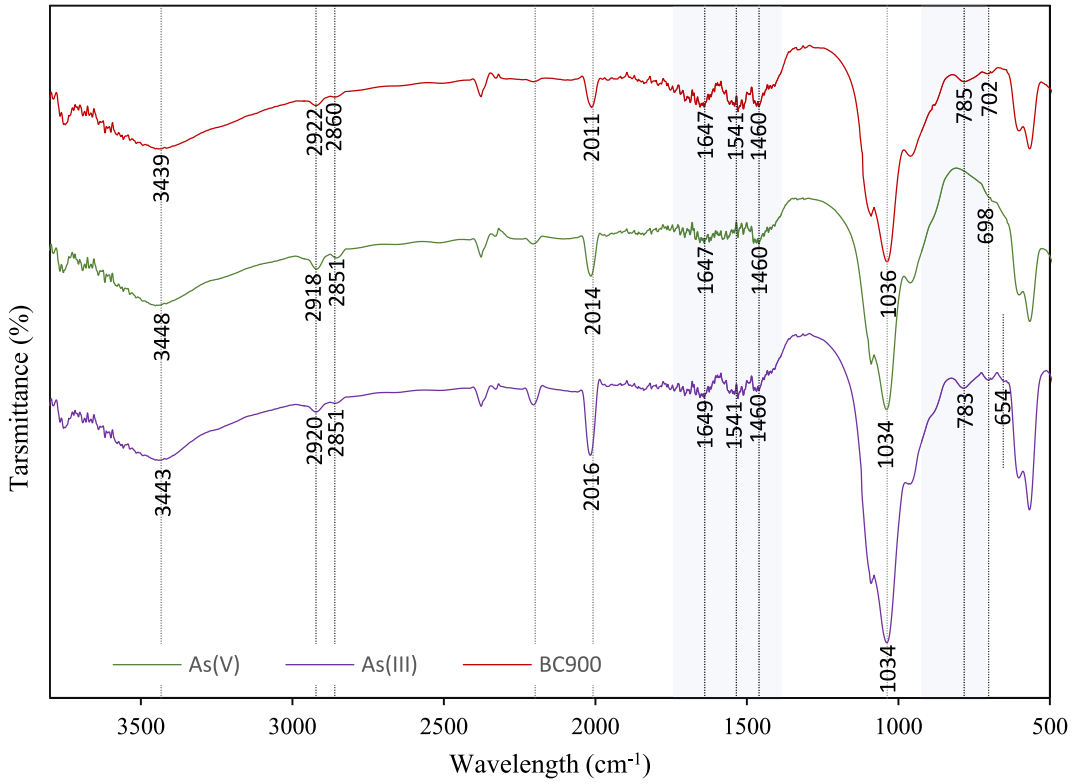

(a)

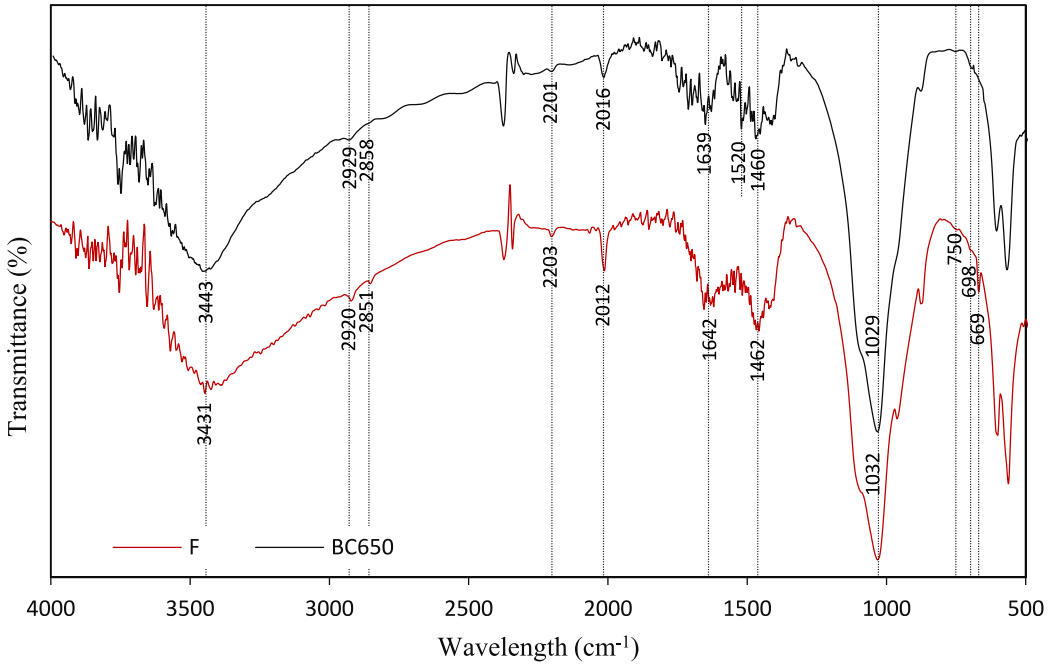

(b)

Fig. 6. FTIR analysis for bone char samples before and after loading with (a) As(III) and As(V) and (b) F^-.

The main As removal mechanisms for bone char are surface complexation, precipitation and/or ligand exchange (Alkurdi et al., 2019a). However, the mechanisms of As(III) removal with bone char have not clearly been presented in literature. Based on the bone char characterization results produced under different conditions, the main factor that was found to affect removal capacity was charring temperature. At high charring pyrolysis temperatures, a higher pH, ash content, CEC and negative surface charge were observed. The effect on acidic functional groups was the opposite, while the basic functional groups were not affected significantly by pyrolysis temperature.

The surface area of bone char prepared at a higher temperature was lower than that of bone char prepared at a lower temperature. It can be said that surface area does not affect bone char's ability to remove As species from solution. Furthermore, the role of basic functional groups on the removal of As species can be ruled out in this study. The adsorption experiments were conducted at an initial pH of 7.0–8.0 for As(III) and As(V) solutions where As(V) is present as $HAsO_4^{2-}$ in the solution. Based on the literature, if ligand exchange is the dominant mechanism, then there will be a decrease in the As(V) uptake on the bone char due to raising pyrolysis temperature, as a consequence of the hydroxyl groups reduction. Hence, it can be inferred that the removal cannot be attributed to ligand exchange mechanism.

According to Bissen and Frimmel (2003), As removal from water was increased due to co-precipitation with Mg compounds due to the ability of As to form solids with this cation (Gupta and Chen, 1978; Park et al., 2010). As can be seen from the results of the CEC, the increase in the CEC was related to the increase in the ability of the bone char to exchange Mg cations. Thus, the increase in the removal capacity may predominantly be related to the formation of surface complexes between the HAP and the metal impurities to form $Ca_{(10-x)}Mg_x(PO_4)_6(OH)_2$ (Alkurdi et al., 2019a). From the observations of this study, it seems that cationic exchange and solids formation may play an important role in increasing removal capacity of bone char. Moreover, FTIR demonstrated the formation of nitrogen functional groups with increased temperatures, as a result of protein degradation. The increase in As binding to the surface of the bone char may be linked to the presence of these nitrogen functional groups as, their increase coincides with improved As removal.

FTIR spectra of As(III) and As(V) loaded bone char are presented in Fig. 6a. The spectra of the 900 °C bone char loaded with As(III) and As(V) revealed a shift in the position of some spectral peaks presented in Fig. 6a. Notably, the main changes were in adsorption bands in the fingerprint region (650–850 cm^{-1}) indicating an intramolecular effect on the adsorption process. Peaks in this region were found to be associated with v_3 of AsO_4 in arsenic-magnesium complexes (Makreski et al., 2015), and this supports the conjecture that the removal happens through surface complexes mechanisms. The Figure shows a significant increase in the intensity of the PO_4^{3-} after As(III) adsorption. Moreover, a new peak was introduced at 654 cm^{-1} in As(III)-loaded bone char. The peak at 785 cm^{-1} disappeared in the case of As(V)-loaded bone char, while the formation of a new peak at 977 cm^{-1} could also be recognized after As(V) adsorption. In addition, As(V)-loaded bone char showed a change in the spectral range associated with C=O indicating that oxygen-containing functional groups are involved in As(V) removal.

In order to better understand the interaction between As species and bone char, a thorough investigation of sorption kinetics and isotherms is required. We conducted such investigations for the char that produced the highest removal with minimal DOC release. However, for the sake of keeping the article focused and succinct, the detailed results of this investigation are not presented here. It was found that the As(III) and As(V) follow pseudo first-order kinetics with R^2 of 0.99 and 0.98, respectively. Based on the linear fittings of Langmuir and Freundlich models, the isotherms that best describe the removal of As(III) and As(V) are the Freundlich and Langmuir isotherm models, respectively. Similar information for F^- removal will be presented in the following section.

4.2. Fluoride removal on bone char samples

Charring temperature and bone source are the two most significant factors that affect the ability of bone char to remove F^- from aqueous media. Based on our recent literature survey, the optimum temperature to achieve a maximum removal capacity of F^- on bone char is in the range of 500 °C–700 °C (Alkurdi et al., 2019a). In this study, sheep bones were used to remove 10 mg/L F^- from synthetic water to optimize the pyrolysis conditions. Fig. 7 shows the results achieved for the removal of 10 mg/L F^- from synthetic water using 1 g bone char/L solution. As can be seen from the results, the lower the pyrolysis temperature and residence time, the greater the F^- uptake. However, the incomplete degradation of the organics contained in the bone structure at 500 °C make the latter unsuitable for water treatment applications. For all of the temperatures examined, purging N_2 gas has resulted in a higher removal capacity (p-value < 0.05) up to 800 °C. Thus, the highest removal capacity of F^- was 2.33 mg/g using bone char samples prepared at 650 °C with purging N_2 gas. Samples made at 800 °C and 900 °C showed a very low uptake of F^- from solution. This can be explained by the lower OH groups which resulted in the reduction of surface functional groups and lower ion exchange capability, which is the main removal mechanism (Medellin-Castillo et al., 2014). Additionally, the increase in the negative surface charge of the char as pyrolysis temperature increased may negatively affect the electrostatic interaction between F^- and bone char. Electrostatic interaction was found to have an important role in F^- removal using bone char (Alkurdi et al., 2019a). Fig. 6b shows the FTIR results that compares between the 650 °C unloaded and F^- loaded bone chart. The effect of electrostatic interaction can be clearly seen when comparing the removal of the bone char with or without N_2. At low temperatures, N_2 decreased the negative surface charge resulting in higher removal. However, as temperature increased, the effect of N_2 on surface charge decreased and consequently F^- removal dropped. In addition, pH_{pzc} being close to neutral pH values for the bone char samples provided a wider pH range to attract the negatively charged F^- ions to the surface of the adsorbent. Thus, controlling the pH conditions can offer a higher removal capacity of the bone char to the different contaminates targeted. With regards to the effect of surface properties on F^-

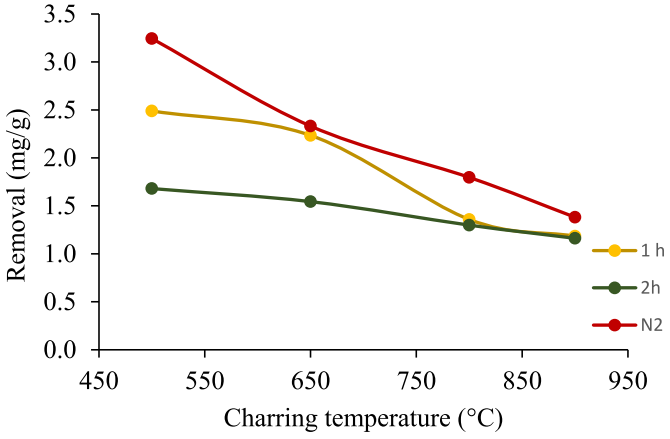

Fig. 7. Removal of F^- on bone char samples.

removal, it appears that the removal is more affected by the surface area than pore size.

As mentioned in the previous section, the kinetics and isotherms of the best removal scenario of F^- are presented here. F^- removal followed Pseudo-second-order kinetics. The isotherm that best represents F^- removal on bone char is the Langmuir model.

5. Conclusions

This study investigated the effect of pyrolysis conditions on bone char characteristics and their As and F^- removal capacity. Pyrolysis temperature was found to be the most effective factor in controlling the surface characteristics of samples. Increased pyrolysis temperature resulted in increases in pH, negative surface charge and roughness, ash content, crystallinity, pore size and CEC. At the same time such increases led to decreased number of acidic functional groups, surface area and DOC releases from the bone char. The change in CEC was mainly attributed to Mg concentration on the bone char surface. While basic functional groups were not affected by pyrolysis temperature. Applying N_2 purging gas had an insignificant effect on pH, surface charge and morphology, while slightly decreasing ash content, crystallinity, CEC and DOC.

FTIR analysis and DOC measurements were applied to unravel the cause behind organic carbon release from bone char prepared at low temperatures. The headline of this exercise was that the growing FTIR peak at 2013 cm^{-1} was found to have a strong and significant inverse correlation with DOC release. This peak was associated with protein decomposition and production of carbon-nitrogen-sulfur compounds. Protein decomposition was also evident in the decreasing nitrogen percentage in the elemental analysis. Based on this correlation, it was postulated that protein structure on bones is a major contributor to carbon release from bone char in aqueous solutions.

Bone char samples prepared under different experimental conditions were examined for inorganic As species and F^- removal from synthetic water samples. It was observed that the higher the temperature, the more As species were removed from water. However, the effect of residence time and purging gas were found to be only minor. As(V) was more effectively removed with bone char as opposed to As(III), especially at low temperature of 500 °C. However, this temperature level was found to produce a high concentration of DOC and thus it was not feasible from the water treatment perspective given the potential risk of DOC in forming disinfection by-products. Close examination of bone char characterization with different pyrolysis temperatures suggests that the likely As removal mechanisms are predominantly surface complexation and to a lesser extent precipitation and interaction with nitrogen groups. Conversely, F^- removal decreased with an increase in pyrolysis temperature. This may be related to the availability of the higher amount of oxygen functional groups on the surface of the bone char, which increased exchange activities with such groups. The increase of the char negative surface charge with the increasing pyrolysis temperature may negatively affect electrostatic interactions between the char and F^-. Based on the results of this study, the recommended pyrolysis temperatures for As and F^- removal are 900 °C and 650 °C, respectively, where highest removal was achieved with the minimal DOC release. In order to conduct a thorough evaluation of bone char applications for As removal, a more comprehensive investigation of the various experimental conditions is recommended for future research work.

Declaration of competing interests

The authors declare that they have no known competing financial interests or personal relationships that could have appeared to influence the work reported in this paper.

Acknowledgements

This research was performed as a part of PhD research which was supported in part by the Iraqi Government and the Australian Research Training Program.

Appendix A. Supplementary data

Supplementary data to this article can be found online at https://doi.org/10.1016/j.envpol.2020.114221.

References

Alarcón-Herrera, M.T., Bundschuh, J., Nath, B., Nicolli, H.B., Gutierrez, M., Reyes-Gomez, V.M., Nunez, D., Martín-Dominguez, I.R., Sracek, O., 2013. Co-occurrence of arsenic and fluoride in groundwater of semi-arid regions in Latin America: genesis, mobility and remediation. J. Hazard Mater. 262, 960–969.

Alarcón-Herrera, M.T., Martin-Alarcon, D.A., Gutiérrez, M., Reynoso-Cuevas, L., Martín-Domínguez, A., Olmos-Márquez, M.A., Bundschuh, J., 2020. Co-occurrence, possible origin, and health-risk assessment of arsenic and fluoride in drinking water sources in Mexico: geographical data visualization. STOTEN 698, 134168.

Ali, I., Aboul-Enein, H.Y., 2002. Speciation of arsenic and chromium metal ions by reversed phase high performance liquid chromatography. Chemosphere 48, 275–278.

Alkurdi, S.S., Al-Juboori, R.A., Bundschuh, J., Hamawand, I., 2019b. Bone char as a green sorbent for removing health threatening fluoride from drinking water. Environ. Int. 127, 704–719.

Alkurdi, S.S., Herath, I., Bundschuh, J., Al-Juboori, R.A., Vithanage, M., Mohan, D., 2019a. Biochar versus bone char for a sustainable inorganic arsenic mitigation in water: what needs to be done in future research? Environ. Int. 127, 52–69.

Angın, D., Şensöz, S., 2014. Effect of pyrolysis temperature on chemical and surface properties of biochar of rapeseed (Brassica napus L.). Int. J. Phytoremediation 16, 684–693.

ASTM D1762-84, Annual Book of ASTM Standards D1762-84. 281–282.

Australian Bureau of Statistics, 2018. Livestock Products, Australia, Sep 2018. Australian Government.

Begum, S.A., Golam Hyder, A., Vahdat, N., 2016. Adsorption isotherm and kinetic studies of as (V) removal from aqueous solution using cattle bone char. J. Water Supply Res. T. 65, 244–252.

Bissen, M., Frimmel, F.H., 2003. Arsenic—a review. Part II: oxidation of arsenic and its removal in water treatment. Acta Hydrochim. Hydrobiol. 31, 97–107.

Boehm, H., 1994. Some aspects of the surface chemistry of carbon blacks and other carbons. Carbon 32, 759–769.

Boskey, A.L., Mendelsohn, R., 2005. Infrared analysis of bone in health and disease. J. Biomed. Optic. 10, 031102.

Brunson, L.R., Sabatini, D.A., 2014. Role of surface area and surface chemistry during an investigation of eucalyptus wood char for fluoride adsorption from drinking water. J. Environ. Eng. 141, 8.

Butt, H.-J., Graf, K., Kappl, M., 2003. Physics and Chemistry of Interfaces. Wiley Online Library.

Chen, Y.-N., Chai, L.-Y., 2008. Equilibrium and Kinetics of Arsenic (V) Sorption by Bone Char, 2nd International Conference on Bioinformatics and Biomedical Engineering. IEEE, pp. 3140–3143.

Chen, Y.-N., Chai, L.-Y., Shu, Y.-D., 2008. Study of arsenic (V) adsorption on bone char from aqueous solution. J. Hazard Mater. 160, 168–172.

Clogston, J.D., Patri, A.K., 2011. Zeta Potential Measurement, Characterization of Nanoparticles Intended for Drug Delivery. Springer, pp. 63–70.

Cruz, M.A.P., Guimarães, L.C.M., da Costa Júnior, E.F., Rocha, S.D.F., Mesquita, P.d.L., 2019. Adsorption of crystal violet from aqueous solution in continuous flow system using bone char. Chem. Eng. Commun. 1–10.

Czerniczyniec, M., Farías, S., Magallanes, J., Cicerone, D., 2007. Arsenic (V) adsorption onto biogenic hydroxyapatite: solution composition effects. Water Air Soil Pollut. 180, 75–82.

Dang, T., Marschner, P., Fitzpatrick, R., Mosley, L., 2018. Assessment of the binding of protons, Al and Fe to biochar at different pH values and soluble metal concentrations. Water 10, 55.

de Melo, N.H., de Oliveira Ferreira, M.E., Neto, E.M.S., Martins, P.R., Ostroski, I.C., 2018. Evaluation of the adsorption process using activated bone char functionalized with magnetite nanoparticles. Environ. Nanotechnol. Monit. Manages. 10, 427–434.

Dotto, G.L., Salau, N.P.G., Piccin, J.S., Cadaval, T.R.S.A., de Pinto, L.A.A., 2017. Adsorption Kinetics in Liquid Phase: Modeling for Discontinuous and Continuous Systems, Adsorption Processes for Water Treatment and Purification. Springer, pp. 53–76.

Eaton, A.D., Clesceri, L.S., Rice, E.W., Greenberg, A.E., Franson, M., 2005. APHA: standard methods for the examination of water and wastewater, Centennial Edition. APHA, AWWA, WEF, Washington, DC.

Fairhurst, D., 2013. An overview of the zeta potential-Part 1: the concept. Am. Pharmaceut. Rev.
Figueiredo, M., Fernando, A., Martins, G., Freitas, J., Judas, F., Figueiredo, H., 2010. Effect of the calcination temperature on the composition and microstructure of hydroxyapatite derived from human and animal bone. Ceram. Int. 36, 2383–2393.
Gezahegn, S., Sain, M., Thomas, S.C., 2019. Variation in feedstock wood chemistry strongly influences biochar liming potential. Soil Sys 3, 26.
Grace, N., 1983. Amounts and distribution of mineral elements associated with fleece-free empty body weight gains in the grazing sheep. New Zeal. J. Agr. Res. 26, 59–70.
Grafe, M., Eick, M.J., Grossl, P.R., Saunders, A.M., 2002. Adsorption of arsenate and arsenite on ferrihydrite in the presence and absence of dissolved organic carbon. J. Environ. Qual. 31, 1115–1123.
Gu, C., Katti, D.R., Katti, K.S., 2013. Photoacoustic FTIR spectroscopic study of undisturbed human cortical bone. Spectrochim. Acta, Part A 103, 25–37.
Gumus, R., Wauton, I., Aliu, A., 2012. Investigation of the effect of chemical activation and characterization of bone char: cow bone. J. Eng. Appl. Sci. 4, 34–45.
Gupta, S.K., Chen, K.Y., 1978. Arsenic removal by adsorption. J. Water Pollut. Control Fed. 493–506.
Herath, H., Kawakami, T., Tafu, M., 2018. The Extremely High Adsorption Capacity of Fluoride by Chicken Bone Char (CBC) in Defluoridation of Drinking Water in Relation to its Finer Particle Size for Better Human Health, Healthcare. Multidisciplinary Digital Publishing Institute, p. 123.
Herath, I., Vithanage, M., Bundschuh, J., Maity, J.P., Bhattacharya, P., 2016. Natural arsenic in global groundwaters: distribution and geochemical triggers for mobilization. Current Pollut. Rep. 2, 68–89.
Hernández-Hernández, L., Bonilla-Petriciolet, A., Mendoza-Castillo, D., Reynel-Ávila, H., 2017. Antagonistic binary adsorption of heavy metals using stratified bone char columns. J. Mol. Liq. 241, 334–346.
Ip, A.W., Barford, J.P., McKay, G., 2010. A comparative study on the kinetics and mechanisms of removal of Reactive Black 5 by adsorption onto activated carbons and bone char. Chem. Eng. J. 157, 434–442.
Jiang, J.-Q., 2001. Removing arsenic from groundwater for the developing world-a review. Water Sci. Technol. 44, 89–98.
Kang, D.-S., Lee, S.-M., Lee, S.-H., Roh, J.-S., 2018. X-ray diffraction analysis of the crystallinity of phenolic resin-derived carbon as a function of the heating rate during the carbonization process. Carbon Lett. (Carbon Lett.) 27, 108–111.
Kawasaki, N., Ogata, F., Tominaga, H., Yamaguchi, I., 2009. Removal of fluoride ion by bone char produced from animal biomass. J. Oleo Sci. 58, 529–535.
Ko, D.C., Porter, J.F., McKay, G., 2000. Optimised correlations for the fixed-bed adsorption of metal ions on bone char. Chem. Eng. Sci. 55, 5819–5829.
Kumar, R., Patel, M., Singh, P., Bundschuh, J., Pittman Jr., C.U., Trakal, L., Mohan, D., 2019. Emerging technologies for arsenic removal from drinking water in rural and peri-urban areas: methods, experience from, and options for Latin America. Sci. Total Environ. 694, 133427.
Leinweber, P., Hagemann, P., Kebelmann, L., Kebelmann, K., Morshedizad, M., 2019. Bone Char as a Novel Phosphorus Fertilizer, Phosphorus Recovery and Recycling. Springer, pp. 419–432.
Li, M., Liu, Q., Lou, Z., Wang, Y., Zhang, Y., Qian, G., 2014. Method to characterize acid–base behavior of biochar: site modeling and theoretical simulation. ACS Sustain. Chem. Eng. 2, 2501–2509.
Litter, M.I., Morgada, M.E., Bundschuh, J., 2010. Possible treatments for arsenic removal in Latin American waters for human consumption. Environ.l Pollut. 158, 1105–1118.
Liu, J., He, L., Dong, F., Hudson-Edwards, K.A., 2016. The role of nano-sized manganese coatings on bone char in removing arsenic (V) from solution: implications for permeable reactive barrier technologies. Chemosphere 153, 146–154.
Liu, J., Huang, X., Liu, J., Wang, W., Zhang, W., Dong, F., 2014. Adsorption of arsenic (V) on bone char: batch, column and modeling studies. Environ. Earth Sci. 72, 2081–2090.
Lopes, C.d.C.A., Limirio, P.H.J.O., Novais, V.R., Dechichi, P., 2018. Fourier transform infrared spectroscopy (FTIR) application chemical characterization of enamel, dentin and bone. Appl. Spectrosc. Rev. 53, 747–769.
Luo, L., Xu, C., Chen, Z., Zhang, S., 2015. Properties of biomass-derived biochars: combined effects of operating conditions and biomass types. Bioresour. Technol. 192, 83–89.
Makreski, P., Stefov, S., Pejov, L., Jovanovski, G., 2015. Theoretical and experimental study of the vibrational spectra of (para) symplesite and hörnesite. Spectrochim. Acta, Part A 144, 155–162.
Medellin-Castillo, N., Leyva-Ramos, R., Padilla-Ortega, E., Perez, R.O., Flores-Cano, J., Berber-Mendoza, M., 2014. Adsorption capacity of bone char for removing fluoride from water solution. Role of hydroxyapatite content, adsorption mechanism and competing anions. J. Ind. Eng. Chem. 20, 4014–4021.
Mendoza-Castillo, D.I., Bonilla-Petriciolet, A., Jáuregui-Rincón, J., 2015. On the importance of surface chemistry and composition of bone char for the sorption of heavy metals from aqueous solution. Desalin. Water Treat. 54, 1651–1662.
Mohan, D., Pittman Jr., C.U., 2007. Arsenic removal from water/wastewater using adsorbents—a critical review. J. Hazard Mater. 142, 1–53.
Mohapatra, M., Anand, S., Mishra, B.K., Giles, D.E., Singh, P., 2009. Review of fluoride removal from drinking water. J. Environ. Manag. 91, 67–77.
Mukherjee, A., Sengupta, M.K., Hossain, M.A., Ahamed, S., Das, B., Nayak, B., Lodh, D., Rahman, M.M., Chakraborti, D., 2006. Arsenic contamination in groundwater: a global perspective with emphasis on the Asian scenario. JHPN 142–163.
OA, O., Abhulimen, K., Adeleke, A., Njoku, C., Amoo, K., 2019. Production and characterization of derived composite biosorbents from animal bone. Afr. J. Pure Appl. Chem. 13, 12–26.
Park, Y.Y., Tran, T., Lee, Y.H., Nam, Y.I., Senanayake, G., Kim, M.J., 2010. Selective removal of arsenic (V) from a molybdate plant liquor by precipitation of magnesium arsenate. Hydrometallurgy 104, 290–297.
Patel, S., Han, J., Qiu, W., Gao, W., 2015. Synthesis and characterisation of mesoporous bone char obtained by pyrolysis of animal bones, for environmental application. J. Environ. Chem. Eng. 3, 2368–2377.
Person, A., Bocherens, H., Saliège, J.-F., Paris, F., Zeitoun, V., Gérard, M., 1995. Early diagenetic evolution of bone phosphate: an X-ray diffractometry analysis. J. Archaeol. Sci. 22, 211–221.
Prado, A.G., Pertusatti, J., Nunes, A.R., 2011. Aspects of protonation and deprotonation of humic scid durface on molecular conformation. J. Braz. Chem. Soc. 22, 1478–1483.
Rocha, S., Ribeiro, M., Viana, P., Mansur, M., 2012. Bone Char: an Alternative for Removal of Diverse Organic and Inorganic Compounds from Industrial Wastewater. Application of Adsorbents for Water Pollution. Bentham Science Publishers Ltd, pp. 502–522.
Rojas-Mayorga, C., Bonilla-Petriciolet, A., Aguayo-Villarreal, I.A., Hernandez-Montoya, V., Moreno-Virgen, M., Tovar-Gómez, R., Montes-Morán, M., 2013. Optimization of pyrolysis conditions and adsorption properties of bone char for fluoride removal from water. J. Anal. Appl. Pyrol. 104, 10–18.
Rojas-Mayorga, C.K., Mendoza-Castillo, D.I., Bonilla-Petriciolet, A., Silvestre-Albero, J., 2016. Tailoring the adsorption behavior of bone char for heavy metal removal from aqueous solution. Adsorpt. Sci. Technol. 34, 368–387.
Shahid, M.K., Kim, J.Y., Choi, Y.-G., 2019. Synthesis of bone char from cattle bones and its application for fluoride removal from the contaminated water. Groundwater Sustain. Develop. 8, 324–331.
Shen, W., Li, Z., Liu, Y., 2008. Surface chemical functional groups modification of porous carbon. Recent Pat. Biomed. Eng. 1, 27–40.
Siebers, N., Godlinski, F., Leinweber, P., 2014. Bone char as phosphorus fertilizer involved in cadmium immobilization in lettuce, wheat, and potato cropping. J. Plant Nutr. Soil Sci. 177, 75–83.
Smith, B.C., 2011. Fundamentals of Fourier Transform Infrared Spectroscopy. CRC press.
Smith, B.C., 2018. The C= O Bond, Part III: Carboxylic Acids.
Sneddon, I., Garelick, H., Valsami-Jones, E., 2005. An investigation into arsenic (V) removal from aqueous solutions by hydroxylapatite and bone-char. Mineral. Mag. 69, 769–780.
Soltani, R.D.C., Safari, M., Maleki, A., Rezaee, R., Shahmoradi, B., Shahmohammadi, S., Ghahramani, E., 2017. Decontamination of arsenic (V)-contained liquid phase utilizing Fe3O4/bone char nanocomposite encapsulated in chitosan biopolymer. Environ. Sci. Pollut. Res. 1–10.
Stuart, B., 2000. Infrared Spectroscopy. Kirk-Othmer Encyclopedia of Chemical Technology, pp. 1–18.
Tomasini, E., Siracusano, G., Maier, M., 2012. Spectroscopic, morphological and chemical characterization of historic pigments based on carbon. Paths for the identification of an artistic pigment. Microchem. J. 102, 28–37.
Van Geen, A., Ahsan, H., Horneman, A.H., Dhar, R.K., Zheng, Y., Hussain, I., Ahmed, K.M., Gelman, A., Stute, M., Simpson, H.J., 2002. Promotion of well-switching to mitigate the current arsenic crisis in Bangladesh. Bull. World Health Organ. 80, 732–737.
Waghmare, S., Arfin, T., Rayalu, S., Lataye, D., Dubey, S., Tiwari, S., 2015. Adsorption behavior of modified zeolite as novel adsorbents for fluoride removal from drinking water: surface phenomena, kinetics and thermodynamics studies. IJSETR 4, 4114–4124.

3.3 Concluding remarks

This study examined the potential removal of dissolved arsenic and fluorine species from using bone char produced from sheep bone waste under various pyrolysis conditions. Testing of bone char showed that as pyrolysis temperature and holding time increased, the surface pH, surface charge, surface roughness, crystallinity and CEC increased with an accompanying decrease in the acidic functional groups. Protein decomposition trends with pyrolysis temperature, determined by an FTIR peak at 2013 cm^{-1} showed a strong inverse correlation with released DOC from the bone char. This indicates that bone protein is a major contributor to DOC release, especially for low temperature bone char, i.e., ≤ 500 °C. Increased pyrolysis temperature resulted in higher removal of arsenite [As(III)] and arsenate [As(V)]. The highest F^- removal was achieved with bone char prepared at 500 °C. However, DOC release from the char prepared at this temperature was significant. Given the health concerns and technical problems associated with DOC, this study does not recommend bone char preparation at this temperature for dissolved As and F species removal.

CHAPTER 4

Arsenic removal from water using bon char: A detailed study on adsorption kinetic and isotherm models

Paper IV

Alkurdi, S.S., Al-Juboori, R.A., Bundschuh, J., Bowtell, L. and Marchuk, A. (2020). Bone char for arsenic species removal from water: A detailed study on adsorption kinetics and isotherm models. (Prepared for submission to the Journal of Hazardous Materials).

4.1 Introduction

This chapter explored the kinetics, diffusion and isotherms of As(III) and As(V) removal on bone char samples prepared at 900 °C (BC900). This approach is crucial to address the mechanism of the removal, which is not yet explored for As(III) removal with bone char. Different experimental conditions were examined for each of the inorganic As(III) and As(V) species, by varying the pH, initial concentration, adsorbent dose and contact time. The mechanisms of the removal were examined based on the results of the SEM-EDS and FTIR analyses, where the composition of the As-loaded bone char was compared to the unloaded bone char, in order to detect structural changes. This Chapter is a continuation from Chapter 3., in which preliminary experiments were undertaken to optimize the bone char production conditions for As(III) and As(V) removal.

Arsenic removal from water using bon char: A detailed study on adsorption kinetic and isotherm models

Susan S.A. Alkurdi[a,b], Raed A. Al-Juboori[c], Jochen Bundschuh[a,d]*, Les Bowtell[e], Alla Marchuk[f]

[a] *School of Civil Engineering and Surveying, Faculty of Health, Engineering and Sciences, University of Southern Queensland, West Street, Toowoomba, 4350, Queensland, Australia.*

[b] *Northern Technical University, Engineering Technical College/Kirkuk, Iraq.*

[c] *Water Engineering Research Group, Department of Civil and Environmental Engineering, Aalto University, P.O. Box 15200, Aalto, FI-00076 Espoo, Finland.*

[d] *UNESCO Chair on Groundwater Arsenic within the 2030 Agenda for Sustainable Development, University of Southern Queensland, West Street, Toowoomba, 4350, Queensland, Australia.*

[e] *School of Mechanical and Electrical Engineering, Faculty of Health, Engineering and Sciences, University of Southern Queensland, Toowoomba, 4350, QLD, Australia.*

[f] *University of Southern Queensland, Centre for Sustainable Agricultural Systems, Toowoomba, 4350, Queensland, Australia.*

Corresponding author*: Jochen Bundschuh

Faculty of Health, Engineering and Sciences & UNESCO Chair on Groundwater Arsenic within the 2030 Agenda for Sustainable Development, University of Southern Queensland, West Street, Toowoomba, 4350, Queensland, Australia.

Phone: +61 7 4631 2694

Email: Jochen.Bundschuh@usq.edu.au

Abstract

Inorganic arsenic is classified as a carcinogen and one of the most hazardous contaminants in drinking-water globally. This study investigated removal mechanisms of inorganic arsenic (As) species: As(III) and As(V) from water using bone char pyrolyzed at 900 °C. Four isotherm models namely Sips, Langmuir, Freundlich, Redlich-Peterson were used to study As adoption onto bone char. Linearized and nonlinear forms of these models were tested. Linearized forms were found to be inaccurate due to the high error values. Therefore, nonlinear regression methods were utilized to calculate parameters of the models. The Sips equation provided the best As(III) experimental data fit, while As(V) data was best represented by the Langmuir model. The mechanism of As removal was investigated using kinetic models (the Pseudo-first-order, Pseudo-second-order, Elovich and Ritchie models) and diffusional models (Intraparticle and Pore diffusion model). At low As(III) and As(V) concentrations of 0.5 and 2.5 mg/L, the removal was found to be due to intra-particle interactions and pore diffusion following Pseudo-first-order kinetics. However, at higher concentrations of 5 and 10 mg/L, the pore diffusion mechanism was ineffective, and the adsorption was best described by Pseudo-second-order and Elovich models. The changes in bone char surface chemistry were examined using FTIR and SEM-EDS. The study demonstrated that As oxide and complexes with metals such as Mg, were the confirmed immobilised forms of As on the bone-char surface. To the authors' knowledge, this study is the first attempt at As(III) adsorption analysis using bone char.

Keywords

Arsenic, kinetic models, isotherm models, bone char.

1. Introduction

Arsenic is found in groundwater originating from natural and anthropogenic sources constituting a global problem. Arsenic is classified as a Class I carcinogenic

contaminant, and has affected millions of people globally causing chronic disease and death (Kumarathilaka et al., 2020). Arsenic in groundwater is derived from the weathering and erosion of the crystalline and sedimental rocks (Yadav et al., 2020). Many countries, especially in Asia, the Americas and Europe source potable water from groundwater with As concentration much higher than the recommended limit for drinking water of 10 µg/L (WHO, 2011). Inorganic As is the dominant form of As in groundwater represented by arsenite [As(III)] and arsenate [As(V)]. Under reducing conditions, As(III) which is the most toxic and mobile phase of As is the dominant inorganic As species in groundwater. For instance, Kumar and Ramanathan (2019) reported that 74% of samples from different areas in Central India, West Bengal and Bangladesh, where reducing aquifers dominate, show a prevalence of As(III) in their groundwaters. The significant population size and low socio-economic status of these communities highlights the need for development of sustainable and low-cost As removal technologies.

Recently, a number of researchers investigated As(V) and As(III) removal from water using different adsorbent materials and methods (Liu et al., 2020), such as activated carbon (Dieme et al., 2017; Hashim et al., 2019; Kalaruban et al., 2019), zeolite (Meher et al., 2016; Soni and Shukla, 2019), biochar (Niazi et al., 2018; Singh and Mohan, 2020; Tabassum et al., 2019). Waste-based adsorbents from the meat industry, such as bone char, can be a potential solution for the contamination problem. Bone char has been reported to be an excellent adsorbent for fluoride ions (F^-) removal from water and discoloration in the sugar industry (Minja, 2020; Nigri et al., 2019). However, there are limited studies examined the use of bone char for As(V) removal (Alkurdi et al., 2019a) and not known studies for the removal of As(III) due to its less amenability to adsorption as in the normal pH range of groundwater As(III) species are neutral (Zeltner, 2002). With regards to As(V), despite the availability of limited investigations that explored its removal with bone char, the mechanism of the removal is still not elucidated properly. The thermal transformation of the meat bones into bone char to be used for As removal recently has become of crucial interest in the field of water treatment (Alkurdi et al., 2020; Alkurdi et al., 2019b; Alkurdi et al., 2019a; Amin, 2020). Hence, this study is dedicated to scrutinizing As species adsorption onto bone char for the first time through detailed and careful examination for the effect of the treatment conditions on the efficiency and the nature of adsorption process.

The aim of this study was to investigate the adsorption of As species onto bone char under different controlling factors such as pH, adsorbent concentration, adsorbate concentration and reaction time. Specific isotherms, kinetics and diffusion models were tested to gain a better understanding of the adsorption mechanisms for different As species onto bone char. SEM-EDS and FTIR were also applied to explore the changes in the bone char structure post adsorption.

2. Materials and methods

2.1 Reagents and equipment

All reagents were AR grade chemicals. Stock solutions of 1000 mg/L As(III) and As(V) in 2% HNO_3 were purchased from Choice Analytical, New South Wales, Australia. The pH of the test solutions was adjusted using 0.1 M nitric acid (70%, RCI Labscan) and sodium hydroxide (Labscan Asia Co. Ltd). The pH measurements were made using a TPS smart Chem-Lab pH meter. Arsenic assays were analyzed using ICP-MS (Perkin Elmer NEXION 300 ICP-MS). The adsorption of As species onto bone char surface was examined using SEM-EDS (JEOL JSM-7500FA). The applied accelerating voltage and probe current were 10 kV and 7.475 nA, respectively.

2.2 Source and preparation of bone char

The bone waste was obtained from a local meat shop in Toowoomba, Australia. Meat bones were boiled and cut into small pieces prior to the pyrolysis process as described in our previous study. The pyrolysis was conducted at 900 °C for 1 h, in a limited oxygen environment (Alkurdi et al., 2020). The pyrolysis conditions selected in this study were based on the outcomes of our earlier investigations into the optimization of bone char for As removal. This pyrolysis temperature provided the highest removal for both As(III) and As(V) when the removal efficiency was examined over a temperature range of 500 - 900 °C. The pyrolyzed bone char was washed with distilled water and then dried at 60 °C for 24 h, and then ground and sieved to the desired

particle size (1 - 2 mm). The ground dried material was then sealed for later use in the adsorption experiments.

2.3 Sorption experiments

Batch sorption experiments were performed at room temperature. Each 50 ml test tube was filled with 15 mL of As(III) or As(V) solution of varying concentrations (1-50 mg/L) and adjusted to the optimum pH. The optimum pH for each As species was determined by examining the maximum As removal from water in the pH range 4-10 using 1 mg/L initial As concentration. A 5 g/L of bone char was added to each test tube and agitated for 4h to reach equilibrium (based on the preliminary experiments). The optimal contact time and other conditions were selected on the basis of preliminary experiments which demonstrated that equilibrium was reached within 4 h. Then, the samples were filtered using Whatman No. 42 filter paper and analyzed for the final concentrations of As(III) and As(V) in the solution by ICP-MS. Arsenic concentrations retained in the adsorbent phase (mg/g) were calculated using the following formula:

$$R = \frac{C_0 - C_f}{W} * v \qquad (1)$$

where R is the sorption capacity (mg/g), C_0 and C_f are the initial and equilibrium concentrations (mg/L) of As in the solution, v is the volume (L) and W is the weight (g) of the adsorbent.

2.4 Data analysis

Analysis of variance (ANOVA) was carried out to test the differences between treatments. Five different error functions were used to compare the fit of the experimental data to the isotherm and kinetic models used to interpret the mechanisms of removal, based on the procedures described by Anirudhan and Radhakrishnan (2009) and Ho et al. (2002).

In brief, minimized errors were determined using the Solver add-in with Microsoft Excel software. Then, the sum of the normalized errors was calculated, by calculating the sum of the values achieved from the division of each error function by the function's maximum value for each run. These values were compared to each other and the minima were provided as the best fit of these models.

The standard error values which were used to ensure the accuracy of the data fitted to the models were the sum of the square of the error (SSE), hybrid fractional error function (HYBRID), Marquardt's percent standard deviation (MPSD), average relative error (ARE) and the sum of the absolute error (SAE). These standard errors were calculated applying the formulae (2 - 6) as presented below:

$$SSE = \sum_{i=1}^{n} (q_{exp} - q_{cal})_i^2 \qquad (2)$$

$$HYBRID = \frac{100}{n-p} \sum_{i=1}^{n} \left[\frac{(q_{exp} - q_{cal})^2}{q_{exp}} \right]_i \qquad (3)$$

$$\text{MPSD} = \left[\sqrt{\frac{1}{n-p} \sum_{i=1}^{n} \left(\frac{q_{exp} - q_{cal}}{q_{exp}}\right)_i^2} \right] * 100 \qquad (4)$$

$$ARE = \frac{100}{n} \sum_{i=1}^{n} \left(\frac{|q_{exp} - q_{cal}|}{q_{exp}} \right)_i \qquad (5)$$

$$\text{SAE} = \sum_{i=1}^{n} |q_{exp} - q_{cal}|_i \qquad (6)$$

where q_{exp} is the data collected from batch experiments in (mg/g), q_{cal} is the data obtained from the theoretical models in (mg/g), n is the number of data points and p is the number of the parameters for each model.

3. Results and discussion

3.1 Summary of bone char characteristics

A detailed characterization of BC900 was presented in our previous study (Alkurdi et al., 2020). The effect of pyrolysis temperature on bone char ability to remove As(III) was not stated in the literature. However, a higher As(V) removal on bone char was observed at 500 °C compared to 900 °C by Czerniczyniec et al. (2007). Similarly, Begum et al. (2016) and Liu et al. (2014) reported the suitability of commercial bone char samples produced at 450 °C and 500 °C, respectively, to remove As(V) from water. Table 1 shows the results for the BC900's characteristics.

Table 1. Characteristics of bone char.

Charring temperature (°C)	900
Surface pH	11.64
Point of zero charge	8.3
Surface acid groups (mmol/g)	3.526
Surface basic groups (mmol/g)	2.382
Surface area	69.063 m^2/g
Pore volume	0.235 cm^3/g
Pore size	13.588 nm

3.2 Sorption studies

3.2.1 Effect of adsorbent dose

Adsorbent dose plays a significant role in the optimization of adsorption capacity. The effect of the adsorbent dose was examined by adding 2.5, 5 and 7.5 g/L of BC900 to 50 mL of 1 mg/L As(III) and As(V) aqueous solution and shaking for 4 h. It was observed that the As(III) removal capacity increased from 0.009 mg/g to 0.079 mg/g with an increase in adsorbent dose from 2.5 to 5 g/L due to the increase in the availability of more adsorption sites occupying the adsorbate. However, the further

increase in BC900 dose to 7.5 g/L resulted in a decrease in As(III) uptake on the adsorbent to 0.009 mg/g.

A similar procedure for evaluating the effect of adsorbent dosage on As(V) adsorption was conducted. The removal capacity was increased from 0.075 mg/g to 0.11 mg/g after increasing the dose from 2.5 to 5 g/L, followed by a significant decrease (0.03 mg/g) after using 7.5 g/L BC900. Thus, the adsorbent dose for carrying out the rest of the experimental work was selected to be 5 g/L. Mondal and George (2015) studied the effect of adsorbent dose on the removal capacity of total As, As(III) and As(V) on activated carbon. The same trend with adsorbent levels was reported in their study as there was a positive relationship between the removal capacity and the adsorbent dose. However, after a certain limit of 8 g/L, there was no further increase in percentage removal (i.e. a decrease in removal when calculated on the basis of mg adsorbate per g adsorbent).

3.2.2 Effect of pH

To study the influence of solution pH on the adsorption of As(III) and As(V), experiments were performed with 1 mg/L initial concentration and 5 g/L adsorbent at different pH levels. Since hydroxyapatite dissociates at low pH levels <4 (Ramsey et al., 1973), therefore, the effect of pH was examined in the range of pH 4-10. Fig. 1 shows the changes in the removal capacity of BC900 at different pH levels for As(III) and As(V). The removal capacity was increased as the initial pH was raised from 4 to 8.6 for As(III) and to 7.5 for As(V). Then, As uptake decreased after raising the pH value to 12. The effect of pH on As(III) removal with bone char has not been addressed in previous studies. However, there has been a plethora of studies that investigated the optimum pH levels of As(V) removal using bone char. For example, Liu et al. (2014) and Begum et al. (2016) reported that the maximum As(V) removal on commercial bone char samples was achieved at pH 4. On the other hand, Chen et al. (2008) achieved the highest As(V) removal on a commercial bone char, but from a different source, at pH 10.

The pH dependence of the adsorption process is mainly influenced by the overall charge of the adsorbent in an aqueous solution. As previously reported in Table 1, the Point of zero charge (pH_{pzc}) for BC900 is 8.3.

The increases in As(V) uptake with increasing pH could be attributed to the electrostatic attraction of negatively charged As(V) species and the positively charged BC900 surface at pH levels below pH_{pzc}. On the other hand, the maximum removal of As(III) was at a pH level greater than pH_{pzc}, which suggests that the mechanisms involved in the adsorption process of arsenite differ from those of arsenate. Zeta potential reached its highest value between pH 5 and 7. However, the higher removal capacity was not in the same range of the plateau, indicating the contribution of mechanisms other than electrostatic attraction in the removal capacity. After identifying the optimum pH level for As species removal (i.e pH of 8.6 for As(III) and 7.5 for As(V)), these pH levels were applied in the kinetic and isotherm experiments.

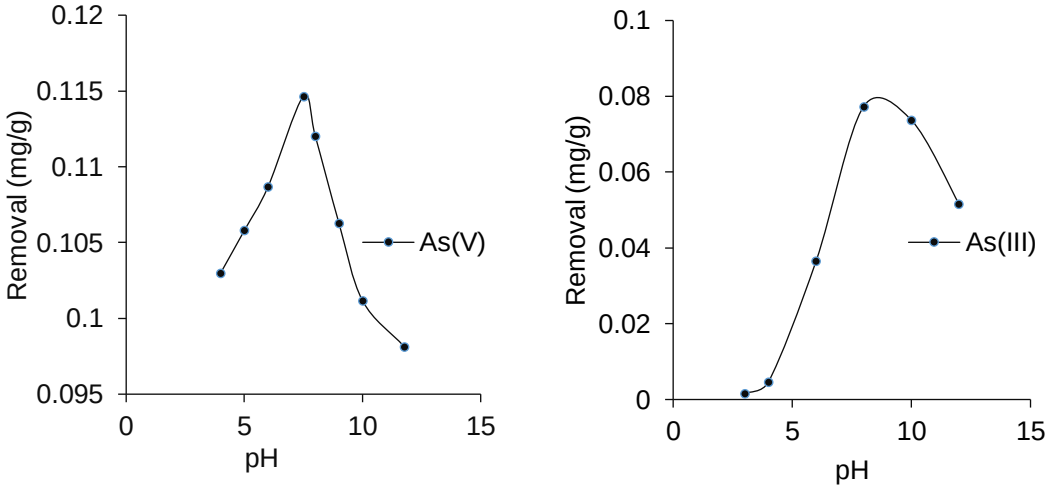

(a) (b)

Fig. 1. The effect of solution pH on the removal capacity of 1 mg/L (a) As(V) and (b) As(III) using 5 g/L BC900.

3.2.3 Effect of initial As concentration

The effect of As concentration was studied with initial As(III) and As(V) concentrations ranging from 0.05 to 50 mg/L. Fig. 2. shows the adsorption capacity

versus initial concentrations of As(III) (centre line) and As(V) (dashed line), respectively. The figure shows that the adsorption capacity of As(V) increased with the initial concentration from 0.05 to 50 mg/L. The higher concentration provided the necessary driving force to oppose resistance toward the mass transfer of As(V) between the adsorbent and the adsorbate. However, the case is different for As(III) where the adsorption capacity increased with an increase in the initial concentration up to 20 mg/L, and then decreased as the initial concentration increased to 50 mg/L. Comparing the effect of initial concentration to the results reported by Alam et al. (2018), but in a lower range of 0.5-5 mg/L, the same trend was noticed for both As species. Similar results were reported by Roy (2018) with a sharper decrease in the percentage removal of As(V) following the rise in the initial concentration to 0.5 mg/L using thioglycolated sugarcane carbon.

The maximum removal of As(III) was 2.543 mg/g at an initial concentration of 50 mg/L, while maximum removal of As(V) was achieved at the initial concentration of 20 mg/L with an equilibrium removal of 1.23 mg/g, and the removal capacity declined at 50 mg/L to 0.898 mg/g. The removal of As(III) was half the removal of As(V) at the same concentrations up to 2 mg/L. After this concentration, the uptake of As(III) reached almost the same value of As(V) removal at 20 mg/L before the removal trend reversed at 50 mg/L.

To design a fixed bed column for the purpose of continuous flow treatment, the contact time is of great importance in controlling removal efficiency. As can be seen from Fig. 2, As(V) had a higher removal rate when compared to As(III) removal at concentrations below 20 mg/L. With a maximum inorganic As concentration of <2 mg/L in natural groundwater globally (Herath et al., 2016; Mukherjee et al., 2006), bone char samples used in this study are more efficient in removing As(V) than As(III) at these concentrations ranges. However, with the higher percentage of As(III) in groundwater, due to its presence in reducing conditions, physical and chemical modification may be required to either improve the ability to remove As(III) or oxidize As(III) to As(V).

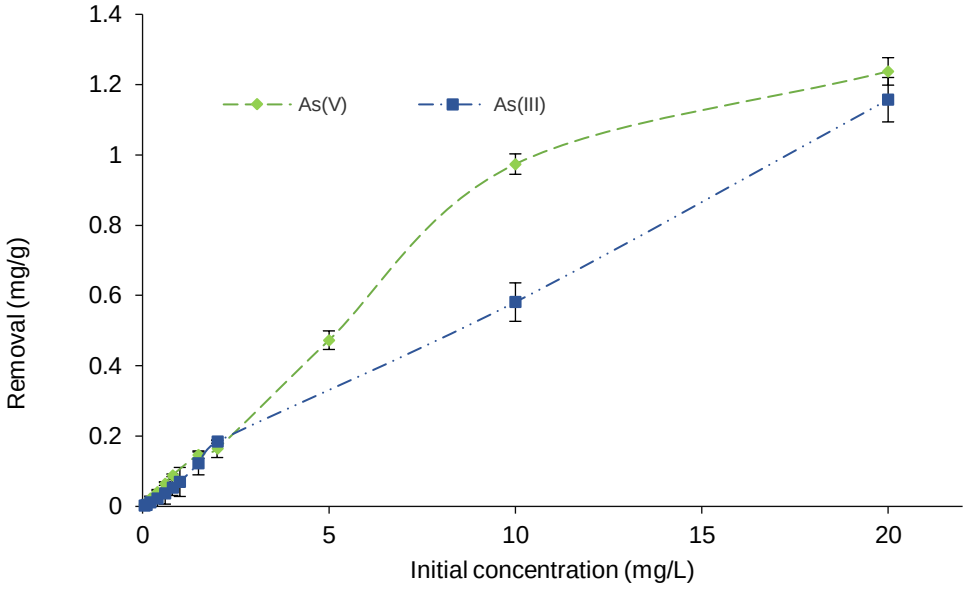

Fig. 2. Effect of initial concentration of As(III) and As(V) on removal capacity using 5 g/L BC900 at pH 8.6 and 7.5, respectively.

3.3 Isotherm models

To optimise the design of a sorption system, it is important to use adsorption isotherms to establish the appropriate correlation for the equilibrium curves. The experimental data of the As adsorption onto BC900 were substituted into equilibrium isotherm models to determine the best fit model for the removal process. Four different isotherm models were tested in this study. These models include two-parameters Langmuir and Freundlich models and three-parameters Redlich-Peterson (R-P) and Sips models.

The Langmuir isotherm model was originally proposed to describe gas adsorption onto activated carbon. Later, the Langmuir model was used to describe adsorption/desorption performance for different bio-sorbents. The Langmuir model is a chemical adsorption model that assumes a monolayer homogeneous adsorption process in which all sites provide an equal affinity to the adsorbate. The nonlinear form of the Langmuir model is given by:

$$q_e = \frac{Q_o \, k_L \, C_e}{1 + k_L \, C_e} \qquad (7)$$

where k_L is Langmuir isotherm constant representing the ratio between the adsorption and desorption rate (L/mg), C_e is equilibrium concentration (mg/L), Q_o is the maximum coverage capacity estimated by the model (mg/g) and q_e is the amount of adsorbate at equilibrium (mg/g). Different linearized formulae were proposed for presenting equilibrium data. In this study, the formula presented below was used and compared to the non-linear regression results:

$$\frac{1}{q_e} = \frac{1}{Q_o} + \frac{1}{k_L\, Q_o C_e} \qquad (8)$$

The Freundlich isotherm model represents an exponential distribution of the active sites of a heterogenous surface and its energy. It is an empirical equation that does not have a physical meaning (Wang and Guo, 2020). The nonlinear form of the Freundlich isotherm is given as:

$$q_e = K_F\, C_e^{1/n} \qquad (9)$$

where K_F is the adsorption capacity ($L^{1/n}.\ mg^{1-1/n}.\ g^{-1}$) and *1/n* is the adsorption intensity which represents the relative distribution of the heterogeneity and the energy of the adsorption sites. When the value of *n* =1, the Freundlich model reduces to its linear form, while when n <1 or n >1 the adsorption process is described as favorable and unfavorable adsorption, respectively.

These parameters may also be determined from the intercept and the slope of the linear trend after plotting the *log* C_e versus *log* q_e based on the linearized form of the model as shown in equation 10:

$$logq_e = logK_F + \frac{1}{n} logC_e \qquad (10)$$

The Redlich-Peterson (PR) model is a hybrid empirical formula incorporating three parameters from the amendment of the Langmuir and Freundlich isotherms, which assumes the presence of both homogeneous and heterogeneous surfaces on the adsorbent. The parameters of the nonlinear formula of this model (equation 11) were calculated by the non-linear regression method:

$$q_e = \frac{K_{RP} C_e}{1 + a_{RP}\, C_e^{\beta_{RP}}} \qquad (11)$$

where q_e is the experimental adsorption capacity (mg/g), C_e is the final concentration at equilibrium (mg/L), K_{RP} is the isotherm constant (L g^{-1}), a_{RP} is the isotherm constant (L mg^{-1}) and β_{RP} is the isotherm exponent. Based on the value of β_{RP}, the models either reduces to the Langmuir model at β_{RP} =1 or to linear model when β_{RP}=0 or C_e approaches 0 (Wang and Guo, 2020). On the other hand, if C_e approaches infinity, the model will reduce to Freundlich (Wang and Guo, 2020). The linearized form of this equation is:

$$\ln\left(k_{RP}\frac{C_e}{q_e} - 1\right) = \beta_{RP} \ln C_e + \ln a_{RP} \qquad (12)$$

Another three-parameters model that is a combination of the Langmuir and Freundlich models is the Sips model presented by the equation below:

$$q_e = \frac{q_m\, b\, C_e^{1/n}}{1 + b\, C_e^{1/n}} \qquad (13)$$

while the linearized form of this equation is:

$$\ln\left(\frac{q_e}{q_m - q_e}\right) = \frac{1}{n}\ln(c_e) + \ln(b)^{1/n} \qquad (14)$$

where b is the Sips constant related to the energy of adsorption process and n is the exponential factor of the isotherm. At low adsorbate concentrations, the Sips model is reduced to the Freundlich equation. Then, the removal follows the Langmuir equation at higher concentrations (Kumara et al., 2014).

Fig. 3 shows the plot of the isotherm models and the experimental data for the As(III) and As(V) adsorption experiments in the range of 0.05-50 mg/L. It is clear from this figure that the experimental data of As(III) were well fitted with all of the isotherm models. However, the comparison for the best fit were based on the coefficient of determination and minimal normalized errors provided in Tables 2 and 3.

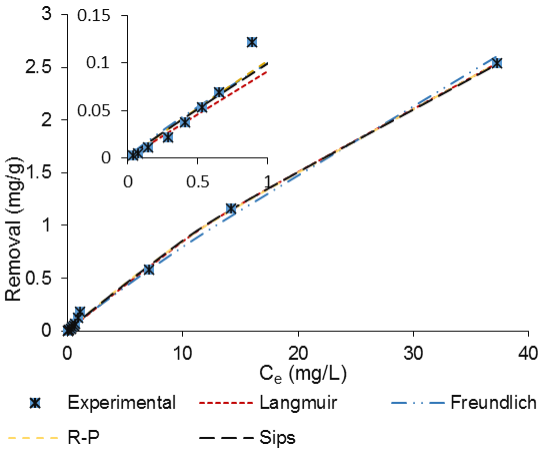

(a) Plot of isotherm models for As(III)

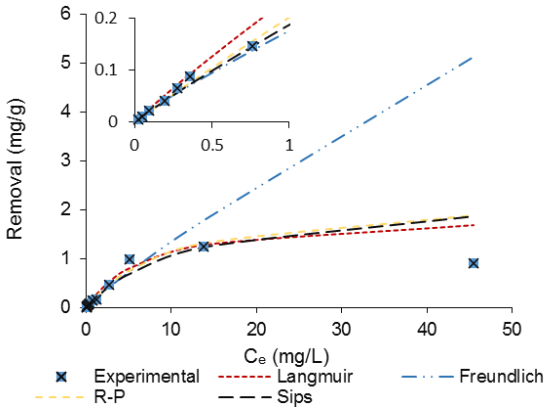

(b) Plot of isotherm models for As(V)

Fig. 3. Isotherm models fit for the experimental data of (a) As(III) and (b) As(V) using 5 g/L BC900 at pH 8.3 and 7.5, respectively.

Table 2 shows the values of the parameters calculated by nonlinear regression fits for the Langmuir and Freundlich isotherms along with the Redlich-Peterson and Sips isotherms using the experimental data from the batch experiments. Fitting to the linearized isotherm models was also conducted, however, the nonlinear regression results produced a lower error values and higher R^2 values compared to those provided from the linearized form (data presented in SM, Table SM1). The error functions for the examined isotherm models were computed for further evaluation of the goodness of the fit of the models and the results are presented in Table 3. The use of the linearized form of isotherm models showed that the data of As(III) and As(V) adsorption onto bone char best fitted by the Redlich-Peterson and Langmuir models,

respectively. However, the error analysis showed that the nonlinear method was a better way to calculate the isotherm parameters.

Comparing the data of As(III) adsorption results using two parameters models, the data showed a better fit to the Freundlich model which can be further affirmed by the higher RSQ and lower SNE. In addition, the value of 1/n (1/n =1.02) at the lowest error value calculated confirms the favorable adsorption of As(III) on bone char (Table 2). This could be also noticed from the very low value of K_L presented in Table 2, which refers to a low affinity in the case of the Langmuir model (Li et al., 2008). The value of K_L in the Langmuir model is correlated to the surface area and pore volume, showing that their increase would result in a higher removal capacity. However, our previous study showed a negative correlation between surface area/pore volume and the removal efficiency (Alkurdi et al., 2020). This may be explained by the results achieved by Samsuri et al. (2013) who examined the removal of As(III) and As(V) using empty fruit bunch and rice husk biochar. Both of the adsorbent removed almost the same amount of As species regardless of the larger surface area of rice husk. The study alluded to the contribution of some other factors in the removal process such as the point of zero charge and the aromaticity and polarity indices.

Comparing the data of As(III) adsorption fits to the Langmuir and Freundlich models with those of the three parameters models (R-P and Sips models), the data of As(III) removal from aqueous solution best fitted the Sips isotherm model with the lowest SNE value as shown in Table 3. The Sips model fitted the data with R^2 value of 0.999 at an exponent factor of n= 0.858. This result confirms that the removal of As(III) on bone char followed the Freundlich model at the lower concentrations and the Langmuir model when the concentrations were raised. This may be related to the contribution of both the physical and chemical adsorption processes in removal (which may be confirmed by examining the kinetic models).

Fig. 3b shows the plot of the four models for As(V) data along with the experimental data. Similarly, the parameters were calculated using both linearized and nonlinear forms of the models, but the analyses were based on the nonlinear results due to the lower SNE value provided by this form rather than those of the linearized forms. The least fit of the data was with the Freundlich models with either forms; linearized or nonlinearized due to the low R^2 values provided and the higher SNE values calculated.

In addition, the value of the 1/n was found to be <1, referring to an unfavorable adsorption. The Langmuir model constant K_L was found to be higher for As(V) adsorption than the one calculated for As(III) adsorption (0.114 and 0.009, respectively), which explains the best fit of the data to the Langmuir model. Furthermore, the lowest SNE value (Tables 4) was obtained by the Langmuir model with R^2 of 0.977 (Tables 2 and SM1) suggesting a monolayer homogeneous adsorption of As(V) on bone char. Similar results were reported by Begum et al. (2016) and Liu et al. (2014) for As(V) removal on bone char where the data best fitted the Langmuir model.

Table 2. Parameters of isotherm models for As(III) and As(V) adsorption onto bone char based on the error function calculation from nonlinear regression fitting.

	2-Parameters			3-Parameters			
	Freundlich			Redlich-Peterson			
	K_F	1/n	R^2	K_{RP}	a_{RP}	β	R^2
As(V)	0.189	0.939	0.888	0.220	0.095	1	0.969
As(III)	0.100	1.0204	0.998	0.113	0.102	0.517	0.999
	Langmuir			Sips			
	K_L	Q_o	R^2	q_m	b	n	R^2
As(V)	0.114	2.042	0.969	2.453	0.083	1.000	0.964
As(III)	0.009	9.822	0.999	2.659	0.040	0.858	0.999

Table 3. Error analysis comparison for As(III) isotherm parameters.

	Langmuir isotherm				
	SSE	HYBRID	MPSD	ARE	SAE
Q_o	9.822	8.305	21.379	21.379	21.375
K_L	0.009	0.012	0.004	0.004	0.004
RSQ	0.999	0.998	0.997	0.997	**0.997**
SSE	**0.010**	0.0121	0.029	0.027	0.028
HYBRID	0.601	**0.576**	0.873	0.9990	1.025

MPSD	30.341	33.077	**27.739**	28.104	28.200
ARE	20.533	22.656	19.544	**19.437**	19.517
SAE	0.187	0.245	0.375	0.353	**0.351**
SNE	**3.255**	3.626	4.553	4.530	4.605

	Freundlich isotherm				
	SSE	HYBRID	MPSD	ARE	SAE
K_F	0.119	0.100	0.080	0.078	0.102
1/n	0.847	1.020	0.900	1.015	0.889
RSQ	0.999	0.998	0.993	0.993	0.998
SSE	**0.008**	0.015	0.473	0.302	0.008
HYBRID	0.970	**0.651**	2.631	1.997	1.013
MPSD	103.619	60.693	**27.569**	27.721	106.656
ARE	62.579	37.178	19.592	**19.200**	64.324
SAE	0.245	0.245	0.245	0.245	**0.245**
SNE	3.329	**2.427**	3.563	2.956	3.401

	Redlich-Peterson isotherm				
	SSE	HYBRID	MPSD	ARE	SAE
K_{RP}	0.189	0.113	0.081	0.081	0.081
a_{RP}	0.679	0.102	0.004	0.005	0.005
β	0.265	0.517	1.000	1.000	1.000
RSQ	0.999	0.999	0.997	0.998	0.998
SSE	**0.008**	0.009	0.029	0.019	0.019
HYBRID	0.716	**0.573**	0.970	0.950	0.950
MPSD	73.772	45.273	**29.239**	29.288	29.288
ARE	44.370	27.996	19.544	**19.409**	19.409
SAE	0.219	0.196	0.375	0.288	**0.288**
SNE	3.587	**2.655**	3.839	3.243	3.244

	Sips isotherm				
	SSE	HYBRID	MPSD	ARE	SAE
q_m	2.659	8.305	9.822	1.957	4.729
b	0.040	0.012	0.040	0.061	0.010
n	0.858	1.000	1.000	0.824	0.768
RSQ	0.999	0.998	0.960	0.922	0.997

SSE	**0.010**	0.012	0.399	0.884	0.028
HYBRID	0.668	**0.640**	2.617	4.684	2.415
MPSD	31.982	34.866	**21.298**	21.895	63.380
ARE	20.533	22.656	14.068	**12.988**	47.855
SAE	0.187	0.245	0.978	1.227	**0.372**
SNE	**1.240**	1.373	2.438	3.617	2.851

Table 4. Error analysis comparison for As(V) isotherm parameters.

	Langmuir isotherm				
	SSE	HYBRID	MPSD	ARE	SAE
Q_o	1.961	2.042	2.217	2.042	2.313
K_L	0.138	0.114	0.098	0.114	0.095
RSQ	0.977	0.969	0.969	0.974	0.974
SSE	**0.104**	0.143	0.227	0.991	0.155
HYBRID	5.126	**1.888**	2.510	9.158	2.230
MPSD	153.069	39.166	**20.556**	30.398	50.690
ARE	99.622	27.041	16.567	**15.42**	32.492
SAE	0.758	0.659	0.827	1.171	**0.568**
SNE	3.312	**1.440**	1.510	3.353	1.543
	Freundlich isotherm				
	SSE	HYBRID	MPSD	ARE	SAE
K_F	0.251	0.182	0.164	0.189	0.179
1/n	0.637	0.779	0.866	0.939	0.736
RSQ	0.906	0.913	0.905	0.888	0.932
SSE	**0.045**	0.057	0.061	0.055	0.055
HYBRID	1.396	**0.948**	0.976	1.010	1.010
MPSD	28.843	17.715	**17.536**	18.912	18.912
ARE	19.733	11.127	11.303	**10.693**	10.693
SAE	0.440	0.406	0.385	0.344	**0.348**
SNE	4.733	3.704	3.7545	**3.596**	3.596

		Redlich-Peterson isotherm			
	SSE	HYBRID	MPSD	ARE	SAE
K_{RP}	0.271	0.220	0.242	0.245	0.245
a_{RP}	0.138	0.095	0.297	0.322	0.322
β	1.000	1.000	0.612	0.645	0.642
RSQ	0.977	0.969	0.947	0.953	0.953
SSE	**0.045**	0.057	0.101	0.109	0.109
HYBRID	1.570	**1.067**	1.511	1.650	1.649
MPSD	30.593	18.790	**17.655**	18.001	18.008
ARE	19.733	11.127	11.272	**10.733**	10.733
SAE	0.440	0.402	0.529	0.460	**0.460**
SNE	4.196	**3.109**	3.991	4.003	4.003
		Sips isotherm			
	SSE	HYBRID	MPSD	ARE	SAE
q_m	1.373	1.897	2.982	2.453	2.453
b	0.120	0.117	0.067	0.083	0.083
n	0.581	0.897	0.995	1.0	0.997
RSQ	0.992	0.978	0.957	0.964	0.964
SSE	**0.018**	0.041	0.082	0.084	0.084
HYBRID	2.046	**0.979**	1.269	1.324	1.324
MPSD	73.059	28.991	**17.313**	17.548	17.548
ARE	51.181	20.803	10.982	**10.345**	10.345
SAE	0.389	0.380	0.476	0.407	**0.407**
SNE	4.817	3.065	3.036	**2.915**	2.915

3.4 Equilibrium experiments

Adsorption and desorption are time dependent processes. Thus, the evaluation of the design and the regeneration of an adsorbent requires the determination of the adsorption rate to reach equilibrium (Azizian, 2004). Mathematical models proposed to describe the kinetics process of adsorption can be classified into adsorption diffusion models and adsorption reaction models. Adsorption diffusion models are

based on three main steps: external diffusion followed by an internal diffusion or intra-particle diffusion, and finally an exchange process between the adsorbate and the active sites of the adsorbent (Qiu et al., 2009). On the other hand, adsorption reaction models are based on chemical reactions that are not normally considered in adsorption process modelling (Qiu et al., 2009). In this study, some of the widely used batch kinetic models were examined to study the behaviour of the bone char as an adsorbent for As species removal from the water.

3.4.1 Kinetic models

Kinetic models provide an important tool for understanding the underlying mechanism of removal in the adsorption process. Four different kinetic models along with the intraparticle diffusion model were used to gain an understanding of the main removal mechanisms of As(III) and As(V). The Pseudo-first-order (PFO) model was tested by exercising the fitting procedure for the experimental removal of data against the theoretical model presented in Equation 15 (Qiu et al., 2009):

$$ln\frac{(q_e - q)}{q_e} = -k_1 t \qquad (15)$$

where q_e and q represent the amount of solute adsorbed at equilibrium and at any time of the adsorption (mg/g), respectively, k_1 is the constant rate of first order sorption (min^{-1}) and t is the time (s).

The Pseudo-second-order (PSO) rate equation assumes a second order uptake of the chemical constituents onto the surface of the adsorbent (Tan and Hameed, 2017). This model is expressed as:

$$q = \frac{q_e^2 k_2 t}{1 + q_e\, k_2 t} \qquad (16)$$

where k_2 is the Pseudo-second-order rate constant. These two models are widely applied to examine the removal of As from water on different adsorbents. For instance, Liu et al. (2014) reported that the removal of As(V) from an aqueous solution followed the Pseudo-second-order model. Similarly, Darvishi Cheshmeh Soltani et al. (2017)

reported that the removal of As(V) on Fe_2O_3/bone char nanocomposite followed the Pseudo-second-order model.

The Elovich model was established in 1937 by Zeldowitsch to identify the rate of chemisorption reaction (Qiu et al., 2009). This model does not account for desorption with an assumption that the equilibrium occurs over a long period of time (Tan and Hameed, 2017). The Elovich equation was first used to interpret the data of C_o removal on manganese oxide (Tan and Hameed, 2017). The linearized form of this model is given by equation 17:

$$q = \frac{1}{\beta}\ln(\alpha\beta) + \frac{1}{\beta}\ln t \qquad (17)$$

where α is the initial adsorption rate in mg/g.min and β is the desorption constant. The plot of ln t versus q should provide a straight line, for which the slope is 1/β and the intercept represents ln(αβ)/β. This model was found to fit the data of cadmium removal on bone char very well (R^2> 0.99) (Cheung et al., 2000). Similarly, Cheung et al. (2001) reported that The Elovich equation best fitted the removal of cadmium on bone char when compared to the Pseudo-first-order, Ritchie second order and Ritchie modified models.

The Ritchie equation was also used first for gas adsorption in 1977 (Ho, 2006). The model assumes that at t=0, the surface of the adsorbent is not occupied with any molecules and the adsorption rate is a function of the sites that are not occupied at time t. The rate of reaction using the Ritchie formula can be expressed as follows:

$$\frac{q_e}{q_e - q_t} = kt + 1 \qquad (18)$$

where q_e is the amount of dye adsorbed at time t (mg/g), k is the rate constant of the Ritchie model (min^{-1}) and t is the time (min).

Examining the suitability of these models to represent the experimental data of the As(III) and As(V) batch experiments was evaluated by determining the parameters of fitting and error function as described earlier. The examination of the goodness of the fit applying the linearized forms of the aforementioned kinetic models revealed that these forms do not provide adequate representation of the experimental data confirmed

by the value of the errors presented in the SNE calculation tables in most of the fittings (Tables SM2 and SM3). However, the use of nonlinear regression methods had resulted in a deviation of the calculated q_e values from the experimental with a lower R^2 in some cases. The explanation for these differences was studied and reported by Lin and Wang (2009). They authors reported that using the nonlinear form of the models is much more accurate for two reasons. First, the alteration of a nonlinear form to linear changes the error structure of these functions, and thus the parameters of the models. Second, the use of experimental q_e to fit the empirical model increased the error of the parameters, while this value is calculated independently from the mathematical forms in the case of the nonlinear form of the models. Thus, regardless of the lower R^2 value (in some cases), the nonlinear form of the models was presented in the study and the differences were stated in the supplementary materials (Table SM4).

Fig. 4. shows the fitting curves of the kinetic models to the data of As(III). Based on these results, As(III) adsorption onto bone char was found to follow the Pseudo-first-order kinetic model at an initial concentration of 0.5 mg/L with R^2=0.996. However, increasing the initial concentration to 2.5 and 5 mg/L revealed removal kinetic behaviour following the Pseudo-second-order model with R^2 of 0.988 and 0.978, respectively. At 10 mg/L initial concentration, the data were found to best fit the Elovich model due to its very low value of SNE compared to the other models (R^2=0.986). This indicates the significant effect of the initial concentration on the mechanism of As(III) removal on bone char. The parameters that were found to best fit the data (used in the Fig. 4) are presented in Table 5.

Table 5 shows the error analysis of the kinetic models for As(III) removal at 0.5 mg/L initial concentration. The results of the same analysis for 2, 5 and 10 mg/L initial concentration are provided in the supplementary materials (Tables SM5-SM67). Given the unavailability of data in the literature pertaining to As(III) removal with bone char, we believe that this study is the first attempt to scrutinize As(III) adsorption onto bone char, and can be used as a base for further investigations.

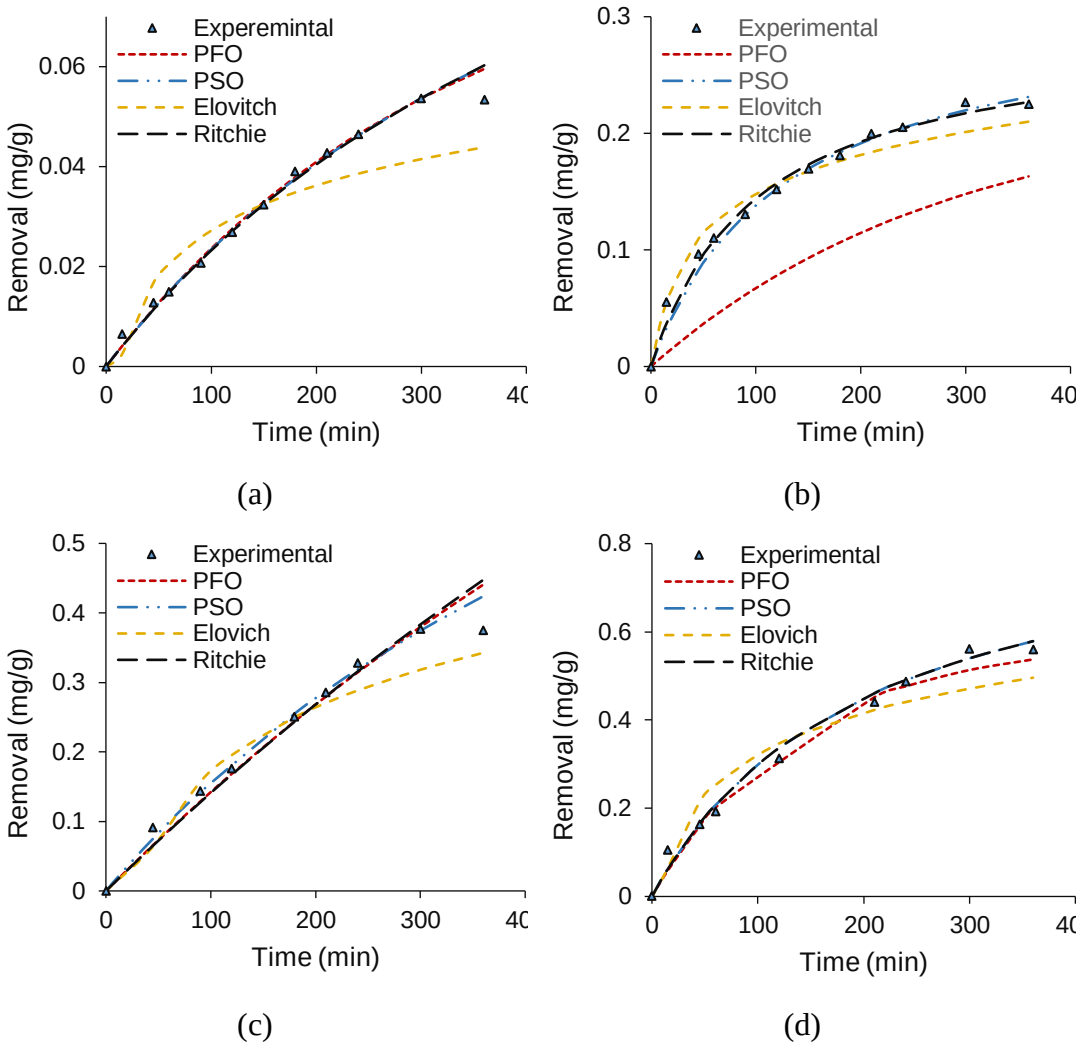

Fig. 4. Fitting of the kinetic models and the experimental data for As(III) at an initial concentration of (a) 0.5 mg/L, (b) 2.5 mg/L, (c) 5 mg/L and (d) 10 mg/L using 5 g/L BC900 at pH 8.3.

Table 5. Kinetic models' parameters for As(III) adsorption onto bone char from nonlinear regression.

	PFO			PSO		
Conc. (mg/L)	k_1	q_e	R^2	k_2	q_e	R^2
0.5	0.001	0.345	0.996	0.012	0.152	0.992
2.5	0.010	0.226	0.963	0.059	0.247	0.988
5.0	0.001	1.261	0.973	0.001	1.258	0.978

10.0	0.007	0.583	0.979	0.006	0.904	0.983

	Elovich			Sips		
	α	β	R^2	k_2	q_e	R^2
0.5	0.001	76.623	0.858	0.002	0.156	0.996
2.5	0.009	18.592	0.976	0.292	0.010	0.956
5.0	0.005	7.460	0.975	0.001	0.954	0.971
10.0	0.015	7.368	0.986	0.005	0.904	0.983

Table 6. Error analysis for kinetic models of As(III) adsorption onto bone char.

	Pseudo-first-order (PFO)				
	SSE	HYBRID	MPSD	ARE	SAE
q_e	0.345	0.089	0.075	0.096	0.096
k_1	0.001	0.003	0.004	0.003	0.003
RSQ	0.997	0.996	0.993	0.997	0.992
SSE	**0.0001**	0.000	0.000	0.000	0.000
HYBRID	0.044	**0.014**	0.016	0.015	0.015
MPSD	20.747	13.933	**13.571**	14.525	14.525
ARE	12.582	5.767	7.552	**5.507**	5.507
SAE	0.023	0.007	0.013	0.007	**0.007**
SNE	5.000	**1.903**	2.456	1.925	1.925
	Pseudo-second-order (PSO)				
	SSE	HYBRID	MPSD	ARE	SAE
q_e	0.302	0.140	0.101	0.152	0.152
k_2	0.003	0.015	0.033	0.012	0.012
RSQ	0.996	0.995	0.986	0.992	0.996
SSE	**3.1E-05**	9.9E-06	3.5E-05	9.6E-06	9.6E-06
HYBRID	0.030	**0.014**	0.021	0.015	0.015
MPSD	18.798	13.822	**12.739**	14.543	14.543
ARE	9.5541	6.0720	8.5852	**5.5367**	5.5367
SAE	0.0148	0.0075	0.0168	0.0063	**0.0063**
SNE	4.776	2.573	4.287	**2.498**	2.498

	Elovich				
	SSE	HYBRID	MPSD	ARE	SAE
α	0.001	0.001	0.001	0.001	0.001
β	60.636	76.623	100.317	102.173	49.128
RSQ	0.975	0.975	0.975	0.975	0.975
SSE	**0.0003**	0.0004	0.001	0.001	0.0004
HYBRID	0.264	**0.185**	0.258	0.253	0.656
MPSD	55.860	35.724	**29.991**	31.699	98.657
ARE	30.157	25.422	24.049	**22.715**	34.526
SAE	0.046	0.054	0.072	0.068	**0.037**
SNE	2.805	**2.585**	3.393	3.209	3.994
	Ritchie				
	SSE	HYBRID	MPSD	ARE	SAE
q_e	0.268	0.149	0.122	0.156	0.156
K_R	0.001	0.002	0.003	0.002	0.002
RSQ	0.996	0.996	0.993	0.996	0.996
SSE	**2.9E-05**	10E-06	1.9E-05	1.1E-05	1.1E-05
HYBRID	0.026	**0.014**	0.0159	0.014	0.014
MPSD	17.539	13.653	**13.265**	14.017	14.017
ARE	9.046	5.914	7.640	**5.590**	5.590
SAE	0.015	0.007	0.013	0.007	**0.007**
SNE	5.000	2.801	3.738	**2.797**	**2.797**

Similar to As(III), kinetic models of As(V) adsorption onto bone char were examined for an initial concentration of 0.5 mg/L and the results are presented in Table 5. Error analyses were also conducted for the fitted models to help identify the best fit for the experimental data of As(V) adsorption. Fig. 5 shows the data fittings of As(V) using these models. The outcome of the kinetic models fitting of As(V) adsorption with higher initial concentrations is presented in Table 7. The data show that the Pseudo-first-order model produces the best fit for As(V) adsorption with the highest coefficient of determination value and lowest SNE. However, when raising the initial concentration to 2.5 and 5 mg/L, the Pseudo-second-order model had the best fit for the experimental adsorption data (Table SM8-SM10). While at 10 mg/L the data best

fitted the Elovich model indicating a chemical adsorption at higher concentrations. The removal of As(V) on bone char was reported in recent studies to follow the Pseudo-first-order model by Chen et al. (2008) and Pseudo-second-order by Begum et al. (2016) at an initial concentration of 10 mg/L. Furthermore, Liu et al. (2014) reported that the removal of As(V) at 2.5, 5 and 10 mg/L also followed the Pseudo-second-order model. Recent studies for As(V) removal on bone char mostly use the Pseudo-first and second-order models to examine the fit of experimental data. Therefore, the comparison was only made with these two models.

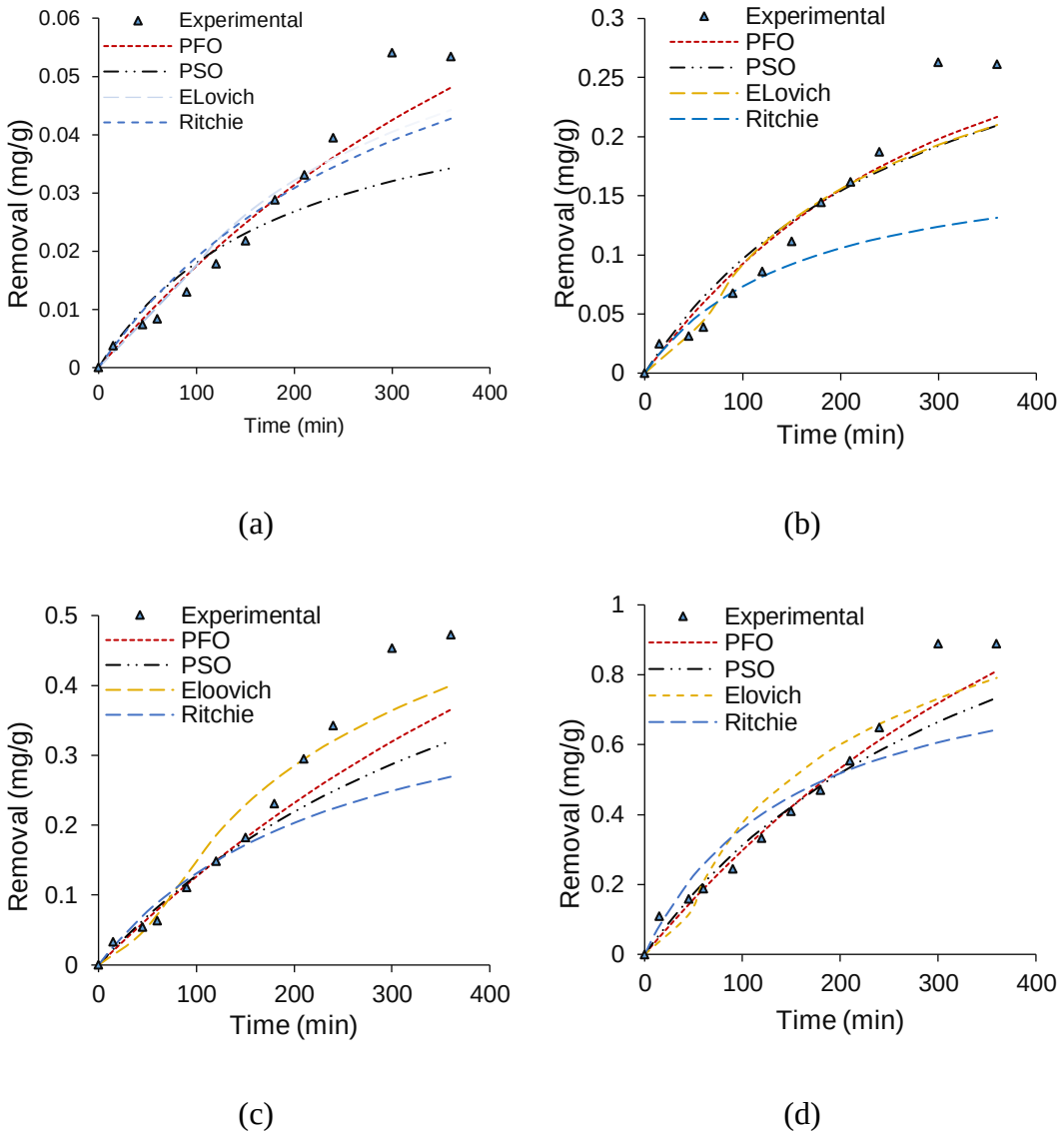

Fig. 5. Fitting of the kinetic models of As(V) removal on bone char to the experimental data at (a) 0.5 mg/L, (b) 2.5 mg/L, (c) 5 mg/L and (d) 10 mg/L using 5 g/L BC900 at pH 7.5.

Based on the observations obtained from the kinetic models, both As(III) and As(V) removal followed the PFO model indicating physical adsorption at low concentrations. However, the best fit provided by the Pseudo-second-order and Elovich models is due to the chemical interaction between the adsorbate and the adsorbent.

Table 7. Kinetic models' parameters for As(V) adsorption onto bone char based on the nonlinear form of the model.

	PFO			PSO		
Conc. (mg/L)	k_1	q_e	R^2	k_2	q_e	R^2
0.5	0.002	0.087	0.963	0.104	0.048	0.878
2.5	0.100	0.228	0.942	0.059	0.247	0.988
5.0	0.001	0.261	0.973	0.001	1.258	0.978
10.0	0.003	1.191	0.922	0.003	1.134	0.903

	Elovich			Sips		
	α	β	R^2	k_2	q_e	R^2
0.5	49E-7	43.544	0.945	0.004	0.062	0.896
2.5	0.009	18.592	0.976	0.100	0.292	0.956
5.0	0.005	7.460	0.975	0.001	0.954	0.971
10.0	0.015	7.368	0.986	0.005	0.904	0.983

Table 8. Error analysis for kinetic models of As(V) adsorption onto bone char at an initial concentration of 0.5 mg/L.

	Pseudo-first-order (PFO)				
	SSE	HYBRID	MPSD	ARE	SAE
q_e	0.065	0.072	0.079	0.079	0.087
k_1	0.004	0.003	0.002	0.002	0.002
RSQ	0.945	0.956	0.963	0.964	0.963
SSE	**0.0002**	0.0002	0.0003	0.000	0.0002
HYBRID	0.111	**0.078**	0.084	0.098	0.064

MPSD	26.718	18.177	**14.951**	15.351	17.739
ARE	19.018	13.417	10.432	**9.874**	12.564
SAE	0.036	0.032	0.033	0.035	**0.028**
SNE	4.629	3.642	3.627	3.930	**3.148**

	Pseudo-second-order (PSO)				
	SSE	HYBRID	MPSD	ARE	SAE
q_e	0.054	0.048	0.043	0.048	0.052
k_2	0.122	0.122	0.129	0.104	0.100
RSQ	0.851	0.868	0.867	0.878	0.873
SSE	**0.001**	0.001	0.001	0.001	0.001
HYBRID	0.283	**0.244**	0.311	0.273	0.219
MPSD	45.640	31.484	**29.371**	27.943	30.650
ARE	33.187	23.614	22.411	**21.183**	22.907
SAE	0.057	0.059	0.067	0.062	**0.056**
SNE	4.283	3.774	4.319	**3.928**	3.520

	Elovich				
	SSE	HYBRID	MPSD	ARE	SAE
α	486E-7	491E-7	488E-7	491E-7	469E-7
β	43.544	48.659	53.939	56.939	44.780
RSQ	0.945	0.945	0.945	0.945	0.945
SSE	**0.0001**	0.0001	0.000	0.000	0.0001
HYBRID	0.052	**0.041**	0.048	0.057	0.054
MPSD	19.544	14.035	**12.657**	13.061	20.181
ARE	11.825	10.373	9.730	**9.452**	10.63
SAE	0.019	0.019	0.022	0.023	**0.017**
SNE	4.164	**3.693**	4.071	4.447	4.121

	Ritchie				
	SSE	HYBRID	MPSD	ARE	SAE
q_e	0.057	0.062	0.068	0.0752	0.083
K_R	0.006	0.004	0.003	0.0026	0.003
RSQ	0.861	0.896	0.916	0.9263	0.918
SSE	**0.001**	0.001	0.001	0.0006	0.0003
HYBRID	0.263	**0.176**	0.177	0.1767	0.135

MPSD	27.469	43.772	**23.404**	22.9378	28.329
ARE	31.745	21.253	17.932	**16.9302**	20.717
SAE	0.050	0.055	0.049	0.0486	**0.040**
SNE	4.362	**4.203**	3.648	3.6120	3.059

3.4.2 Adsorption diffusion models.

Understanding the dynamic behaviour of an adsorption system is a pivotal step in the design and control of any treatment. Adsorption processes take place throughout three stages, in which one or two of these stages are the controlling mechanisms of the removal. First, the adsorbent reaches the adjacent layers of the adsorbent particles. In next stage, the adsorbent particles diffuse through these adjacent layers to reach the pores on the surface. Finally, the interaction between the adsorbate and adsorbent takes place. The adsorption of targeted constituents in water onto adsorbents occurs through either intraparticle diffusion or pore diffusion, or the combination of these two mechanisms (Malash and El-Khaiary, 2010). Thus, the experimental data of As(III) and As(V) adsorption onto bone char was fitted to the aforementioned models to identify which mechanisms best describe the As species removal with bone char. In the case of the intra-particle diffusion model, the following formula was adopted in this study (Valderrama et al., 2008):

$$q_t = k_{ip} t^{0.5} + c \qquad (19)$$

where q_t is the amount of adsorbed As (mg/g), k_{ip} is the rate constant of intraparticle diffusion model (mg/g $min^{0.5}$) and c is the intercept. Fitting q_t versus $t^{0.5}$ may provide a straight line indicating that the intraparticle diffusion is one of the controlling steps in the adsorption process (based on the value of c). If the value of c is zero (the straight line passes through the origin), then the intraparticle is the main controlling mechanism, otherwise there is another mechanism contributing to the process. If the plot is not a straight line, then different mechanisms are involved in the adsorption process other than intraparticle diffusion.

To test the pore diffusion mechanisms, the Boyd model shown in equation 20 was applied (El-Khaiary and Malash, 2011). Following the same interpretation of the

intraparticle model, the plot of B_t versus ln (1-q_t/q_e) from the Boyd model determines whether or not the pore diffusion mechanisms contributed to the adsorption process. This kinetic model can be applied to differentiate between internal and external diffusion in the adsorption process (Ermolenko et al., 2020).

$$B_t = -0.4977 - \ln(1 - q_t/q_e) \qquad (20)$$

where B_t is the mathematical function of the fractional attainment of equilibrium at different time (t). The fit of the experimental data to these two models is illustrated in Fig. 6 and 7. The plot of As(III) data using the intraparticle diffusion model showed that this model is one of the mechanisms that controls the rate of the removal on bone char at all concentrations. However, other mechanisms are also contributing into removal process as the lines did not pass through the origin. Similar results were achieved when examining the suitability of the Boyd model to fit the data at 0.5, 2.5 and 5 mg/L as the fit of the straight line had a high R^2. On the other hand, the experimental data at 10 mg/L failed to produce a straight line with an R^2 of 0.87, suggesting the contribution of other diffusion mechanisms at a concentration of 10 mg/L (Fig. 7).

As(V) adsorption onto bone char could also be said to employ an intraparticle diffusion mechanism as the plot of q_t versus $t^{0.5}$ resulted in a linear relationship. However, there seem that two phases of the intraparticle diffusion occurred; low adsorption, represented by the first segment of the fitting line (at time of approximately $\leq$ 45 min), followed by high adsorption beyond 45 min. The fitting lines of the all the concentrations did not pass through zero indicating that intraparticle is not the only diffusion mechanism that can describe the adsorption of As(V). Fig. 7 shows the plot of data after applying the model for the four concentrations of each As(III) and As(V). Two concentrations are presented on each sub-figure for the sake of clarity as the data interfere with each other when the presented together. From Fig. 7, it can be seen that the pore diffusion mechanism might also contribute to the removal process at 0.5 and 2.5 mg/L initial concentration. Raising the initial concentrations to 5 and 10 mg/L reduced the linearity of the fit. This means that at higher concentrations, the pore diffusion mechanism had no contribution to the adsorption process. Similar results were reported by Chen et al. (2008) when examining the mechanism of As(V) removal on bone char at initial concentrations of 0.5,1,and 1.5 mg/L. Their study confirmed

that the removal was complex and due to surface adsorption and the intraparticle diffusion mechanism. Moreover, studying the controlling rate of As(III) and As(V) on graphene showed that the intraparticle and the outer diffusion were both contributing to the adsorption process (Yu et al., 2015). Similarly, the outer diffusion is the controlling mechanism of the removal when the pore diffusion is applicable since the line fittings do not pass through the origin.

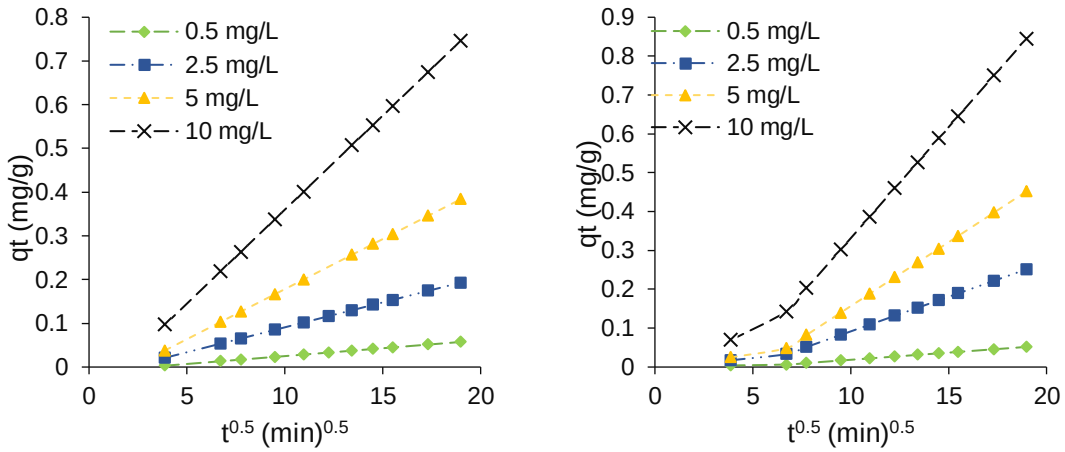

(a) Plot of As(III) (b) Plot of As(V)

Fig. 6. Plot of intra particle diffusion model for (a) As(III) and (b) As(V) experimental data using 5 g/L BC900 at pH 8.6 and 7.5, respectively.

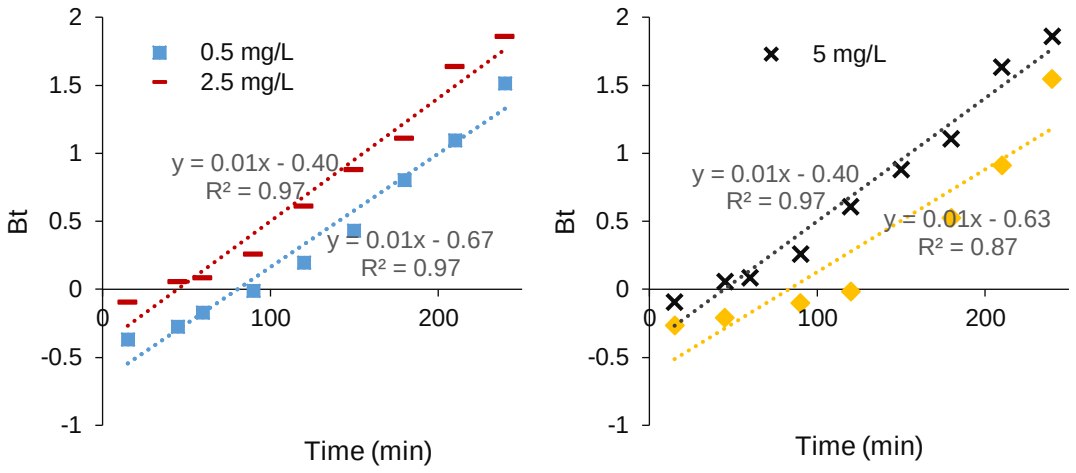

(a) Data plot for As(III) at 0.5, 2.5, 5 and 10 mg/L

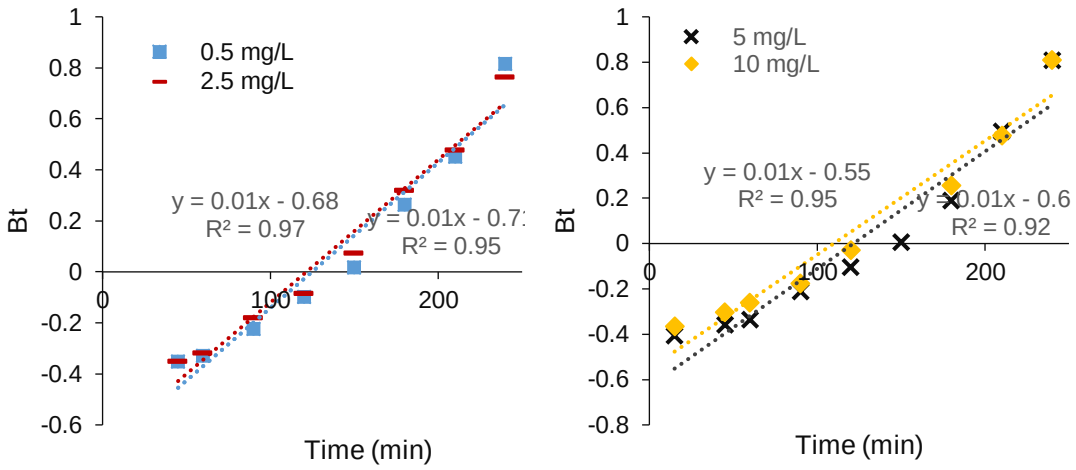

(b) Data plot for As(V) at 0.5, 2.5, 5 and 10 mg/L

Fig. 7. Plot of the Boyd model for different concentration of (a) As(III) and (b) As(V) experimental data using 5 g/L bone char at pH 8.6 and 7.5, respectively

4. SEM-EDS and FTIR analyses

The adsorption of As(III) and As(V) onto BC900 was investigated through SEM-EDS analysis as illustrated in Fig. 8. The surface elemental analyses of vergine bone char are in line with those reported in (Rojas-Mayorga et al., 2016) where Ca, P and O being the major elements of the structure. Comaparing the mass percentage of surface elements of BC900 to those loaded with As species, it can be seen from Fig. 8 that there are changes in the elemental composition after adsorption. The main changes due to loading As(III) on the bone char was due to the reduction in the C, O, Na, Mg and P percentage mass and the appearance of As(III). On the other hand, As(V) affected the content of C, O, Na and Mg. The changes in these elements suggest that the amobilisation of As species onto bone char was in the form of As oxides and metal complexes (Alkurdi et al., 2020; Cheng et al., 2016). The FTIR analysis was used to detect the changes in the bone char structure after loading it with As(III) or As(V). The main changes was in the region were the the oxygen functional group peaks were found with a higher alteration of these peaks position and shape for As(III) loaded samples. Therefore, the removal mechanism may be exaplaind as a result of the

formations of precipitants with Mg on the surface of the BC900 as provided by Makreski et al. (2015).

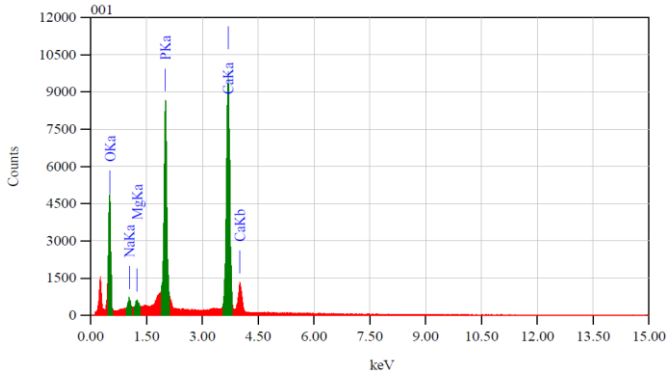

(a)

Elements	Mass %
C	3.07
O	38.15
Ca	38.03
P	19.7
Mg	0.66
Na	0.42

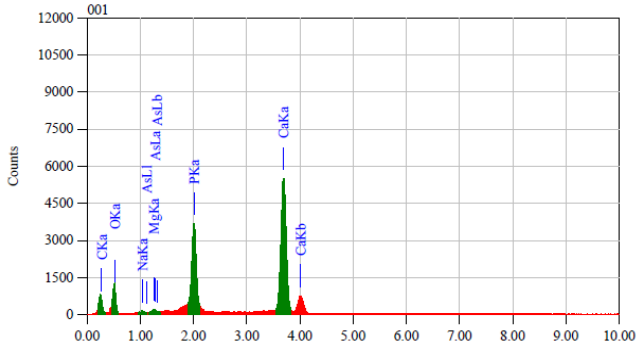

(b)

Elements	Mass %
C	3.01
O	38.08
Ca	42.11
P	16.24
Mg	0.35
Na	0.19
As	0.03

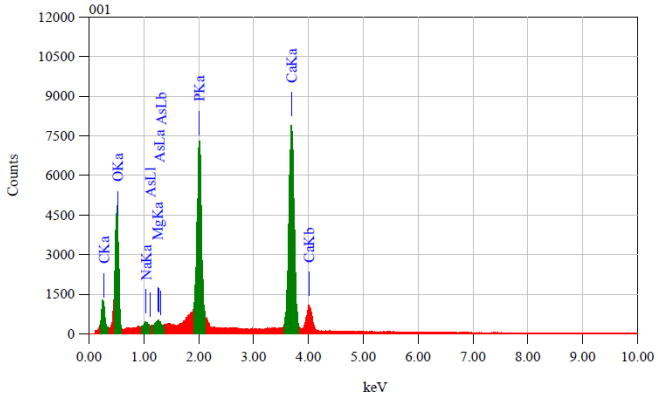

(c)

Elements	Mass %
C	2.85
O	40.17
Ca	36.69
P	19.48
Mg	0.30
Na	0.31
As	0.20

Fig. 8. EDS analyses for (a) BC900, (b) As(III) and (c) As(V).

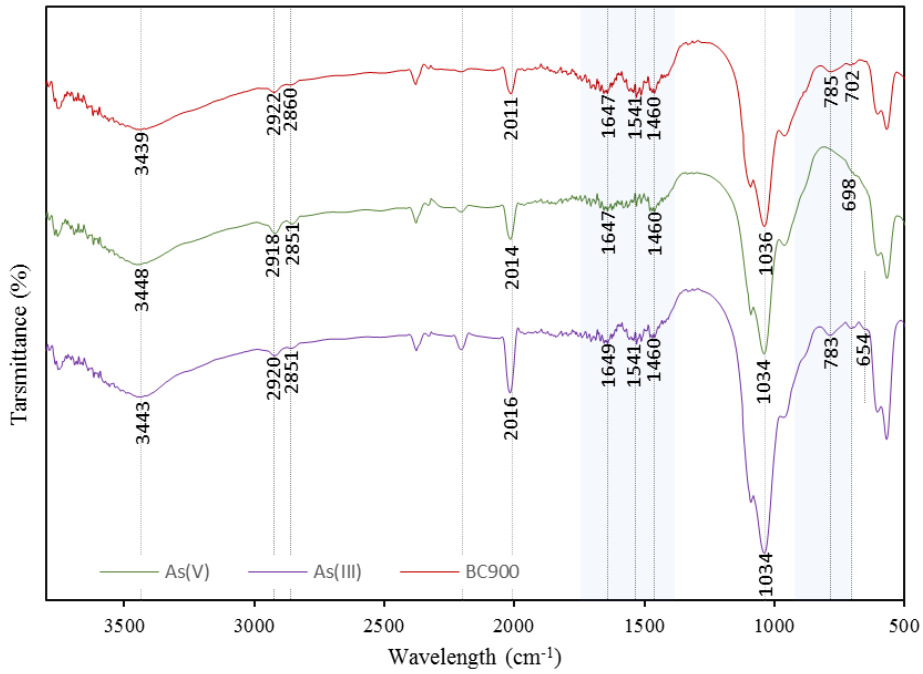

Fig. 9. FTIR analysis for As-loaded and unloaded BC900 [8].

5. Conclusion

The removal of As(III) and As(V) with bone char was thoroughly examined in this study taking into consideration the adsorption kinetics, isotherms and diffusion models. Four isotherm models were tested for each of the As species: Langmuier, Freundlich Redlich-Peterson and Sips models. Similarly, the kinetics were examined using Pseudo-first-order, Pseudo-second-order, Elovich and Ritchie models. Both the linear and nonlinear forms of the models were tested for fitting of the experimental data. The results of the fitting for isotherm and kinetic models for these two As species were found to be different, with a best fit provided by the Sips model for As(III) and the Langmuir model for As(V). On the other hand, the knietic models were dependent on the initial concentration of As species. It was found that at low concentration, intraparticle diffusion and pore diffusion were both effective for As(III) and As(V). However, the pore diffusion model was not suitable for describing adsoption when the initial concentration of As(III) increased beyond 10 mg/L. For As(V) adsoption, fitting against the intrapartcile diffusion model exhibited a two stage linear trend; low adsoption capacity at time $\leq$ 45 min and high adsoption capacity byond this time. Furthermore, the effect of the pore difusion model was valid up to 5 mg/L for As(V)

adsorption. Structural analysis using SEM-EDS was used to confirm the adorption of As species by BC900 and examining the changes in the chemical composition of the As loaded samples. FTIR was used to detect the changes in the functional groups and the fingerprint region after adsorption. The results showed that the adsorption of As species onto bone char was possibly due to the formation of As oxides and metal complexes as in the imobalised phase on bone char. For futre work recommendations, tt would be useful to explore the effciency of the identifed optimum removal paramters for As species in column packed reactors.

Acknowledgments

This research was performed as a part of PhD research which was supported in part by the Iraqi Government and the Australian Research Training Program.

4.3 Concluding remarks

The effect of experimental conditions on As(III) and As(V) removal were studied. The optimum conditions of the removal were applied to examine the isotherm, kinetic and diffusion models. The parameters of the models were calculated based on the linearized and nonlinear forms. The results were compared based on the values of the coefficient of the determination and the normalized sum of errors (calculated from five different error functions). The results provided by the nonlinear regressions were more accurate than those of the linearized forms. The Langmuir, Freundlich, Redlich-Peterson isotherm models were applied. The Sips and Langmuir models provided the best fit for the experimental data of As(III) and As(V) respectively. The kinetics were studied using the Pseudo-first-order, Pseudo-second-order, Elovich and Ritchie models. Four different initial concentrations (0.5, 2.5, 5 and 10 mg/L) were fitted to the kinetic models. Removal was found to be by physical adsorption at 0.5 mg/L, and through chemisorption at higher concentrations. The diffusion models provided that the intraparticle diffusion mechanism is the controlling rate of removal. The pore diffusion model also contributed to removal at the lower concentrations examined (0.5 and 2.5 mg/L).

CHAPTER 5

Evaluating the ability of $nTiO_2$/bone char composite and UV radiation for simultaneous oxidation and removal of arsenite

PAPER V

Alkurdi, S. S., Al-Juboori, R. A., Bundschuh, J. and Marchuk, A. (2020). Evaluating the ability of $nTiO_2$/bone char composite and UV radiation for simultaneous oxidation and removal of arsenite **(**Prepared for submission to the Environmental Pollution).

5.1 Introduction

This chapter explores the chemical modification of bone char to produce a composite that functions as an adsorbent and oxidizer for inorganic As mitigation. Animal bone residues were used as a precursor for the preparation of bone char at 900 °C and its composite using nanoparticles of titanium dioxide ($nTiO_2$) for the oxidation of As(III) in the presence of UV light. The pyrolysis temperature was selected based on the results of Chapter 3, while the need for an oxidant was based on the results of Chapter 4. The composite coated using two different methods: after the pyrolysis process at 300 °C and during the pyrolysis at 900 °C. The outcomes of the study show that the composite can be successfully used for oxidizing As(III) and adsorbing the resultant As(V) in solution in one step (no pre-treatment required). Furthermore, the study examined the transformation of the TiO_2 from anatase to rutile due to exposure to high temperature when coated during the pyrolysis process. FTIR and SEM-EDS analysis were used to examine the changes in the composite structure due to coating and loading As.

Evaluating the ability of $nTiO_2$/bone char composite and UV radiation for simultaneous oxidation and removal of arsenite

Susan S.A. Alkurdi[a,b], Raed A. Al-Juboori[c,] Jochen Bundschuh[a,d*], Alla Marchuk[e]

[a] *School of Civil Engineering and Surveying, Faculty of Health, Engineering and Sciences, University of Southern Queensland, West Street, Toowoomba, 4350, Queensland, Australia.*

[b] *Northern Technical University, Engineering Technical College/Kirkuk, Iraq.*

[c] *Water Engineering Research Group, Department of Civil and Environmental Engineering, Aalto University, P.O. Box 15200, Aalto, FI-00076 Espoo, Finland.*

[d] *UNESCO Chair on Groundwater Arsenic within the 2030 Agenda for Sustainable Development, University of Southern Queensland, West Street, Toowoomba, 4350, Queensland, Australia.*

[e] *University of Southern Queensland, Centre for Sustainable Agricultural Systems, Toowoomba, 4350, Queensland, Australia.*

Corresponding author*: Jochen Bundschuh
Faculty of Health, Engineering and Sciences & UNESCO Chair on Groundwater Arsenic within the 2030 Agenda for Sustainable Development, University of Southern Queensland, West Street, Toowoomba, 4350, Queensland, Australia.
Phone: +61 7 4631 2694
Email: Jochen.Bundschuh@usq.edu.au

Abstract:

The reuse of waste materials for water treatment purposes is an important approach for promoting circular economy and achieving effective environmental remediation. This study examined the use of bone char/titanium dioxide nanoparticles composite (BC/nTiO_2) and UV for As(III) and As(V) removal from water. Two different procedures were followed to produce (BC/nTiO_2) composite. nTiO_2 deposition onto BC led to a decrease in the specific surface area and pore volume from 69.063 to 37.679 m^2/g and 0.234 to 0.162 cm^3/g, respectively, however, the pore size increased from 13.588 to 16.884 nm. BC/nTiO_2 prepared by covering the raw bone with nTiO_2 and then pyrolyzing it at 900 °C had better As removal (57.3 % vs 24.8%) and oxidation (3.5 times higher arsenate produced) than that of which was prepared after pyrolysis. The effect of three UV power levels of 4, 8 and 12 W on arsenite oxidation and removal with the best BC/nTiO_2 composite were tested and benchmarked against treatments of BC/nTiO_2 with visible light and BC alone. The highest UV power was found to be the most effective treatment with removal capacity of 281.36 µg/g followed by BC alone with removal capacity of 195.76 µg/g. This suggests that the effect of surface area and pore volume loss due to TiO_2 deposition can only be compensated by applying high level of UV power.

Keywords: Bone char, nTiO_2, pyrolysis, UV, visible light.

1. Introduction

Elevated arsenic (As) concentrations in ground water are a global concern that affects not only the availability of drinking water, but also food safety (Kumarathilaka et al. 2020). Arsenite [As(III)] is the most toxic form of inorganic As. It is present as uncharged arsenious acid in the pH range of 6.5-8.5, which makes it less amenable to adsorption compared to arsenate [As(V)] at the same pH range (Clifford and Ghurye 2001, Zeltner 2002). Therefore, oxidizing As(III) to As(V) was introduced as a viable means of improving the removal of inorganic As from water. Recent studies have provided an extensive explanation for the mechanism of oxidizing organic and inorganic As(III) to As(V). The oxidation process may be chemically achieved using ozone or iron and manganese compounds, microbiologically, e.g. using

Herminiimonas arsenicoxydans (known as ULPAs1) (Weiss et al. 2009), or photochemically by applying ultraviolet radiation (UV) with or without activating agents such as TiO_2, H_2O_2 or sulfur (Bissen and Frimmel 2003).

With the predicted growth in world population, there is a global concern about an accompanying rise in waste disposed which will be a substantial challenge to address. For instance, increasing demands on the meat industry lead to an increase in the bone waste, particularly in countries that invest in livestock such as Australia (Alkurdi et al. 2019b, OECD 2018). Exploring ways of utilizing these waste materials for different environmental applications can have a significant impact on protecting the environment in an economic and sustainable fashion. Incinerating the bone waste simultaneously produces energy and useful products such as bone char (BC). Bone char has been reported to have great potential for removing different contaminants from water (Minja 2020, Rojas-Mayorga et al. 2015). Regardless of the high performance of bone char to remove F^- and dyes from solutions, different studies have reported its limited ability to remove As species, especially As(III). Thus, applying chemical and/or physical modification is crucial to improve its performance in this application.

Modification with nanomaterials are considered to be a promising method for improving the sorption capacity of adsorbents for water treatment because of their special physical and chemical properties. Some of these characteristics are related to their particle size and surface area, photoelectronic and photocatalytic properties (Liu et al. 2011). Metal-containing nanoparticles, carbonaceous nanomaterials, zeolites and dendrimers have been demonstrated to enhance sorption capacities for water treatment purposes (Savage and Diallo 2005).

Titanium dioxide (or titania) nanoparticles are versatile, durable, non-toxic, and thermodynamically stable photocatalysts (Woan et al. 2009). It has been reported to be a promising oxidative and reductive catalyst that is widely explored for water/wastewater purification from organic and inorganic contaminants (Savage and Diallo 2005). TiO_2 is mainly used as a semiconductor that can create a mobile electron by adsorbing the right amount of energy. Hence, it is commonly applied in combination with UV radiation. TiO_2 absorbs UV radiation with wavelengths of ~380 nm with a band-gap larger than 3.2 eV where the electron can move from the valence

band to the conduction band (Xu et al. 2007). TiO_2 is available in three different forms: anatase, rutile and brookite. Thermodynamically, rutile is the most stable form of TiO_2 with a higher surface energy than anatase with the same particle size (Mancardi et al. 2018).

The photocatalyst activity of TiO_2 nanoparticles in oxidizing As(III) species was explored from different perspectives. For instance, Xu et al. (2007) reported that the methylated arsenic species were effectively oxidized by hydroxyl radicals formed in catalytic photolysis. Wei et al. (2019) reported that high pH levels (11 and 12) are the optimum pH of the highest photocatalytic activity for three different facets of anatase. Guan et al. (2012) reviewed the removal of As species using TiO_2. Their study revealed that TiO_2 had a low sorption capacity for As species at low concentrations (less than 1 g/L). It recommended that increasing the specific surface area and decreasing the degree of crystallinity may be applicable by supporting TiO_2 onto porous materials. This can also reduce the need for separating nanoparticles after treatment. Several studies introduced new composites such as TiO_2 with Ag_2O (Ren et al. 2019) or Fe_3O_4 (Deng et al. 2019) for As oxidation and removal from water. The present study is designed to evaluate the effect of UV radiation on concurrent As oxidation and removal of As on a composite of $nTiO_2$ and bone char ($BC/nTiO_2$). To the knowledge of the authors, As removal with simultaneous photocatalytic oxidation and adsorption on bone char and TiO_2 composite has not been studied in previous research work, and this study attempts to provide some insight into this treatment process.

Based on the results achieved by our previous study that examined the effect of pyrolysis temperature in the range 500-900 °C on As removal from water, BC pyrolysed at 900°C (BC900) was found to have the highest removal capacity for As species in water (Alkurdi et al. 2020). However, BC900 was more effective for As(V) removal than for As(III) removal under the same experimental conditions. Therefore, this bone char was selected to prepare the adsorptive catalytic composite with TiO_2 to remove inorganic As from water without the need for pre-oxidation. The effectiveness of the composite for catalyzing the photo oxidation of As(III) was evaluated along with the overall removal capacity. The change in the absorbent structure with different treatment regimens was also tracked using a range of advanced analytical equipment.

2. Materials and methods

2.1 Reagents and equipment

Bone samples were collected from local shop in Toowoomba, QLD, Australia. All reagents used were of analytical grade. Arsenite standard with a concentration of 1000 mg/L was purchased from Choice Analytical, New South Wales, Australia. Nitric acid (70%, RCI Labscan) and sodium hydroxide (Labscan Asia Co. Ltd) were used to control the pH of the solutions. TiO_2 nanoparticles (anatase, 99.9%, 18 nm) were purchased from US Research Nanomaterials, Inc. Potassium bromide was purchased from BDH Chemicals Ltd, Poole, England.

Arsenic assays were performed using Inductively Coupled Plasma Mass Spectrometry (ICP-MS) (PerkinElmer NEXION 300 ICP-MS). ICP-MS hyphenated to Ultra-High Performance Liquid Chromatography (UHPLC) was used for As speciation applying the method reported in (Herath et al. 2020). Throughout the study, pH measurements were made using TPS smart Chem-Lab pH meter. The point of zero charge of the char samples was measured applying dynamic light scattering topology using a Nano-S Zetasizer (Malvern Instruments Ltd., UK). Ultrasonic cleaner model FXP 14 provided by Unisonic Australia Cleaning Systems, NSW, Australia was used for the composite preparation.

Pyrolysis process of bone char and the composite were performed using Rio Grande kiln, model CS2, USA. Surface morphology and the porous structure visualization of the samples were conducted using Scanning Electron Microscopy (SEM) (JEOL, model JSM-6000 Plus). The elemental surface analyses were carried out using SEM-EDS (JEOL JSM-7500FA) with accelerating voltage of 10 kV and probe current of 7.475 nA. The composition and the functional groups were analyzed based on the results obtained from Fourier Transform Infrared (FTIR) spectroscopy (IRAffinity-1S FTIR spectrometer, Shimadzu) following the same procedure for the characterization of the BC900 reported in our previous work (Alkurdi et al. 2020). UV light was applied using 4-W Mini Ultra-violet Fluoro Lights (λmax = 360 nm). The surface area, pore size and volume were performed by Particle and Surface Science Pty Limited. BET surface area was estimated from the results of N_2 adsorption at 77.3 K using Brunauer–Emmer–Teller.

2.2 Adsorbent preparation

Bone char samples used in this study were the same as those tested in our previous study (Alkurdi et al. 2020). Two different procedures were followed for the preparation of the composite. These were ultrasound-assisted methods (composite denoted as $(BC/nTiO_2)_{US}$) after the pyrolysis of the bone samples and during the pyrolysis where the raw bone was covered with $nTiO_2$ and then pyrolysed at 900 °C (composite denoted as $(BC/nTiO_2)_P$).

For the preparation of $(BC/nTiO_2)_{US}$, $nTiO_2$ slurry was prepared by adding 1 g of $nTiO_2$ nanoparticles to 100 mL double distilled water. The slurry was then stirred for 4 h to disperse and suspended the particles in the solution (Jia et al. 2007). Thereafter, $nTiO_2$ slurry was shaken in ultrasonic cleaner along with 5 g of washed BC900 (1-2 mm size) for 30 min. The composite was separated using filtration and then dried at 120 °C for 2 h. Afterward, the resultant solids were calcinated at 300 °C for 2h to obtain the final $(BC/nTiO_2)_{US}$ composite.

The second composite ($(BC/nTiO_2)_P$) was prepared following a simplified one step method. Briefly, 1g $nTiO_2$ was added to 5g of cleaned crushed bone pieces. Then the mixture was sprayed with 20 mL distilled water to instigate the adhesion of $nTiO_2$ particles onto the cleaned bone. Next, the final product was placed in the kiln at 900 °C for 1h. Later, the sample was grinded into 1-2 mm in diameter, washed with distilled water thoroughly to remove the excess nanoparticles on the surface and then dried at 60 °C for 24 h. The whole samples were sealed in plastic bags for later use in the adsorption experiments to avoid moisture entrapment into the composite.

2.3 Adsorbent experiments

2.3.1 Experimental setup

The setup used in this study for carrying out the experiments is illustrated in Fig. 1. UV light was applied through three lamps with power level of 4 W for each lamp (Yoon and Lee 2005). The solution and the adsorbent were placed in a glass beaker (300 mL) and stirred using a magnetic stirrer. In order to avoid the breakage of the composite particles due to the friction between the magnetic bar and the bottom of the

beaker, a vent cowl with metal mesh was used to cover the bar while conveying the stirring motion to the solution. Three power levels were tested in this study: 4, 8 and 12 W. For the 4 W test, the lamp was fixed on top of the beaker, whereas for the 8 and 12 W tests, the lamps were secured around the beaker at fixed distance between them.

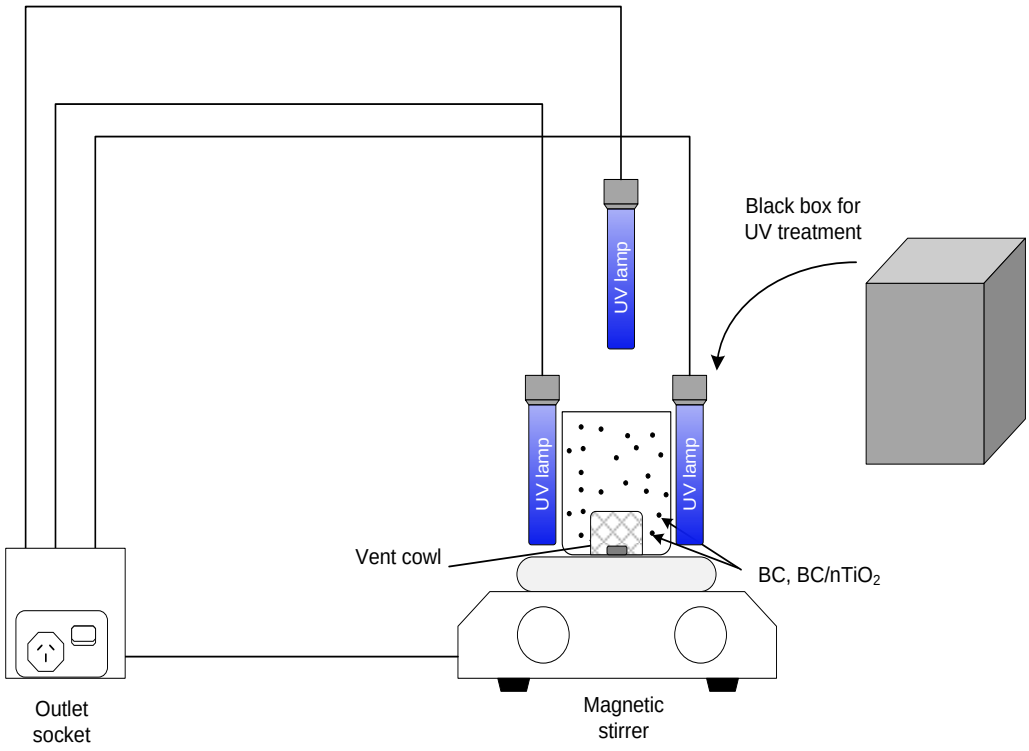

Fig. 1. Experimental setup

2.3.2 Experimental procedure

Adsorption experiments were performed to evaluate As removal with BC900 alone and in combination with $nTiO_2$ and UV. The oxidation of arsenite under the effect of the aforementioned treatment scenarios was also examined. Adsorption experiments were performed by adding 5 g/L of the adsorbent to 100 mL of 2.5 mg/L As(III) solution and mixed for 4 h at pH 8. The experimental conditions were selected based on a thorough kinetic experimental work on As adsorption with BC900. A summary of the kinetic study outcome is provided in Table 1. For UV treatment, a black box was used to cover the solution to prevent the interference of natural light effects. The same reaction time and stirring process were applied with BC900 alone and $BC/nTiO_2$ but without UV source. After the elapse of reaction time, stirring was halted and

samples were filtrated and analyzed for the residual As in solution to calculate the removal capacity applying the following formula:

$$R = \frac{(C_o - C_f)}{D} \quad (1)$$

where R is the removal capacity in mg/g, C_o is the initial concentration in mg/L, C_f is the final concentration and D is the adsorbent dose in g/L.

Table 1. Optimum operating conditions for As species removal with BC900

Experimental condition	**Range**	**As species**	
		As(III) optimum	As(V) optimum
Initial concentration (mg/L)	0.5-50	Maximum removal of 45.99% at 2.5 mg/L	Maximum removal of 55.29% at 1 mg/L
pH	4-10	8.6	7.5
Contact time (h)	0-12	4	4
Bone char dose (g/L)	2.5, 5 and 7.5	5	5

To examine the effect of UV light power on the oxidation of arsenite, a speciation process was carried out using HPLC/ICP-MS as mentioned earlier. All the results are presented in mean values of three repeats for each experiment, except for the UHPLC analysis, were only two repeats were analyzed.

3. Results and discussion

3.1 BC/nTiO$_2$ characteristics

The efficiency of the two composite preparation methods for improving As removal was investigated through preliminary tests. It was found that $(BC/nTiO_2)_P$ was more effective than $(BC/nTiO_2)_{US}$. Hence, only $(BC/nTiO_2)_P$ will be characterized using a range of advanced analytical measurements. However, FTIR analysis is an exception where comparison between the spectra of $(BC/nTiO_2)_{US}$ and $(BC/nTiO_2)_P$ will be presented due to the observed interesting shifts in the peaks for the two composites.

The adherence of $nTiO_2$ onto bone char surface was confirmed using EDS analysis for BC900 and $(BC/nTiO_2)_P$ as shown in Fig. 2. It can clearly be seen that there is a fair amount of Ti detected on $(BC/nTiO_2)_P$ composite indicating that this method was effective for preparing such composite.

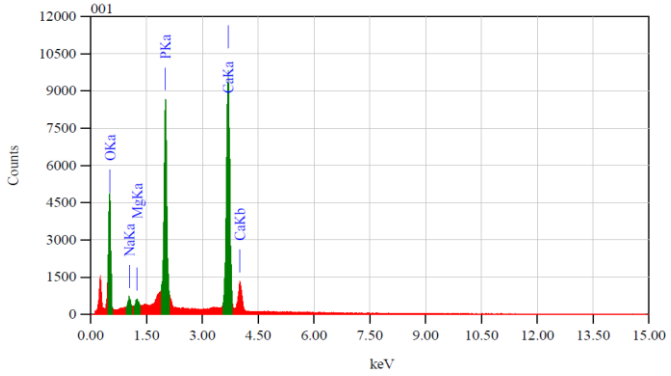

Elements	Mass %
C	4.07
O	41.15
Ca	34.00
P	19.7
Mg	0.66
Na	0.42

(a)

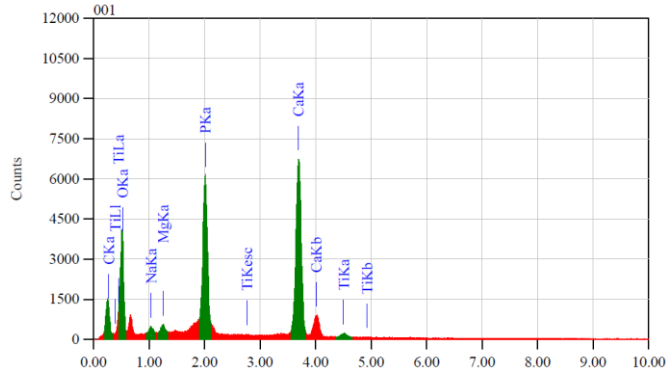

Elements	Mass %
C	4.08
O	39.62
Ca	35.38
P	18.76
Mg	0.58
Na	0.49
Ti	1.08

(b)

Fig. 2. EDS analyses for (a) BC900 and (b) $(BC/nTiO_2)_P$

$(BC/nTiO_2)_P$ was also characterized for the surface pH, surface area, pore volume and pore size as presented in Table 2. Compared to the bone char pyrolysed under the same conditions, the BET surface area was about half of that of the BC900's (69.063 m^2/g). Similarly, the pore volume was reduced from 0.235 cm^3/g to 0.162 cm^3/g for $(BC/nTiO_2)_P$ compared to BC900. However, the pore size was higher for $(BC/nTiO_2)_P$, 16.884 nm as opposed to 13.588 nm for BC900 (Alkurdi et al. 2020). The SEM images presented in Fig. 3 show that the morphology of the char surface became rougher after the deposition of $nTiO_2$ particles. The pores on $(BC/nTiO_2)_P$ surface were larger but

less dense in number compared to BC900 and this agrees with the results presented in Table 2. Similar results were observed by a recent study on coating activated carbon with copper where surface area and pore volume decreased while pore diameter increased with coating (Zhao et al. 2020).

The surface charge of $(BC/nTiO_2)_P$ was also examined and the results are depicted in Fig. 4. The composite surface charge at its initial pH was -9.03 mV. This value increased after reducing the pH of the solution up to pH 5, and then dropped as pH decreased to provide 2 points of zero charge (pH_{pzc}) at 3.82 and 8.79. In comparison, BC900 has only one pH_{pzc} at a pH of ~8.3 (Alkurdi et al. 2020).

Table 2. $(BC/nTiO_2)_P$ characteristics

Pyrolysis temperature (°C)	900
Surface pH	9.9
pH_{pzc}	3.82 and 8.79
BET surface area (m^2/g)	38.483
Pore volume (cm^3/g)	0.162
Pore size (nm)	16.884

FTIR analysis was carried out to detect the changes which resulted after depositing of $nTiO_2$ particles onto the BC900. Fig. 5 shows that the deposition of $nTiO_2$ particles decreased the amount of functional groups present on the surface. The composite $(BC/nTiO_2)_{US}$ exhibited a significant decrease in the peaks related to the presence of amide groups and the oxygen surface groups in the range 1585-1700 cm^{-1}. It was established that these groups are likely to be related to bone protein decomposition during pyrolysis (Alkurdi et al. 2020). This indicates that TiO_2 interacts with these groups during pyrolysis and this led to the disappearance of their corresponding peaks. This is supported by the findings of Roguska et al. (2011), who reported the high adsorption capacity of protein onto TiO_2. However, these peaks changed only a little for the case of $(BC/nTiO_2)_P$. This may be related to the decomposition of the protein in the first stage of the pyrolysis process and less interaction of TiO_2 at a lower temperature (300 °C).

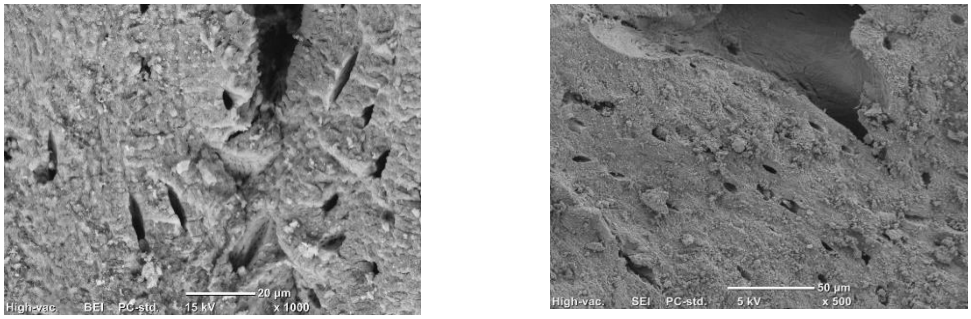

(a)

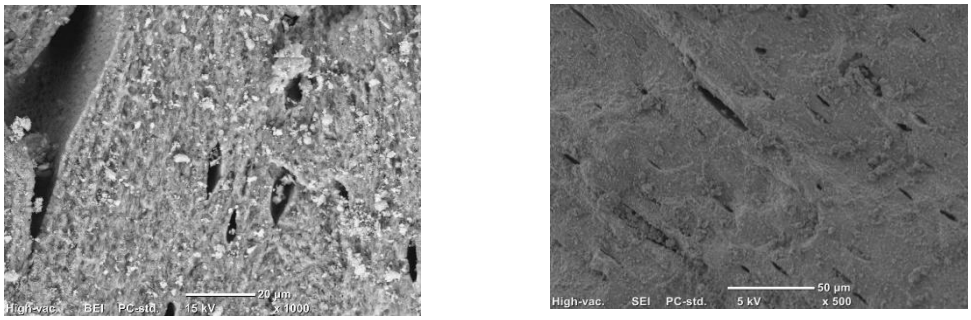

(b)

Fig. 3. SEM images for (a) BC900 and (b) $(BC/nTiO_2)_P$

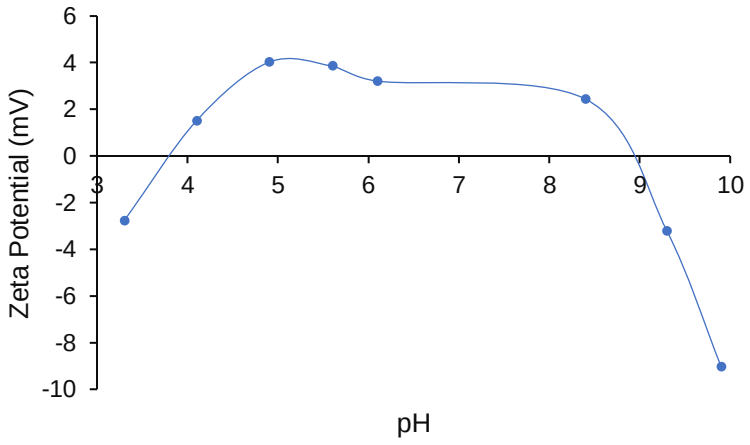

Fig. 4. $(BC/nTiO_2)_P$ surface charge at various pH levels

Compared to BC900, the peaks associated with PO_4^{3-} shifted slightly from 1032 to 1041 cm^{-1}, 962 to 956 cm^{-1} and 563 to 570 cm^{-1} after TiO_2 deposition. Similarly, the

peaks at 1408 and 880 cm^{-1} that are related to CO_3^{2-} shifted to 1420 and 887 cm^{-1}. In addition, the peak of the hydroxyl group shifted from 3443 to 3448 cm^{-1} due to the deposition of $nTiO_2$ particles. The shifting in the position of the main peaks of the composite compared to BC900 highlights the change in the BC structure due to $nTiO_2$ particles deposition onto the char surface. Furthermore, the reduction in the BET surface area and pore volume are other evidences of the incorporation of the nanoparticles into the bone char structure. FTIR spectrum of $(BC/nTiO_2)_{US}$ showed the formation of a small peak at 1342 cm^{-1}, due to the formation of Ti-O-Ti bond (Kannaiyan et al. 2010, Thamir et al. 2016). Depositing $nTiO_2$ particles after pyrolysis resulted in a boarder peak of PO_4^{3-} at 1033 cm^{-1} and a higher intensity for the peaks related to the presence of PO_4^{3-} at 570 and 601 cm^{-1}. This may be related to the formation of new complexes between PO_4^{3-} and the nanoparticles.

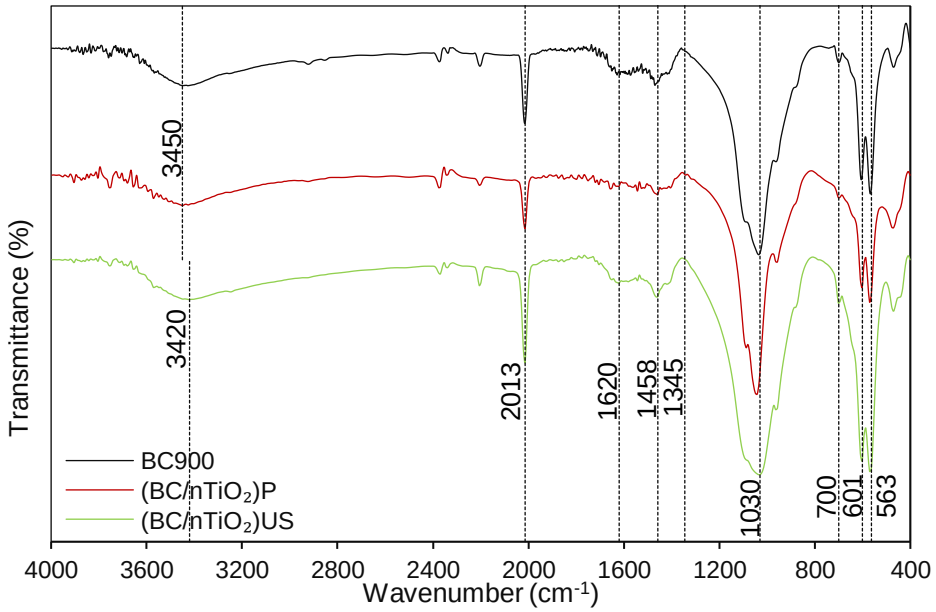

Fig. 5. FTIR spectra of BC900 and the composites prepared following two different procedures

The difference in the properties of the composites prepared during or after pyrolysis conditions can be attributed to the effect of temperature on $nTiO_2$. For the case of $(BC/nTiO_2)_P$, TiO_2 was exposed to a temperature of 900 °C, which probably resulted in the transformation of the photocatalyst from anatase to rutile as such a transformation was reported to occur at 600 °C (Hanaor and Sorrell 2011). In

comparison, the anatase in the composite $(BC/nTiO_2)_{US}$ was exposed only to 300 °C, and hence TiO_2 remained in its original polymorph. The transformation of $nTiO_2$ from anatase to rutile form was confirmed by taking the FTIR spectra for the $nTiO_2$ before and after exposure to 900°C and compare it with the spectra of previous studies as demonstrated in Fig. 6. The analogy between the spectra obtained for $nTiO_2$ before and after pyrolysis at 900°C in this study and those reported by Kalaivani and Anilkumar (Kalaivani and Anilkumar 2018) is clear. It seems that anatase form has few characteristic peaks that contract to one characteristic peak as it transforms to rutile.

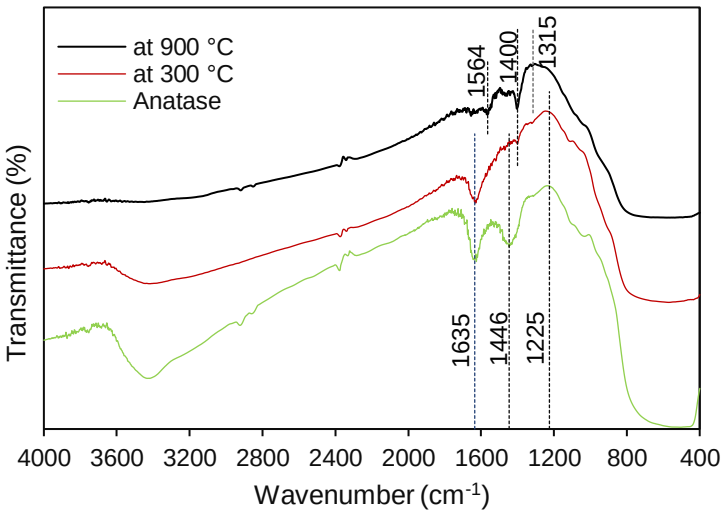

(a)

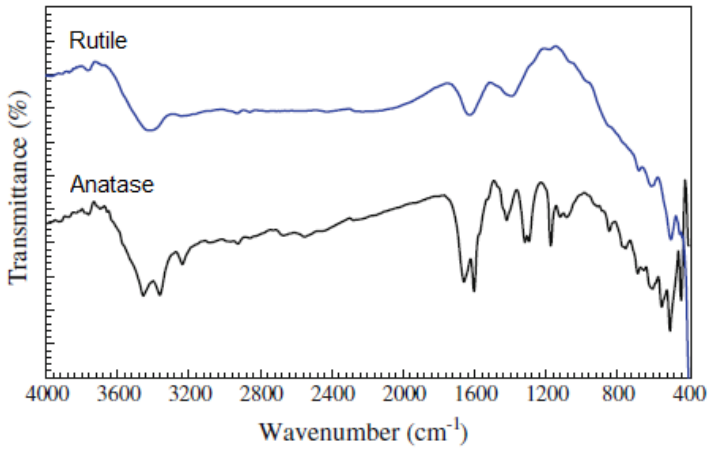

(b)

Fig. 6. FTIR spectra for (a) $nTiO_2$ (anatase) and after exposure to 300°C and 900°C in this study and (b) anatase and rutile (El-Sherbiny et al. 2014)

3.2 Arsenic adsorption

The initial As(III) concentration was measured to check for any oxidation that might have happened due to solution mixing. The first step of the adsorption experiments involved comparing the two composites' efficiency in removing As in the presence of 12 W UV light source. Fig. 7 shows As speciation for untreated and treated samples with the two composites. It can be seen that the removal capacity and arsenite oxidation of $(BC/nTiO_2)_P$ was higher than that of $(BC/nTiO_2)_{US}$. The removal achieved with the former was 57.3% while the removal level of the latter was 24.8%. Recent studies compared the removal of As(III) and As(V) on the two phases of $nTiO_2$ (namely anatase and rutile) report that anatase had a higher removal capacity compared to rutile (Gupta et al. 2013, Ma and Tu 2011). However, in our study, the reverse action was observed as the TiO_2 exposed to 900°C (rutile form) was more efficient than that exposed to 300 °C (anatase form). This suggests that TiO_2 behaves differently when interacting with bone char. The composite of rutile with bone char creates a more effective adsorbent than the composite of anatase with bone char. Based on the measured residual arsenate after adsorption, the oxidation with $(BC/nTiO_2)_P$ was about 3.5 times higher than that of $(BC/nTiO_2)_{US}$.

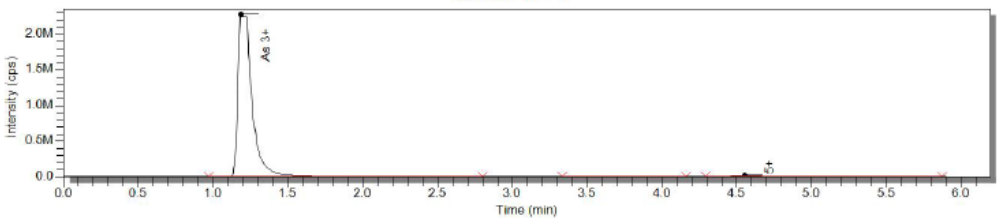

RT (min)	Component Name	Isotope	Area	Height	Internal Standard	Int Std Resp Ratio	Conc	Units
1.185	As 3+	As 75	15,106,266	2,286,023			2.457	ppm
3.442		As 75	6,715	300				
4.059		As 75	2,045	204				
4.555	As 5+	As 75	274,035	19,787			0.022	ppm
5.728		As 75	3,029	257				
Total			15,392,091				2.479	

(a)

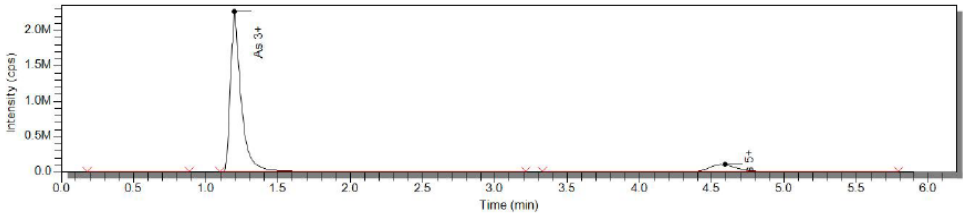

RT (min)	Component Name	Isotope	Area	Height	Internal Standard	Int Std Resp Ratio	Conc	Units
0.305		As 75	4,155	216				
0.850		As 75	1,363	241				
1.198	As 3+	As 75	11,645,912	2,227,567			1.743	ppm
2.931		As 75	11,979	357				
3.414		As 75	6,585	256				
4.594	As 5+	As 75	1,408,336	103,798			0.122	ppm
Total			13,078,330				1.865	

(b)

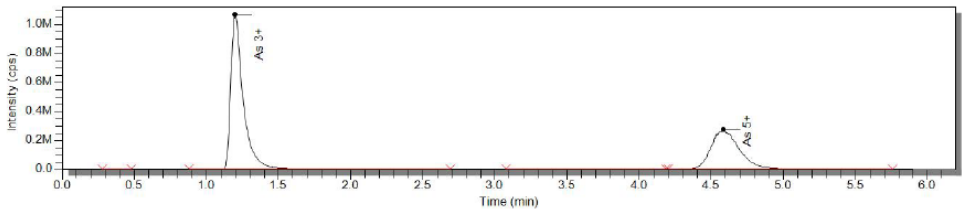

RT (min)	Component Name	Isotope	Area	Height	Internal Standard	Int Std Resp Ratio	Conc	Units
0.333		As 75	2,867	350				
1.199	As 3+	As 75	6,320,417	1,056,795			0.645	ppm
3.286		As 75	12,373	318				
4.583	As 5+	As 75	3,706,422	276,743			0.414	ppm
Total			10,042,079				1.058	

(c)

Fig. 7. Arsenic speciation for (a) untreated sample, (b) treated sample with UV and $(BC/nTiO_2)_{US}$ (c) treated sample with UV and $(BC/nTiO_2)_P$

Considering the abovementioned results, $(BC/nTiO_2)_P$ was used to further investigate the effect of UV power level on As removal capacity. These tests were compared with treatments of BC900 alone and $(BC/nTiO_2)_P$ with visible light to evaluate UV effect on As removal (Fig. 8). Increasing UV power from 4 to 8 and then to 12 W increased the As removal capacity of the solution from 116.8 to 123.13 to 281.36 µg/g, respectively. Surprisingly, the removal capacity of the $(BC/nTiO_2)_P$ with visible light was slightly higher than those of 4 and 8 W of UV light. This indicates that the minimum UV light required to enhance the removal capacity was 12 W per 100 mL for water with As concentration of 2.5 mg/L. BC900 had better removal capacity than

$(BC/nTiO_2)_P$ with low UV power and visible light. This could be ascribed to the loss of surface area and pore volume due to TiO_2 deposition. In order to make up for the loss of these traits, high UV power needs to be applied to obtain better removal outcome. It should be noted that even with the chemical modification of bone char and UV application, the maximum removal capacity (281.4 µg As/g of $(BC/nTiO_2)_P$) could not bring down the concentration of As to the acceptable limit for human consumption (i.e. 10 µg/L based on WHO recommendation). Bone char alone (BC900) achieved As removal capacity of 195.8 µg/g. Although the increase in the removal capacity with $nTiO_2$ modification and UV application is little considering the cost associated with these additions, thorough investigation for the removal mechanisms and kinetics of $(BC/nTiO_2)_P$ + UV is required to draw a firm conclusion regarding the feasibility of this process for As removal. In comparison to commercially available adsorbents such as GHE and Bayoxide and their high As removal capacity (Driehaus 2002, Katsoyiannis et al. 2015), bone char might score low. However, bone char has the advantage of being sourced from waste and as by-product of energy producing processes (i.e. gasification (Alkurdi et al. 2019b)) as well as its ability to be regenerated and reused. These traits make it worth investigation for future potential use for As removal under different environmental conditions.

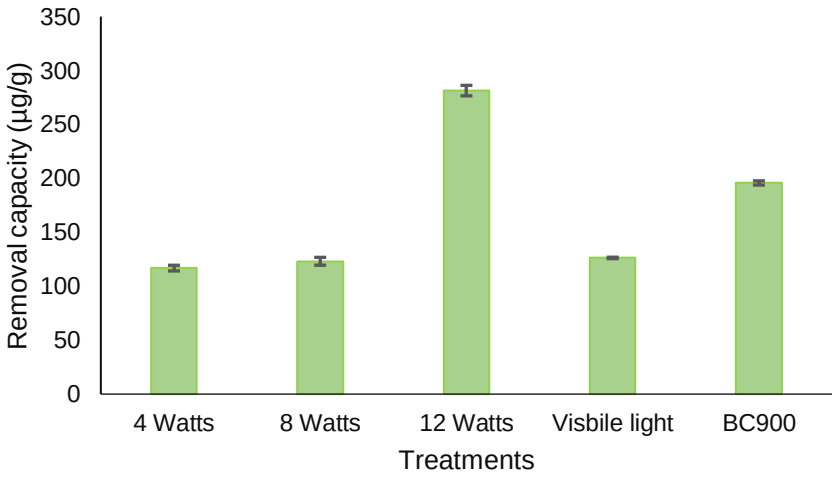

Fig. 8. As removal capacity with different treatment scenarios. Experimental conditions: pH = 8, As(III) initial concentration = 2.5 mg/L, adsorbent dose = 5 g/L

The changes in bone char and $(BC/nTiO_2)_P$ structure after As loading and exposure to UV radiation was studied using FTIR analysis and the results are presented in Fig. 8. The most prominent peak in Fig. 9 a is the peak at 1381 cm^{-1}. This peak is assigned to the presence of nitro compounds (Janakiraman and Johnson 2015). The formation of this peak is accompanied by the reduction of the peak at 2013 cm^{-1}, which is assigned to the cyanate compounds that were formed due to the decomposition of the protein in the bone structure at high pyrolysis temperature (Alkurdi et al. 2020). The peak at 1639 cm^{-1} could be associated with the formation of Ti-OH bond. This peak is the result of hydrolysis of the surface oxides of TiO_2 in water (Foratirad et al. 2017, Sheng et al. 2015). The peak at 1647 cm^{-1} was found to be linked to sodium arsenate (Li et al. 2011) and this suggests that an interaction between arsenate and the sodium in the bone char structure might have occurred. The increase intensity of the broad OH peak at 3425 cm^{-1} is due to the high potency of TiO_2 to attract OH. The reduction in the intensity of the peak related to the presence of PO_4^{3-} at 1033 cm^{-1} suggests the possibility of ion contribution to the removal process. The change in the peaks intensity and width in the region 400-1000 cm^{-1} is believed to be due to As interaction with oxygen containing moieties on the char surface (Cowen et al. 2008, Min et al. 2017).

Fig. 9b shows the differences in the adsorbents composition after they were loaded with As species in different treatment scenarios. It appears that UV improves the decomposition of cyanate and promotes the formation of nitro compounds represented by the diminishing peak at 2013 cm^{-1} and the rise of the peak at 1380 cm^{-1}. The other obvious effect of UV is the change in the spectra for wavenumber less than 1000 cm^{-1} and this could be due to the formation of hydroxyl radicals in the photocatalytic decomposition of water molecules and the reaction of the latter with As forming As-O compounds on the char.

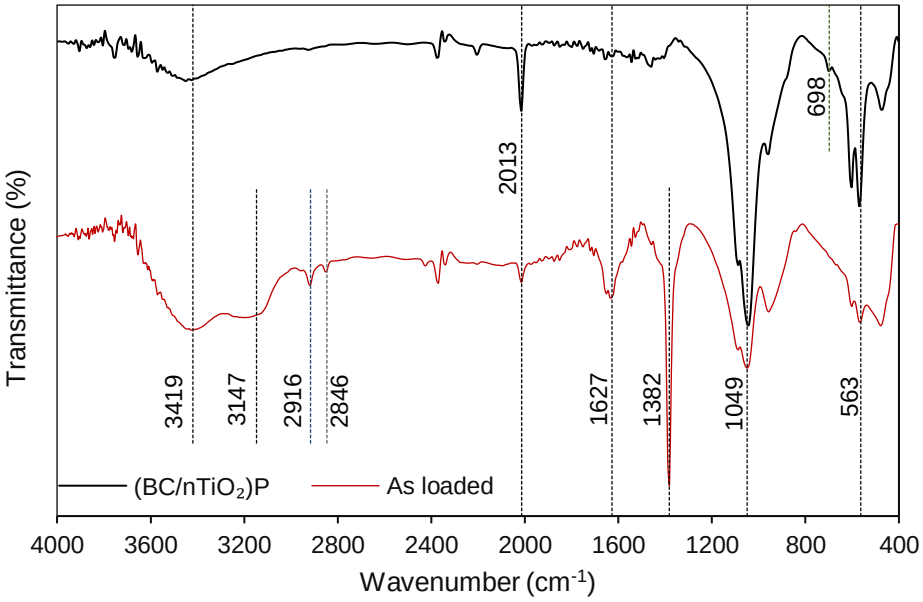

(a)

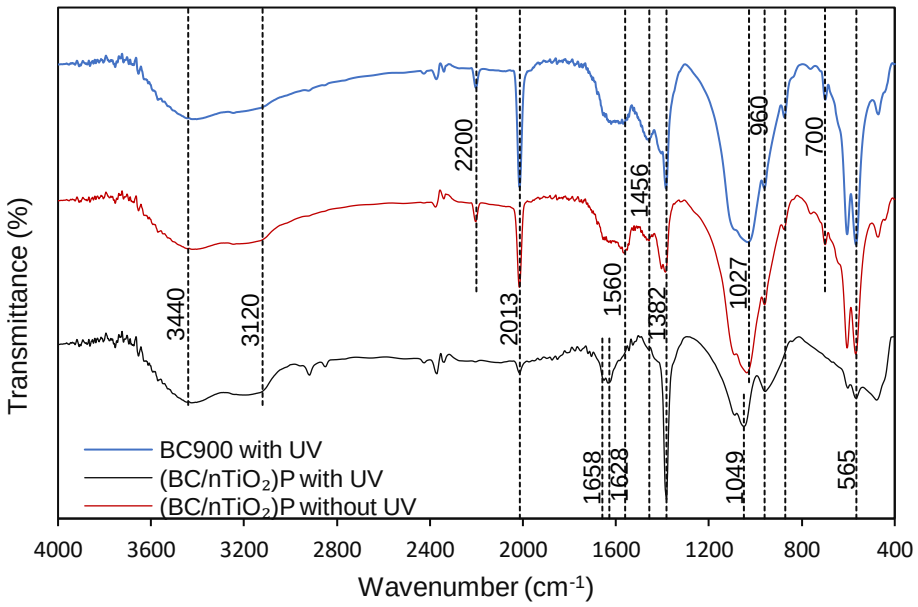

(b)

Fig. 9. FTIR analysis for (a) As loading effect on $(BC/TiO_2)_P$ structure and (b) UV and $nTiO_2$ effect on BC900 structure

4. Conclusions

$BC/nTiO_2$ composite was prepared following two different procedures: during and after pyrolysis. The two composites were compared for their effectiveness in removing inorganic As from the aqueous solution. The composite $(BC/nTiO_2)_P$ proved to be more effective in arsenite removal (57.3 % vs 24.8%) and photocatalytic oxidation (3.5 times higher arsenate produced). Arsenic removal using $(BC/nTiO_2)_P$ and UV power of 4, 8 and 12 W was tested and compared to the treatment with visible light and BC900. It was found that power levels of 4 and 8 W had a lower As removal capacity than that of $(BC/nTiO_2)_P$ with visible light and BC900. It was concluded that the loss of bone char surface area and pore volume due to $nTiO_2$ deposition can only be compensated by applying high UV power. This study showed that depositing $nTiO_2$ onto bone char and applying UV radiation was successful in achieving simultaneous oxidation and removal of arsenite. Further studies for identifying As removal mechanisms and kinetics and isotherms with $(BC/nTiO_2)_P$ and UV are recommended for future research work.

Acknowledgments: This research was performed as a part of PhD research which was supported in part by the Iraqi Government and the Australian Research Training Program. The authors are thankful to Mr Prasanna Kumarathilaka for his contribution and support in As speciation using UHPLC.

Conflicts of Interest: The authors declare no conflict of interest. The funders had no role in the design of the study; in the collection, analyses, or interpretation of data; in the writing of the manuscript, or in the decision to publish the results.

5.3 Concluding remarks

This paper investigated the performance of a newly prepared composite material from bone char and nanoparticles of TiO_2 for the oxidation and removal of As(III) and As(V) from water. The characteristic of the composite investigated by a range of experimental and analytical means. The surface area of the composite was reduced compared to the bone char sample prepared under the same conditions (BC900). The FTIR analysis showed the formation of new peaks due to the coating process. SEM-EDS results confirmed the deposition of $nTiO_2$ on the bone char samples. The As removal and oxidation capability of the prepared BC/$nTiO_2$ composite material and the unmodified bone char were examined and compared via batch experiments using three different levels of UV light. The higher oxidation of As(III) were examined using 12 W of UV light levels. The composite is a promising way to combine the oxidation of As(III) and adsorbing As(V) without pretreatment.

CHAPTER 6

Simultaneous immobilization of co-occurring fluoride and arsenic from water using bone char packed columns and the application of CDI for enhancing As removal

Paper VI

Alkurdi, S.S., Al-Juboori, R.A., Bundschuh, J., Bowtell, L. Hamawand, I. and Kumarathilaka, P. (2020). Simultaneous immobilization of co-occurring fluoride and arsenic from water using bone char packed columns and the application of CDI for enhancing As removal. (Prepared for submission to the Journal of Hazardous Materials).

6.1 Introduction

Adsorption experiments with bone char packed fixed-bed columns for the individual and concurrent removal of As(III), As(V) and F^- were carried out in this study. It demonstrated that breakthrough occurred more slowly with an increasing influent concentration and a decreasing flow rate. The concentrations of contaminant were selected based on the average concentrations reported in the literature. The removal behaviour was explained using Yoon-Nelson, Thomas, and Bohart and Adams models. The effect of the coexisting anions was examined using natural well water. Experiments on competitive adsorption illustrated that the removal of As(III) and As(V) decreased when additional metal ions were present in the solution. The simultaneous removal of As(III), As(V) and F^- were examined. The effect of F^- existence was more significant for As removal than the other anions. A capacitive deionization (CDI) assisted bone char (BC) column was used to assess the relative improvement in the removal capacity of As on the bone char.

Simultaneous immobilization of co-occurring fluoride and arsenic from water using bone char packed columns and the application of CDI for enhancing As removal

Susan S.A. Alkurdi[a,b], Raed A. Al-Juboori[a,c], Jochen Bundschuh[a,d]*, Les Bowtell[e], Ihsan Hamawand[a] and Prasanna Kumarathilaka[a]

[a] *School of Civil Engineering and Surveying, Faculty of Health, Engineering and Sciences, University of Southern Queensland, West Street, Toowoomba, 4350, Queensland, Australia.*

[b] *Northern Technical University, Engineering Technical College/Kirkuk, Iraq.*

[c] *Water Engineering Research Group, Department of Civil and Environmental Engineering, Aalto University, P.O. Box 15200, Aalto, FI-00076, Espoo, Finland.*

[d] *UNESCO Chair on Groundwater Arsenic within the 2030 Agenda for Sustainable Development, University of Southern Queensland, West Street, Toowoomba, 4350, Queensland, Australia.*

[e] *School of Mechanical and Electrical Engineering, Faculty of Health, Engineering and Sciences, University of Southern Queensland, Toowoomba, 4350, QLD, Australia.*

Corresponding author*: Jochen Bundschuh
Faculty of Health, Engineering and Sciences & UNESCO Chair on Groundwater Arsenic within the 2030 Agenda for Sustainable Development, University of Southern Queensland, West Street, Toowoomba, 4350, Queensland, Australia.
Phone: +61 7 4631 2694
Email: Jochen.Bundschuh@usq.edu.au

Abstract

This study examines the removal of dissolved arsenic and fluorine species from groundwater based on column experiments. Three different flow rates (2.5, 5 and 10 mL/min) were used to study the adsorption of 1 and 1.5 mg/L As(III) and As(V) from water. The columns used in this study were 13.3 cm in height with a diameter of 3.85 cm. The solution feed was passed through a cross section area of 11.642 cm^2. The removal of fluoride ions (F^-) was examined at the same flow rates as As(III) and As(V), but at different concentrations of 10 and 20 mg/L. The removal As from synthetic solutions was compared to its removal when natural well water was spiked with 1 mg/L. The presence of other anions in the well water inhibited the removal of As. The simultaneous removal of aqueous As and F species showed that the most inhibitory effect in the lowering of As removal was due to the presence of 10 mg/L F^-. Applying capacitive deionization (CDI) technology improved the removal of As from water. The performance of adsorption was interpreted by applying the Yoon-Nelson, Thomas, and the Bohart and Adams models. The findings of this study confirm the ability of bone char to remove aqueous As and F species concurrently after applying modifications to overcome competition between these two contaminants to occupy the active sites on the surface.

Keywords

Arsenic, fluoride, column experiments, capacitive deionization (CDI)

1. Introduction

Groundwater is the primary source of potable water around the world. The deteriorating quality of surface water as a result of population growth and industrial developments affects the quality of groundwater through drainage, leaching and runoff (Cerejeira et al. 2003). These factors add to the natural geogenic contaminant sources and (bio)geochemical processes which mobilize them into the groundwater, contributing to a significant increase in the concentration of heavy metals/metalloids in groundwater.

The source of dissolved arsenic and fluorine species in groundwater is mainly geogenic due to a series of reactions between the water and rocks of aquifers. The co-occurrence of these two contaminants was reported in many areas such as Latin America (Alarcón-Herrera et al. 2020, Reyes-Gómez et al. 2013), Pakistan (Rasool et al. 2015) and India (Kumar et al. 2016). The health consequences associated with the consumption of these co-occurring contaminants is the reason behind research efforts to investigate a cost-effective material for the simultaneous removal of these contaminants. Recently, numerous studies have been performed to remove As or F^- from water using naturally available minerals, agricultural or waste based materials (Kikuchi et al. 2019, Kumar et al. 2019, Niazi et al. 2018, Soni and Shukla 2019). However, very limited studies have the simultaneous removal of these two contaminants.

For decades, bone char has been known for its excellent ability to remove F^- from water on a small to large scale (Chatterjee et al. 2018, Nigri et al. 2019). However, there are limited studies exploring As removal with bone char. Furthermore, the studies dealing with As adsorption onto bone char are limited to the lab scale. There are benefits from the high ability of this adsorbent to remove F^- therefore, it is crucial to modify it in a way that provides a high removal capacity for both contaminants. The best pyrolysis temperature for bone char to optimise its ability to remove dissolved As and F species was reported to be 900 °C and 650 °C, respectively (Alkurdi et al. 2020). Thus, modifications are crucial to increase the ability of bone char to remove As from water in the presence of F^-.

Capitative deionization (CDI) is a technology used for water deionization by supplying electrical current. CDI uses two porous carbon rods as electrodes providing two different charges on each side. The electrically charged carbon rods attract the dissolved ions in solution following the electric double layer theory (Welgemoed and Schutte 2005). The main application of this process for water treatment is the desalination of brackish water. Applying this technology to a fixed bed column may enhance the removal capacity of the cations and anions due to electrostatic attraction.

This study aims to examine the removal of As and F species from water separately and in combination using fixed-bed columns. It also examines the validity of connecting CDI to the column to improve the ability of the packed bone char to remove As.

Furthermore, the study explores the simultaneous removal of these two contaminants from natural water.

2. Materials and methods

2.1 Reagents and equipment

Fixed bed adsorption experiments for the removal of dissolved As and F species were conducted using bone char samples pyrolysed at 900 °C (BC900) and 650 °C (BC650) without and with purging N_2 gas, respectively. The selection of the pyrolysis temperature was based on the results reported in our previous study (Alkurdi et al. 2020). All chemicals used were of analytical grades. As(III) and As(V) were purchased from Choice Analytical, New South Wales, Australia with a concentration of 1000 mg/L. A F^- stock solution of 1000 mg/L was prepared by dissolving NaF (AR grade, Chem-Supply) in distilled water. The pH of the solutions was controlled using nitric acid (70%, RCI Labscan) and sodium hydroxide (Labscan Asia Co. Ltd).

The columns used in this study were plastic columns 13.30 cm in height and with an internal diameter of 3.85 cm. The columns were packed with 90 g of bone char with two layers of sand at the top and bottom to provide a uniform flow of the solution onto the bone char layer. The height of the bone char bed was 8.8 cm, occupying 100 mL of the column volume. The sand was separated from the bone char using fibreglass filters.

Before packing, all columns were washed with distilled water; the sand filter was washed with 0.1 M HCl (32%, AR grade, RCI Labscan) and bone char samples (of 1-2 mm size) were washed with distilled water until a stable pH was achieved. The EC was below 50 µS/cm (using EUTECH instruments, model PC2700). All media were dried at 60 °C overnight and then packed into the columns. The cover of the columns was attached using commercial silicon.

All adsorption experiments were operated at up-flow mode using silicone tubes with a cross sectional area of 11.642 cm^2 attached to Masterflex (Cole Parmer) peristaltic pumps (model 7528-10) for the flow rate of 10 mL/min and an ISMATEC ecoline pump (model ISM1067A, Germany) for the lower flow rates. The flow rate of the

peristaltic pumps was calibrated before each experiment. Samples were analyzed for the residual As and F concentrations using Ion Chromatography coupled with Mass Spectroscopy (PerkinElmer NEXION 300 ICP/MS) and Thermo Scientific Dionex ICS-2000 Ion Chromatography, respectively.

2.2 Adsorption experiments

For a continuous wastewater treatment system, flow rate is one of the main factors that control the removal of the contaminants to reduce their concentrations below permissible limits. The breakthrough curve, which indicates the adsorption progress through a column, can be examined by plotting the concentration profile at different times. Thus, samples were collected at different times and plotted versus the concentration. Fig. 1 shows the experimental setup, used in this study. To evaluate the potential use of bone char under natural pH conditions and the inapplicability of pH adjustment for practical uses, experimental trials were performed at pH 6.5±0.1 at room temperature. The feed flow rates of 2.5, 5 and 10 mL/min for each of the two concentrations were examined for As(III), As(V) and F^-.

Arsenic feed concentrations were selected based on the results reported in previous studies that examine the average range of As concentrations reported in groundwater. Two different concentrations of 1 and 1.5 mg/L were examined for As(III) and As(V) at the previously mentioned flow rates using BC900 packed columns. Then, a flow rate of 90 mL/min with an initial input solution of 1 mg/L was used to compare the removal of total As to a commercial column. Furthermore, natural water was spiked with the same concentration of As. The natural water was collected from an inland desalination facility located in Dalby, Queensland, Australia to explore the effect of the presence of some other anions on filter efficiency.

Similarly, F^- removal using bone char BC650 columns was examined at the previously mentioned flow rates, but at an initial concentration of 10 and 20 mg/L. These concentrations were selected based on the average F^- concentrations reported in the literature which is 0-50 mg/L (Figoli et al. 2016) and 0.01-48 mg/L (Mumtaz et al. 2015). Afterwards, the simultaneous removal of aqueous As and F species was examined using both BC650 and BC900. As a final stage of these experiments, the

removal capacity was explored in the presence of CDI. All the results reported in this study were the average of three repeats.

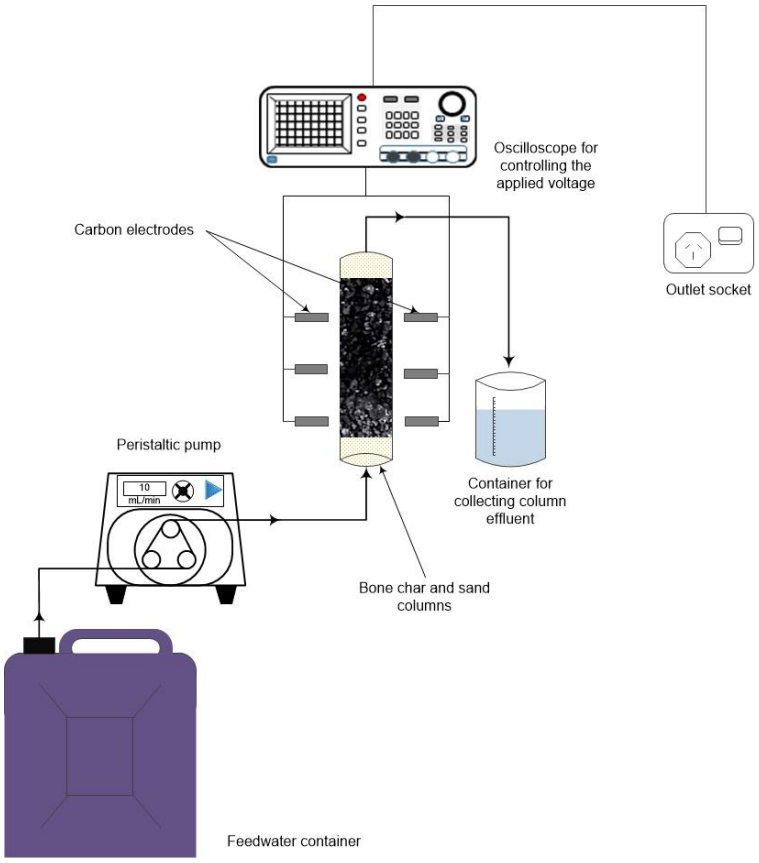

Fig. 1. Schematic representation of the experimental setup

The breakthrough curve, which indicates the adsorption progress through a column, can be examined by plotting the concentration profile at different times.

For the CDI experiments, the carbon electrodes were powered by a 6 V battery (Eveready heavy duty). The electrodes were cleaned thoroughly with ethanol to remove any chemicals from the surface. Then they were washed with distilled water, placed on the two sides of the column and connected to a power source. Three electrodes were placed on each side of the column, as presented in Fig. 1. The current and voltage were adjusted to 0.2 A and 1.2 V to each electrode.

2.3 Breakthrough analysis

In a fixed-bed column, adsorption processes occur first at the inlet of the column where saturation initially takes place. As a result of the decrease in the number of active sites adsorb contaminants, the saturation zone moved gradually towards the outlet of the column over time. Thus, the plot of the outlet concentration versus the elapsed time shows the breakthrough curve of the column. The bed capacity of a column at breakthrough time can be calculated based on the following formula:

$$q_b = \int_{t=0}^{t=t_b} \left(\frac{C_0 - C_t}{m}\right) Q\, dt \qquad (1)$$

where q_b is the bed capacity in mg/g, m is the mass of adsorbent packed in the column in g, C_0 and C_t are the inlet and the outlet concentration in mg/L, Q is the flow rate in mL/min, and t is the time.

The number of bed volumes (V_b) that are processed before reaching the point of breakthrough indicates the adsorption performance. This parameter is the ratio between the volume of the adsorbate treated at a breakthrough point in L and the volume of the adsorbent bed occupied in the column in L (Onyango et al. 2009). The adsorbent exhaustion rate (ARE) will provide information on the mas exhausted per unit volume of the treated water:

$$ARE = \frac{mass\ of\ adsorbent\ (g)}{Volume\ of\ the\ treated\ water\ at\ breakthrough\ (L)}$$

2.4 Modelling breakthrough

The maximum adsorption capacity of an adsorbent is a critical factor in designing the process. Mathematical models of adsorption processes in a fixed bed column assume the presence of axial dispersion, external mass transfer, nonlinear isotherm and intraparticle diffusion (Patel 2019). Breakthrough behaviour for the column experiments was modelled using three different mathematical models: Thomas, Yoon-Nelson, and Bohart Adams models.

The Thomas model is based on Langmuir kinetics that assumes a second-order reversible reaction with no axial dispersion (Patel 2019). The Thomas model was used to analyze the experimental data, and the model parameters were evaluated based on Formula (3) (Bhaumik et al. 2013):

$$\ln\left(\frac{C_o - C_t}{C_t}\right) = \frac{K_{TH} q_o m}{v} - K_{TH} C_o t \qquad (3)$$

where C_o is the feed concentration, C_t is the outlet concentration at any time t, K_{TH} is Thomas rate constant in mL/min mg, q_o is the adsorption capacity in mg/g, ν is the flow rate in mL/min and m is the mass of the adsorbent packed in the column in g.

Yoon-Nelson's model is a simple mathematical formula (Equation 4) that correlates the experimental data regardless of the adsorbate and adsorbent characteristics and the bed properties of the column:

$$\ln\left(\frac{C_t}{C_o - C_t}\right) = k_{YN} t - \tau k_{YN} \qquad (4)$$

where K_{YN} is the rate constant of the Yoon-Nelson model (min^{-1}), and τ is the time required to reach 50% adsorbate breakthrough (min), (Ahmad and Hameed 2010).

The Bohart and Adams model is another mathematical model used to examine the fit of the data based on the experimental column parameters and the adsorbate concentration. This model assumes that the adsorption rate is a function of the adsorbate concentration and the residual capacity of the adsorbent (Patel 2019). The formula presented by Bohart and Adams is:

$$\ln\left(\frac{C_o - C_t}{C_t}\right) = K_{BA} N_o \frac{z}{u} - K_{BA} C_o t \qquad (5)$$

where K_{BA} is the rate constant of Bohart and Adam's model (L/mg min), N_o is the saturation concentration in mg/L, z is the adsorbent bed depth in cm, and *u* is the ratio of the volumetric flow rate in cm^3/min to the cross-sectional area of the column in cm^3.

3. Results and discussion

3.1 Bone char characteristics

The bone char samples used in this study were previously described for their adsorption capacity of As(III), As(V) and F^- in our previous studies (Alkurdi et al. 2020) where full details of the characteristics of these two samples due to altering pyrolysis conditions were reported.

3.2 As removal

Fig. 2 and 3 show the experimental and modelled As(III) and As(V) breakthrough curves using BC900 in packed columns at tested operating conditions. All the curves showed a typical asymmetric S-curved profile. Generally, the feed concentration affects the mass transfer and the adsorption rate. At the same time, contact time between adsorbent and adsorbate and the hydrodynamics of the column are related to the feed flow rate. As can be seen from the figures, the effect of changing the flow rate and the initial concentration impacted on the breakthrough curve for As(III). Increasing the flow rate resulted in a reduction in the time that the column took to reach saturation. Raising the feed rate and concentration resulted in decreasing the breakthrough time. This effect is due to the reduction in the contact time between the adsorbate and the adsorbent. Furthermore, providing a higher concentration of the adsorbate feed resulted in a higher occupation of the active sites as time proceeded, and thus a lower breakthrough time.

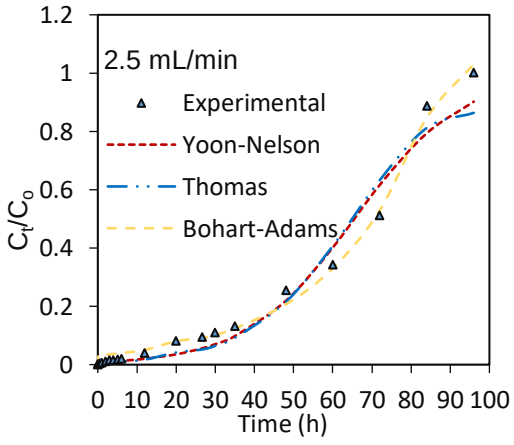

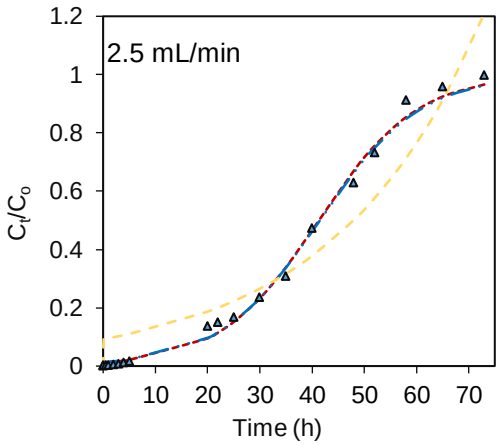

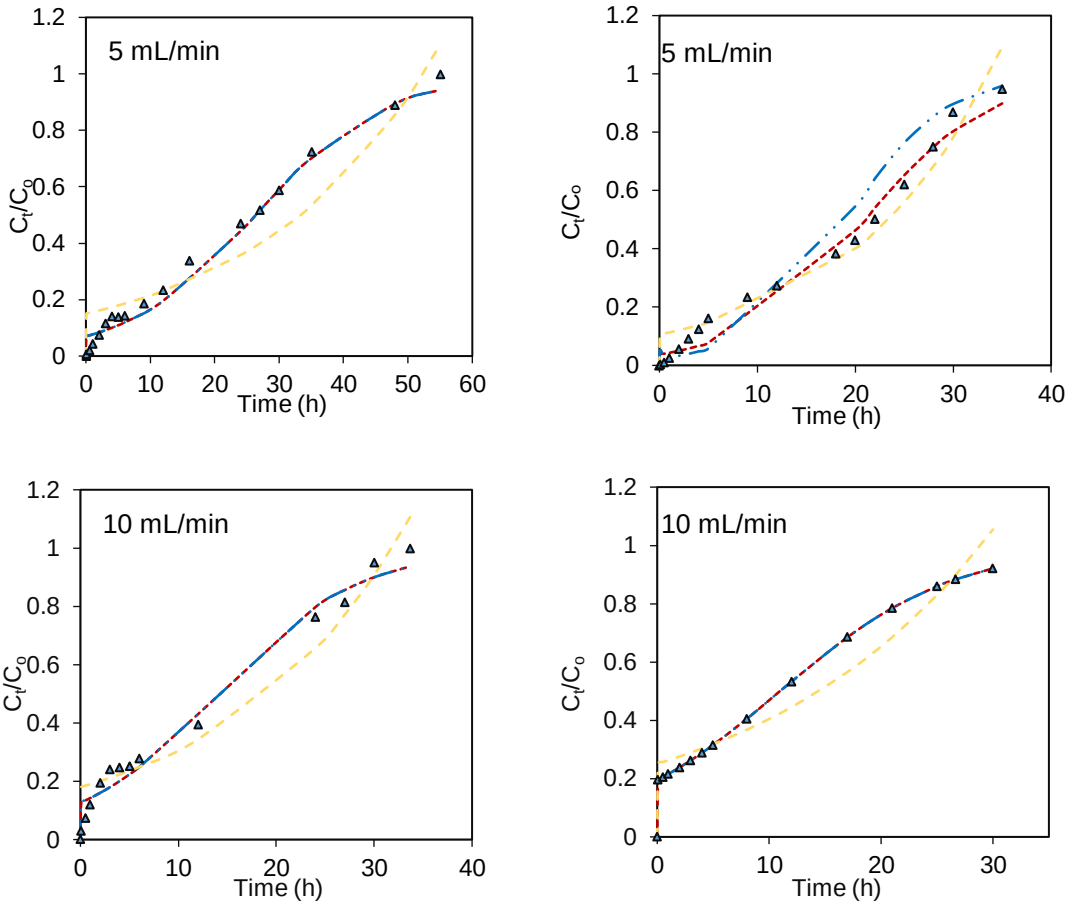

(a) Inlet concentration of 1 mg/L (b) Inlet concentration of 1.5 mg/L

Fig. 2. As(III) experiments and models plot at (a) 1 mg/L and (b) 1.5 mg/L at three different flow rates

Comparing the breakthrough curve of As(III) to those of As(V) which were run under the same experimental conditions, the ability of the column to remove As(V) was higher as it can be seen that the increase in the outlet concentration occured after a longer period of time. This behaviour was also noticed in the batch experiments where the removal of As(V) was almost double that of As(III) at low concentrations (<20 mg/L). This may be explained by the electrostatic attraction of the negatively charged As(V) to the positively charged bone char surface at pH levels lower than the $pH_{PZC,}$ which was counted as one of the mechanisms that contributed to the removal process on bone char. At an initial concentration of 1.5 mg/L and 10 mL/min flow rate, the column was unable to reduce the As(III) concentration below the allowable limits from the first sample collection at 5 min. For both of the examined concentrations, the feed rate of 2.5 mL/min was able to reduce the concentration of both As species effectively

at the beginning of the experiment, with better results provided by As(V) removal. However, running the column at a flow rate of 10 mL/min, at 1.5 mg/L significantly affected the removal of As(III) and showed a very low capacity for the first 5 min of sample collection.

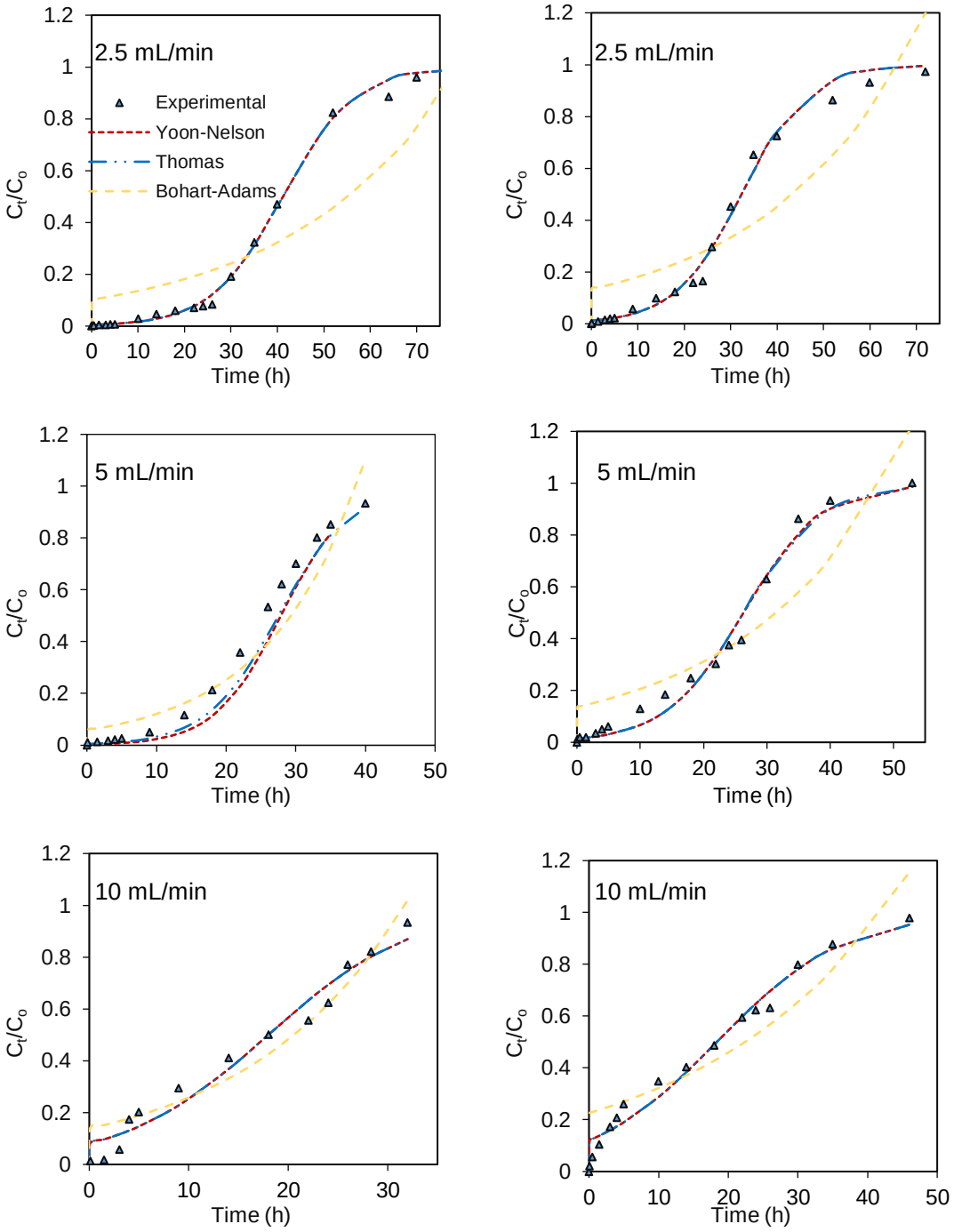

(a) Inlet concentration of 1 mg/L (b) Inlet concentration of 1.5 mg/L

Fig. 3. As(V) experimental and models plot at (a) 1 mg/L and (b) 1.5 mg/L at three different flow rates

The adsorption models of Yoon-Nelson, Thomas, and Bohart and Adams for As(III) and As(V) are presented in Fig. 2 and 3. The parameters were determined based on the linear and nonlinear regression fittings using the Solver add-in with Microsoft Excel by minimizing the sum of the squared error between the experimental and the predicted data. Data of both regressions, along with their parameters, are presented in Tables 1 and 2 for As(III) and As(V) fittings.

For both of the As species, Bohart and Adams's model failed to fit the experimental data at all feed rates and concentrations. Based on the values reported in Table 1 and 2, the data of As(III) and As(V) best fitted both the Yoon-Nelson and Thomas models. However, the results of the calculated sum of error functions showed that the Yoon-Nelson model provided a slightly better fit for As(III) and Thomas' model was better for presenting the data of As(V). For the Yoon-Nelson model, an increase in both the flow rate and initial concentrations led to an increase of K_{YN} and τ which indicates that the column saturation was reached more quickly at a higher initial concentration and flow rate. Examining the parameters of the Thomas model showed that the value of K_{TH} decreased due to the increase of the initial concentrations of As(III). This is due to the difference in As(III) concentration in solution and on the bone char. The increase in the flow rate resulted in a decrease in the q values due to the decrease in the availability of the reaction sites. However, the opposite was observed for the experimental data of As(V). The value of q increased, indicating an increase in the removal capacity with the increase in the initial concentration. Thus, the better fit provided by the Thomas model suggests an adsorption-desorption process with a negligible axial dispersion.

Passman et al. (2014) examined the removal of 500 µg/L total As in a column experiment using a layer of commercial bone char attached to a clay filter. The filter was able to reduce the concentration of As in the solution to below the WHO guidelines value. However, the study did not show the impact of the bone char layer on removal performance. Liu et al. (2014) examined the removal of As(V) on bone char in a continuous flow experiment. The study applied the Convection Dispersion Equation to quantify the adsorption process at different flow rates and column dimensions. The model fitted the experimental data indicating that As(V) removal followed ligand exchange and electrostatic interaction. Hu et al. (2015) used biochar modified with Fe

in a fixed bed column to remove As(V) from water. The study showed that using a small column packed with 9.4 g of modified biochar, resulted in a high removal capacity of As(V) whereas the column was exhausted in about 70 min. Thus, bone char modification is essential to increase its ability to remove As species. To the knowledge of the authors, there are no studies investigating the application of bone char for As(III) removal from water.

Table 1. Parameters of column models for As(III) experimental data fittings

Yoon-Nelson model

Parameters		Linear			Nonlinear		
C_o (mg/L)	Flow rate (mL/min)	K_{YN}	τ	R^2	K_{YN}	τ	R^2
1.0	2.5	0.001	3783.0	0.965	0.001	3929.848	0.978
	5.0	0.002	1655.833	0.982	0.002	1581.580	0.984
	10.0	0.003	742.1875	0.965	0.002	843.1083	0.9779
1.5	2.5	0.002	2344.750	0.982	0.002	2478.561	0.995
	5.0	0.003	1145.0	0.960	0.003	1257.320	0.984
	10.0	0.002	744.0	0.905	0.002	659.134	0.995

Thomas Model

Parameters		Linear			Nonlinear		
C_o (mg/L)	Flow rate (mL/min)	K_{TH}	q	R^2	K_{TH}	q	R^2
1.0	2.5	1.318	103.612	0.965	1.295	116.672	0.970
	5.0	2.231	79.834	0.975	2.211	101.848	0.978
	10.0	3.245	81.311	0.962	2.327	92.367	0.977
1.5	2.5	1.499	104.275	0.980	1.082	117.707	0.995
	5.0	2.061	101.840	0.960	1.541	110.692	0.978
	10.0	1.374	132.407	0.905	1.345	104.251	0.915

Bohart Adams model

Parameters		Linear			Nonlinear		
C_o (mg/L)	Flow rate (mL/min)	K_{BA}	N_o	R^2	K_{BA}	N_o	R^2
1.0	2.5	0.001	113.799	0.959	0.001	127.385	0.994
	5.0	0.001	125.273	0.771	0.001	151.037	0.904
	10.0	0.001	169.578	0.945	0.001	183.644	0.951
1.5	2.5	0.001	132.884	0.627	0.0003	158.473	0.928

	5.0	0.001	139.640	0.831	0.001	157.942	0.969
	10.0	0.001	240.587	0.841	0.0004	270.916	0.878

Table 2. Parameters of column models for As(V) experimental data fittings

Yoon-Nelson Model

Parameters		Linear			Nonlinear		
C_o (mg/L)	Flow rate (mL/min)	K_{YN}	τ	R^2	K_{YN}	τ	R^2
1.0	2.5	0.002	2638.800	0.991	0.002	2467.745	0.997
	5.0	0.003	1507.538	0.975	0.003	1578.317	0.976
	10.0	0.002	1100.364	0.968	0.002	1101.033	0.976
1.5	2.5	0.002	2122.905	0.977	0.002	1942.160	0.991
	5.0	0.003	1514.733	0.966	0.003	1671.021	0.979
	10.0	0.003	1101.414	0.955	0.003	1079.727	0.966

Thomas model

Parameters		Linear			Nonlinear		
C_o (mg/L)	Flow rate (mL/min)	K_{TH}	q	R^2	K_{TH}	q	R^2
1.0	2.5	1.692	86.627	0.997	1.667	89.113	0.997
	5.0	2.000	108.878	0.975	2.072	113.990	0.982
	10.0	2.692	158.941	0.968	2.391	159.038	0.979
1.5	2.5	1.3125	94.351	0.978	1.436	86.318	0.996
	5.0	1.875	134.643	0.965	2.017	146.626	0.987
	10.0	2.813	195.870	0.956	2.411	191.951	0.966

Bohart Adams model

Parameters		Linear			Nonlinear		
C_o (mg/L)	Flow rate (mL/min)	K_{BA}	N_o	R^2	K_{BA}	N_o	R^2
1.0	2.5	0.001	124.435	0.782	0.0003	150.679	0.823
	5.0	0.001	155.548	0.598	0.0005	183.326	0.836
	10.0	0.001	257.219	0.859	0.0001	319.409	0.864
1.5	2.5	0.001	120.724	0.513	0.0003	154.699	0.816
	5.0	0.001	167.454	0.886	0.0007	181.260	0.965
	10.0	0.001	260.870	0.858	0.0006	296.967	0.943

The parameters of the adsorbent are presented in Table 3. The results show that bone char performed better for As(III) removal at 1 mg/L, but As(V) had a higher removal for the higher feed concentration.

Table 3. The parameters calculated for the breakthrough curve at saturation

	Conc. (mg/L)	q_b	V_b
As(III)	1	0.143	1.43
	1.5	0.110	1.10
As(V)	1	0.110	1.10
	1.5	0.139	1.39

3.3.1 Total As removal at different experimental conditions

For an efficient removal of As species from water, the same columns were used to remove total As at 90 mL/min from a synthetic solution. This flow rate was chosen by comparing the dimension of the column to the commercial filter size and calculating the equivalent flow rate. Bone char was found unsuitable for use at this speed as the removal started with an efficiency of 41.075% for 1 mg/L total As (Fig. 4).

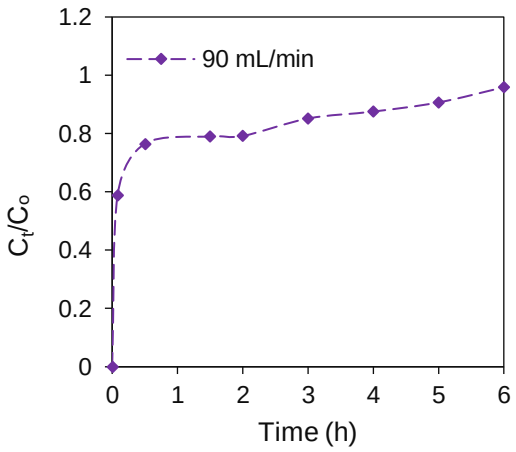

Fig. 4. The removal 1 mg/L total As at 90 mL/min

To simulate the removal of As in natural water, an additional experiment was carried out by spiking natural well water with 1 mg/L total As. The same fixed-bed adsorption methodology as that described above was applied for examining the effect of co-

existing anions on the removal capacity at 10 mL/min. The characteristics of the natural water used are presented in Table 4, and it confirmed with the reported values by Rioyo et al. (2018). As presented in Fig. 5, the saturation of the column was reached after 25 h. During the first five hours, the removal was rapid, and then decreased gradually. The presence of competing ions impeded the removal of As as it showed a shorter period to reach saturation (compared to As(III) and As(V)). Comparing the effect of the contact time and the existence of competing anions showed that the feed rate had the most significant effect on the removal capacity of the bed (Fig. 5). The effect of coexisting anions on As(V) removal from the water was reported to follow the order of SiO_3^{2-}> PO_4^{3-}> NO_3^-> SO_4^{2-} (Alkurdi et al. 2019a). Table 4 shows that there is a high concentration of SiO_3^{2-} which may be the main reason to reduce the removal capacity of As from water. The percentage reduction in As(V) removal due to the existence of 10 mg/L SiO_3^{2-} was reported to be 16% and 14% using synthesized hydroxyapatite and Fe impregnated rice husk biochar, respectively (Cope et al. 2014, Islam et al. 2011). The contribution of PO_4^{3-}, NO_3^- and SO_4^{2-} in reducing the removal efficiency of As(V) may be ignored as they are lower than the limits reported (in the literature) to affect the As removal. On the other hand, PO_4^{3-} and Cl^- had a bigger influence on As(III) removal as stated by Baig et al. (2014). The negative charge of these two anions increases their affinity to the surface of the adsorbent via electrostatic attraction and thus they occupy the active sites on the surface of the adsorbent, thus reducing As(III) uptake.

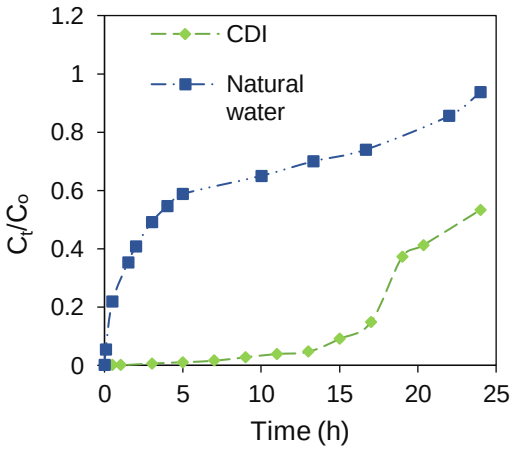

Fig. 5. Total As removal at 1 mg/L and 10 mL/min using (a) natural well water and (b) applying CDI using distilled water

Based on the results achieved after raising the flow rate to fulfil the commercial requirements of water filters and the effect of the different anions in groundwater, the CDI method was added to the fixed bed column to enhance As removal from the water. In this experiment, the removal of total As was examined to simulate As(III) and As(V) co-existence in groundwater. The procedure of connecting the power source to the column is presented in Fig. 1. Fig. 5 (b) shows that there was a significant improvement in the column's ability to remove As under this condition. This improvement in the removal capacity is mainly related to the increased attraction of the charged anions (mainly As(V)) toward the electrodes (Fig. 7).

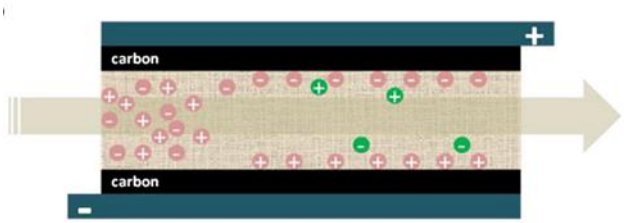

Fig. 6. Principle of CDI application (Li and Zou 2011)

Table 4. The characteristic of well water supplied by Western Downs Regional Council

Parameter	Min	Max
pH (Units)	7.5	7.85
Conductivity (mS/cm)	3.4	3.5
Turbidity (NTU)	0.1	0.6
TDS (mg/L)	1860	2050
Alkalinity (mg/L $CaCO_3$)	324	370
Sodium (mg/L)	526	580
Potassium (mg/L)	2.8	3.2
Calcium (mg/L)	44	52
Magnesium (mg/L)	69.6	84.7
Strontium (mg/L)	2	2.5
Barium (mg/L)	0.05	0.06
Sulphate (mg/L)	130	160

Chloride (mg/L)	786	934
Fluoride (mg/L)	-	-
Silica (mg/L SiO_2)	31	35
Phosphate (mg/L)	0.23	0.32
Nitrate (mg/L)	1.8	2

3.3 F^- removal

Bone char was reported to be a superior adsorbent for F^- removal from water (Abe et al. 2004, Rojas-Mayorga et al. 2013). The mechanism of the removal is based on the ion exchange between F^- and OH^- ions which forms fluorapatite. Fixed bed columns were used to explore the capacity of the packed bone (BC650) to remove F^- in a continuous system. A fixed bed study for F^- adsorption was conducted at pH 6.5 (the natural groundwater pH). Variation of the feed amount with time was determined at two different concentrations (10 and 20 mg/L using distilled water). Fig. 7 shows the breakthrough curves and the plot of the models for a flow rate of 2.5, 5 and 10 mg/L. The breakthrough curves for all flow rates and concentrations were asymmetric, typical S curve, but with different rates of saturation. The packed columns at 2.5 and 5 mL/min flow rates adsorb all of the 10 mg/L F^- up to about 60 and 20 minutes, respectively. Then a gradual decrease in the removal capacity followed. The columns were able to reduce the concentration below the limits applied by the WHO for F^- regulations (150 mg/L) up to 12, 4 and 1.5 h at the feed rate of 2.5, 5 and 10 mL/min, respectively.

At 20 mg/L inlet concentration, the removal of F^- was below the limits for about 6 and 2 h for 2.5 and 5 mL/min. However, running the same concentration at 10 mL/min resulted in an insufficient removal capacity from the first 5 minutes of sample collection. The decrease in the removal was based on the feed flow rate and concentration. The increase in flow rate shifted the curve to the right due to the shorter contact time. The increased feed concentration increased the driving force that opposed the mass transfer action. As a consequence, the decrease in the removal capacity shifted the curve towards the origin.

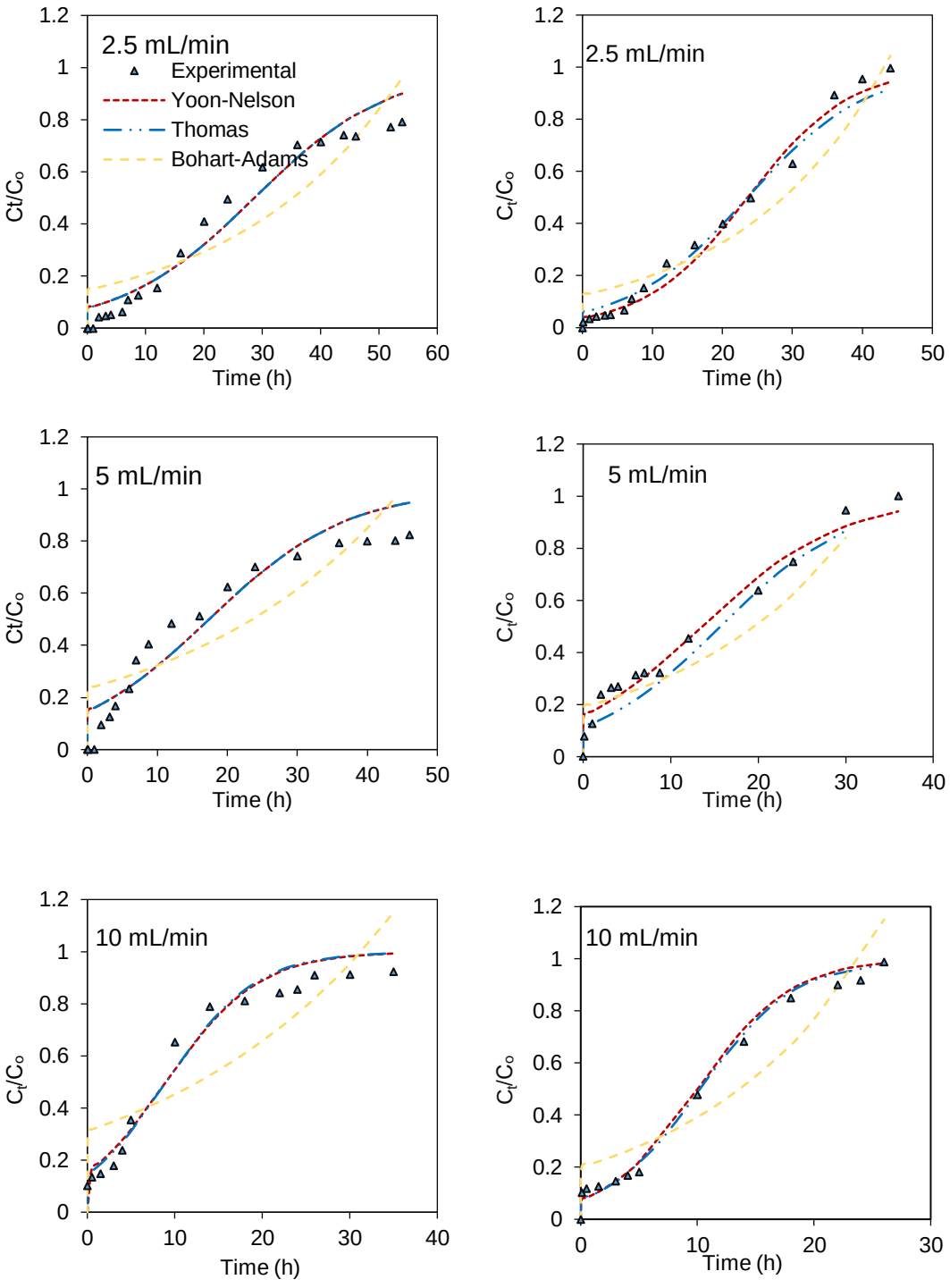

(a) Inlet 10 mg/L (b) 20 mg/L

Fig. 7. Breakthrough curve and model plot for F^- at (a) 10 mg/L and (b) 20 mg/L

The Yoon-Nelson, Thomas, and Bohart and Adams model were used for simulating the experimental data in Fig. 7. The Bohart and Adams's model was unable to explain the data when compared to the other two models as can be seen from the R^2 values provided in Table 5. The table shows the result of using the linear and nonlinear forms

of the models for the determination of the parameters. The values of the nonlinear regression, which was calculated based on minimizing the value of the sum of the squared errors, were found to provide a better fit to the experimental data. The Yoon-Nelson and the Thomas models provided the best fit to the experimental data of F^- removal. Our fittings results are in agreement with the previous work. Tovar-Gómez et al. (2013) and Rojas-Mayorga et al. (2015a) reported a better fit for F^- data by modelling the data using artificial neural networks based on Thomas's model parameters.

Table 5. Parameters of adsorption models applied for F^- removal from water

Yoon-Nelson model

Parameters		Linear			Nonlinear		
C_o (mg/L)	Flow rate (mL/min)	K_{YN}	τ	R^2	K_{YN}	τ	R^2
10	2.5	0.001	1879.800	0.940	0.001	1719.433	0.956
	5.0	0.001	1174.077	0.891	0.002	1044.325	0.902
	10.0	0.002	662.667	0.940	0.003	541.208	0.969
20	2.5	0.002	1417.609	0.981	0.002	1417.609	0.988
	5.0	0.002	834.163	0.946	0.002	815.752	0.975
	10.0	0.004	600.738	0.987	0.002	942.378	0.951

Thomas model

Parameters		Linear			Nonlinear		
C_o (mg/L)	Flow rate (mL/min)	K_{TH}	q	R^2	K_{TH}	q	R^2
10	2.5	0.0001	513.648	0.912	0.0001	477.620	0.960
	5.0	0.0002	652.265	0.886	0.0002	580.181	0.905
	10.0	0.0003	736.296	0.940	0.0003	602.884	0.974
20	2.5	0.0001	812.929	0.979	0.0001	786.039	0.985
	5.0	0.0001	926.818	0.984	0.0001	1047.086	0.951
	10.0	0.0002	1334.974	0.987	0.0002	1366.497	0.987

Bohart Adams model

Parameters		Linear			Nonlinear		
C_o (mg/L)	Flow rate (mL/min)	K_{BA}	N_o	R^2	K_{BA}	N_o	R^2
10	2.5	0.0001	728.651	0.728	0.001	806.675	0.854

	5.0	0.0001	1148.273	0.714	0.001	1318.656	0.756
	10.0	0.0001	1661.464	0.660	0.001	1831.130	0.859
20	2.5	0.0001	1055.158	0.809	4E-05	1262.562	0.917
	5.0	4E-05	1893.468	0.903	4E-05	1963.435	0.906
	10.0	0.0002	2417.578	0.767	6E-05	2801.780	0.851

3.4 Simultaneous removal of aqueous As and F

As stated in the earlier sections, dissolved As and F species are often present simultaneously in the groundwater at elevated levels around the globe at different concentrations. Therefore, the same experimental setup was used for the simultaneous removal of 1 mg/L total As and 10 mg/L F^- at a flow rate of 10 mL/min These experiments were examined using either BC900 or BC650 to remove the contaminants from Dalby's well water. Fig. 6 shows the experiment's breakthrough curve.

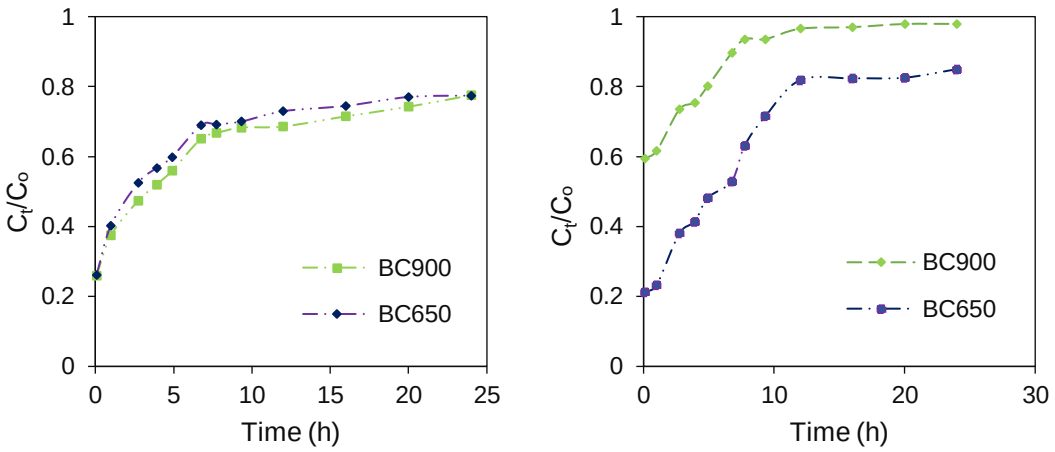

(a) (b)

Fig. 8. The simultaneous removal of (a) 1 mg/L total As and (b) 10 mg/L F^- from natural well water

As it can be seen from Fig. 8, BC900 performed slightly better than BC650 for As removal in the presence of other competing anions. This trend varied from the results of As removal reported for bone char pyrolysed at a different temperature (Alkurdi et al. 2020). The existence of other competing anions lowered the removal of BC900 and made it almost equivalent to BC650. In this case, modifying the BC650 for As removal

may provide similar results with a lower energy demand of production, which needs to be investigated in future works. The column was not able to reduce the concentration of As below the standards specified by WHO from the first run through the column. However, the presence of competing anions greatly affected the ability of BC900 to remove As. The effect of the different anions present in the water samples on removal capacity was presented in the previous section. When comparing Fig. 8 to Fig. 5 (the effect of the anions without 10 mg/L F^-), it is clear that the main contributor to the significant reduction of As removal was the presence of F^- which competed to occupy the adsorbents' active sites. These results are in agreement with the results reported by Mlilo et al. (2009) who showed that the presence of 10 mg/L F^- in the solution reduced the removal of As(V) and As(III) by about 63 and 38%, respectively. This may be related to the reactivity of F^- which has a high tendency to form complexes with the metal oxides on the surface, and thus reduces the potential of precipitation of As species on the surface

Based on the results shown in Fig. 8 (b), there was a smaller change in the ability of BC650 to remove F^- due to the existence of 1 mg/L As and the rest of the well water constituents. BC900 was able to remove F^- from water to a lower extent than BC650, which is similar to the results obtained in our previous work reported by Alkurdi et al. (2020). This may be related to the high affinity of F^- ions to OH exchange groups as reported in (Alkurdi et al. 2019b).

4. Conclusions

Bone char is a potent adsorbent for the simultaneous removal of aqueous As and F species from water if suitable modifications, either chemical or physical, are applied. This study examined the removal of these two contaminants through fixed-bed columns. The initial concentrations examined were based on the average concentration of As and $^-$ in groundwater, which are 1 and 1.5 mg/L for As and 10 mg/L for F. Three different flow rates of 2.5, 4 and 10 mL/min were used to investigate the ability of the column to remove these contaminants. Adsorption models were applied to simulate the removal of the contaminants. The Bohart and Adams's model was found to be unrepresentative of the experimental data. Arsenic removal was profoundly affected by the presence of F^- and other coexisting anions in the well water. To compare the removal of As from water to a commercial filter, a flow rate of 90 mL/min was found

to be adequate based on the hydraulic retention time of the column. However, this flow rate was found to be unable to reduce the concentration below the limits specified by the WHO. Thus, modifications were required to enhance the removal capacity. CDI technology was found to improve the removal capacity of As from water significantly. For future studies, more investigations are required to explore the effect of CDI from natural water samples.

Acknowledgement

This research was performed as a part of PhD research which was supported in part by the Iraqi Government and the Australian Research Training Program.

6.3 Concluding remarks

This chapter explored the application of bone char for the removal of dissolved arsenic and fluorine species using fixed bed columns. Each of these contaminants was examined individually and simultaneously using feed concentrations of 1 and 1.5 mg/L for As(III) and As(V). Fluoride ions removal was examined using feed concentrations of 10 and 20 mg/L. The feed rate varied with each concentration to study the effect of each of these factors on the removal capacity. Breakthrough curves for these contaminants were compared to those plotted by fitting the experimental data to the three different models. The parameters were calculated from both linear and nonlinear forms with a lower error achieved by the nonlinear regression methods. Data for all contaminants were found to well fit the Thomas and Yoon-Nelson models. Examining the removal of As in natural well water showed a decrease in the removal capacity due to competition with the existing anions. However, adding 10 mg/L F^- to the well water significantly impeded the removal of As from the solution. The removal performance of As in the presence of F^- using BC900 was reduced to the same level of BC650. Adding the CDI process to the adsorption method increased the removal capacity of the column significantly. This needs to be examined in future work for natural water applications.

CHAPTER 7

Conclusions and Recommendations

This chapter summarizes the contribution of this thesis and discusses the recommendations for future work.

7.1 Conclusion

The preparation, characterization and application of bone char and its composites for enhancing the performance of conventional removal of dissolved As and F species from water was investigated in-depth in this study. Locally available animal bone was explored as a precursor for bone char production with the final goal of converting animal waste material into a potential material for environmental applications. For the first time, this study postulates the mechanism of As(III) on bone char. The removal of F^- and inorganic As species from water was examined in batch and fixed bed experiments. Isotherm, kinetics and diffusion models were used to investigate the mechanism and capacity of bone char samples to uptake these contaminants.

In the first stage of the experiments, bone char was produced at different pyrolysis temperatures (500-900 °C) in a limited oxygen or N_2 gas environment at two different residence times (1 h and 2 h). Generally, bone char samples which were produced at 500 °C under all conditions (with or without N_2 at 1 and 2 h residence time) were unsuitable for water treatment due to the high dissolved organic carbon (DOC) released when used as an adsorbent. Therefore, the minimum pyrolysis temperature for bone char use in water treatment processes was found to be 650 °C, which is the point when the protein starts to dissociate. Furthermore, purging N_2 gas slightly affected the surface texture and the oxygen functional groups on the surface when compared to those prepared at the same residence time and pyrolysis temperature.

The characterization of each bone char sample was examined using a wide range of analytical and technical procedures. The textural composition of the char samples was compared based on the results of the surface area, pore volume and pore size experiments. There was a negative correlation between the pyrolysis temperature, and

the surface area and pore volume parameters, as an increase in pyrolysis temperature resulted in a decrease in the surface area sand pore volumes. However, the opposite was found for the pore size with a higher pore volume at the highest temperature. The Scanning Electron Microscopy (SEM) images provided information about the morphology of the surface, showing that it was rough with an undefined geometry. Elemental analysis using Scanning Electron Microscopy-Energy Dispersive Spectroscopy (SEM-EDS) showed a reduction in oxygen content after raising the pyrolysis temperature to 900 °C, which was supported by the results of the Boehm titrations and Fourier-transform infrared spectroscopy (FTIR) analyses. Similarly, the increase in Mg content at 900 °C was supported by the cation exchange capacity examination. The point of zero charge was measured and found to shift to higher pH values after raising the pyrolysis temperatures, giving a wider range of neutral pH values for anionic removal. Similarly, a rise in pyrolysis temperature resulted in larger crystallites.

The bone char samples produced were examined for their ability to remove As(III), As(V) or F^- from water. Generally, the factors that affected the removal capacity of both of the contaminates were in the following order: pyrolysis temperature > purging gas > residence time. Bone char samples produced at 900 °C were found to have the highest removal capacity for both As species, with a lower removal capacity for As(III) due to its uncharged state in the pH range of 6.5-8.5. On the other hand, the best removal capacity for F^- was at the lowest pyrolysis temperature (500°C). However, due to the high DOC obtained using the 500°C samples, the samples pyrolysed at 650°C were used for the rest of the study. Hence the effect of purging gas was significant for F^- removal from water as there was a higher removal capacity for the samples purged with N_2 gas.

Based on the characterization results, the mechanism of As(III) and As(V) removal on bone char was found to be surface complexation with the Mg compounds, which were found to be the highest at 900 °C, and coprecipitation. The results of the FTIR analysis showed a major change in the fingerprint area due to the intramolecular effect on the adsorption process. The new peaks introduced in this region were due to the formation of As-Mg complexes. In addition, the reduction in the intensity of the oxygen functional groups was mainly noticed in the case of As(V) adsorption, while As(III)

adsorption increased the intensity of the PO_4^{3-} peaks, confirming the formation of surface complexes.

In Chapter 4, a detailed experimental and theoretical analysis of As removal on bone char was performed. Batch experiments were conducted to investigate the mechanism of As(III) and As(V) adsorption using linear and nonlinear regression analyses for the isotherm, kinetics and diffusion models. The removal efficiency was strongly dependent on the pH of the solution. The maximum removal achieved was at a pH of 8.6 and 7.5 for As(III) and As(V), respectively. The isotherms of As(III) and As(V) were examined using the Langmuir, Freundlich, Redlich-Peterson and Sips model in the concentration range of 0.05-50 mg/L. The data obtained from the As(III) experiments best fit the Sips model, which confirmed the dependence of the removal mechanisms on the initial concentration of As(III) in the solution. Meanwhile, As(V) removal was best represented by the Langmuir model confirming a homogenous monolayer adsorption for As(V).

The Pseudo-first-order, Pseudo-second-order, Elovich and Ritchie models were used to examine the kinetics of the removal of As(III) and As(V) onto bone char. The experimental data was examined for four concentrations (0.5, 2.5, 5 and 10 mg/L) of As(III) and As(V), respectively. The mechanism of the removal for both of As(III) and As(V) species was found to be based on the initial concentration of the solution. At a low concentration of 0.5 mg/L, the removal followed the Pseudo-first-order model, expressing a physical adsorption on the bone char surface. Increasing the initial concentration showed a better fit to the Pseudo-second-order or Elovich model, which means chemisorption removal was the main removal mechanism.

Diffusional models represented by the intraparticle diffusion model and pore diffusion model (the Boyd model) were used to explain the removal of these two species. The results showed that the intraparticle model was the limiting step for the removal of both of As species. Moreover, the results of the Boyd model showed the contribution of pore diffusion mechanisms in the adsorption process at the lower concentrations of 0.5 and 2.5 mg/L. Finally, SEM-EDS results confirmed that removal was complex due to the formation of precipitants on the surface of the bone char where significant changes in the percentage mass of Mg, Na and Ca content were noticed.

Chapter 5 examined the oxidation of As(III) to As(V) through the modification of the bone char with the highest removal capacity (BC900) with nanoparticles of TiO_2. The modification was made following two different procedures: after pyrolysis and during the pyrolysis of the bone precursor. Depositing $nTiO_2$ resulted in a decrease of surface area and pore volume of the new composite compared to the unmodified bone char, but pore size was increased. Coating during the pyrolysis procedure was found to result in a higher oxidation efficiency for As(III). Adsorption batch experiments using the composite were conducted using three different levels of ultraviolet (UV) light (4, 8 and 12 W) with $\lambda max = 360$ nm. The findings of these experiments confirmed that the increase in removal of As from the water (from 24.8 for BC to 57.3% for the composite) was due to the change in the oxidation state of As(III) using 12 W of UV light. The study also investigated the changes in the phase of the TiO_2 from anatase to rutile after exposing the bone char to 900 °C, and FTIR analyses explained the formation of the new bonds after the adsorption process.

The last part of the study (Chapter 6) examined the individual and simultaneous removal of F^- and As in fixed bed columns packed with bone char. It also explored the enhanced removal capacity of As(V) on bone char using the capitative deionization (CDI) method. As(III) and As(V) were examined at two initial concentrations of 1 and 1.5 mg/L. Fluoride removal was studied at 10 and 20 mg/L initial concentration. In addition, the feed rate was varied from 2.5-10 mL/min passing through a column with a cross sectional area of 11.642 cm^2 for all of the concentrations examined to study the effect of these varied conditions on the removal capacity. These concentrations were selected based on the average concentration of each of the groundwater contaminants reported in the literature.

The experimental data was fitted against the Yoon-Nelson, Thomas, and Bohart and Adams kinetic models. In all cases, the Bohart and Adams model did not fit the experimental data. The best fit was provided using the Thomas and Yoon-Nelson models indicating the reversable removal of these contaminants with neglected axial forces contribution in the removal.

The efficiency of As removal using the packed bed was compared to a commercial filter by increasing the flow rate to 90 mL/min. However, removal was found to be very low at this flow rate and modifications were recommended to enhance removal

capacity. The concurrent applications of adsorption and the electrochemical treatment of water were combined to increase the removal capacity of the bed. Therefore, CDI was added to remove the As at a concentration of 10 mg/L and 1 mg/L of the inlet feed and a flow rate of 10 mL/min. Removal increased significantly after combining these two methods. Breakthrough occurred after about 10 h of running the column. This application of CDI is a promising, efficient and cost-effective method of removing As from groundwater resources at a household scale.

The main proposed removal mechanism that controlled the uptake of As on bone char was found to be the formation of surface Mg-As complexes in addition to the contribution of electrostatic attraction. As(V) removal was affected by the presence of coexisting anions, such as PO_4^{3-}, SiO_3^{2-}, NO_3^- and SO_4^{2-}, due to competition to occupy the active sites on the bone char surface. On the other hand, As(III) is uncharged at the pH of the experiments (6.5). However, the higher ability of the negatively charged anions to form magnesium nitrates, phosphates, etc. reduces the chances of the interaction between As(III) and Mg on the surface.

The simultaneous removal of aqueous As and F species from natural water was compared to the ability of the bone char to remove from As-spiked well water. It was noticed that F^- had the greatest effect on impeding the removal of As from well water. Furthermore, the effect of pyrolysis temperature almost disappeared for As removal as the BC900 and BC650 acted almost the same in the presence of F^- and other competing anions, while F^- removal was slightly affected by the existence of other anions. This may be explained by the strong electronegativity of F^- which makes it very reactive and able to for*m* complexes with metal ions.

7.2 Recommendations

The results obtained in this study show that bone char and the modification methods adopted are promising green sorbents that can significantly improve the performance of water treatment processes at a small scale (single households); paving the way for more applications on a large domestic and industrial scale. However, several aspects were identified for further exploration to improve the performance of these waste

materials for environmental remediation. The following aspects are worthy of further investigation in future work:

1. In this study, a BC/nTiO_2 composite was prepared following two different procedures, but only one ratio of BC:nTiO_2 was used. While optimization of this ratio on the oxidation/removal efficiency of As(III) was not within the scope of this study, it is recommended that the production methods be optimized for further application, for instance the in industrial wastewater treatment. In addition, studying the cost effectiveness of the composite needs to be evaluated

2. In this study, the removal of As on the coated bone char was improved compared to the uncoated BC. To optimize the experimental condition of As(III) oxidation and As(V) to maximize the removal of the BC/nTiO_2 composite, the isotherm and kinetic models need to be examined. In addition, the oxidation performance of the composite was examined in the presence or the absence of pure UV light. However, investigation on the effect of sunlight on oxidation performance needs to be considered as this would lower costs of the technology

3. The simultaneous removal of dissolved As and F species was examined in this study using fixed bed columns. The effect of the presence of co-existing anions in groundwater was investigated individually and simultaneously using two different samples of bone char (pyrolyzed at 650 °C with N_2, and pyrolyzed at 900 °C in a limited oxygen environment). While the contribution of the CDI technology was found to enhance the removal of As from water, it needs to be investigated with natural water for As and F species simultaneously

4. Coating BC with TiO_2 was used to oxidize As(III) to As(V) which can be more easily adsorbed due to its negative charge state at neutral pH levels. CDI was then used to increase the removal of As(V) from solution. While each modification method is used to target one of these species, it would be interesting to use the composite with CDI in a fixed bed column

5. Bone char has been used to remove F^- on a large scale in many different areas of Africa and Asia. However, the application of As removal on bone char is

still in the lab scale. Therefore, examining the removal of As with F^- is of great interest.

References

Abe, I., Iwasaki, S., Tokimoto, T., Kawasaki, N., Nakamura, T. and Tanada, S., 2004. Adsorption of fluoride ions onto carbonaceous materials. *J. Colloid. Interface. Sci.* 275(1), 35-39.

Ahmad, A. and Hameed, B., 2010. Fixed-bed adsorption of reactive azo dye onto granular activated carbon prepared from waste. *J. Hazard. Mater.* 175(1-3), 298-303.

Akter, K.F., Owens, G., Davey, D.E. and Naidu, R. (2005) Rev. Environ. Contam Tox., pp. 97-149, Springer.

Alam, M.A., Shaikh, W.A., Alam, M.O., Bhattacharya, T., Chakraborty, S., Show, B. and Saha, I., 2018. Adsorption of As (III) and As (V) from aqueous solution by modified Cassia fistula (golden shower) biochar. *Appl. Water Sci.* 8(7), 198.

Alam, R. and McPhedran, K., 2019. Applications of biological sulfate reduction for remediation of arsenic–A review. *Chemosphere* 222, 932-944.

Alarcón-Herrera, M.T., Bundschuh, J., Nath, B., Nicolli, H.B., Gutierrez, M., Reyes-Gomez, V.M., Nunez, D., Martín-Dominguez, I.R. and Sracek, O., 2013. Co-occurrence of arsenic and fluoride in groundwater of semi-arid regions in Latin America: Genesis, mobility and remediation. *J. Hazard. Mater.* 262, 960-969.

Alarcón-Herrera, M.T., Martin-Alarcon, D.A., Gutiérrez, M., Reynoso-Cuevas, L., Martín-Domínguez, A., Olmos-Márquez, M.A. and Bundschuh, J., 2020. Co-occurrence, possible origin, and health-risk assessment of arsenic and fluoride in drinking water sources in Mexico: Geographical data visualization. *Sci. Total. Environ.* 698, 134168.

Alkurdi, S.S., Al-Juboori, R.A., Bundschuh, J., Bowtell, L. and McKnight, S., 2020. Effect of pyrolysis conditions on bone char characterization and its ability for arsenic and fluoride removal. *Environ. Pollut.*, 114221.

Alkurdi, S.S., Al-Juboori, R.A., Bundschuh, J. and Hamawand, I., 2019b. Bone char as a green sorbent for removing health threatening fluoride from drinking water. *Environ. Inter.* 127, 704-719.

Alkurdi, S.S., Herath, I., Bundschuh, J., Al-Juboori, R.A., Vithanage, M. and Mohan, D., 2019a. Biochar versus bone char for a sustainable inorganic arsenic mitigation in water: What needs to be done in future research? *Environ. Inter.* 127, 52-69.

Amin, A.E.-E.A.Z., 2020. Sulfur, Na_2-EDTA and their mixture effects on phosphorus release from cow bone char in P-poor sandy soil. *Environ. Technol. Innov.* 17, 100636.

Anirudhan, T. and Radhakrishnan, P., 2009. Kinetic and equilibrium modelling of Cadmium (II) ions sorption onto polymerized tamarind fruit shell. *Desalination* 249(3), 1298-1307.

Appelo, T. and Heederik, J.P., 2008. Arsenic in groundwater. *A world problem*.

Azizian, S., 2004. Kinetic models of sorption: a theoretical analysis. *J. Colloid. Interface. Sci.* 276(1), 47-52.

Baig, S.A., Zhu, J., Muhammad, N., Sheng, T. and Xu, X., 2014. Effect of synthesis methods on magnetic Kans grass biochar for enhanced As (III, V) adsorption from aqueous solutions. *Biomass Bioenergy* 71, 299-310.

Begum, S.A., Golam Hyder, A. and Vahdat, N., 2016. Adsorption isotherm and kinetic studies of As (V) removal from aqueous solution using cattle bone char. *J. Water Supply Res. T.* 65(3), 244-252.

Bertoni, E., Bigi, A., Cojazzi, G., Gandolfi, M., Panzavolta, S. and Roveri, N., 1998. Nanocrystals of magnesium and fluoride substituted hydroxyapatite. *J. Inorg. Biochem.* 72(1-2), 29-35.

Bhaumik, M., Setshedi, K., Maity, A. and Onyango, M.S., 2013. Chromium (VI) removal from water using fixed bed column of polypyrrole/Fe_3O_4 nanocomposite. *Sep. Purif. Technol.* 110, 11-19.

Bissen, M. and Frimmel, F.H., 2003. Arsenic—a review. Part II: oxidation of arsenic and its removal in water treatment. *Acta Hydrochim. Hydrobiol.* 31(2), 97-107.

Bordajandi, L.R., Gómez, G., Fernandez, M., Abad, E., Rivera, J. and González, M.J., 2003. Study on PCBs, PCDD/Fs, organochlorine pesticides, heavy metals and arsenic content in freshwater fish species from the River Turia (Spain). *Chemosphere* 53(2), 163-171.

Bullough, P.G. (2010) Orthopaedic Pathology Mosby.

Bundschuh, J., Maity, J.P., Mushtaq, S., Vithanage, M., Seneweera, S., Schneider, J., Bhattacharya, P., Khan, N.I., Hamawand, I. and Guilherme, L.R., 2017. Medical geology in the framework of the sustainable development goals. *Sci. Total Environ.* 581, 87-104.

Cai, Q., Turner, B.D., Sheng, D. and Sloan, S., 2017. Application of kinetic models to the design of a calcite permeable reactive barrier (PRB) for fluoride remediation. *Water Res.* 130, 300-311.

Cerejeira, M., Viana, P., Batista, S., Pereira, T., Silva, E., Valério, M., Silva, A., Ferreira, M. and Silva-Fernandes, A., 2003. Pesticides in Portuguese surface and ground waters. *Water research* 37(5), 1055-1063.

Chatterjee, S., Mukherjee, M. and De, S., 2018. Defluoridation using novel chemically treated carbonized bone meal: batch and dynamic performance with scale-up studies. *Environ. Sci. Pollut. Res.* 25, 18161-18178.

Chen, Y.-N., Chai, L.-Y. and Shu, Y.-D., 2008. Study of arsenic (V) adsorption on bone char from aqueous solution. *J. Hazard. Mater.* 160(1), 168-172.

Cheng, Z., Fu, F., Dionysiou, D.D. and Tang, B., 2016. Adsorption, oxidation, and reduction behavior of arsenic in the removal of aqueous As (III) by mesoporous Fe/Al bimetallic particles. *Water Res.* 96, 22-31.

Cheung, C., Porter, J. and McKay, G., 2001. Sorption kinetic analysis for the removal of cadmium ions from effluents using bone char. *Water Res.* 35(3), 605-612.

Cheung, C.W., Porter, J.F. and McKay, G., 2000. Elovich equation and modified second-order equation for sorption of cadmium ions onto bone char. *J. Chem. Technol. Biotechnol* 75(11), 963-970.

Choy, K.K. and McKay, G., 2005. Sorption of cadmium, copper, and zinc ions onto bone char using Crank diffusion model. *Chemosphere* 60(8), 1141-1150.

Clifford, D. and Ghurye, G., 2001. Arsenic III to Arsenic V. *Water Quality Products*, 28.

Co-operation, O.f.E. and Development (2018) OECD-FAO agricultural outlook 2018-2027, OECD Publishing.

Cope, C.O., Webster, D.S. and Sabatini, D.A., 2014. Arsenate adsorption onto iron oxide amended rice husk char. *Sci. Total Environ.* 488, 554-561.

Cowen, S., Duggal, M., Hoang, T. and Al-Abadleh, H.A., 2008. Vibrational spectroscopic characterization of some environmentally important organoarsenicals—A guide for understanding the nature of their surface complexes. *Can. J. Chem.* 86(10), 942-950.

Czerniczyniec, M., Farías, S., Magallanes, J. and Cicerone, D., 2007. Arsenic (V) adsorption onto biogenic hydroxyapatite: solution composition effects. *Water Air Soil Pollut.* 180(1-4), 75-82.

Dalin, C., Taniguchi, M. and Green, T.R., 2019. Unsustainable groundwater use for global food production and related international trade. *Global Sustainability* 2.

Darvishi Cheshmeh Soltani, R., Safari, M., Maleki, A., Rezaee, R., Shahmoradi, B., Shahmohammadi, S. and Ghahramani, E., 2017. Decontamination of arsenic(V)-contained liquid phase utilizing Fe_3O_4/bone char nanocomposite encapsulated in chitosan biopolymer. *Environ. Sci. Pollut. Res.* 24(17), 15157-15166.

Delgadillo-Velasco, L., Hernández-Montoya, V., Cervantes, F.J., Montes-Morán, M.A. and Lira-Berlanga, D., 2017. Bone char with antibacterial properties for fluoride removal: Preparation, characterization and water treatment. *J. Environ. Manage.* 201, 277-285.

Deng, M., Wu, X., Zhu, A., Zhang, Q. and Liu, Q., 2019. Well-dispersed TiO_2 nanoparticles anchored on Fe_3O_4 magnetic nanosheets for efficient arsenic removal. *J. Environ. Manage.* 237, 63-74.

Dieme, M., Villot, A., Gerente, C., Andres, Y., Diop, S. and Diawara, C., 2017. Sustainable conversion of agriculture wastes into activated carbons: energy balance and arsenic removal from water. *Environ. Technol.* 38(3), 353-360.

Dotto, G.L., Salau, N.P.G., Piccin, J.S., Cadaval, T.R.S.A. and de Pinto, L.A.A. (2017) Adsorption Processes for Water Treatment and Purification, pp. 53-76, Springer.

Driehaus, W., 2002. Arsenic removal-experience with the GEH® process in Germany. *Water Sci. Technol* 2(2), 275-280.

Dubey, C.S., Mishra, B.K., Shukla, D.P., Singh, R.P., Tajbakhsh, M. and Sakhare, P., 2012. Anthropogenic arsenic menace in Delhi Yamuna flood plains. *Environ. Earth Sci.* 65(1), 131-139.

Edvantoro, B.B., Naidu, R., Megharaj, M., Merrington, G. and Singleton, I., 2004. Microbial formation of volatile arsenic in cattle dip site soils contaminated with arsenic and DDT. *Appl. Soil Ecol.* 25(3), 207-217.

El-Khaiary, M.I. and Malash, G.F., 2011. Common data analysis errors in batch adsorption studies. *Hydrometallurgy* 105(3-4), 314-320.

El-Sherbiny, S., Morsy, F., Samir, M. and Fouad, O.A., 2014. Synthesis, characterization and application of TiO_2 nanopowders as special paper coating pigment. *Appl. Nanosci.* 4(3), 305-313.

Environment Australia 1998 Treatment technologies for destruction or management of arsenic wastes, Environment Australia, Environment protection group.

Ermolenko, A., Shevelev, A., Vikulova, M., Blagova, T., Altukhov, S., Gorokhovsky, A., Godymchuk, A., Burmistrov, I. and Offor, P.O., 2020. Wastewater treatment from lead and strontium by potassium polytitanates: Kinetic analysis and adsorption mechanism. *Processes* 8(2), 217.

Fan, C.-S., Liou, S.Y.H. and Hou, C.-H., 2017. Capacitive deionization of arsenic-contaminated groundwater in a single-pass mode. *Chemosphere* 184, 924-931.

Fan, C.-S., Tseng, S.-C., Li, K.-C. and Hou, C.-H., 2016. Electro-removal of arsenic (III) and arsenic (V) from aqueous solutions by capacitive deionization. *J. Hazard. Mater.* 312, 208-215.

Figoli, A., Bundschuh, J. and Hoinkis, J., 2016. Fluoride, uranium and arsenic: Occurrence, mobility, chemistry, human health impacts and concerns. *Membr. Technol. Water Treat.*, 3-19.

Foratirad, H., Baharvandi, H.R. and Maragheh, M.G., 2017. Chemo-rheological behavior of aqueous titanium carbide suspension and evaluation of the gelcasted green body properties. *Mater. Res.* 20(1), 175-182.

Garelick, H., Jones, H., Dybowska, A. and Valsami-Jones, E. (2009) Rev. Environ. Contam Tox., pp. 17-60, Springer.

Guan, X., Du, J., Meng, X., Sun, Y., Sun, B. and Hu, Q., 2012. Application of titanium dioxide in arsenic removal from water: a review. *J. Hazard. Mater.* 215, 1-16.

Gunneriusson, L., Sandström, Å., Holmgren, A., Kuzmann, E., Kovacs, K. and Vértes, A., 2009. Jarosite inclusion of fluoride and its potential significance to bioleaching of sulphide minerals. *Hydrometallurgy* 96(1-2), 108-116.

Guo, H., Wen, D., Liu, Z., Jia, Y. and Guo, Q., 2014. A review of high arsenic groundwater in Mainland and Taiwan, China: distribution, characteristics and geochemical processes. *Appl. Geochemistry* 41, 196-217.

Gupta, K., Singh, N., Pandey, A., Shukla, S., Upadayay, S., Mishra, V., Srivastava, P., Lalla, N. and Mishra, P., 2013. Effect of anatase/rutile TiO_2 phase composition on arsenic adsorption. *J. Disper. Sci. Technol.* 34(8), 1043-1052.

Hanaor, D.A. and Sorrell, C.C., 2011. Review of the anatase to rutile phase transformation. *J. Mater. Sci.* 46(4), 855-874.

Hashim, M.A., Kundu, A., Mukherjee, S., Ng, Y.-S., Mukhopadhyay, S., Redzwan, G. and Gupta, B.S., 2019. Arsenic removal by adsorption on activated carbon in a rotating packed bed. *J. Water Process. Eng.* 30, 100591.

Herath, I., Kumarathilaka, P., Bundschuh, J., Marchuk, A. and Rinklebe, J., 2020. A fast analytical protocol for simultaneous speciation of arsenic by Ultra-High Performance Liquid Chromatography (UHPLC) hyphenated to Inductively Coupled Plasma Mass Spectrometry (ICP-MS) as a modern advancement in liquid chromatography approaches. *Talanta* 208, 120457.

Herath, I., Vithanage, M., Bundschuh, J., Maity, J.P. and Bhattacharya, P., 2016. Natural Arsenic in Global Groundwaters: Distribution and Geochemical Triggers for Mobilization. *Curr. Pollut. Rep.* 2(1), 68-89.

Ho, Y.-S., 2006. Review of second-order models for adsorption systems. *J. Hazard. Mater.* 136(3), 681-689.

Ho, Y., Porter, J. and McKay, G., 2002. Equilibrium isotherm studies for the sorption of divalent metal ions onto peat: copper, nickel and lead single component systems. *Water Air Soil Pollut.* 141(1-4), 1-33.

Hu, X., Ding, Z., Zimmerman, A.R., Wang, S. and Gao, B., 2015. Batch and column sorption of arsenic onto iron-impregnated biochar synthesized through hydrolysis. *Water Res.* 68, 206-216.

Huang, H., Liu, J., Zhang, P., Zhang, D. and Gao, F., 2017. Investigation on the simultaneous removal of fluoride, ammonia nitrogen and phosphate from semiconductor wastewater using chemical precipitation. *Chem. Eng. J.* 307, 696-706.

Hubadillah, S.K., Othman, M.H.D., Ismail, A., Rahman, M.A. and Jaafar, J., 2019. A low cost hydrophobic kaolin hollow fiber membrane (h-KHFM) for arsenic removal from aqueous solution via direct contact membrane distillation. *Sep. Purif. Technol.* 214, 31-39.

Inam, M.A., Khan, R., Akram, M., Khan, S., Park, D.R. and Yeom, I.T., 2019. Interaction of Arsenic Species with Organic Ligands: Competitive Removal from Water by Coagulation-Flocculation-Sedimentation (C/F/S). *Molecules* 24(8), 1619.

Ingallinella, A.M., Pacini, V.A., Fernández, R.G., Vidoni, R.M. and Sanguinetti, G., 2011. Simultaneous removal of arsenic and fluoride from groundwater by

coagulation-adsorption with polyaluminum chloride. *J. Environ. Sci. Health A* 46(11), 1288-1296.

Islam, M., Mishra, P.C. and Patel, R., 2011. Arsenate removal from aqueous solution by cellulose-carbonated hydroxyapatite nanocomposites. *J. Hazard. Mater.* 189(3), 755-763.

Jadhav, S.V., Bringas, E., Yadav, G.D., Rathod, V.K., Ortiz, I. and Marathe, K.V., 2015. Arsenic and fluoride contaminated groundwaters: a review of current technologies for contaminants removal. *J. Environ. Manag.* 162, 306-325.

Janakiraman, N. and Johnson, M., 2015. Functional groups of tree ferns (Cyathea) using FTIR: Chemotaxonomic implications. *Rom. J. of Biophys.* 25(2), 131-141.

Jia, B.Y., Duan, L.Y., Ma, C.L. and Wang, C.M., 2007. Characterization of TiO_2 loaded on activated carbon fibers and its photocatalytic reactivity. *Chin. J. Chem.* 25(4), 553-557.

Juhasz, A.L., Smith, E., Smith, J. and Naidu, R., 2002. Biosorption of organochlorine pesticides using fungal biomass. *J. Ind. Microbiol. Biotechnol.* 29(4), 163-169.

Kalaivani, T. and Anilkumar, P., 2018. Role of temperature on the phase modification of TiO 2 nanoparticles synthesized by the precipitation method. *Silicon* 10(4), 1679-1686.

Kalaruban, M., Loganathan, P., Nguyen, T.V., Nur, T., Johir, M.A.H., Nguyen, T.H., Trinh, M.V. and Vigneswaran, S., 2019. Iron-impregnated granular activated carbon for arsenic removal: application to practical column filters. *J. Environ. Manage.* 239, 235-243.

Kannaiyan, D., Kochuveedu, S.T., Jang, Y.H., Jang, Y.J., Lee, J.Y., Lee, J., Lee, J., Kim, J. and Kim, D.H., 2010. Enhanced photophysical properties of nanopatterned titania nanodots/nanowires upon hybridization with silica via block copolymer templated sol-gel process. *Polymers* 2(4), 490-504.

Katsoyiannis, I.A., Mitrakas, M. and Zouboulis, A.I., 2015. Arsenic occurrence in Europe: Emphasis in Greece and description of the applied full-scale treatment plants. *Desalination Water Treat.* 54(8), 2100-2107.

Kawasaki, N., Ogata, F., Tominaga, H. and Yamaguchi, I., 2009. Removal of fluoride ion by bone char produced from animal biomass. *J Oleo Sci* 58(10), 529-535.

Khan, K.M., Chakraborty, R., Bundschuh, J., Bhattacharya, P. and Parvez, F., 2020. Health effects of arsenic exposure in Latin America: An overview of the past eight years of research. *Sci. Total Environ.* 710, 136071.

Kikuchi, M., Arioka, Y., Tafu, M. and Irie, M., 2019. Changes in Fluoride Removal Ability of Chicken Bone Char with Changes in Calcination Time. *IJCES.*

Konikow, L.F. and Kendy, E., 2005. Groundwater depletion: A global problem. *Hydrogeol. J.* 13(1), 317-320.

Kumar, H., Patel, M. and Mohan, D., 2019. Simplified Batch and Fixed-Bed Design System for Efficient and Sustainable Fluoride Removal from Water Using Slow Pyrolyzed Okra Stem and Black Gram Straw Biochars. *ACS omega* 4(22), 19513-19525.

Kumar, M., Das, A., Das, N., Goswami, R. and Singh, U.K., 2016. Co-occurrence perspective of arsenic and fluoride in the groundwater of Diphu, Assam, Northeastern India. *Chemosphere* 150, 227-238.

Kumar, M. and Ramanathan, A. 2019. Arsenic speciation of groundwater and agricultural soils in central Gangetic basin, India, p. 225, CRC Press.

Kumara, N., Hamdan, N., Petra, M.I., Tennakoon, K.U. and Ekanayake, P., 2014. Equilibrium isotherm studies of adsorption of pigments extracted from kuduk-kuduk (Melastoma malabathricum L.) pulp onto TiO_2 nanoparticles. *J. Chem.* 2014.

Kumarathilaka, P., Seneweera, S., Ok, Y.S., Meharg, A.A. and Bundschuh, J., 2020. Mitigation of arsenic accumulation in rice: An agronomical, physico-chemical, and biological approach–A critical review. *Crit. Rev. Environ. Sci. Technol.* 50(1), 31-71.

Lapworth, D., Krishan, G., MacDonald, A. and Rao, M., 2017. Groundwater quality in the alluvial aquifer system of northwest India: New evidence of the extent of anthropogenic and geogenic contamination. *Sci. Total Environ.* 599, 1433-1444.

Lazar, M.A., Varghese, S. and Nair, S.S., 2012. Photocatalytic water treatment by titanium dioxide: recent updates. *Catalysts* 2(4), 572-601.

Li, G.-Y., Jiang, Y.-R., Huang, K.-L., Ding, P. and Yao, L.-L., 2008. Kinetics of adsorption of Saccharomyces cerevisiae mandelated dehydrogenase on magnetic Fe_3O_4–chitosan nanoparticles. *Colloids Surf. A Physicochem. Eng. Asp.* 320(1-3), 11-18.

Li, H. and Zou, L., 2011. Ion-exchange membrane capacitive deionization: A new strategy for brackish water desalination. *Desalination* 275(1-3), 62-66.

Li, M., Luo, Z., Yan, Y., Wang, Z., Chi, Q., Yan, C. and Xing, B., 2016. Arsenate accumulation, distribution, and toxicity associated with titanium dioxide nanoparticles in Daphnia magna. *Environ. Sci. Technol.* 50(17), 9636-9643.

Li, Z., Hong, H., Jean, J.-S., Koski, A.J., Liu, C.-C., Reza, S., Randolph, J.J., Kurdas, S.R., Friend, J.H. and Antinucci, S.J., 2011. Characterization on arsenic sorption and mobility of the sediments of Chia-Nan Plain, where Blackfoot disease occurred. *Environ. Earth Sci.* 64(3), 823-831.

Lin, J. and Wang, L., 2009. Comparison between linear and non-linear forms of pseudo-first-order and pseudo-second-order adsorption kinetic models for the removal of methylene blue by activated carbon. *Front Environ. Sci. Eng.* 3(3), 320-324.

Liu, B., Kim, K.-H., Kumar, V. and Kim, S., 2020. A review of functional sorbents for adsorptive removal of arsenic ions in aqueous systems. *J. Hazard. Mater.* 388, 121815.

Liu, J., Huang, X., Liu, J., Wang, W., Zhang, W. and Dong, F., 2014. Adsorption of arsenic (V) on bone char: batch, column and modeling studies. *Environ. Earth Sci.* 72(6), 2081-2090.

Liu, Y., Su, G., Zhang, B., Jiang, G. and Yan, B., 2011. Nanoparticle-based strategies for detection and remediation of environmental pollutants. *Analyst* 136(5), 872-877.

Long, T. and Xu, X.-J. 2017. Research of groundwater fluoride removal by coagulation-filtration, pp. 501-510, World Scientific.

Ma, L. and Tu, S., 2011. Removal of arsenic from aqueous solution by two types of nano TiO 2 crystals. *Environ. Chem. Lett.* 9(4), 465-472.

Makreski, P., Stefov, S., Pejov, L. and Jovanovski, G., 2015. Theoretical and experimental study of the vibrational spectra of (para) symplesite and hörnesite. *Spectrochim. Acta, Part A* 144, 155-162.

Malash, G.F. and El-Khaiary, M.I., 2010. Piecewise linear regression: A statistical method for the analysis of experimental adsorption data by the intraparticle-diffusion models. *Chem. Eng. J.* 163(3), 256-263.

Mancardi, G., Hernandez Tamargo, C., Terranova, U. and De Leeuw, N.H., 2018. Calcium Phosphate Deposition on Planar and Stepped (101) Surfaces of

Anatase TiO_2: Introducing an Interatomic Potential for the TiO_2/Ca-PO_4/Water Interface. *Langmuir* 34(34), 10144-10152.

Meher, A., Pillewan, P., Rayalu, S. and Bansiwal, A., 2016. Arsenic removal from water using metal and metal oxide modified zeolites. *Arsen. Res. Glob. Sustain.*, 482-483.

Min, X., Li, Y., Ke, Y., Shi, M., Chai, L. and Xue, K., 2017. Fe-FeS2 adsorbent prepared with iron powder and pyrite by facile ball milling and its application for arsenic removal. *Water Sci. Technol* 76(1), 192-200.

Minja, R.J., 2020. Practical Approach for Removal of Natural Organic Matter and Defluoridation of Maji ya Chai River Water: Use of Acid Pre-treated Bone Char and Coagulants. *Tanz. J. Engrg. Technol.* 38(2).

Mlilo, T., Brunson, L. and Sabatini, D., 2009. Arsenic and fluoride removal using simple materials. *J. Environ. Eng.* 136(4), 391-398.

Mondal, P. and George, S., 2015. A review on adsorbents used for defluoridation of drinking water. *Rev. Environ. Sci. Bio.* 14(2), 195-210.

Mukherjee, A., Sengupta, M.K., Hossain, M.A., Ahamed, S., Das, B., Nayak, B., Lodh, D., Rahman, M.M. and Chakraborti, D., 2006. Arsenic contamination in groundwater: a global perspective with emphasis on the Asian scenario. *JHPN*, 142-163.

Mumtaz, N., Pandey, G. and Labhasetwar, P.K., 2015. Global fluoride occurrence, available technologies for fluoride removal, and electrolytic defluoridation: a review. *Crit. Rev. Environ. Sci. Technol.* 45(21), 2357-2389.

Nasir, A.M., Goh, P.S. and Ismail, A.F., 2019. Highly adsorptive polysulfone/hydrous iron-nickel-manganese (PSF/HINM) nanocomposite hollow fiber membrane for synergistic arsenic removal. *Sep. Purif. Technol.* 213, 162-175.

Nevárez, L.M., Casarrubias, L.B., Canto, O.S., Celzard, A., Fierro, V., Gómez, R.I. and Sánchez, G.G., 2011. Biopolymers-based nanocomposites: Membranes from propionated lignin and cellulose for water purification. *Carbohydr. Polym.* 86(2), 732-741.

Niazi, N.K., Bibi, I., Shahid, M., Ok, Y.S., Burton, E.D., Wang, H., Shaheen, S.M., Rinklebe, J. and Lüttge, A., 2018a. Arsenic removal by perilla leaf biochar in aqueous solutions and groundwater: an integrated spectroscopic and microscopic examination. *Environmental Pollution* 232, 31-41.

Niazi, N.K., Bibi, I., Shahid, M., Ok, Y.S., Shaheen, S.M., Rinklebe, J., Wang, H., Murtaza, B., Islam, E. and Nawaz, M.F., 2018b. Arsenic removal by Japanese oak wood biochar in aqueous solutions and well water: Investigating arsenic fate using integrated spectroscopic and microscopic techniques. *Sci. Total Environ.* 621, 1642-1651.

Nigri, E.M., Santos, A.L., Bhatnagar, A. and Rocha, S.D., 2019. Chemical regeneration of bone char associated with a continuous system for defluoridation of water. *Braz. J. Chem. Eng.* 36(4), 1631-1643.

OECD (2018) OECD-FAO Agricultural Outlook 2018-2027.

Onyango, M.S., Leswifi, T.Y., Ochieng, A., Kuchar, D., Otieno, F.O. and Matsuda, H., 2009. Breakthrough analysis for water defluoridation using surface-tailored zeolite in a fixed bed column. *Ind. Eng. Chem. Res.* 48(2), 931-937.

Padhi, S. and Muralidharan, D., 2012. Fluoride occurrence and mobilization in geo-environment of semi-arid Granite watershed in southern peninsular India. *Environ. Earth Sci.* 66(2), 471-479.

Passman, S.D., White, T.J. and Lewis, R.D., 2014. Point-of-use water filtration for arsenic: a sustainable and simple solution in resource-poor settings. *IJSLE* 9(1), 79-91.

Patel, H., 2019. Fixed-bed column adsorption study: a comprehensive review. *Appl. Water Sci.* 9(3), 45.

Pillai, P., Kakadiya, N., Timaniya, Z., Dharaskar, S. and Sillanpaa, M., 2020. Removal of arsenic using iron oxide amended with rice husk nanoparticles from aqueous solution. *Materials Today: Proceedings*.

Porada, S., Zhao, R., Van Der Wal, A., Presser, V. and Biesheuvel, P., 2013. Review on the science and technology of water desalination by capacitive deionization. *Prog. Mater. Sci* 58(8), 1388-1442.

Qi, P., Luo, R., Pichler, T., Zeng, J., Wang, Y., Fan, Y. and Sui, K., 2019. Development of a magnetic core-shell Fe_3O_4@ TA@ UiO-66 microsphere for removal of arsenic (III) and antimony (III) from aqueous solution. *J. Hazard. Mater.* 378, 120721.

Qiu, H., Lv, L., Pan, B.-c., Zhang, Q.-j., Zhang, W.-m. and Zhang, Q.-x., 2009. Critical review in adsorption kinetic models. *J. Zhejiang Univ. Sci. A* 10(5), 716-724.

Ramsey, A.C., Duff, E., Paterson, L. and Stuart, J., 1973. The Uptake of F^- by Hydroxyapatite at Varying pH. *Caries research* 7(3), 231-244.

Rasool, A., Farooqi, A., Xiao, T., Ali, W., Noor, S., Abiola, O., Ali, S. and Nasim, W., 2017. A review of global outlook on fluoride contamination in groundwater with prominence on the Pakistan current situation. *Environ. Geochem. Health* 40(4), 1-17.

Rasool, A., Xiao, T., Baig, Z.T., Masood, S., Mostofa, K.M. and Iqbal, M., 2015. Co-occurrence of arsenic and fluoride in the groundwater of Punjab, Pakistan: source discrimination and health risk assessment. *Environ. Sci. Pollut. Res.* 22(24), 19729-19746.

Ren, H.-T., Han, J., Li, T.-T., Sun, F., Lin, J.-H. and Lou, C.-W., 2019. Visible light-induced oxidation of aqueous arsenite using facile Ag_2O/TiO_2 composites: Performance and mechanism. *J. Photochem. Photobiol* 377, 260-267.

Reyes-Gómez, V.M., Alarcón-Herrera, M.T., Gutiérrez, M. and López, D.N., 2013. Fluoride and arsenic in an alluvial aquifer system in Chihuahua, Mexico: contaminant levels, potential sources, and co-occurrence. *Water, Air, & Soil Pollution* 224(2), 1433.

Rioyo, J., Aravinthan, V., Bundschuh, J. and Lynch, M., 2018. Research on 'high-pH precipitation treatment'for RO concentrate minimization and salt recovery in a municipal groundwater desalination facility. *Desalination* 439, 168-178.

Roguska, A., Pisarek, M., Andrzejczuk, M., Dolata, M., Lewandowska, M. and Janik-Czachor, M., 2011. Characterization of a calcium phosphate–TiO_2 nanotube composite layer for biomedical applications. *Mater. Sci. Eng* 31(5), 906-914.

Rojas-Mayorga, C., Bonilla-Petriciolet, A., Aguayo-Villarreal, I.A., Hernandez-Montoya, V., Moreno-Virgen, M., Tovar-Gómez, R. and Montes-Morán, M., 2013. Optimization of pyrolysis conditions and adsorption properties of bone char for fluoride removal from water. *J. Anal. Appl. Pyrolysis* 104, 10-18.

Rojas-Mayorga, C.K., Bonilla-Petriciolet, A., Sánchez-Ruiz, F.J., Moreno-Pérez, J., Reynel-Ávila, H.E., Aguayo-Villarreal, I. and Mendoza-Castillo, D., 2015a. Breakthrough curve modeling of liquid-phase adsorption of fluoride ions on aluminum-doped bone char using micro-columns: effectiveness of data fitting approaches. *Journal of Molecular Liquids* 208, 114-121.

Rojas-Mayorga, C.K., Mendoza-Castillo, D.I., Bonilla-Petriciolet, A. and Silvestre-Albero, J., 2016. Tailoring the adsorption behavior of bone char for heavy metal removal from aqueous solution. *Adsorpt. Sci. Technol.* 34(6), 368-387.

Rojas-Mayorga, C.K., Silvestre-Albero, J., Aguayo-Villarreal, I.A., Mendoza-Castillo, D.I. and Bonilla-Petriciolet, A., 2015b. A new synthesis route for bone chars using CO_2 atmosphere and their application as fluoride adsorbents. *Micropor. Mesopor. Mat.* 209, 38-44.

Rousseau, M.-C., Straif, K. and Siemiatycki, J., 2005. IARC carcinogen update. *Environ. Health Prerspec.* 113(9), A580-A581.

Roy, S., 2018. Synthesis of graphene oxide using tea-waste biochar as green substitute of graphite and its application in de-fluoridation of contaminated water. *Am. J. Chem. Res.* 1(1), 1-19.

Rubinos, D.A. and Spagnoli, G., 2019. Assessment of red mud as sorptive landfill liner for the retention of arsenic (V). *J. Environ. Manage.* 232, 271-285.

Samsuri, A.W., Sadegh-Zadeh, F. and Seh-Bardan, B.J., 2013. Adsorption of As (III) and As (V) by Fe coated biochars and biochars produced from empty fruit bunch and rice husk. *J. Environ. Chem. Eng.* 1(4), 981-988.

Savage, N. and Diallo, M.S., 2005. Nanomaterials and water purification: opportunities and challenges. *J. Nanopart. Res* 7(4-5), 331-342.

Shen, J., Richards, B.S. and Schäfer, A.I., 2016. Renewable energy powered membrane technology: Case study of St. Dorcas borehole in Tanzania demonstrating fluoride removal via nanofiltration/reverse osmosis. *Sep. Purif. Technol.* 170, 445-452.

Sheng, H., Zhang, H., Song, W., Ji, H., Ma, W., Chen, C. and Zhao, J., 2015. Activation of water in titanium dioxide photocatalysis by formation of surface hydrogen bonds: an in situ IR spectroscopy study. *Angew. Chem. Int. Ed.* 54(20), 5905-5909.

Singh, P. and Mohan, D., 2020. Rice-husk and wheat-husk iron oxide biochar nanocomposites for the sustainable removal of arsenic from water, p. 30.

Singh, S., Mahalingam, H. and Singh, P.K., 2013. Polymer-supported titanium dioxide photocatalysts for environmental remediation: A review. *Appl. Catal, A.* 462, 178-195.

Smith, E., Smith, J., Smith, L., Biswas, T., Correll, R. and Naidu, R., 2003. Arsenic in Australian environment: an overview. *J. Environ. Sci. Health A* 38(1), 223-239.

Soni, R. and Shukla, D.P., 2019. Synthesis of fly ash based zeolite-reduced graphene oxide composite and its evaluation as an adsorbent for arsenic removal. *Chemosphere* 219, 504-509.

Sternitzke, V., Kaegi, R., Audinot, J.-N., Lewin, E., Hering, J.G. and Johnson, C.A., 2012. Uptake of fluoride from aqueous solution on nano-sized hydroxyapatite: examination of a fluoridated surface layer. *Environ. Sci. Technol.* 46(2), 802-809.

Tabassum, R.A., Shahid, M., Niazi, N.K., Dumat, C., Zhang, Y., Imran, M., Bakhat, H.F., Hussain, I. and Khalid, S., 2019. Arsenic removal from aqueous solutions and groundwater using agricultural biowastes-derived biosorbents and biochar: a column-scale investigation. *Int. J. Phytoremediation* 21(6), 509-518.

Tan, K. and Hameed, B., 2017. Insight into the adsorption kinetics models for the removal of contaminants from aqueous solutions. *J. Taiwan Inst. Chem. Eng.* 74, 25-48.

Thamir, A.D., Haider, A.J. and Ali, G.A., 2016. Preparation of NanostructureTiO2 at Different Temperatures by Pulsed Laser Deposition as Solar Cell. *Engineering and Technology Journal* 34(2 Part (A) Engineering), 193-204.

Tovar-Gómez, R., Moreno-Virgen, M., Dena-Aguilar, J., Hernández-Montoya, V., Bonilla-Petriciolet, A. and Montes-Morán, M., 2013. Modeling of fixed-bed adsorption of fluoride on bone char using a hybrid neural network approach. *Chemical engineering journal* 228, 1098-1109.

UN 2019 World water develeopment report.

Valderrama, C., Gamisans, X., De las Heras, X., Farran, A. and Cortina, J., 2008. Sorption kinetics of polycyclic aromatic hydrocarbons removal using granular activated carbon: intraparticle diffusion coefficients. *J. Hazard. Mater.* 157(2-3), 386-396.

Wang, H., Liang, D., Wang, Y.-n., Sun, Y., Li, W., Zhang, D., Tsang, Y.F. and Pan, X., 2019. Fabricating biogenic Fe (III) flocs from municipal sewage sludge using NAFO processes: Characterization and arsenic removal ability. *J. Environ. Manage.* 231, 268-274.

Wang, J. and Guo, X., 2020. Adsorption isotherm models: Classification, physical meaning, application and solving method. *Chemosphere*, 127279.

Wei, Z., Fang, Y., Wang, Z., Liu, Y., Wu, Y., Liang, K., Yan, J., Pan, Z. and Hu, G., 2019. pH effects of the arsenite photocatalytic oxidation reaction on different anatase TiO_2 facets. *Chemosphere* 225, 434-442.

Weiss, S., Carapito, C., Cleiss, J., Koechler, S., Turlin, E., Coppee, J.-Y., Heymann, M., Kugler, V., Stauffert, M. and Cruveiller, S., 2009. Enhanced structural and functional genome elucidation of the arsenite-oxidizing strain Herminiimonas arsenicoxydans by proteomics data. *Biochimie* 91(2), 192-203.

Welgemoed, T. and Schutte, C.F., 2005. Capacitive deionization technology™: an alternative desalination solution. *Desalination* 183(1-3), 327-340.

WHO, G., 2011. Guidelines for drinking-water quality. *World Health Organization* 216, 303-304.

Woan, K., Pyrgiotakis, G. and Sigmund, W., 2009. Photocatalytic carbon-nanotube–TiO_2 composites. *Adv. Mater.* 21(21), 2233-2239.

Xu, T., Cai, Y. and O'Shea, K.E., 2007. Adsorption and photocatalyzed oxidation of methylated arsenic species in TiO_2 suspensions. *Environ. Sci. Technol.* 41(15), 5471-5477.

Yadav, S.K., Ramanathan, A., Kumar, M., Chidambaram, S., Gautam, Y. and Tiwari, C., 2020. Assessment of arsenic and uranium co-occurrences in groundwater of central Gangetic Plain, Uttar Pradesh, India. *Environ. Earth Sci.* 79(6), 1-14.

Yoon, S.-H. and Lee, J.H., 2005. Oxidation mechanism of As(III) in the UV/TiO_2 system: evidence for a direct hole oxidation mechanism. *Environ. Sci. Technol.* 39(24), 9695-9701.

Yu, F., Sun, S., Ma, J. and Han, S., 2015. Enhanced removal performance of arsenate and arsenite by magnetic graphene oxide with high iron oxide loading. *Phys. Chem. Chem. Phys.* 17(6), 4388-4397.

Zeltner, W.A., 2002. Simultaneous Removal of Arsenite As (III) and Arsenate As (V) From Drinking Water Using a Novel Photoactive Adsorbent, EPA.

Zhang, Q., Bolisetty, S., Cao, Y., Handschin, S., Adamcik, J., Peng, Q. and Mezzenga, R., 2019a. Selective and efficient removal of fluoride from water: in situ engineered amyloid fibril/ZrO_2 hybrid membranes. *Angew. Chem. Int. Ed.* 58(18), 6012-6016.

Zhang, T., Zhao, Y., Kang, S., Li, Y. and Zhang, Q., 2019b. Formation of active Fe $(OH)_3$ in situ for enhancing arsenic removal from water by the oxidation of Fe (II) in air with the presence of $CaCO_3$. *J. Clean. Prod.* 227, 1-9.

Zhao, X., Zhang, A., Zhang, J., Wang, Q., Huang, X., Wu, Y. and Tang, C., 2020. Enhanced Selenate Removal in Aqueous Phase by Copper-Coated Activated Carbon. *Materials* 13(2), 468.

Appendix A

Supplementary Materials

Arsenic removal from water using bon char: A detailed study on adsorption kinetic and isotherm models

Susan S.A. Alkurdi[a,b], Raed A. Al-Juboori[c], Jochen Bundschuh[a,d]*, Les Bowtell[e], Alla Marchuk[f]

[a] *School of Civil Engineering and Surveying, Faculty of Health, Engineering and Sciences, University of Southern Queensland, West Street, Toowoomba, 4350, Queensland, Australia.*

[b] *Northern Technical University, Engineering Technical College/Kirkuk, Iraq.*

[c] *Water Engineering Research Group, Department of Civil and Environmental Engineering, Aalto University, P.O. Box 15200, Aalto, FI-00076 Espoo, Finland.*

[d] *UNESCO Chair on Groundwater Arsenic within the 2030 Agenda for Sustainable Development, University of Southern Queensland, West Street, Toowoomba, 4350, Queensland, Australia.*

[e] *School of Mechanical and Electrical Engineering, Faculty of Health, Engineering and Sciences, University of Southern Queensland, Toowoomba, 4350, QLD, Australia.*

[f] *University of Southern Queensland, Centre for Sustainable Agricultural Systems, Toowoomba, 4350, Queensland, Australia.*

Table captions

Table SM1. Parameters of isotherm models for As(III) and As(V) adsorption onto bone char based on linear regression fittings

Table SM2. Parameters of kinetic models for As(III) data calculated from the linear forms of the models

Table SM3. Parameters of kinetic models for As(V) data calculated from the linear forms of the models

Table SM4. Error functions for each of the concentrations after determining the parameters of kinetic models using linear (L) and nonlinear (NL) regression methods for As(III) data

Table SM5. Error analysis for kinetic models of As(III) adsorption onto bone char at an initial concentration of 2.5 mg/L

Table SM6. Error analysis for kinetic models of As(III) adsorption onto bone char at an initial concentration of 5 mg/L

Table SM7. Error analysis for kinetic models of As(III) adsorption onto bone char at an initial concentration of 10 mg/L

Table SM8. Error analysis for kinetic models of As(V) adsorption onto bone char at an initial concentration of 2.5 mg/L

Table SM9. Error analysis for kinetic models of As(V) adsorption onto bone char at an initial concentration of 5 mg/L

Table SM10. Error analysis for kinetic models of As(V) adsorption onto bone char at an initial concentration of 10 mg/L

Table SM1. Parameters of isotherm models for As(III) and As(V) adsorption onto bone char based on linear regression fittings

	2-Parameters			3-Parameters			
	Freundlich			Redlich-Peterson			
	K_f	1/n	R^2	K_{RP}	a_{RP}	β	R^2
As(V)	0.175	1.132	0.891	0.340	0.342	0.997	0.908
As(III)	0.089	1.0224	0.943	0.647	0.053	0.51	0.984
	Langmuir			Sips			
	K_L	Q_o	R^2	q_m	b	n	R^2
As(V)	0.287	0.8518	0.960	0.204	0.0172	0.608	0.653
As(III)	0.6	0.0985	0.781	2.661	0.089	0.854	0.892

Table SM2. Parameters of kinetic models for As(III) data calculated from the linear forms of the models

	PFO			PSO		
Conc. (mg/L)	k_1	q_e	R^2	k_2	q_e	R^2
0.5	0.008	0.054	0.953	0.151	0.054	0.943
2.5	0.009	0.227	0.961	0.215	0.227	0.756
5.0	0.009	0.377	0.988	0.096	0.096	0.723
10.0	0.008	0.561	0.980	0.037	0.037	0.906

	Elovich			Sips		
	α	β	R^2	k_2	q_e	R^2
0.5	0.001	44.053	0.902	0.009	0.053	0.947
2.5	0.005	13.736	0.898	0.011	0.277	0.942

5.0	0.004	4.831	0.899	0.007	0.487	0.932
10.0	0.009	4.864	0.923	0.016	0.504	0.930

Table SM3. Parameters of kinetic models for As(V) data calculated from the linear forms of the models

	PFO			PSO		
Conc. (mg/L)	k_1	q_e	R^2	k_2	q_e	R^2
0.5	0.005	0.054	0.915	0.145	0.054	0.851
2.5	0.005	0.263	0.918	0.064	0.263	0.738
5.0	0.005	0.473	0.902	0.019	0.473	0.819
10.0	0.005	0.889	0.917	0.025	0.889	0.675
	Elovich			Sips		
	α	β	R^2	k_2	q_e	R^2
0.5	0.001	44.131	0.898	0.006	0.047	0.892
2.5	0.003	12.346	0.912	0.016	0.129	0.748
5.0	0.005	6.730	0.894	0.007	0.310	0.845
10.0	0.012	4.312	0.878	0.018	0.519	0.730

Table SM4. Error functions for each of the concentrations after determining the parameters of kinetic models using linear (L) and nonlinear (NL) regression methods for As(III) data

Conc. (mg/L)	Error Functions	PFO		PSO		Elovich		Ritchie	
	and RSQ	L	NL	L	NL	L	NL	L	NL
0.5	SSE	2.4E-04	9.7E-06	5.2E-04	9.6E-06	7.7E-04	3.8E-04	5.1E-04	1.1E-05
	HYBRID	1.5E-01	1.4E-02	1.6E-01	1.5E-02	3.7E-01	1.8E-01	1.6E-01	1.4E-02
	MPSD	3.0E+01	1.4E+01	2.0E+01	1.5E+01	4.2E+01	3.6E+01	2.3E+01	1.4E+01
	ARE	2.0E+01	5.8E+00	1.6E+01	5.5E+00	3.4E+01	2.5E+01	1.7E+01	5.6E+00
	SAE	4.1E-02	6.9E-03	5.1E-02	6.3E-03	8.3E-02	5.4E-02	5.4E-02	6.9E-03
	RSQ	9.5E-01	1.0E+00	9.4E-01	1.0E+00	9.8E-01	9.8E-01	9.5E-01	1.0E+00
2.5	SSE	3.3E-03	5.0E-02	1.6E-02	2.12E-03	5.8E-03	2.8E-03	2.1E-03	2.0E-03
	HYBRID	4.8E-01	4.3E+00	2.1E+00	3.83E-01	9.4E-01	2.7E-01	2.8E-01	2.9E-01
	MPSD	2.4E+01	5.9E+01	4.4E+01	2.22E+01	3.5E+01	1.6E+01	1.8E+01	1.9E+01
	ARE	1.2E+01	5.0E+01	3.0E+01	9.30E+00	1.3E+01	1.1E+01	9.6E+00	9.4E+00
	SAE	1.3E-01	7.0E-01	3.2E-01	7.49E-02	1.2E-01	1.5E-01	1.1E-01	9.7E-02

	RSQ	9.6E-01	9.8E-01	7.6E-01	9.62E-01	9.1E-01	9.8E-01	9.4E-01	9.4E-01
5	SSE	2.5E-02	1.7E-03	6.0E-02	3.7E-03	5.9E-03	1.0E-02	1.4E-02	1.6E-03
	HYBRID	3.3E+00	2.7E-01	1.0E+01	8.5E-01	1.1E+00	1.0E+00	1.8E+00	2.7E-01
	MPSD	4.9E+01	1.6E+01	9.6E+01	3.2E+01	3.3E+01	2.6E+01	3.6E+01	1.6E+01
	ARE	3.1E+01	8.4E+00	5.9E+01	1.6E+01	1.6E+01	1.9E+01	2.3E+01	8.3E+00
	SAE	3.5E-01	8.2E-02	5.3E-01	1.2E-01	1.5E-01	2.4E-01	2.7E-01	8.2E-02
	RSQ	8.8E-01	9.8E-01	7.2E-01	9.7E-01	9.5E-01	9.7E-01	9.0E-01	9.8E-01
10	SSE	5.3E-03	4.6E-03	3.6E-02	3.6E-03	2.1E-03	1.8E-02	3.6E-02	3.6E-03
	HYBRID	6.4E-01	6.3E-01	4.6E+00	5.6E-01	1.5E-01	1.5E+00	1.9E+00	4.5E-01
	MPSD	2.2E+01	2.3E+01	5.1E+01	2.1E+01	8.3E+00	2.9E+01	2.5E+01	1.9E+01
	ARE	1.2E+01	1.0E+01	3.2E+01	1.2E+01	6.0E+00	2.0E+01	1.9E+01	1.0E+01
	SAE	1.5E-01	1.2E-01	4.1E-01	1.4E-01	1.1E-01	3.1E-01	4.2E-01	1.4E-01
	RSQ	9.8E-01	9.8E-01	9.1E-01	9.8E-01	9.9E-01	9.9E-01	9.3E-01	9.8E-01

Table SM5. Error analysis for kinetic models of As(III) adsorption onto bone char at an initial concentration of 2.5 mg/L

	Pseudo-first-order (PFO)				
	SSE	HYBRID	MPSD	ARE	SAE
q_e	0.226	0.213	0.196	0.228	0.227
k_1	0.010	0.012	0.015	0.010	0.011
RSQ	0.963	0.910	0.857	0.942	0.941
SSE	**0.003**	0.003	0.004	0.003	0.005
HYBRID	0.385	**0.371**	0.404	0.395	0.393
MPSD	21.881	20.917	**20.394**	22.255	22.250
ARE	10.461	11.407	12.338	**10.120**	10.114
SAE	0.108	0.128	0.154	0.102	**0.102**
SNE	4.048	4.216	4.727	**4.027**	4.453
	Pseudo-second-order (PSO)				
	SSE	HYBRID	MPSD	ARE	SAE
q_e	1.240	0.247	0.213	0.296	0.312
k_2	0.001	0.059	0.102	0.030	0.025
RSQ	0.900	0.988	0.854	0.944	0.951
SSE	**0.008**	0.002	0.003	0.002	0.002
HYBRID	1.221	**0.292**	0.333	0.362	0.383
MPSD	36.961	18.152	**17.383**	21.474	22.161
ARE	23.643	10.278	12.696	**9.450**	9.301
SAE	0.232	0.103	0.145	0.080	**0.075**
SNE	5.000	**1.847**	2.268	1.867	1.885
	Elovich				
	SSE	HYBRID	MPSD	ARE	SAE

α	0.009	0.010	0.012	0.014	0.006
β	18.592	20.571	23.266	22.786	16.231
RSQ	0.976	0.971	0.973	0.971	0.968
SSE	**0.002**	0.003	0.004	0.003	0.003
HYBRID	0.295	**0.272**	0.304	0.317	0.448
MPSD	17.608	15.780	**15.033**	16.436	23.487
ARE	11.270	11.439	11.973	**11.590**	10.894
SAE	0.130	0.146	0.171	0.152	**0.114**
SNE	**3.761**	3.808	4.320	4.125	4.381

	Ritchie				
	SSE	HYBRID	MPSD	ARE	SAE
q_e	0.292	0.267	0.232	0.310	0.314
K_R	0.010	0.012	0.018	0.007	0.008
RSQ	0.956	0.918	0.878	0.939	0.956
SSE	**0.002**	0.002	0.003	0.002	0.002
HYBRID	0.294	**0.280**	0.318	0.341	0.341
MPSD	19.081	17.942	**17.248**	20.870	20.869
ARE	9.398	9.814	11.770	**8.636**	8.636
SAE	0.097	0.112	0.153	0.081	**0.081**
SNE	**3.820**	3.906	4.760	3.927	3.927

Table SM6. Error analysis for kinetic models of As(III) adsorption onto bone char at an initial concentration of 5 mg/L

	Pseudo-first-order (PFO)				
	SSE	HYBRID	MPSD	ARE	SAE
q_e	1.359	1.261	0.848	0.853	0.853

K_1	0.001	0.001	0.002	0.002	0.002
RSQ	0.973	0.973	0.9733	0.973	0.973
SSE	**0.002**	0.0017	0.0020	0.002	0.002
HYBRID	0.272	**0.2713**	0.2885	0.304	0.304
MPSD	15.751	15.685	**15.449**	15.832	15.832
ARE	8.403	8.3823	9.377	**9.320**	9.319
SAE	0.083	0.0819	0.102	0.090	**0.090**
SNE	4.395	**4.3862**	4.926	4.846	4.846

	Pseudo-second-order (PSO)				
	SSE	HYBRID	MPSD	ARE	SAE
q_e	1.258	0.873	0.559	0.645	0.645
k_2	0.001	0.003	0.008	0.006	0.006
RSQ	0.978	0.959	0.926	0.938	0.938
SSE	**0.004**	0.004	0.008	0.006	0.006
HYBRID	0.855	**0.818**	0.959	0.872	0.872
MPSD	32.054	30.451	**29.382**	29.555	29.555
ARE	16.044	16.312	17.285	**16.169**	16.169
SAE	0.119	0.140	0.193	0.161	**0.161**
SNE	**3.923**	4.005	4.917	4.325	4.325

	Elovich				
	SSE	HYBRID	MPSD	ARE	SAE
α	0.005	0.005	0.005	0.006	0.006
β	6.427	7.460	9.085	9.433	7.938
RSQ	0.974	0.975	0.971	0.970	0.971
SSE	**0.008**	0.010	0.017	0.015	0.011
HYBRID	1.185	**1.038**	1.263	1.319	1.374

MPSD	31.148	26.265	**24.156**	26.650	30.475
ARE	19.739	18.702	19.085	**17.388**	18.162
SAE	0.212	0.236	0.296	0.263	**0.226**
SNE	4.065	**3.925**	4.662	4.480	4.325

	Ritchie				
	SSE	HYBRID	MPSD	ARE	SAE
q_e	0.95	1.289	1.142	1.266	1.366
K_R	0.001	0.001	0.001	0.001	0.009
RSQ	0.971	0.969	0.970	0.971	0.960
SSE	**0.0016**	0.002	0.002	0.002	0.019
HYBRID	0.272	**0.270**	0.291	0.306	0.308
MPSD	15.802	15.617	**15.342**	15.813	15.813
ARE	8.314	8.400	9.4988	**9.399**	9.399
SAE	0.082	0.082	0.106	0.092	**0.092**
SNE	**4.303**	4.305	4.918	4.806	4.806

Table SM7. Error analysis for kinetic models of As(III) adsorption onto bone char at an initial concentration of 10 mg/L

	Pseudo-first-order (PFO)				
	SSE	HYBRID	MPSD	ARE	SAE
q_e	1.191	0.980	1.029	1.080	1.134
k_1	0.003	0.004	0.004	0.003	0.003
RSQ	0.922	0.907	0.913	0.920	0.923
SSE	**0.046**	0.064	0.062	0.064	0.058
HYBRID	1.311	**1.456**	1.395	1.404	1.320

MPSD	23.241	22.771	**22.665**	22.901	22.758
ARE	15.260	14.670	14.236	**13.496**	13.483
SAE	0.502	0.529	0.510	0.493	**0.478**
SNE	**4.563**	4.941	4.789	4.761	4.570

	Pseudo-second-order (PSO)				
	SSE	HYBRID	MPSD	ARE	SAE
q_e	0.933	0.980	1.029	1.080	1.134
k_2	0.007	0.005	0.004	0.004	0.003
RSQ	0.857	0.881	0.894	0.906	0.903
SSE	**0.106**	0.109	0.113	0.126	0.093
HYBRID	3.113	**2.434**	2.363	2.552	2.028
MPSD	32.072	25.284	**24.163**	24.774	23.565
ARE	24.513	19.430	17.651	**16.031**	16.692
SAE	0.738	0.665	0.651	0.653	**0.585**
SNE	4.844	4.131	4.015	4.131	**3.601**

	Elovich				
	SSE	HYBRID	MPSD	ARE	SAE
α	0.013	0.015	0.016	0.019	0.010
β	6.376	7.368	9.071	8.208	5.464
RSQ	0.984	0.986	0.983	0.982	0.984
SSE	**0.015**	0.018	0.040	0.023	0.022
HYBRID	1.770	**1.483**	1.968	1.917	3.730
MPSD	36.214	28.812	**25.593**	31.165	58.738
ARE	20.791	19.615	20.740	**17.419**	23.927
SAE	0.257	0.313	0.455	0.305	**0.244**
SNE	2.894	**2.863**	3.830	3.031	4.086

	Ritchie				
	SSE	HYBRID	MPSD	ARE	SAE
q_e	0.904	0.856	0.761	0.899	0.900
K_R	0.005	0.006	0.007	0.005	0.005
RSQ	0.983	0.981	0.975	0.984	0.984
SSE	**0.004**	0.004	0.005	0.004	0.004
HYBRID	0.447	**0.437**	0.486	0.479	0.478
MPSD	19.043	18.425	**17.939**	19.71	19.711
ARE	10.082	10.446	11.098	**9.448**	9.447
SAE	0.142	0.147	0.163	0.132	**0.132**
SNE	**4.334**	4.376	4.910	4.390	4.390

Table SM8. Error analysis for kinetic models of As(V) adsorption onto bone char at an initial concentration of 2.5 mg/L

	Pseudo-first-order (PFO)				
	SSE	HYBRID	MPSD	ARE	SAE
q_e	0.318	0.350	0.385	0.423	0.466
k_1	0.004	0.003	0.002	0.002	0.002
RSQ	0.932	0.945	0.954	0.959	0.957
SSE	**0.005**	0.005	0.007	0.008	0.003
HYBRID	0.595	**0.442**	0.463	0.5099	0.351
MPSD	32.570	25.954	**23.913**	23.992	25.494
ARE	23.435	19.041	16.725	**16.100**	17.729
SAE	0.173	0.162	0.168	0.177	**0.130**
SNE	4.644	3.964	4.049	4.281	**3.304**

	Pseudo-second-order (PSO)				
	SSE	HYBRID	MPSD	ARE	SAE
q_e	0.260	0.286	0.315	0.346	0.381
k_2	0.025	0.015	0.010	0.008	0.009
RSQ	0.849	0.889	0.912	0.923	0.909
SSE	**0.013**	0.014	0.017	0.016	0.008
HYBRID	1.463	**0.835**	1.020	1.003	0.982
MPSD	50.819	33.686	**29.072**	28.421	37.940
ARE	33.502	25.580	22.407	**21.212**	26.489
SAE	0.272	0.255	0.266	0.261	**0.204**
SNE	4.790	**3.766**	3.915	3.828	3.422
	Elovich				
	SSE	HYBRID	MPSD	ARE	SAE
α	0.003	0.003	0.002	0.002	0.003
β	9.004	10.824	12.857	12.603	12.603
RSQ	0.907	0.907	0.907	0.907	0.907
SSE	**0.005**	0.006	0.010	0.012	0.009
HYBRID	0.769	**0.543**	0.681	0.817	0.672
MPSD	39.619	24.533	**21.293**	25.706	24.246
ARE	23.151	17.422	16.982	**16.397**	17.521
SAE	0.169	0.161	0.199	0.203	**0.189**
SNE	4.191	**3.356**	3.942	4.356	3.433
	Ritchie				
	SSE	HYBRID	MPSD	ARE	SAE
q_e	0.156	0.172	0.189	0.208	0.229
K_R	0.019	0.010	0.006	0.006	0.006

RSQ	0.704	0.804	0.853	0.862	0.853
SSE	**0.027**	0.028	0.030	0.026	0.018
HYBRID	2.762	**1.848**	1.846	1.590	1.302
MPSD	34.237	41.588	**35.491**	68.877	38.681
ARE	31.323	47.684	28.009	**26.779**	28.572
SAE	0.401	0.361	0.366	0.336	**0.292**
SNE	4.061	**4.087**	3.684	3.830	2.956

Table SM9. Error analysis for kinetic models of As(V) adsorption onto bone char at an initial concentration of 5 mg/L

	Pseudo-first-order (PFO)				
	SSE	HYBRID	MPSD	ARE	SAE
q_e	0.520	0.572	0.630	0.692	0.762
k_1	0.004	0.003	0.002	0.002	0.002
RSQ	0.916	0.934	0.944	0.950	0.950
SSE	**0.024**	0.026	0.033	0.035	0.022
HYBRID	1.462	**1.028**	1.101	1.156	0.814
MPSD	36.966	26.313	**23.178**	23.025	23.017
ARE	26.976	20.334	17.165	**16.138**	17.503
SAE	0.386	0.345	0.350	0.352	**0.303**
SNE	4.676	3.793	3.858	3.922	**3.226**
	Pseudo-second-order (PSO)				
	SSE	HYBRID	MPSD	ARE	SAE
q_e	0.520	0.572	0.630	0.630	0.692
k_2	0.010	0.006	0.004	0.004	0.004

RSQ	0.861	0.895	0.916	0.916	0.911
SSE	**0.042**	0.046	0.056	0.057	0.034
HYBRID	2.624	**1.733**	1.844	1.865	1.430
MPSD	51.276	32.239	**27.163**	27.168	31.397
ARE	35.898	24.250	20.455	**20.412**	23.426
SAE	0.511	0.4493	0.4592	0.4617	**0.4004**
SNE	4.7278	3.6398	3.6878	**3.7129**	3.1973

	Elovich				
	SSE	HYBRID	MPSD	ARE	SAE
α	0.004	0.004	0.004	0.004	0.004
β	4.960	6.169	7.581	7.578	5.121
RSQ	0.890	0.890	0.890	0.890	0.890
SSE	**0.020**	0.026	0.044	0.054	0.021
HYBRID	1.854	**1.279**	1.625	2.014	1.791
MPSD	46.886	28.389	**24.382**	29.032	46.661
ARE	28.173	21.733	19.274	**18.347**	27.068
SAE	0.353	0.364	0.409	0.424	**0.339**
SNE	4.134	**3.364**	3.797	4.270	4.040

	Ritchie				
	SSE	HYBRID	MPSD	ARE	SAE
q_e	0.341	0.375	0.413	0.454	0.499
K_R	0.011	0.006	0.004	0.004	0.005
RSQ	0.765	0.839	0.876	0.883	0.868
SSE	**0.072**	0.076	0.087	0.074	0.047
HYBRID	4.304	**2.778**	2.857	2.458	2.169
MPSD	66.863	38.388	**31.913**	30.903	41.416

ARE	47.170	27.354	24.701	**23.459**	28.543
SAE	0.651	0.564	0.590	0.537	**0.480**
SNE	4.829	3.536	3.571	3.207	**2.999**

Table SM10. Error analysis for kinetic models of As(V) adsorption onto bone char at an initial concentration of 10 mg/L

	Pseudo-first-order (PFO)				
	SSE	HYBRID	MPSD	ARE	SAE
q_e	1.075	1.183	1.174	1.292	1.421
k_1	0.004	0.003	0.003	0.003	0.002
RSQ	0.912	0.924	0.924	0.931	0.937
SSE	**0.041**	0.049	0.051	0.047	0.053
HYBRID	1.432	**1.239**	1.248	1.181	1.113
MPSD	23.526	22.622	**22.611**	22.681	22.712
ARE	16.006	13.856	13.769	**13.228**	13.117
SAE	0.536	0.466	0.468	0.441	**0.419**
SNE	4.773	4.495	4.526	**4.323**	4.344
	Pseudo-second-order (PSO)				
	SSE	HYBRID	MPSD	ARE	SAE
q_e	1.075	1.183	1.301	1.396	0.978
k_2	0.005	0.003	0.003	0.002	0.005
RSQ	0.881	0.904	0.917	0.925	0.881
SSE	**0.084**	0.080	0.076	0.075	0.110
HYBRID	2.494	**1.873**	1.707	1.669	2.443
MPSD	29.119	23.777	**22.909**	22.913	25.148
ARE	22.503	17.566	15.402	**13.969**	19.223

SAE	0.662	0.573	0.525	0.664	**0.495**
SNE	4.750	3.929	**3.626**	3.753	4.443

	Elovich				
	SSE	HYBRID	MPSD	ARE	SAE
α	0.010	0.011	0.010	0.010	0.009
β	3.071	3.426	4.095	4.095	3.431
RSQ	0.896	0.896	0.896	0.896	0.896
SSE	**0.059**	0.068	0.093	0.098	0.068
HYBRID	2.284	**2.476**	2.359	2.303	1.874
MPSD	26.483	26.915	**22.409**	20.690	22.087
ARE	19.868	19.165	15.772	**15.185**	15.013
SAE	0.586	0.590	0.584	0.584	**0.500**
SNE	4.504	4.657	4.512	4.452	**3.875**

	Ritchie				
	SSE	HYBRID	MPSD	ARE	SAE
q_e	0.919	0.628	0.691	0.760	0.836
K_R	0.007	0.011	0.008	0.006	0.006
RSQ	0.829	0.767	0.805	0.840	0.846
SSE	**0.121**	0.236	0.224	0.235	0.185
HYBRID	2.914	**4.238**	3.845	4.018	3.176
MPSD	29.612	28.981	**26.621**	27.508	25.180
ARE	23.761	23.391	20.522	**18.239**	17.736
SAE	0.833	1.031	0.954	0.926	**0.836**
SNE	4.008	4.963	4.543	4.537	**3.939**

Appendix B

Graphical abstract of the published papers

- **The graphical abstract - PAPER I**

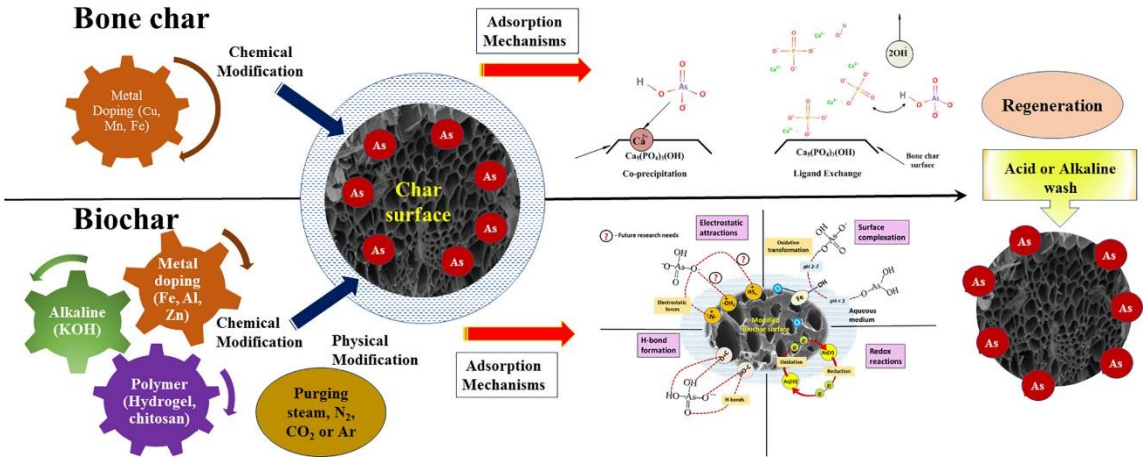

- **The graphical abstract – PAPER II**

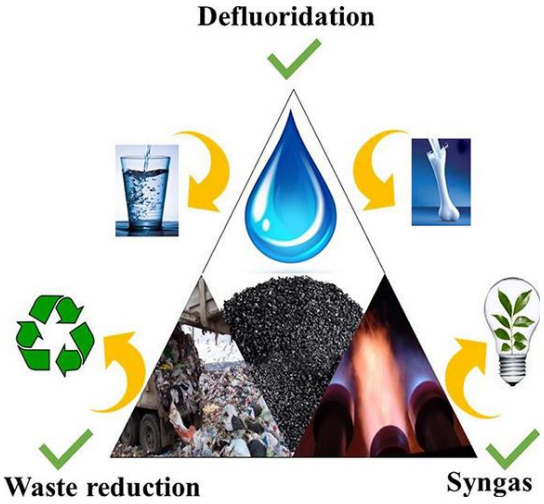

- **The graphical abstract -PAPER III**